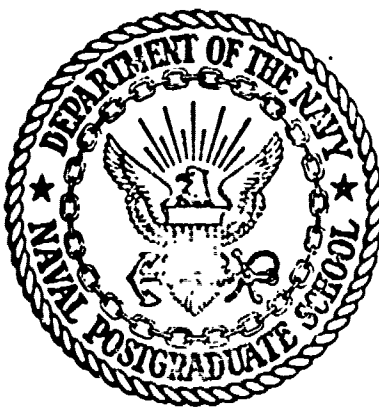


AD 749048

NAVAL POSTGRADUATE SCHOOL

Monterey, California



Reproduced by
**NATIONAL TECHNICAL
INFORMATION SERVICE**
U S Department of Commerce
Springfield VA 22151

THESIS

Holographic Interferometry of The Flow

Field Between a Fin And Flat Plate

by

Robert Ward Heyer

Thesis Advisor:

D. G. Collins

March 1972

Details of illustrations in
this document may be better
studied on microfiche

Approved for public release; distribution unlimited.

UNCLASSIFIED

Security Classification

DOCUMENT CONTROL DATA - R & D

(Security classification of title, body of abstract and indexing annotation must be entered when the overall report is classified)

1. ORIGINATING ACTIVITY (Corporate author) Naval Postgraduate School Monterey, California 93940	2a. REPORT SECURITY CLASSIFICATION Unclassified
	2b. GROUP

3. REPORT TITLE

Holographic Interferometry of The Flow Field Between a Fin And Flat Plate

4. DESCRIPTIVE NOTES (Type of report and, inclusive dates)

Master's Thesis; (March 1972)

5. AUTHOR(S) (First name, middle initial, last name)

Robert Ward Heyer

6. REPORT DATE March 1972	7a. TOTAL NO. OF PAGES 178	7b. NO. OF REFS 27
------------------------------	-------------------------------	-----------------------

8a. CONTRACT OR GRANT NO.

8b. PROJECT NO.

c.

d.

8c. ORIGINATOR'S REPORT NUMBER(S)

8d. OTHER REPORT NO(S) (Any other numbers that may be assigned this report)

10. DISTRIBUTION STATEMENT

Approved for public release; distribution unlimited.

11. SUPPLEMENTARY NOTES

12. SPONSORING MILITARY ACTIVITY

Naval Postgraduate School
Monterey, California 93940

13. ABSTRACT

This study was an attempt to map the density field in a fin-flat plate junction three-dimensionally using holographic interferometry. This investigation has extended the density studies by Matulka [12, 13] and Jagota [3, 4] to include, for the first time, interferometric fringe information obtained through a transparent model in supersonic flow. The fringe information was then inverted by a FORTRAN computer program to produce a plot of the density field around the model. The feasibility of the method was demonstrated.

The factors which are thought to have limited the success of the experiment include vibration of the model, fluctuations of the tunnel flow and the fact that the model was somewhat too large in relation to the size of the wind tunnel test section. Schlieren photography was used to look through and around the model and to verify that the same flow was established as was reported by Thomas [23, 24] and Winkelmann [26, 27].

The data reduction of holographic interferograms was, for the first time, accomplished using photographic enlargements. This technique is considered to be much easier and more accurate than the one used in the previous investigations. However, the data reduction step, because of the time and labor involved, is considered to be the rate controlling process of the whole analysis.

UNCLASSIFIED

Security Classification

14. KEY WORDS	LINK A		LINK B		LINK C	
	ROLE	WT	ROLE	WT	ROLE	WT
fin-flat plate flow field						
wing-root flow field						
holography						
three-dimensional density field						
three-dimensional flow field						
fin						
flat plate						
interferogram						
flow field						
fin flat plate junction						
wing root junction						
holographic interferometry						
supersonic flow						

DD FORM 1 NOV 68 1473 (BACK)
S/N 0101-807-6821

UNCLASSIFIED

Security Classification

A-31409

Holographic Interferometry of The Flow
Field Between a Fin And Flat Plate

by

Robert Ward Heyer
Lieutenant, United States Navy
B.S.E.E., Duke University, 1964

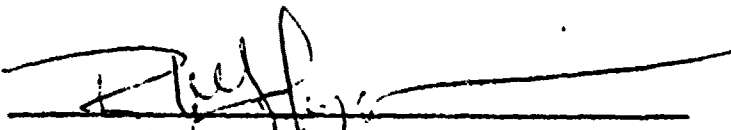
Submitted in partial fulfillment of the
requirements for the degree of

MASTER OF SCIENCE IN AERONAUTICAL ENGINEERING

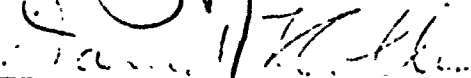
from the

NAVAL POSTGRADUATE SCHOOL
March 1972

Author

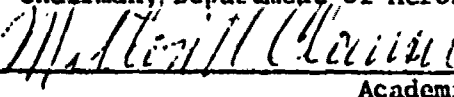


Approved by:



Thesis Advisor

Chairman, Department of Aeronautics



Academic Dean

ABSTRACT

This study was an attempt to map the density field in a fin-flat plate junction three-dimensionally using holographic interferometry. This investigation has extended the density studies by Matulka [12, 13] and Jagota [3, 4] to include, for the first time, interferometric fringe information obtained through a transparent model in supersonic flow. The fringe information was then inverted by a FORTRAN computer program to produce a plot of the density field around the model. The feasibility of the method was demonstrated.

The factors which are thought to have limited the success of the experiment include vibration of the model, fluctuations of the tunnel flow and the fact that the model was somewhat too large in relation to the size of the wind tunnel test section. Schlieren photography was used to look through and around the model and to verify that the same flow was established as was reported by Thomas [23, 24] and Winkelman [26, 27].

The data reduction of holographic interferograms was, for the first time, accomplished using photographic enlargements. This technique is considered to be much easier and more accurate than the one used in the previous investigations. However, the data reduction step, because of the time and labor involved, is considered to be the rate controlling process of the whole analysis.

TABLE OF CONTENTS

I.	INTRODUCTION -----	6
II.	EXPERIMENTAL APPARATUS -----	7
	A. THE WIND TUNNEL -----	7
	B. THE HOLOGRAPHIC ARRANGEMENT -----	7
	C. THE WIND TUNNEL MODELS -----	8
III.	ANALYTICAL EVALUATION OF THE DENSITY FIELD -----	9
	A. THE BASIC INTERFEROMETRIC EQUATION -----	9
	B. THE INTEGRAL INVERSION -----	11
	C. THE NUMERICAL PROCEDURE -----	14
IV.	EXPERIMENTAL PROCEDURE -----	15
	A. LABORATORY TECHNIQUES -----	15
	1. Model Considerations -----	15
	2. Holographic Techniques -----	16
	a. Direct Fin-Root Flow Method -----	18
	b. Total Model Flow Method -----	18
	3. Schlieren Analysis -----	19
	B. PHOTOGRAPHIC TECHNIQUES -----	19
	C. DATA REDUCTION -----	20
V.	EXPERIMENTAL RESULTS AND DISCUSSION -----	22
VI.	CONCLUSIONS AND RECOMMENDATIONS -----	35
	APPENDIX A: Reduction Of An Interferogram To Obtain Fringe Shift Data -----	98
	APPENDIX B: Calculation Of Tunnel Wall And Grid Plastic Refraction Correction -----	101

APPENDIX C: Application Of Computer Program "Holofer"	125
BIBLIOGRAPHY -----	175
INITIAL DISTRIBUTION LIST -----	177
FORM DD-1473 -----	178

ACKNOWLEDGEMENTS

This writer wishes to gratefully acknowledge Dr. D. J. Collins for his most valuable guidance and assistance during the course of this investigation; Dr. T. H. Gawain for his valuable assistance and recommendations in the writing of this report; the technical staff of the Department of Aeronautics under R. Besel and T. Dunton, particularly N. Lechenby, J. Multon, and G. Middleton, for their able assistance in the fabrication and assembly of the models and equipment used in this study; Mrs. John B. Coleman Jr. for her considerable effort in the final preparation; and my wife and family for their noble patience and encouragement.

I. INTRODUCTION

The determination of the flow field in the wing-body junction of an aircraft in supersonic flight presents many problems. The typical approach has been to measure the static pressure on the surface using many small pressure taps [23, 24] and to determine the velocity field in the junction using translatable pressure probes [18, 19, 25]. Thomas [20, 24] and Winkelmann [26, 27] used azobenzene and oil-smear tests to view the flow field around a flat plate-fin junction. From the streak patterns on the plate and fin, they were able to illustrate the three-dimensional flow field, although in a partially speculative fashion. This study has attempted to map the density field in a fin-flat plate junction three-dimensionally using holographic interferometry. Although this objective was not fully achieved, the feasibility of the method has been demonstrated.

By using a Q-switched laser with exposure times of about twenty nanoseconds, it was possible to obtain three-dimensional holographic interferograms of the density field in the fin-flat plate junction. From holograms taken at a number of viewing angles the fringe shifts in different planes could be obtained. By integrating this information using a FORTRAN computer program, the density field can be determined. This technique has been previously demonstrated for the flow field of a free jet by Matulka [12, 13] and for the supersonic flow field around a cone at angle of attack by Jagota [3, 4].

The tests were performed at the Naval Postgraduate School, using the four-inch supersonic wind tunnel.

II. EXPERIMENTAL APPARATUS

A. THE WIND TUNNEL

The investigation was conducted in the Naval Postgraduate School blowdown-to-atmosphere supersonic wind tunnel. The test section is four inches by four inches in cross section and six inches long with two different sets of side walls. The two-inch thick plexiglas side walls, which have a refraction index of 1.49, present a complete field of view of the flow from the nozzle throat to aft of the test section mounting bracket (Figure 1 (a)). The second set of sidewalls used are aluminum with high quality optical glass portholes located in the test section area (Figure 1 (b)). The interchangeable nozzle for a test section Mach number of 2.8 was used for all tests. The nominal run time is five minutes at Mach 2.8 with the maximum stagnation pressure of about 105 pounds per square inch.

B. THE HOLOGRAPHIC ARRANGEMENT

The holographic arrangement is illustrated in Figure 2 and shown in photographs included as Figures 3, 4, and 5. The equipment stand was rested on a portion of the building floor that was vibrationally isolated. A Konrad K-1 pulsed ruby laser with a Pockels cell Q-switching unit was used to produce monochromatic light - a wave length of 6943 Angstroms and exposure time of twenty nano-seconds. The laser cavity length was seventy-three cm. giving a coherence length of about ten cm. To maintain the laser head and output etalon at a constant temperature of 27.5 degrees centigrade, a Lauda constant temperature circulator Model N was used. This was controlled by an electronic relay type R-10 coupled with a Culligan de-ionizer.

Holograms were obtained by routing the reference beam under the wind tunnel and the scene beam through the test section, and intersecting the two beams on the hologram plate at an intersecting angle of approximately 50 degrees. The beam sizes were controlled by translating the concave lenses located between the beam splitter and hologram plate in each beam (Figure 2). The Q-switched laser and optics were aligned using a continuous wave helium-neon laser. For reference purposes, grids were mounted on the outside tunnel walls and aligned using a surveyor's transit. The holographic stand and test section were completely enclosed in a wooden box to enable holograms to be taken in the daylight (Figure 6).

C. THE WIND TUNNEL MODELS

The fin-flat plate models used are shown in Figures 7 (a), (b), (c), and (d). The metal portions of both models were stainless steel. The center section, part of one strake, and all of the other strake of the first model in Figure 7 (a) were made of epoxy while the center section of the second model, Figures 7 (b) and 7 (c), was fabricated from plexiglas. The flat plate grids in both models were etched into the plastic surface and coated with a clear plastic to achieve a smooth surface.

The models were rotated about their sting mounts as shown in Figure 7 (d). Alignment for the desired rotation angle was accomplished by aligning prescribed lines on the sting mount collar with a scribed mark on the sting stand using a surveyor's transit.

III. ANALYTICAL EVALUATION OF THE DENSITY FIELD

A. THE BASIC INTERFEROMETRIC EQUATION

Interferograms are created when two coherent light beams are superimposed on each other and projected on a viewing screen. The light and dark regions observed correspond to the relative phase difference between the two beams which are caused by a difference in the two optical path lengths. Consider a coherent beam which is split and then recombined on a viewing screen. A difference in optical path lengths of the two beams may be achieved in two ways in order to create an interferogram. The first is to make the physical distance traveled by the two beams different. In a vacuum this path length difference is expressed as $L = C_0 \Delta t$ where C_0 is the speed of light in a vacuum. The second way is to maintain equal physical path lengths but to have the beams traverse through different media prior to recombining. In this case each light beam will travel at a speed $\frac{C_0}{n}$ where n is the index of refraction for the medium traversed. The optical path length difference then becomes:

$$\Delta L = L (n_2 - n_1) = C_0 \Delta t \quad (1)$$

The interference pattern or fringes observed may be expressed as a function of the optical path length difference or

$$g = \frac{\Delta L}{\lambda} \quad (2)$$

where: g = fringe shift

λ = wave length of the light source

ΔL = change in optical path

Combining equations (1) and (2), the fringe shift is then

$$g = \frac{L}{\lambda} (n_2 - n_1) \quad (3)$$

The index of refraction is known to be a function of density. Since the speed of light is only slightly less in gases than in a vacuum, the index of refraction could be closely approximated by the series expansion [8]

$$n = 1 + \beta \frac{\rho}{\rho_s} \quad (4)$$

where

β = dimensionless constant related to the Gladstone-Dale constant by $K = \beta/\rho_s$

ρ_s = reference density of 0° C, 760 mm. Hg.

The variation of n with wavelength is small and has a value of 0.000292 for $\lambda = 5893$ angstroms.

Considering a fixed difference in the index of refraction between the two beams in Equation (3), then

$$g = \beta \frac{L}{\lambda} \left(\frac{\rho_a - \rho_\infty}{\rho_s} \right) \quad (5)$$

If the density varies in a beam path, the net change in the optical path length will be the integrated effect along the beam path or

$$g = \frac{\beta}{\lambda \rho_s} \int_0^L (\rho - \rho_\infty) ds = Q \int_0^L f(x, y, z_c) ds \quad (6)$$

where

$$Q = \frac{\beta \rho_\infty}{\lambda \rho_s} \quad (6a)$$

$$f(x, y, z_c) = \frac{\rho(x, y, z_c)}{\rho_\infty} - 1 \quad (6b)$$

z_c = a plane of constant Z

ds = incremental distance along the ray

In order to determine the density along the beam path where the fringe shift is known from an interferogram, Equation (6) must be inverted.

B. THE INTEGRAL INVERSION

The integral inversion technique was first reported by C. D. Maldonado et al in 1965 [9, 10, 11]. R.D. Matulka [12, 13] and R. C. Jagota [3, 4] used this method to determine the density variation in an asymmetric free jet and about a cone at angle of attack, respectively. The technique involves representing the function, $f(x, y, z)$ in Equation (6) by a complete set of orthogonal functions where the unknown coefficients are evaluated using the orthogonality relationship between the set of functions. The functions are orthogonal over the entire plane and also have the property of being invariant in form to any rotation of the coordinate system. Figure 8 illustrates the coordinate system for the inversion where x and y are the fixed laboratory coordinates and x' and y' are the coordinates in which the fringe number function is defined. As the view through the test section is varied the primed coordinates are rotated with respect to the fixed coordinates x and y .

The fringe shift expressed in Equation (6) may be written as the transform

$$g(\xi, y, z_c) = f(x, y, z_c) \quad (7)$$

or, inverting the equation, the density function, f , is equal to:

$$f(x, y, z_c) = \bar{T}^{-1} g(\xi, y, z_c) \quad (8)$$

The density function can be expanded in the following manner using a set of polynomial functions, $U_{m+2k}^{\pm m}(\alpha x, \alpha y)$, and unknown complex coefficients, $C_{m+2k}^{\pm m}(\alpha)$

$$f(x, y, z_c) = \sum_{m=0}^{\infty} \sum_{k=0}^{\infty} \epsilon_m [C_{m+2k}^m(\alpha) U_{m+2k}^m(\alpha x, \alpha y) + C_{m+2k}^{-m}(\alpha) U_{m+2k}^{-m}(\alpha x, \alpha y)] e^{-(\alpha^2 x^2 + \alpha^2 y^2)} \quad (9)$$

where

$$\epsilon_m = \begin{cases} \frac{1}{2} & m=0 \\ 1 & m=1, 2, 3, \dots \end{cases}$$

α = arbitrary scale factor

The polynomial functions, $U_{m+2k}^{\pm m}(\alpha x, \alpha y)$, are invariant in form to a rotation of the coordinate system [10, 12, 13]. They also have a Gauss transform which makes them adaptable to the physical situation and to manipulating into the form of Equation (7). The functions are defined as:

$$U_{m+2k}^{\pm m}(\alpha x, \alpha y) = (-1)^k \alpha \left[\frac{k! (\alpha^2 x^2 + \alpha^2 y^2)^m}{\pi (m+k)!} \right]^{\frac{1}{2}} e^{\pm i m \phi} L_k^m(\alpha^2 x^2 + \alpha^2 y^2) \quad (10)$$

where $\phi = \tan^{-1}\left(\frac{y}{x}\right) - \frac{\pi}{2}$ (10a)

L_k^m = Laguerre polynomial

$$= \sum_{s=0}^k \left[\frac{(m+k)!}{(k-s)!(m-s)! s!} \right] \left[(-1)(\alpha^2 x^2 + \alpha^2 y^2) \right]^s \quad (10b)$$

And the Gauss Transform of $U_{m+2k}^{\pm m}$ is:

$$I_{m+2k}^{\pm m}(\alpha y; \xi) = \int_{-\infty}^{\infty} U_{m+2k}^{\pm m}(\alpha x, \alpha y) e^{-\alpha^2 x'^2} dx' = \frac{e^{\pm im\xi}}{[k!(m+k)!]^{\frac{1}{2}} 2^{m+2k}} H_{m+2k}(\alpha y') \quad (11)$$

where

$H_{m+2k}(\alpha y')$ = Hermite polynomials

By applying the transform above to Equation (9), the fringe function in

Equation (7) can be written as:

$$g(\xi, y, z_c) = \sum_{m=0}^{\infty} \sum_{k=0}^{\infty} \frac{c_m [C_{m+2k}^m(\alpha) e^{im\xi} + C_{m+2k}^{-m}(\alpha) e^{-im\xi}] H_{m+2k}(\alpha) e^{-\alpha^2 y^2}}{[k!(m+k)! 2^{2(m+k)}]^{1/2}} \quad (12)$$

using the following orthogonality relationship on Equation (12)

$$\int_{-\pi}^{\pi} e^{\pm im\xi} e^{\mp im\xi} d\xi \int_{-\infty}^{\infty} H_{m+2k}(\alpha y') H_{n+2l}(\alpha y') e^{-\alpha^2 y'^2} dy' = \\ \frac{2\pi}{\alpha} [(m+2k)!(n+2l)! 2^{m+2k} 2^{n+2l} \delta_{mn} \delta_{(m+2k)(n+2l)}] \quad (13)$$

where δ is the kroneker delta, the expansion coefficients C_{m+2k}^m , can be determined by:

$$C_{m+2k}^m(\alpha) = \frac{\alpha}{2\pi} \left[\frac{(k!(m+k)!)^{1/2}}{(m+2k)!} \right] \int_{-\pi}^{\pi} g(y', \xi, z_c) H_{m+2k}(\alpha y') e^{\mp im\xi} dy' d\xi \quad (14)$$

Substitution of the coefficients in Equation (14) back into Equation (9) results in the density variation being expressed as:

$$f(x, y, z_c) = \left(\frac{\alpha}{\pi} \right)^2 \sum_{m=0}^{\infty} \sum_{k=0}^{\infty} c_m [k!(m+k)!]^{1/2} e^{-(\alpha^2 x^2 + \alpha^2 y^2)} \cdot \\ \text{REAL} \left[\int_{-\pi}^{\pi} \int_{-\infty}^{\infty} g(y', \xi, z_c) e^{-im\xi} H_{m+2k}(\alpha y') dy' d\xi \right] U_{m+2k}^m(\alpha x, \alpha y) \quad (15)$$

or by inserting Equation (10):

$$f(x, y, z_c) = \left(\frac{\alpha}{\pi} \right)^2 \sum_{m=0}^{\infty} \sum_{k=0}^{\infty} c_m \frac{(k!)^m k!}{(m+2k)!} (\alpha^2 x^2 + \alpha^2 y^2)^{m/2} L_k^m(\alpha^2 x^2 + \alpha^2 y^2) \cdot \\ [B_{m+2k}^m(\alpha) \cos(m\phi) + D_{m+2k}^m(\alpha) \sin(m\phi)] e^{-(\alpha^2 x^2 + \alpha^2 y^2)} \quad (16)$$

where:

$$B_{m+2k}^m(\alpha) = \int_{-\pi}^{\pi} \int_{-\infty}^{\infty} g(y', \xi, z_c) \cos(m\xi) H_{m+2k}(\alpha y') dy' d\xi \quad (17)$$

$$D_{m+2k}^m(\alpha) = \int_{-\pi}^{\pi} \int_{-\infty}^{\infty} g(y', \xi, z_c) \sin(m\xi) H_{m+2k}(\alpha y') dy' d\xi \quad (18)$$

Equations (16), (17), and (18) are the basic equations used to calculate the density distribution from the experimentally determined fringe variations.

C. THE NUMERICAL PROCEDURE

The form of the density distribution in Equations (16), (17), and (18) must be modified in order to input the experimentally determined fringe distribution. First from Figure 8 and Equation (6b) it can be seen that it is only necessary to integrate Equations (17) and (18) over an area where the density is changing from a known density, ρ_∞ . Outside of this region where there is no change in density, the function $f(x, y, z_0) = 0$, i.e. outside the test section. Also since the fringe distribution is taken in small increments over the test area the coefficients, B and D, can be approximated as

$$B_{m+2k}^m(\alpha) = \sum_{i=1}^{I-1} \sum_{j=0}^{J-1} g(\xi_j + \Delta\xi_j, x_i + \Delta x_i) \int_{\xi_j}^{\xi_{j+1}} \cos(m\xi) d\xi \int_{x_i}^{x_{i+1}} H_{m+2k}(\alpha x) dx \quad (19)$$

$$D_{m+2k}^m(\alpha) = \sum_{i=1}^{I-1} \sum_{j=0}^{J-1} g(\xi_j + \Delta\xi_j, x_i + \Delta x_i) \int_{\xi_j}^{\xi_{j+1}} \sin(m\xi) d\xi \int_{x_i}^{x_{i+1}} H_{m+2k}(\alpha x) dx \quad (20)$$

The integral of ξ is easily determined and by using the derivative formula for Hermite polynomials the integral of x may be manipulated to yield

$$B_{m+2k}^m(\alpha) = \left[\frac{1}{2\pi m(m+2k+1)} \right] \sum_{i=0}^{I-1} \sum_{j=0}^{J-1} g(\xi_j + \Delta\xi_j, x_i + \Delta x_i) \cdot \\ [\sin(m\xi_{j+1}) - \sin(m\xi_j)] [H_{m+2k+1}(\alpha x_{i+1}) - H_{m+2k+1}(\alpha x_i)] \quad (21)$$

$$D_{m+2k}^m(\alpha) = - \left[\frac{1}{2\pi m(m+2k+1)} \right] \sum_{i=0}^{I-1} \sum_{j=0}^{J-1} g(\xi_j + \Delta\xi_j, x_i + \Delta x_i) \cdot \\ [\cos(m\xi_{j+1}) - \cos(m\xi_j)] [H_{m+2k+1}(\alpha x_{i+1}) - H_{m+2k+1}(\alpha x_i)] \quad (22)$$

In the computation of the density function from Equation (16), obtaining the infinite summations experimentally is not plausible or

possible. It has been demonstrated that by using a finite number of terms and by adjusting the values of $\Delta \xi$, Δx and α , it is possible to obtain the density distribution with very good accuracy [3, 4, 12, 13]. Equation (16) then becomes:

$$f(x, y, z_0) = \left(\frac{\alpha}{\pi}\right)^2 \sum_{k=0}^K \sum_{m=0}^M \epsilon_m (-1)^k \left[\frac{k!}{(m+2k)!} \right] (\alpha^2 x^2 + \alpha^2 y^2) \cdot \quad (23)$$

$$L_k^m (\alpha^2 x^2 + \alpha^2 y^2) \left[B_{m+2k}^m (\alpha) \cos(m\phi) + D_{m+2k}^m (\alpha) \sin(m\phi) \right] \cdot \\ e^{-(\alpha^2 x^2 + \alpha^2 y^2)}$$

IV. EXPERIMENTAL PROCEDURE

A. LABORATORY TECHNIQUES

The analysis of a free jet by Matulka [12, 13] illustrated how holographic interferometry can be used to obtain a complete three dimensional plot of the density within a moving transparent flow field.

Jagota [3, 4] in his study of a cone at angle of attack in supersonic flow went one step further by introducing an opaque object into an assumed steady state flow field and describing the density field three-dimensionally.

This investigation has attempted to determine the three-dimensional density field around a transparent object in a supersonic flow field by passing a light beam through the object. Specifically the interest was to describe the flow field existing in the junction of a fin-root intersection.

1. Model Considerations

In order to obtain uniform flow around the fin-root area, a model of the form shown in Figure 9 was selected. The flat plate has a knife

edge and is intended to remain at zero degrees angle of attack so as to establish the flow conditions illustrated. The fin edges were made circular in order to approach flow conditions similar to those established in Winkelmann's [26, 27] investigation. Plastic and metal strakes were added on the model sides so as to maintain two-dimensional flow as well as to add strength to the flat plate. In the first model constructed (Figure 7(a)), maximum visibility of the plastic fin-flat plate center section was achieved by bolting the leading edge and aft plate together through the plastic center section. Due to model flexure, this design was found to be unsuitable and the second model in Figures 7(b) and 7(c) was constructed. The model was made from a single piece of stainless steel. The model rigidity was satisfactory but unfortunately the strengthening borders around the plastic center section reduced the holographic visibility somewhat.

Since the wind tunnel blocks were fixed, it was possible to make multiple test runs with the same flow conditions over the model provided supersonic flow had been established over the model.

2. Holographic Techniques

In order to obtain holographic interferograms it was necessary to ensure that the optical path lengths of the scene and reference beams remained approximately equal. Since the ruby laser is believed to have a coherence length of approximately ten centimeters, the equality of lengths is far less critical than in the classical Mach-Zehner interferometric approach. Consequently a string was used in the experiment to trace the reference beam and then adjust the scene beam. This method kept the two beam lengths within one centimeter of each other. Since the scene beam traversed approximately 4.5 inches of plastic tunnel walls and

grids which the reference beam did not, it was necessary to compensate by making the scene beam physically 2.25 inches shorter than the reference beam. The reference beam varied in length from 61 inches to 68 inches during the experimentation.

To determine the fringe/density field, finite fringe interferograms were made by three different techniques. In the direct fin-root flow approach the diffuser plate was part of the model. Either the mirror, M_5 , in Figure 2 or the hologram plate holder was translated between the no-flow exposure and the flow-established exposure. In the total model flow method the diffuser plate was located between scene beam lens, L_3 , and the test section (See Figure 2) and it was translated horizontally or vertically. Translations were varied from .001 inches to .006 inches with the translation distance of .003 inches yielding the best fringe separation.

Most of the holograms taken using basically the holographic arrangement shown in Figure 2 gave well-defined fringe patterns. In order to improve upon the fringe definition, a variety of techniques was attempted. The transverse mode selector was varied from 1.0 mm. to 2.5 mm. in increments of 0.5 mm. to determine the best lighting of the model. The hologram plate holder was rotated horizontally to various positions. These positions varied between being perpendicular to the scene beam to being perpendicular to the bisection of the angle between the scene and reference beams. Polarization plates were added in both the scene and reference beams between the test section and hologram plate in the scene beam and between the last mirror, M_4 , and the hologram plate in the reference beam. A one-quarter wave plate was also placed between the first lens, L_1 , and the beam splitter as recommended by Okayama and Emori [14].

The holograms were taken using 4" x 5" Agfa-Gavaert 8E-75 hologram plates. The developing process involved:

1. Five minutes in Kodak D-19 developer
2. Thirty seconds in an acetic acid stop bath
3. Five minutes in standard fixer
4. Five minutes in a flowing water bath
5. One minute emersion in Kodak Photo Flo wetting agent
6. Drying using blowing cool air
 - a. Direct Fin-Root Flow Method

Since the flow field in the fin-root junction is assumed to be identical on either side of the fin, then it is only necessary to determine the density on one side of the fin. To accomplish this it is necessary to obtain holograms for 180° of view as shown in Figure 10. The holograms for the views from 0° to 90° can be obtained by using a frosted fin and flat plate as shown in Figure 11. The advantage of having the frosted plate as part of the model is that the fringe/density information obtained by the interferogram is believed to be only for the area between the fin-root intersection to the tunnel wall vice the whole test section, but this was not verified. In order to obtain the fringe information for angles greater than 90° but less than 180° the fin would be exchanged for one containing a stainless steel reflective surface. The scene beam would then enter the test area from the viewing port below the tunnel and be reflected to the hologram plate as shown in Figure 12.

b. Total Model Flow Method

In this method the diffuser plate was located in the scene beam outside the test section as shown in Figure 14 and the flat plate

center section and fin were made of optically clear plexiglas. By translating the diffuser plate between exposures of the hologram, an interferogram of the whole density field in the test section about the model was obtained. From Figure 13 it can be seen that due to symmetry only 90° of view was required to obtain the density field. This makes it much easier experimentally to take the holograms than the previous method described.

3. Schlieren Analysis

A standard Schlieren knife-edge system was used to verify the establishment of the supersonic flow network around the model as shown in Figure 9. Photographs were also taken of the flow with the model at 0° and 90° rotation in order to compare the fin shock conditions with those obtained by Winkelmann [26, 27].

B. PHOTOGRAPHIC TECHNIQUES

By illuminating the holograms with a helium-neon laser beam which has a wave length of 6328 Angstroms, the original scene was reconstructed. Since the original scene beam and the reconstructed beam were of different wave lengths, there is actually a small distortion in the reconstructed scene but of neglectable effect because the hologram plate emulsion in the development process also shrinks.

The typical method for reconstructing the scene is to illuminate the hologram as illustrated in Figure 15. The diffuse glass used in the construction of the hologram appears to act as an infinite light source of non-parallel rays which illuminates the scene. If a small aperture is positioned at the focal plane of the imaging lense, an almost parallel set of rays may then be selected as shown in Figure 16. A third method

illustrated in Figure 17 uses a small diameter conjugate beam to illuminate the hologram. A large depth of field is achieved because the narrow beam acts as an aperture. This effect was of considerable advantage since it enabled both the front and rear grids, the model, and the fringe patterns to be simultaneously projected on the screen. The best photographs were obtained by focusing on the plane of the fringes.

C. DATA REDUCTION

Photographic interferograms were obtained by illuminating the hologram scene with a thin laser beam and using a camera with a viewing screen located in the film plane as shown in Figure 15. The line of sight in the plane desired was achieved by translating the hologram until common points on the front and rear grids were aligned. The camera, with the aperture set wide open at 7.7, was then adjusted to give the best focus on the fringe plane. The best photographic results were achieved by using an exposure time of 1/10 second with Polaroid Type 55 P/N film.

It was felt that the density field could be well defined three-dimensionally along the fin if the density fields were determined in four planes perpendicular to the Z-axis and equally spaced along the fin as shown in Figure 18. In obtaining the fringe data across a constant Z-plane it would be necessary to take six photographs per rotation angle, aligned at appropriate intervals down the y' axis, and then graphically mate the fringe data to form one complete set. The six photos across the field were felt necessary because the optical path length from the model to the hologram plate varied for those points not on the aligned plane.

The fringe shift reduction was accomplished using two different techniques. The first was to project the negative, using a photo enlarger,

onto a sheet of paper and trace over the fringe pattern, model surfaces and grid lines. The light fringes were traced out since it was much easier to judge their center line. From the fringe lines forward of the fin in the region of uniform flow one fringe line which appeared the straightest and compatible with most others was selected as the bench mark. A straight line was then drawn over that fringe and extended past the aligned Z plane (i.e. y' axis). Lines parallel to the bench mark line were then drawn likewise over the remaining fringe lines. The fringe displacements were then read relative to the lines drawn at the points of intersection of the fringes with the y' axis. The radius of the inversion circle was selected so that the fin-root intersection was the origin and the fin tip was the 100 percent point.

In the second technique an enlarged positive photograph was made from the negative. Again one fringe line in the uniform flow region just forward of the fin which appeared to be parallel with the majority of the fringes was selected as the bench mark. The remaining fringes were likewise traced over with lines parallel to the first. The fringe displacements were then measured relative to the lines drawn. For further details see Appendix A.

The locations at which reference lines crossed the y' axis in both techniques above were further adjusted to account for the tunnel wall refraction displacement as shown in Figure 19 and computed by a computer program in Appendix B. Once these corrections were made, the radial variation of the fringe number could then be plotted for the various y' alignment planes and a smooth curve drawn through the data points. The fringe number at 201 equidistant points across the field can then be obtained for input into the computer program, HOLOFER, in MODE 3. For

further details on how to use the computer program, HOLOFER, see Appendix C. Once the data from all the rotation angles of the model have been put into the computer program, the program will then calculate the density field across the inversion circle for that Z-plane. After the density has been calculated for all four Z-planes in Figure 18, a three-dimensional plot of the density field can be made by connecting points of equal density across the fin.

V. EXPERIMENTAL RESULTS AND DISCUSSION

The initial attempts to establish uniform flow over the flat plate shown in Figure 7(a) were unsuccessful due to model vibration and flexure. Movement of the model sting within its holder and flexure of the model plastic center section allowed the model leading edge to establish a little over 1° angle of attack upward when flow was established. Due to various modifications made in attempts to eliminate the vibration, the sting finally fractured.

In an attempt to eliminate these problems, the second model shown in Figures 7(b) and 7(c) was made of a single piece of stainless steel and the sting was mated to its holder to within .001 inches. The model center section was made of poured epoxy and the strakes were both made of stainless steel with plexiglas inserts. The model rotation about the sting was reduced to approximately 0.3° angle of attack upward. Due to the vibration in passing through the transonic range and a weak glue seal between the metal strakes and plexiglas inserts, the inserts were found to break loose. They were subsequently removed and not replaced.

In order to determine the flow field using the direct fin-root approach, the epoxy fin and model center section were frosted on one side using fine

emery paper (see Figure 20). Holograms were taken of the model at rotation angles of 0° , 12° , 45° and 90° using the holographic arrangement in Figure 2 excluding the diffuser plate between lens, L_3 , and the test section. The mirror, M_5 , was translated in various directions from towards to parallel to the test section between the exposures without flow and with flow established. Fringe patterns were obtained around the model, but only at 0° and 12° rotation could any fringe patterns be observed across the fin. It was found that the fin fringe pattern appeared to remain almost unchanged no matter how or how much the mirror, M_5 , was translated while the fringe around the model changed appropriately. For instance, in Figure 21 the mirror was not translated and in Figure 22 the mirror was translated .006 inches horizontally parallel to the tunnel.

Since fringes could not be observed across the flat plate at 45° and 90° , it was felt that the epoxy center section might be too imperfect optically. Consequently double-exposed holograms were taken with no flow through the test section and various translation distances from 0 to .005 inches. The fringe patterns were excellent across the whole model and their spacing decreased according to the increase in the translation of M_5 . Next the diffuser plate in the scene beam in Figure 2 was inserted with the model at 0° rotation angle and translated between no flow and flow exposures of the hologram. The fringes about the model were of excellent quality but the double diffusion of the scene beam through the model caused all fringe patterns on the model (fin) to disappear.

It was felt at this point that the fringe pattern obtained across the fin was caused by the movement of the model to an angle of attack and possibly by model vibration, although none was observed visually. The

lack of any fringes across the flat plate center section is not well understood but is believed to be caused by vibration of the model.

Since it was not possible to obtain acceptable interferograms with the diffuser plate as part of the model due to model motion, it was felt that the effect of minor model movements could be eliminated by using an optically clear model and an external translating diffuser plate. Therefore the fin and model center sections were replaced with optically clear plexiglas. With these changes it was found that the flat-plate leading-edge angle of attack had been reduced to approximately 0.1° .

Initially double-exposure holograms were taken using the arrangement in Figure 2 and translating the diffuser horizontally. At 0° model rotation the holographic interferograms were excellent. But as observed in Figure 23 it would be extremely difficult to determine the fringe change across the fin since no free stream reference fringes were available, due to the flat plate leading edge Prandtl-Meyer expansion and fin shock intersecting the tunnel top just above the fin. With a larger tunnel or smaller model this would be an excellent technique.

The diffuser plate was then translated vertically between exposures and excellent horizontal fringe patterns were obtained as shown in Figure 24. The model was then rotated to $22\frac{1}{2}^\circ$ and the same holographic technique was used. Excellent fringe patterns were obtained above and below the flat plate center section. Fringe patterns across the flat plate center section and fin in this area were very light and usable interferograms could not be photographed with the polaroid camera. In an attempt to improve on the fringe quality, polarizer plates were inserted in the reference beam between the mirror, M_4 , and the hologram plate and in the scene beam between the lens, L_3 , and the diffuser plate in order to ensure

polarization of both beams. No significant improvement could be noticed and they were subsequently removed. A one-quarter wave polarizer plate was then placed between the lens, L_1 , and the beam splitter in order to utilize circularly polarized light for the reference and scene beams. Okayama and Emori [14] found that their image resolution improved considerably; however, with this particular arrangement little to no improvement in the fringe resolution was observed and the approach was abandoned.

The transverse mode selector was then varied from 2.0 mm. to 1.5 mm. and later to 1.0 mm. in an effort to improve the coherency length of the laser light and consequently the image resolution. Due to the decrease in output light intensity, up to six exposures were taken during a run with flow established. Image and fringe definition were not found to increase possibly due to model vibration which was not visible to the eye.

The model was rotated to 45° and $67\frac{1}{2}^\circ$ and double exposure holograms were taken with a 2.5 mm. transverse mode selector. There were no observable fringe patterns in any portion of the test section. Consequently it was believed that supersonic flow was not established due to tunnel blockage caused by the shock wave from the model and by slight model vibrations in passing through the transonic range. In the transition to supersonic flow, the model leading edge would sometimes flex as much as 0.2° depending upon the transition time.

The test section walls were changed from the total plexiglas side walls shown in Figure 1(a) to the aluminum walls with the optical quality glass port holes (Figure 1(b)). The better quality glass would hopefully improve the viewing and the port holes made the model much more accessible. The metal strakes were also removed from the model since they appeared to have a minimal effect on the flow, were an interference optically,

THIS
PAGE
IS
MISSING
IN
ORIGINAL
DOCUMENT

flow was established. The plate leading edge shock and fin shock appeared quite fuzzy and light. Due to oil from the tunnel supply reservoir mixing in the flow, a light oil smear pattern can be observed across the fin in Figure 26. During one run, which could not be duplicated, the model pitched up as flow was established but did not vibrate. The plate shock and Prandtl-Meyer waves, fin shock system, and tunnel Mach lines became very distinct and well defined as seen in Figure 27. The schematic of the Schlieren photographs in Figure 28 points out the cause for the various flow lines observed. The non-uniformity of the free stream caused by tunnel leakage can be easily seen. Consequently the experimental work was discontinued due to tunnel conditions and time considerations.

It was felt at this point that if the holographic interferogram taken of the clear plexiglas fin at 0° rotation angle could be reduced to useful data for the computer program then the holographic method would be to a certain extent verified even though the actual density field could not yet be determined.

In obtaining interferograms from the hologram, the reconstruction technique shown in Figure 15 was used. The plane of constant z across the model to be reduced was chosen to be the forward most vertical grid line crossing the fin. It should be pointed out that in order to simplify the hologram alignment process, all four reduction planes across the model should have been scribed on the exterior grids. The three photographic points across the Z plane on the y' axis were, for convenience, chosen to be where horizontal exterior grid lines crossed the y' axis on the fin. Five interferogram photographs were taken at points A, B, and C as shown in Figure 29. Photographs 2 and 5 were taken using a Kodak Wratten Gelatin Filter N.D. 2.0 placed in the reconstruction beam in order to reduce the

beam intensity and increase the fringe definition. These two photographs were also used to provide a check on the consistency of the reduction process.

All five negatives were blown up on the photo enlarger in the dark room and the plate, fin, grid lines and fringes were traced out on a sheet of white paper as shown in Figures 30-34. It was very difficult to trace the fringes in the region of the fin tip and fin root due to the photographic resolution and the fin tip shadow. Also fringes were not visible in the region of the fin leading edge shock. Consequently, connecting the fringe in front of the fin to the correct fringe on the fin was a best guess effort. Typical of the problem was that fringe lines in two of the drawings were initially improperly connected across the fin leading edge shock. After being checked against the photograph negatives, the fringes were reconnected and the data taken correlated well with the data from other drawings. The fringes in the fin root area were extremely light in some photographs which made it quite difficult to determine their centerline crossing the y' axis.. Another point of difficulty was determining the location of the top and bottom of the fin. An error in drawing here will have an effect later when the fringe locations are normalized with respect to the fin height.

Enlarged positives were then made from the negatives as shown in Figures 35-39 to see if the data accuracy could be improved by eliminating the difficulties of tracing the fringes in the dark room. This method also made it possible usually to reassess the assumed path of the fringe lines at a later time if the data did no appear to correlate properly. The same problems of locating the fringe lines in the region of the fin tip and of connecting the fringe lines across the fin shock are readily apparent in the figures.

To obtain the fringe change across the fin one of the straightest fringes in the free stream region which paralleled the majority of other free stream fringes was selected. A straight line was drawn through its centerline and extended to cross the y' axis. The other free stream reference lines were then drawn parallel to the first and adjusted so as to best follow the centerline of the selected fringe. This method actually averages the free stream conditions and is only valid if the free stream is essentially uniform. Since it was not possible to obtain in the photographs the free stream fringe pattern forward of the leading edge Prandtl-Meyer expansion for the lower fin region, the fringe reference lines in photo enlargements were drawn over the fringes just prior to the fin shock. In order to adjust them to free stream conditions their location was moved downward a distance $\Delta y'$ equal to 1.1 times the average fringe interval for that photograph. The figure 1.1 was observed in all the enlarged photographs to be the approximate fringe change across the Prandtl-Meyer expansion. In the drawings (Figures 30-34), fringe reference lines for the lower fringes (generally $y' < .8$) were initially aligned along the straightest portion of the fringe prior to intercepting the fin shock. By comparing the reference line location on the drawing with the fringe pattern in the photographic enlargements the reference line location and fringe change were adjusted by an appropriate portion or all of the 1.1 fringe change caused by the Prandtl-Meyer expansion. All of the reference lines were then corrected for the tunnel wall and grid plastic parallax shown in Figure 19 and computed in Appendix B. The reference fringe locations were then normalized with respect to the wing height and the fringe numbers calculated by dividing the fringe change by the average fringe interval. For further details and calculations see Appendix A.

The data obtained for alignment points A and C by the two different reduction processes are plotted in Figures 40-43. The data obtained from the photo enlargements aligned at point C and shown in Figure 43 gave the best data agreement between two photographs. The worst data agreement was obtained from the reduction of the drawings aligned at the same point. The inconsistency in the data was probably caused by connecting the wrong fringe lines across the fin leading edge shock. The data fluctuations and discrepancies between the curves in the figures could have been caused by a number of things. It could have been caused, for instance, by not drawing the fringe reference line parallel to or exactly on the free stream fringe center line or slightly missing the fringe center as it crosses the y' axis or by misconnecting fringe lines across the fin shock as was illustrated in Figure 42. Fringe location errors could be caused by misdrawing the fin tip and root lines as was mentioned earlier. Another contributor would be measurement errors.

To analyze these sources for error, first consider that the typical fin size in the drawings and photo enlargements averaged about 2.5 inches high and 2.75 inches wide and that the fringe spacing averaged about 0.10 inches. All measurements were taken using a ruler graduated in 0.01 inches and readings were made to the nearest .005 inches. Since the average difference between the data points and curves ran around $\frac{1}{2}$ fringe, some figures were calculated to determine what measurement errors could produce this fringe error. It was found that an error of .025 inches in alignment of the fringe reference line with the free stream fringe center line and/or fringe center line crossing the y' axis could produce $\frac{1}{2}$ fringe error. This fringe error will also occur if the fringe reference line differs from the free stream center line by more than 1.4° when drawn 1 inch from the y' axis or by more than 0.36° when drawn 4 inches from the

y' axis. A difference of .01 inches in the average fringe interval could also produce a $\frac{1}{4}$ -fringe error; however, this is not too likely since it is an average of fifteen to twenty-five intervals. By comparing the actual height-to-width ratio with those found in all the drawings and photo enlargements it was found that average error was around 2% or a distance of .02 on the y'-axis.

In order to compare the interferogram negative quality and the two different reduction techniques, a plot of the data for each negative was made as shown in Figures 44-48. Photographs 1 and 3 in Figures 44 and 46 gave the smoothest curves indicating the highest interferogram resolution. Photograph 5 (Figure 48) gave the worst dispersion indicating poor interferogram resolution; yet looking at the enlargement in Figure 39, the fringe line contrast is very good. In comparing Figures 40-48 it appears that the reduction technique using the photographic enlargements gave the most consistent data. This technique also provides a much easier and faster recheck on the proper tracing of fringe lines because it is extremely difficult and tedious to duplicate the fringe pattern to the same scale over the drawings using the photo-enlarger in the dark room.

All the data obtained by either method for one alignment point were then plotted in Figures 49 and 50 in order to observe the dispersion. A fringe number dispersion of about 0.6 fringes was observed in the data taken from the negatives aligned at point A and a dispersion of about 0.8 fringes for the data about point C. The dispersion is attributable to the inaccuracies in the drawings, to the photographic quality of the interferograms, and to the inaccuracies in correcting the lower fringe reference lines to free stream conditions. The last point is based upon the increased dispersion between the fin tip and fin root data.

Figures 51 and 52 show an integrated curve of the fringe change across the wing as determined by each reduction method. In constructing the curve, the data from the three aligned points was plotted so as to just overlap each other. These two curves were then compared in Figure 53. The maximum variation in the fringe number is about $\frac{1}{2}$ a fringe but the variations in the location of the fringe maximums and minimums average about 0.1 inches on the fin. The location difference is probably due to improper drawing of the fringe reference lines compounded with not being able to measure the wing height accurately. Due to the inaccuracies introduced in tracing the negative and then reducing the data it is felt that the photo enlargement method is the more accurate reduction method.

With fringe data from only one field of view, the density field, obviously, could not be obtained. It was felt useful to consider the flow field axisymmetric in order to exercise the computer program and to provide a check on the program's ability to handle these particular curve shapes. Fringe data at 101 equidistant points across the fin from $0 \leq Y' \leq 1.0$ was obtained from Figure 53 for both curves and fed in HOLOFER in Mode 3 for the axisymmetric case. For further details on HOLOFER see Appendix C. The scale factor, α , in Equation 9 was then varied from 0.2 to 2.5 and a value to 1.0 was determined to yield the most accurate density solutions. This value was verified by feeding the function data, ($\rho/\rho_\infty - 1$), calculated by Mode 3 back into the program in Mode 1 and comparing the fringe data calculated with the original fringe data obtained from Figure 53.

The density distribution for both the drawing and photographic reduction cases is plotted in Figure 54. The density as Y' approaches zero actually goes as the drawn lines even though the points indicate a dip.

Matulka [12, 13] pointed out that the computer program accuracy does not converge at the origin. The large variations of the density curves at values of $Y' > 0.8$ are caused by the program trying to adapt to a step or shock wave type function at $Y' = 1.0$. If the remainder of the fringe data in Figure 53 for values of $Y' > 1.0$ had been included as input data the density curves would have smoothed out. This shock wave step function effect was demonstrated and analyzed by Matulka [12, 13].

The low values of density for the photographic data curve around $Y' = 0.38$ were unexpected but not surprising. First, the photographic fringe data curve is more extreme than the drawing fringe data curve and second, the density curves are not true values anyway since the field was considered axisymmetric and this is not the case in reality.

In general the density curves are felt to be reasonable under the assumed conditions. Consequently it is believed that the computer program could very easily and accurately handle a complete analysis of the flow field around the fin-flat plate.

In completing the analysis there are some data reduction problems which would have been encountered in reducing the interferograms at other model rotation angles which merit discussion. With no model rotation, adjusting the fringe reference lines close to the fin root to account for the leading edge Prandtl-Meyer expansion was relatively easy. However, when the model is rotated, the fringe shift across the Prandtl-Meyer expansion can no longer be considered a constant and it will be very difficult to adjust the fringe lines at lower values of Y' to free stream conditions. The best solution would be to increase the scene beam diameter and/or reduce the model size in order to photograph the free stream fringe lines forward of the plate leading edge. The free

stream lines could be connected to the appropriate fringe lines forward of the fin and this would eliminate the numerical correction and increase the fringe data accuracy.

Also at the rotated angles, fringe information will not be available for portions of the reduction plane due to shadows cast by the model sides as shown in Figure 55. In the lower portion of the hologram the fringe curve can be connected with a smooth line because the density field in that portion should be essentially constant. Care must be taken in completing the curve, though, since this information will be used in the integration of other rotation angles. The fringe curve in the upper portion must also be completed carefully but should be easier since the shadow will be smaller. For this particular model it was calculated that for angles greater than 46.6° the upper shadow would not penetrate the fin.

There are two more problems to be coped with which do not have apparent solutions at this time. The first has to do with the superimposing of fringe information from different locations onto one scene beam line as illustrated in Figure 56. In case I the superimposing of the fringe change in Region A onto that in Region C and locating the fringe reference line at point C' is tolerable because the density field in Region A should be fairly constant and uniform. However in case II where the fringe change in all three regions are superimposed and located at point C'', the answer is not readily apparent. If the plate and fin were of equal thicknesses then points A'' and C'' would be the same and the error would be somewhat reduced. If, in addition, the thicknesses were made as thin as structurally possible, the error would be reduced to a minimum. Also it might be possible to integrate the model geometry into the computer program but this has not been attempted.

With the model at rotation angles between 0° and 90° scene beam defraction at the fin root and tip areas would also present problems as seen in Figure 57. A minimization of the problem could again be achieved by minimizing the fin and plate thicknesses.

VI. CONCLUSIONS AND RECOMMENDATIONS

The investigation, although not totally successful, has demonstrated the feasibility of using holographic interferometry to determine the flow field around a transparent model by looking through the model. The problems of model vibration and movement, of superimposing different fringe information on one beam, and of scene beam divergence through the fin root and tip regions must still be solved. The model vibrations and rotation to an angle of attack are attributable to the tunnel pressure fluctuations caused by tunnel leaks and to possible movement of the sting holder. It is felt that all three problems could be decreased to negligible effects by reducing the overall model size and by incorporating the model geometry into the computer program.

The basic holographic arrangement was found to work quite well for this type of experiment. The holograms were generally high quality except when unfavorable tunnel flow conditions existed. The use of circularly polarized light recommended by Okayama and Emori [14] did not increase the hologram resolution appreciably but the method merits further considerations because of their excellent results.

The data reduction process was found to be the rate-controlling step in the investigation due to the time and labor involved. Reducing the data from enlarged photographs of the interferogram saved some time and appeared to increase the data accuracy. The data scatter of $\pm 1/8$ fringe

was considered acceptable considering the fringe resolution in the holograms. It was felt that this could be reduced by using either a larger tunnel or a smaller model. With either of the changes it would be possible either to use the free stream fringe pattern forward of the model as the reference conditions across the whole model or to use a vertical fringe pattern, since the leading edge Prandtl-Meyer expansion and fin shock would not block out the free stream fringes above the fin. It appears that the use of vertical fringes would also considerably reduce the data reduction time.

With the use of Schlieren the flow network described by both Thomas [23, 24] and Winkelmann [26, 27] was verified to exist. From the top view (90° model rotation) the fin shock and its fluctuations were observed and photographed through the flat plate plastic center section.

The computer program, HOLOFER, was found to be quite capable of handling the type of flow field fringe data which would be generated in a complete analysis of this type. As pointed out before it is believed that the program should be modified to incorporate the model geometry.

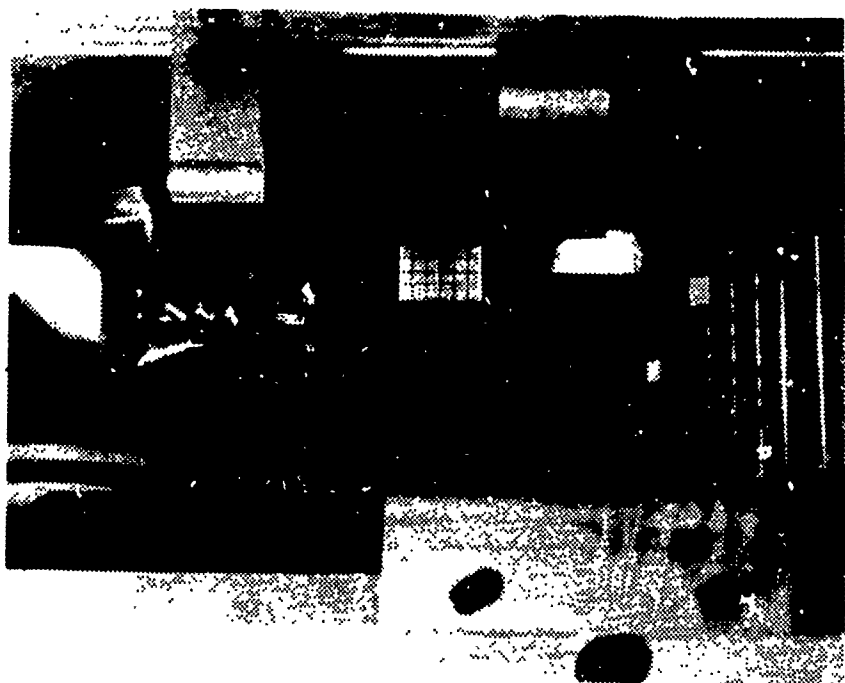
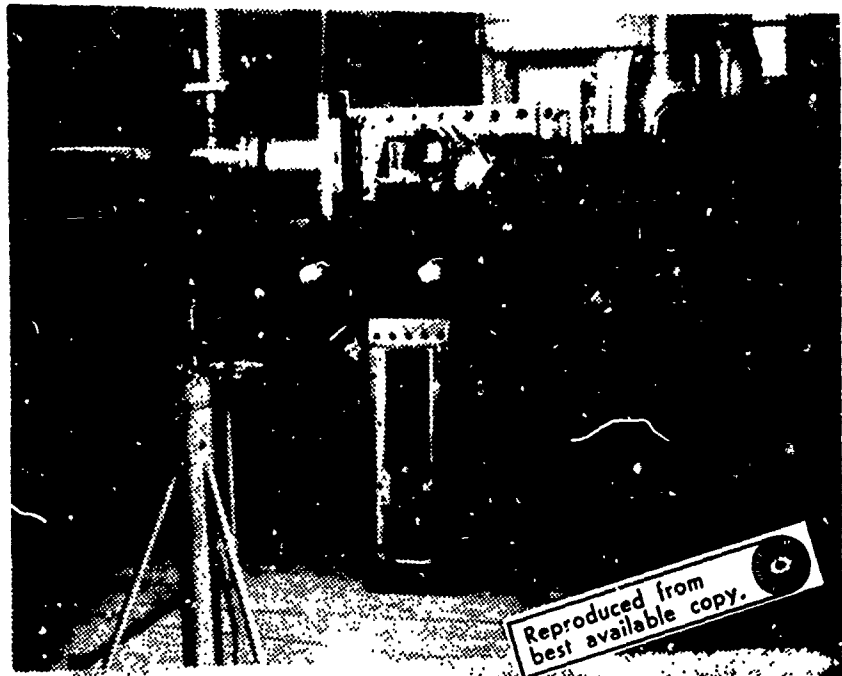


Figure 1(a). Wind Tunnel Test Section with Clear Plastic Side Walls



Reproduced from
best available copy.

Figure 1(b). Wind Tunnel Test Section with Aluminum Side Walls

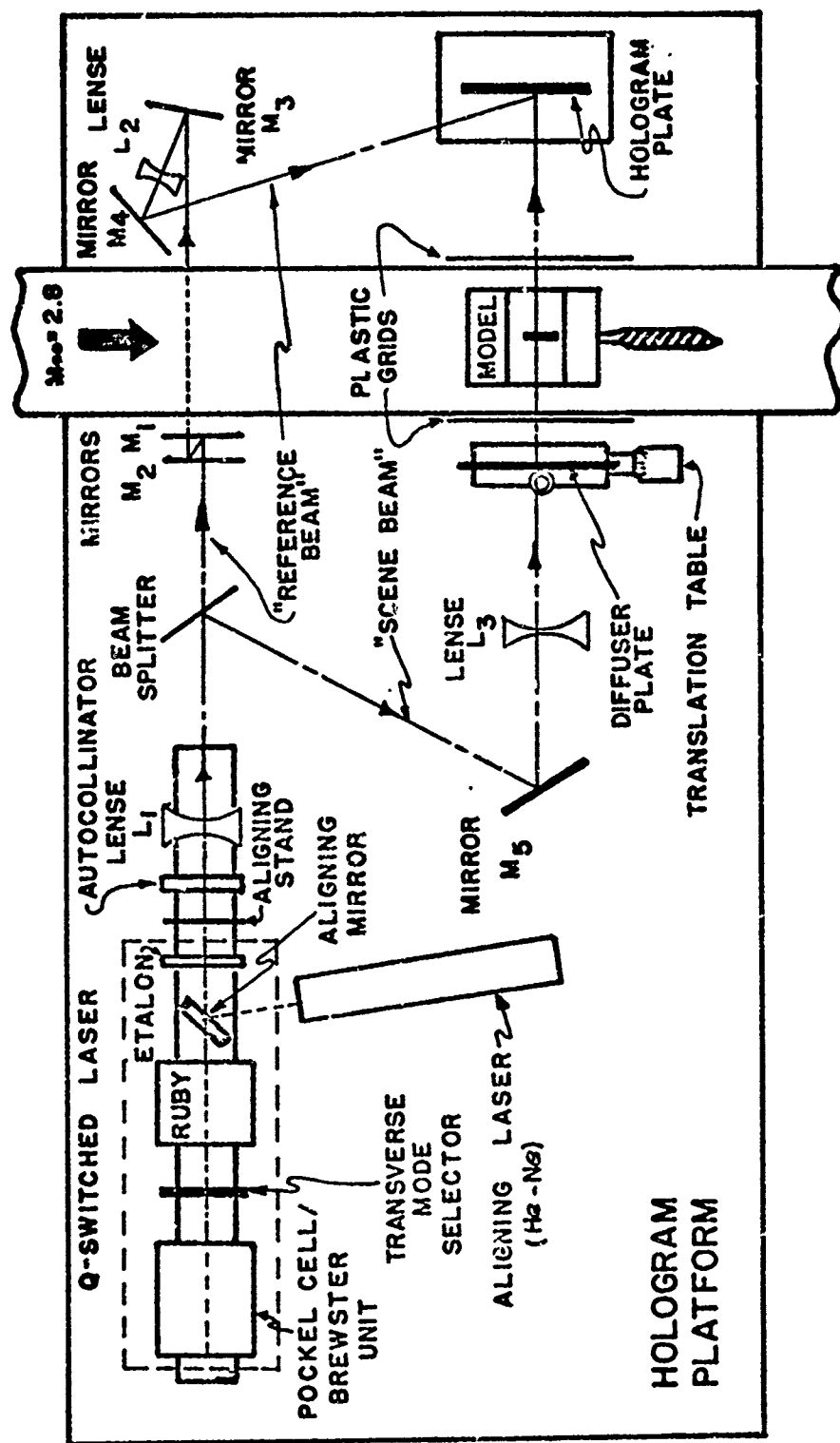


Figure 2. Schematic Representation of the Holographic Arrangement

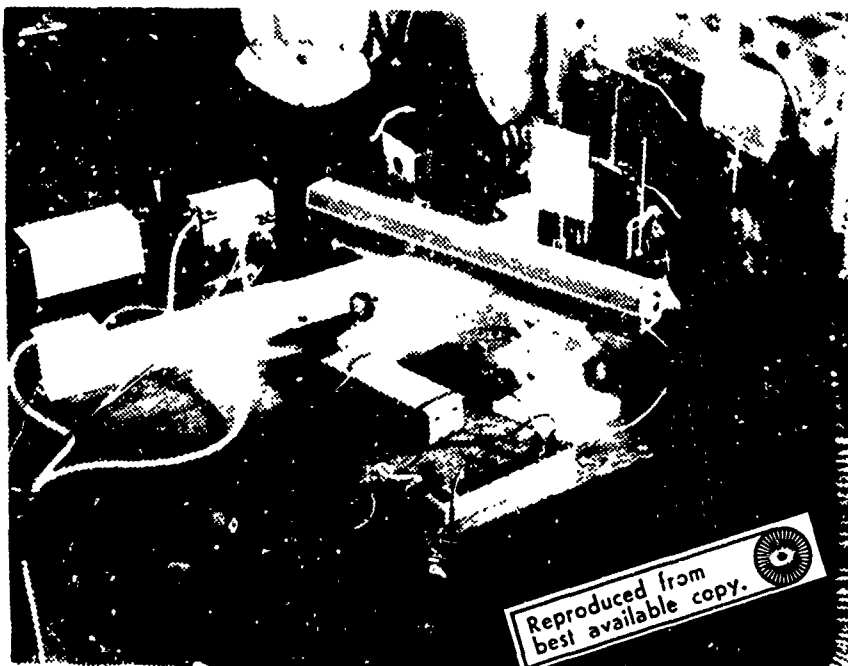


Figure 3. Holographic Arrangement Including the Laser Cooling and Aligning Equipment

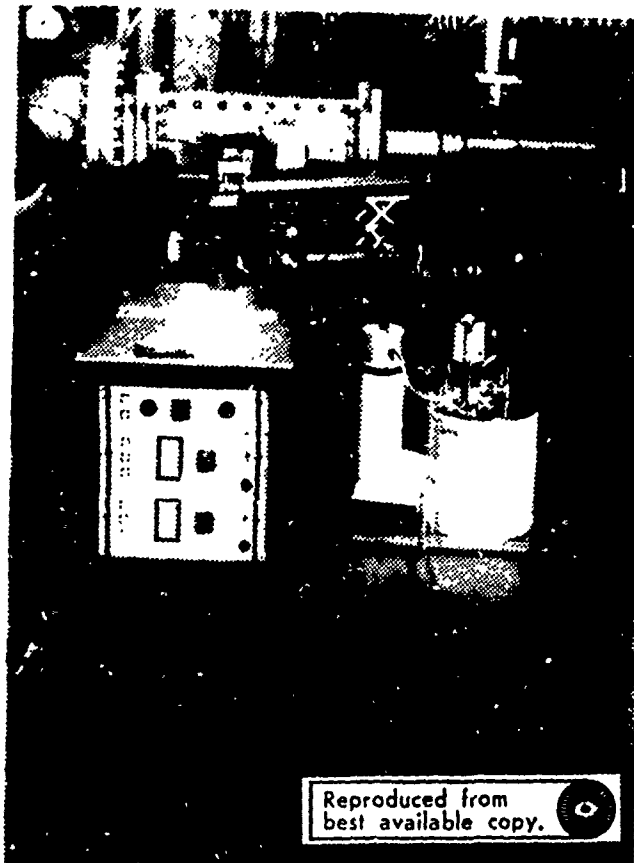
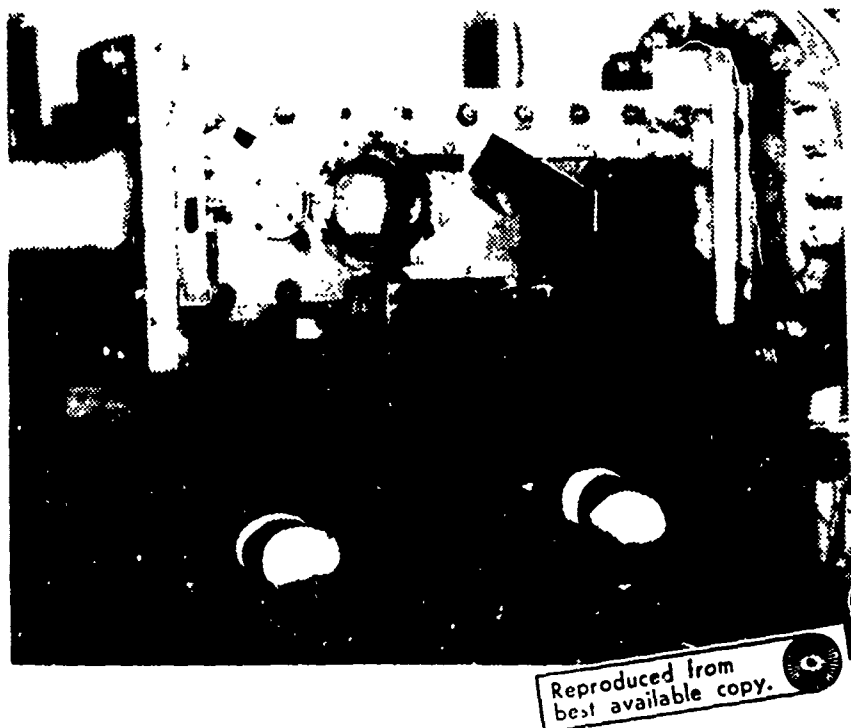


Figure 4. Ruby Laser Power Supply and Cooling Unit

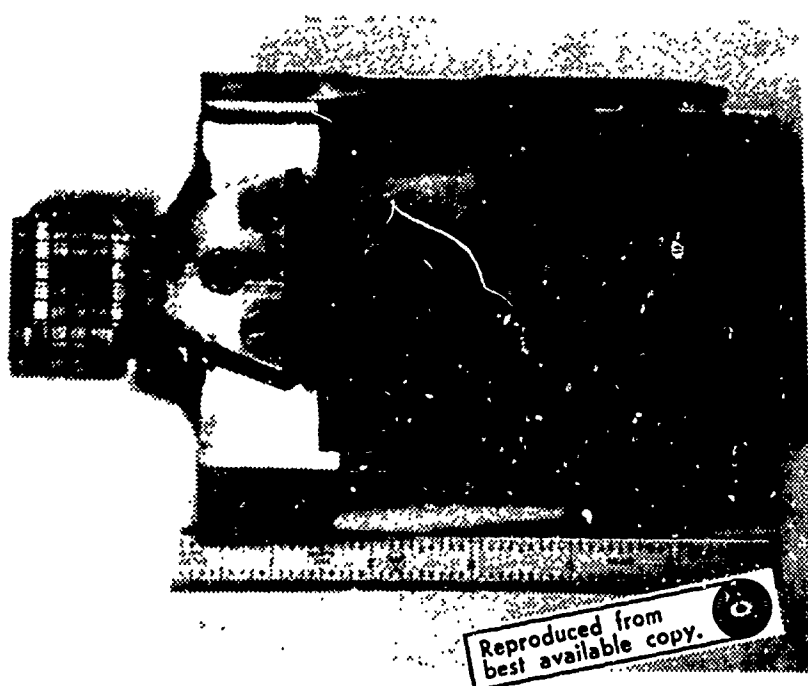


Reproduced from
best available copy.

Figure 5. Hologram Plate Holder and Mirrors on the Reverse Side
of the Wind Tunnel



Figure 6. Hologram Platform Box Cover for Daylight Photography



Reproduced from
best available copy.

Figure 7(a). Initial Fin-Flat Plate Model Used in the Experiment

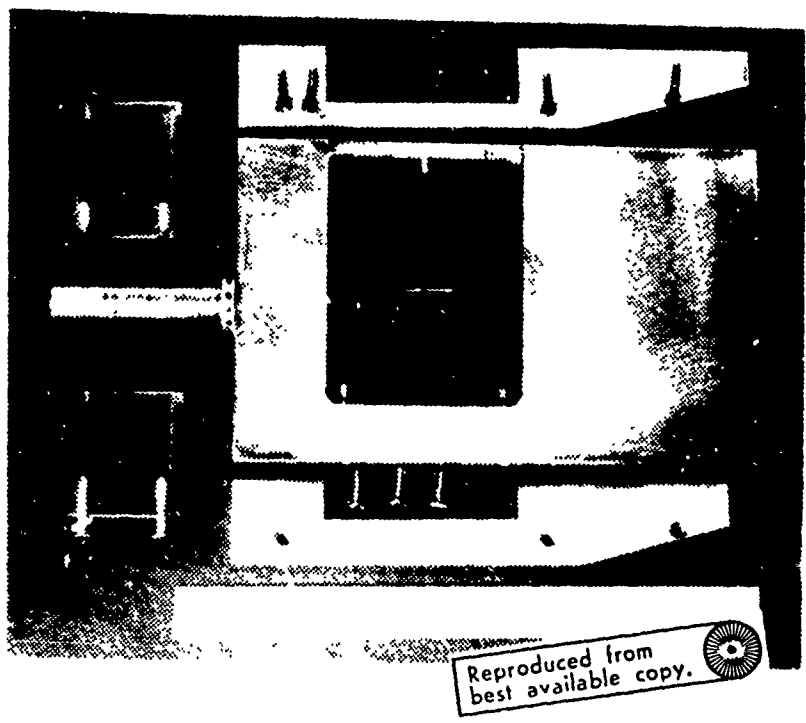


Figure 1(b). Second Fin-Flat Plate Model Used in the Experiment

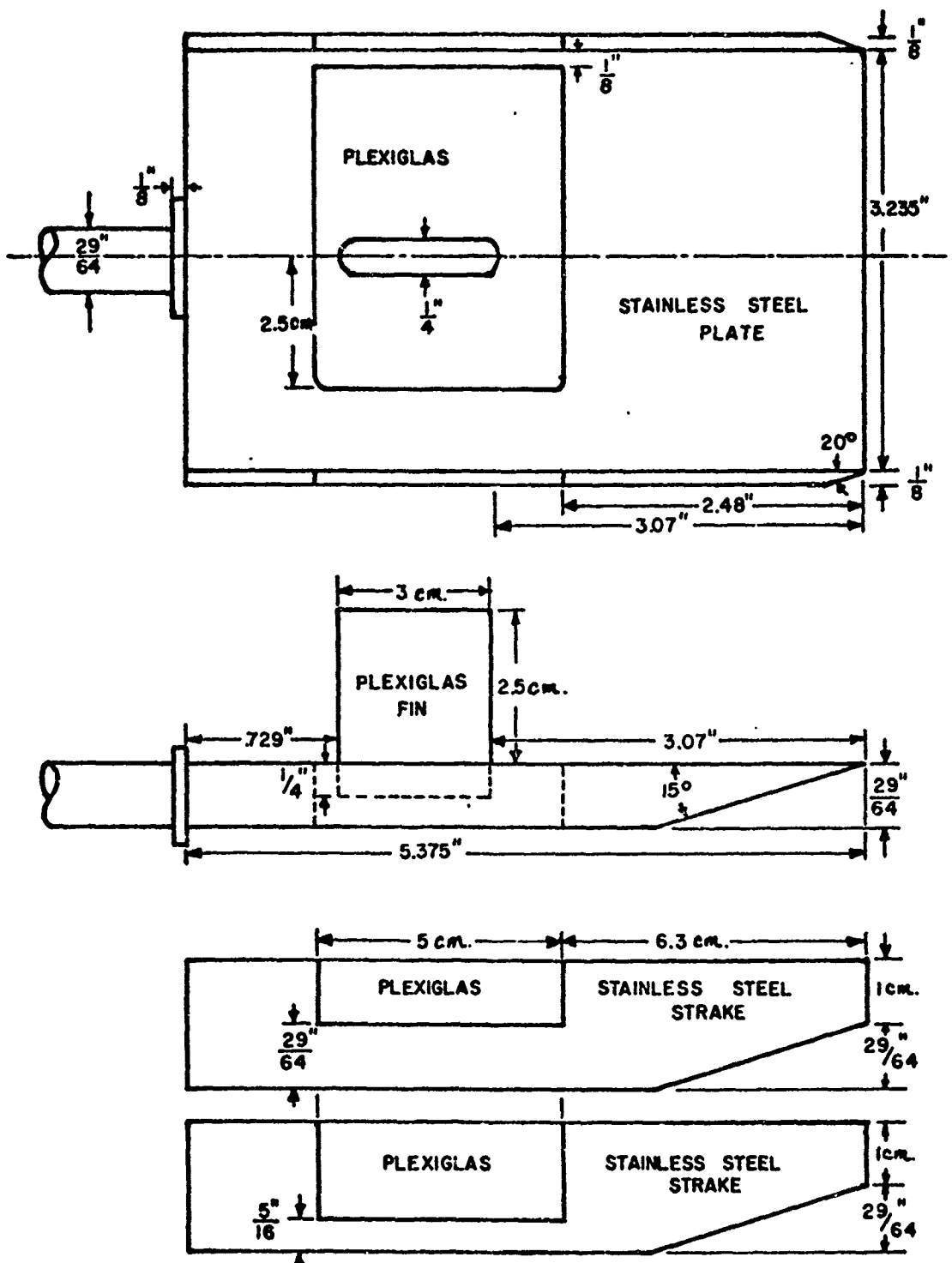


Figure 7(c). Details of the Second Fin-Flat Plate Model

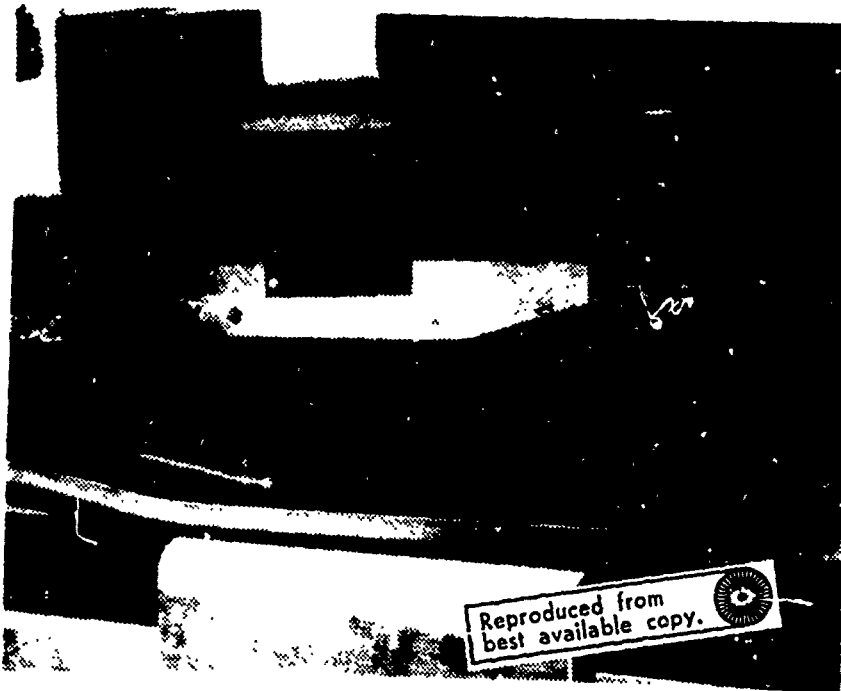


Figure 7(d). Model Mounting in the Wind Tunnel Test Section

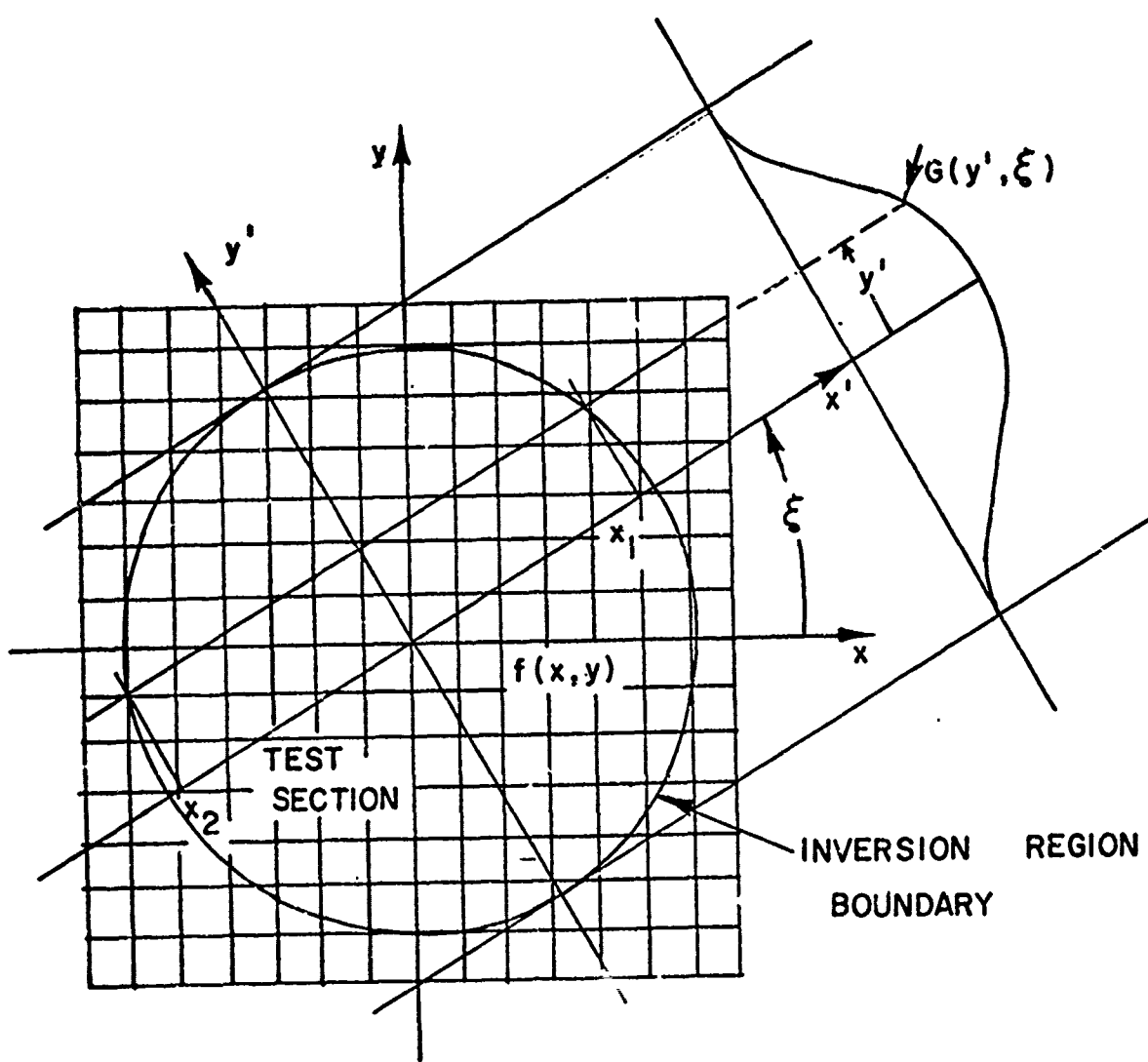


FIGURE 8. CO-ORDINATE SYSTEM USED FOR THE INVERSION OF FRINGE NUMBER TO DENSITY

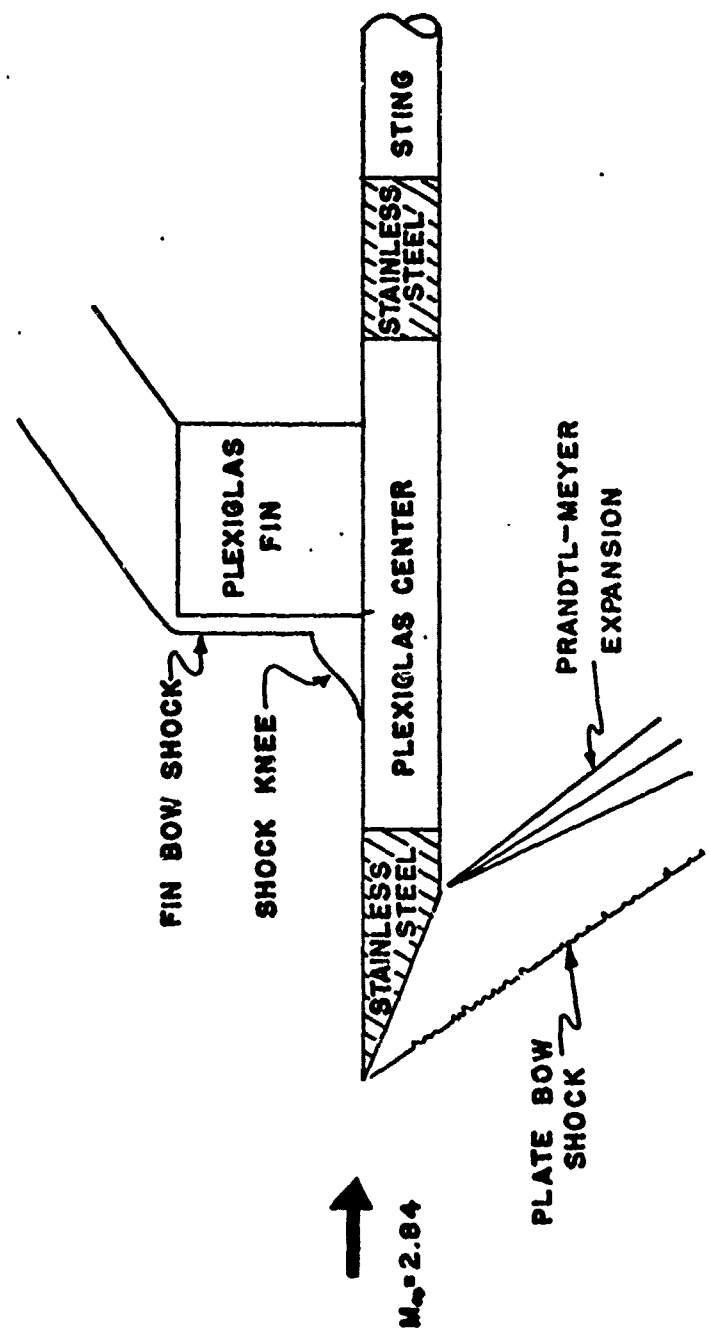


Figure 9. Schematic of the Desired Model Flow Network

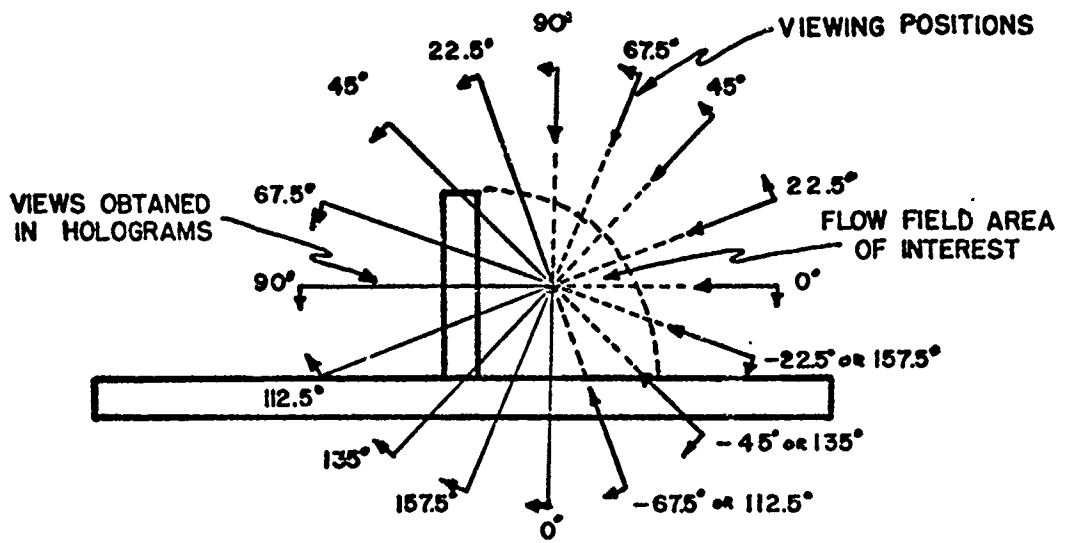


Figure 10. Desired Holographic Views in the Direct Fin-Root Method

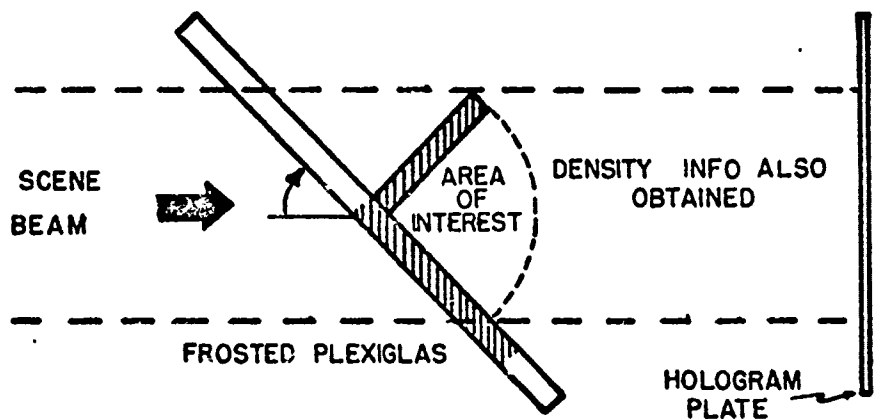


Figure 11. Schematic of the Model Used to Obtain Holographic Views Between 0° and 90° in the Direct Fin-Root Method

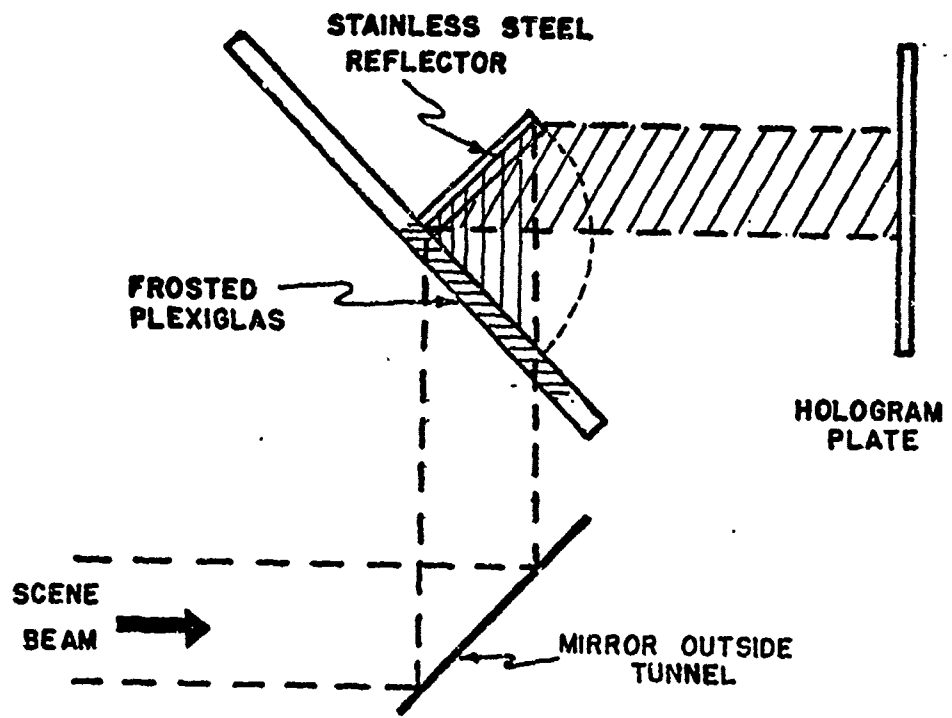


Figure 12. Schematic of the Model Used to Obtain Holographic Views Between 90° and 180° in the Direct Fin-Root Method

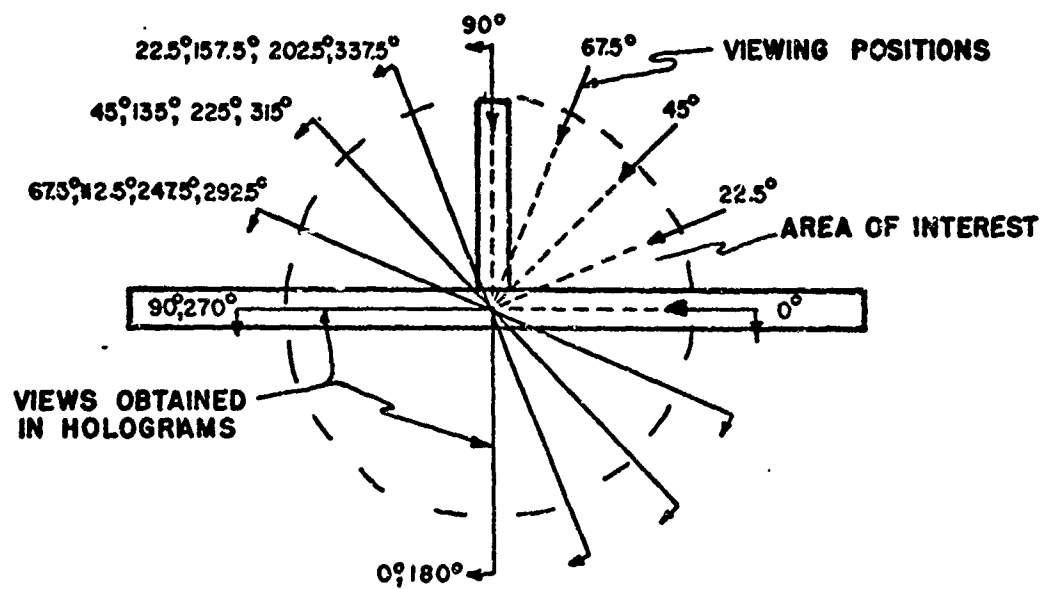


Figure 13. Holographic Viewing Angles Required in the Total Model Flow Method

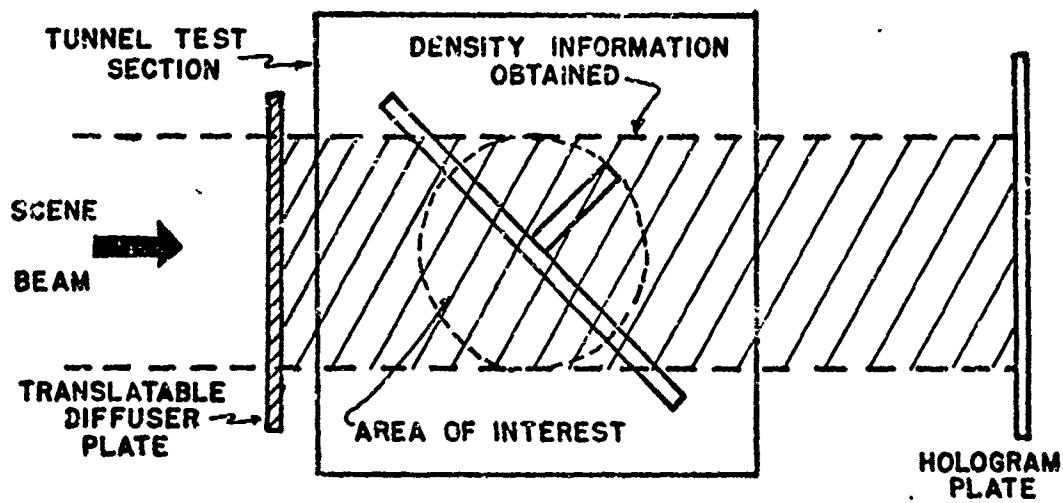


Figure 14. Schematic of the Technique Used to Obtain Holograms in the Total Model Flow Method

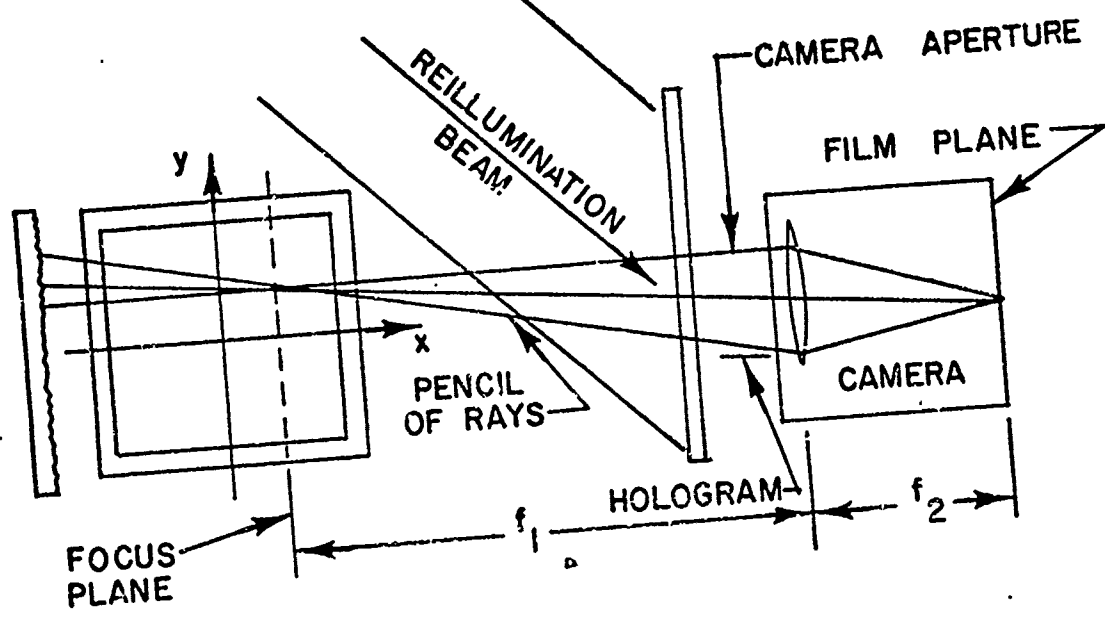


FIGURE 15. EFFECT OF APERTURE SIZE FOCUS PLANE POSITION ON THE PENCIL SIZE OF RAYS ABOUT A LINE OF SIGHT RECORDED BY CAMERA

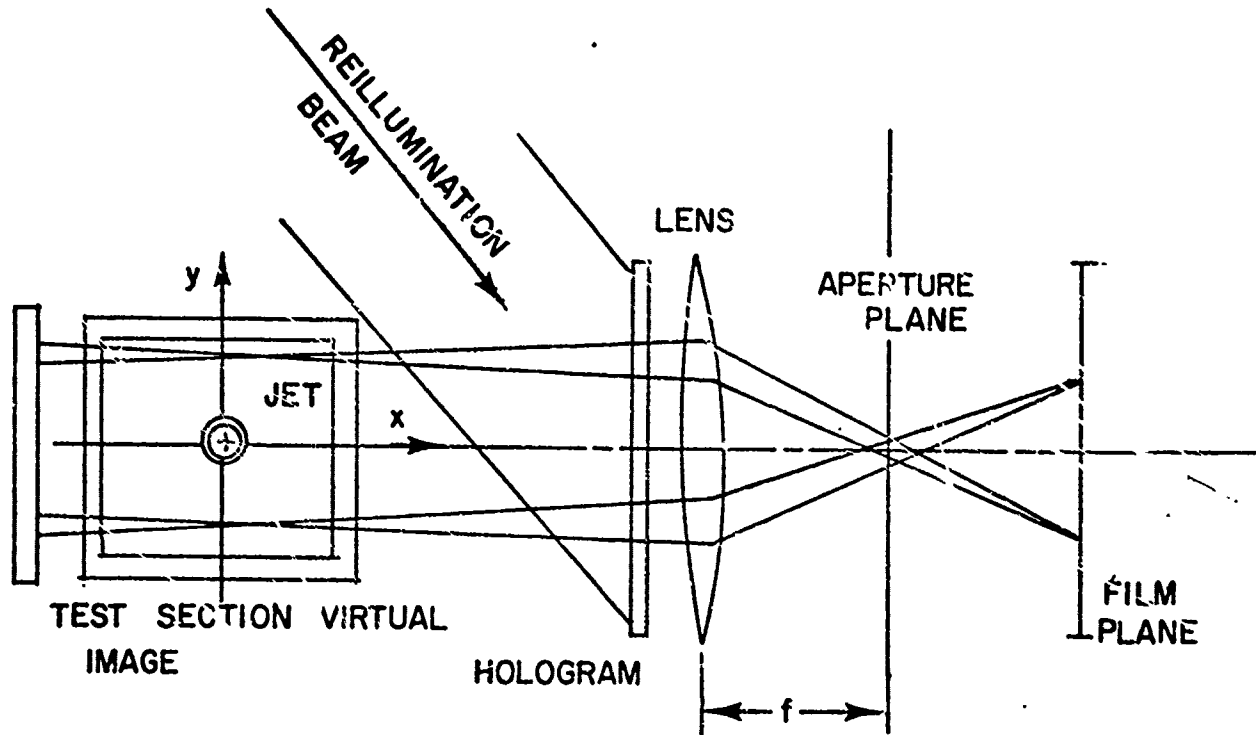


FIGURE 16. SPATIAL FILTERING TECHNIQUE FOR SELECTING PHOTOGRAPH OF CONSTANT ANGLE LINES OF LIGHT

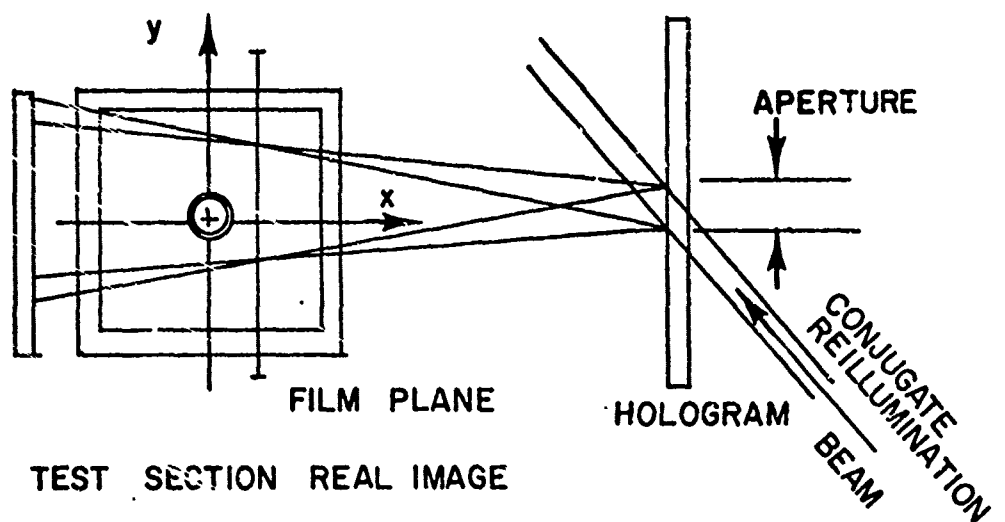


FIGURE 17. LENSLESS PHOTOGRAPHIC TECHNIQUE USING A CONJUGATE REFERENCE BEAM OF SMALL DIAMETER

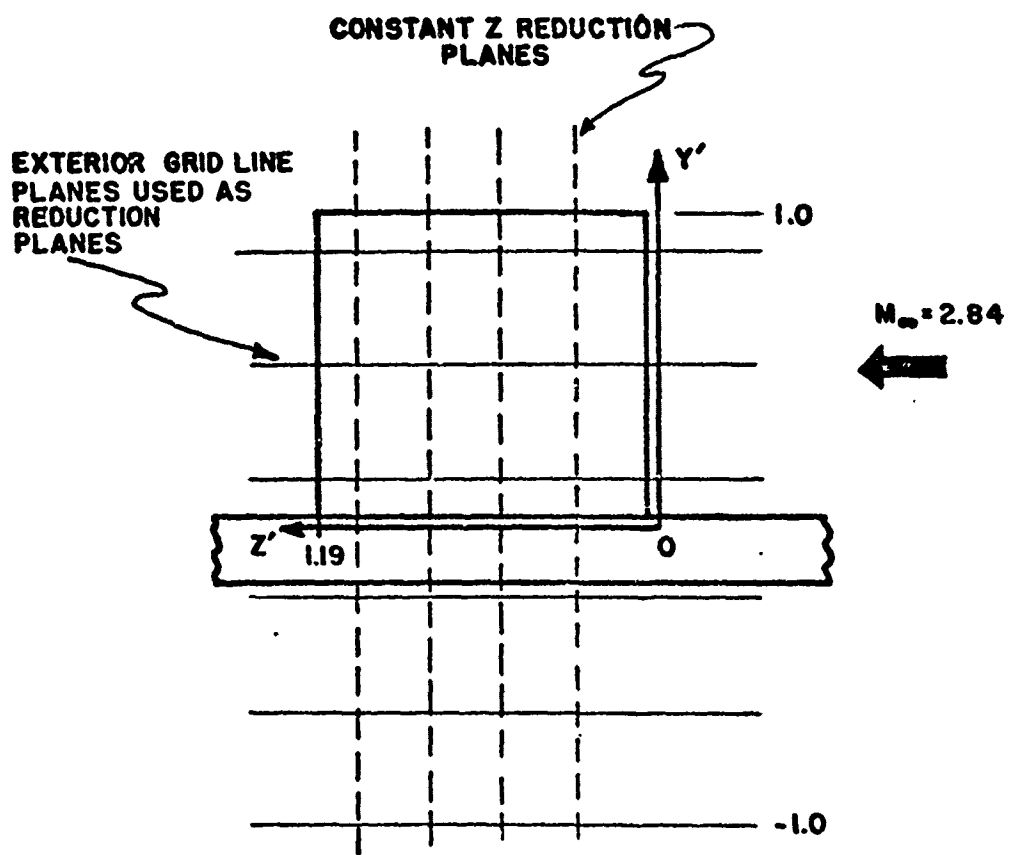


Figure 18. Data Reduction Planes Desired to Describe the Density Field Down the Fin

PLASTIC GRID AND TUNNEL WALL

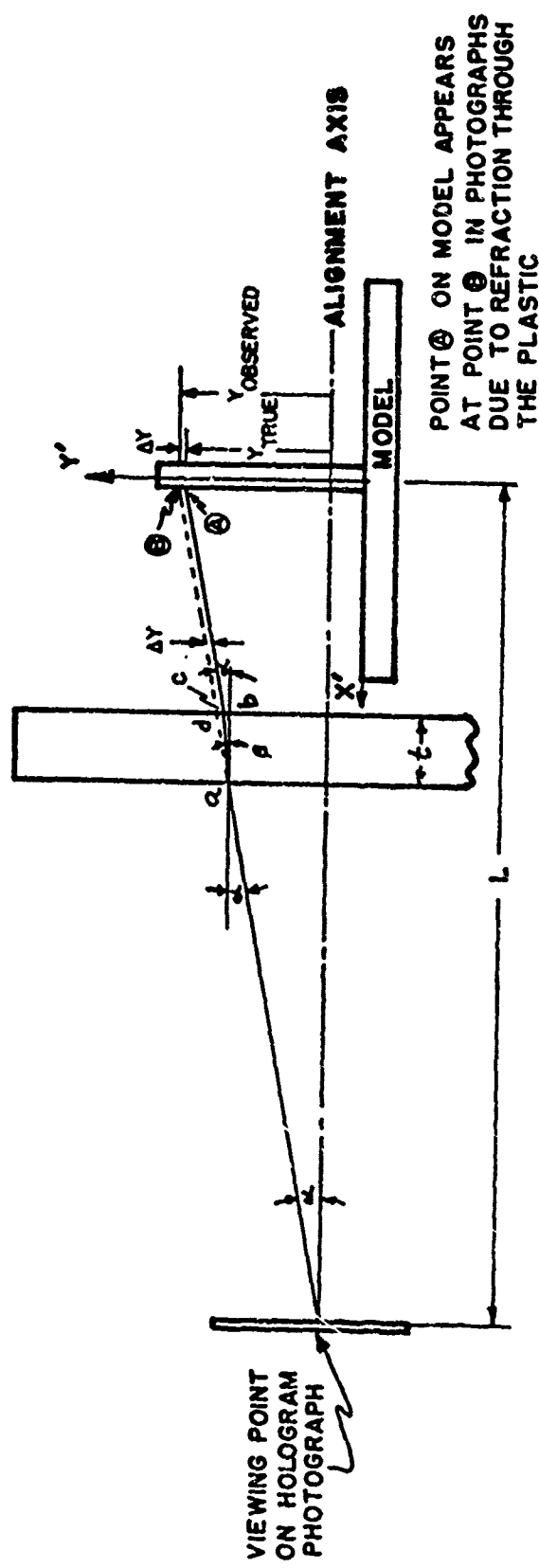


Figure 19. Schematic of the Refraction Displacement in the Photographs of Points Not Located on the Aligned Axis Caused by the Plastic Grid and Tunnel Wall

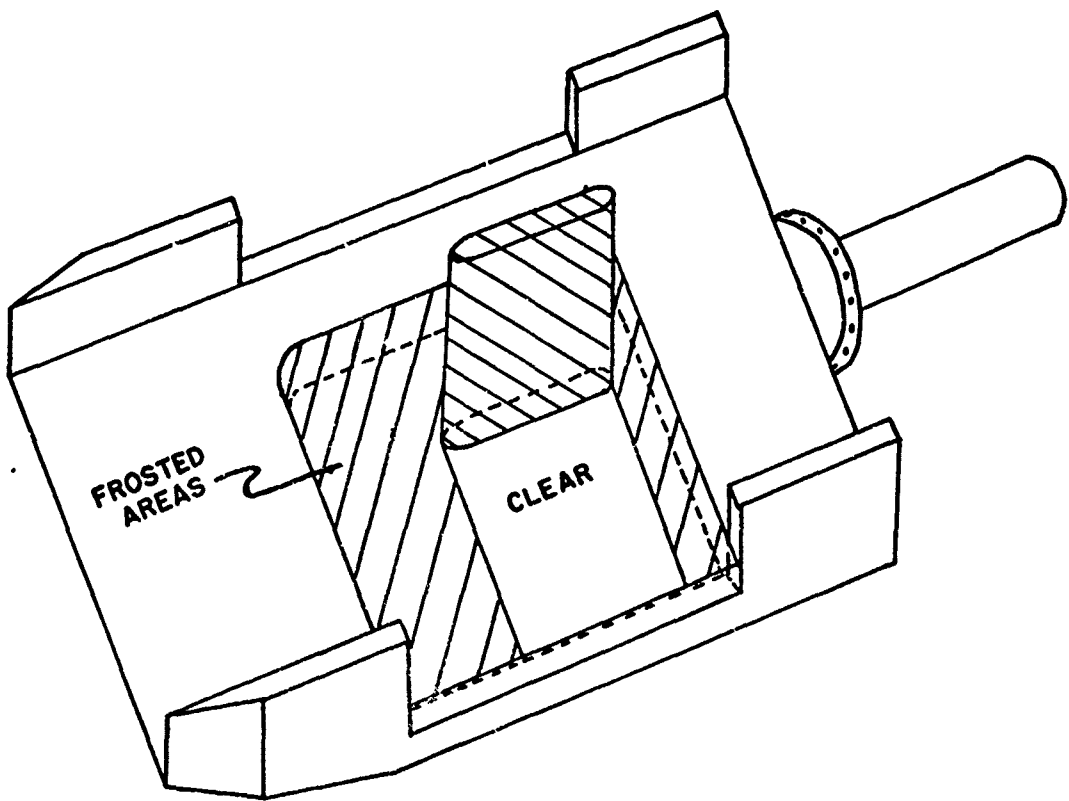


Figure 20. Schematic of the Diffused Plastic Portion of the Model Required in the Direct Fin Flow Method

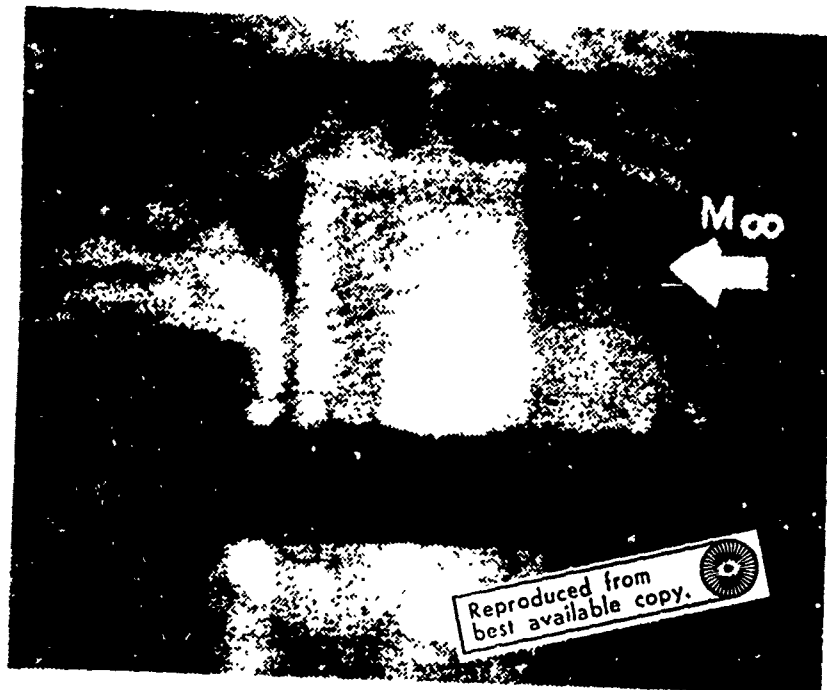


Figure 21. Interferogram Obtained in the Direct Fin Flow Method with the Model at 0° Rotation, Mach 2.84 and no Translation of Mirror, M_5

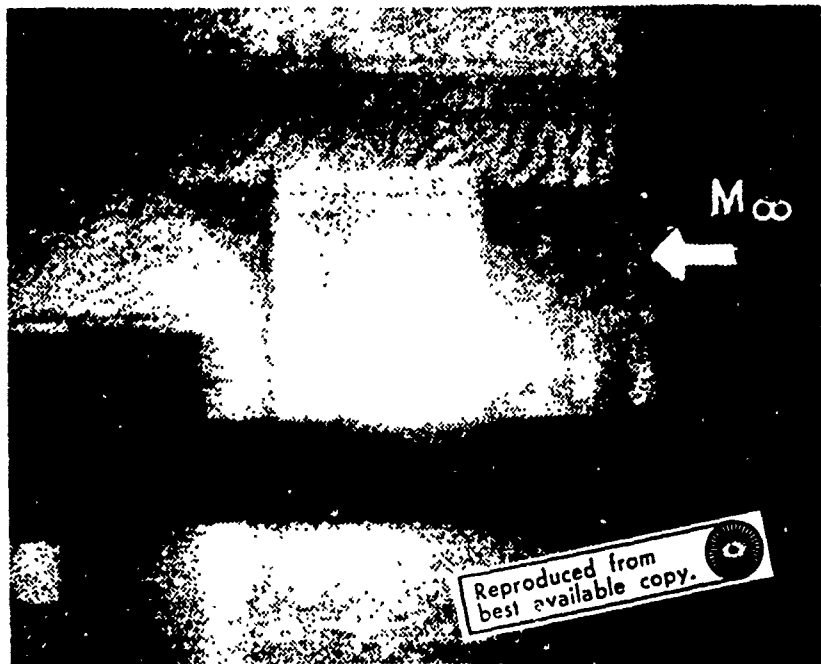


Figure 22. Interferogram Obtained in the Direct Fin Flow Method with the Model at 0° Rotation, Mach 2.84 and a .006 inches Translation of Mirror, M₅, Parallel to the Test Section

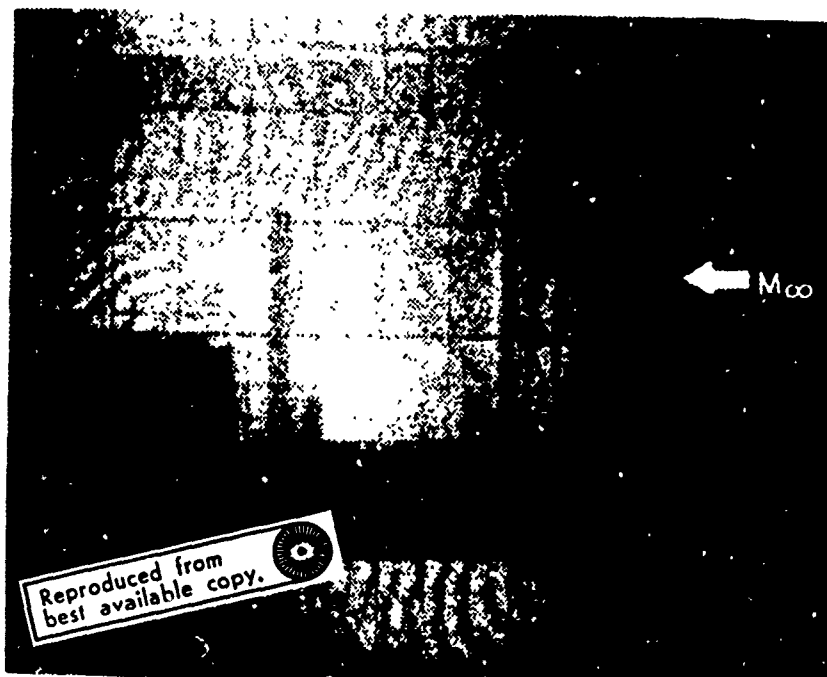


Figure 23. Interferogram Obtained in the Total Flow Method with the Clear Plexiglas Fin Model at 0° Rotation, Mach 2.84 and a .0015 inches horizontal Translation of the Diffuser Plate Parallel to the Test Section

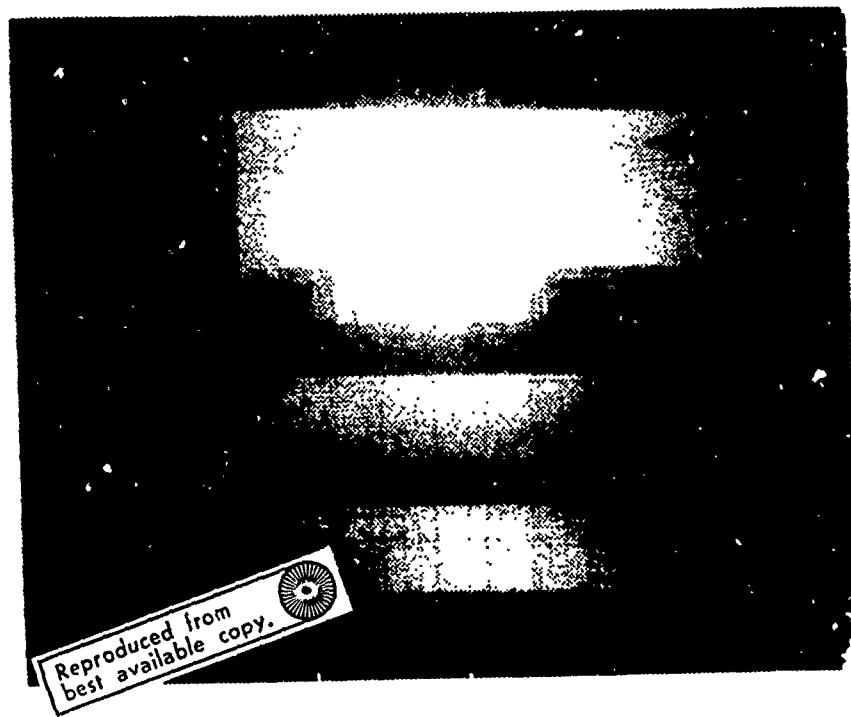
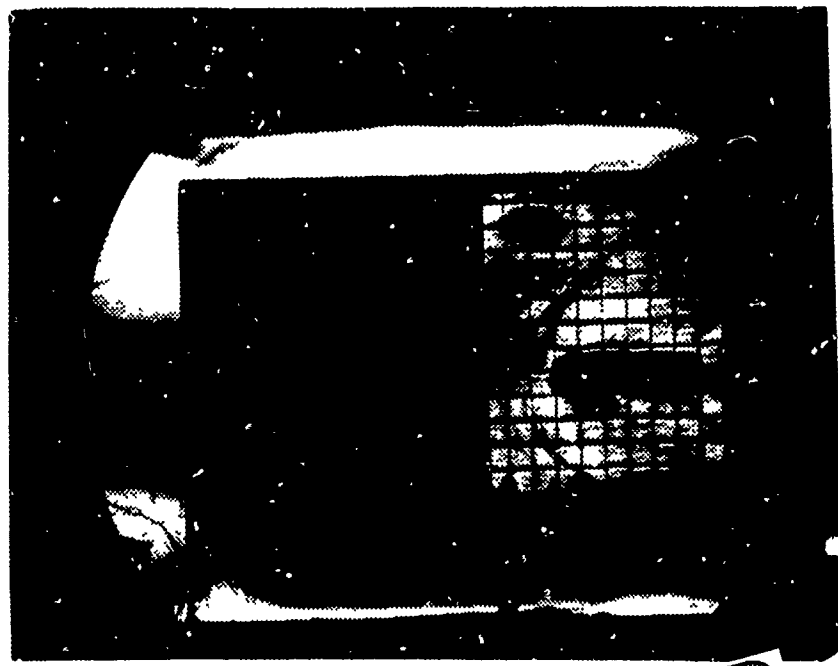
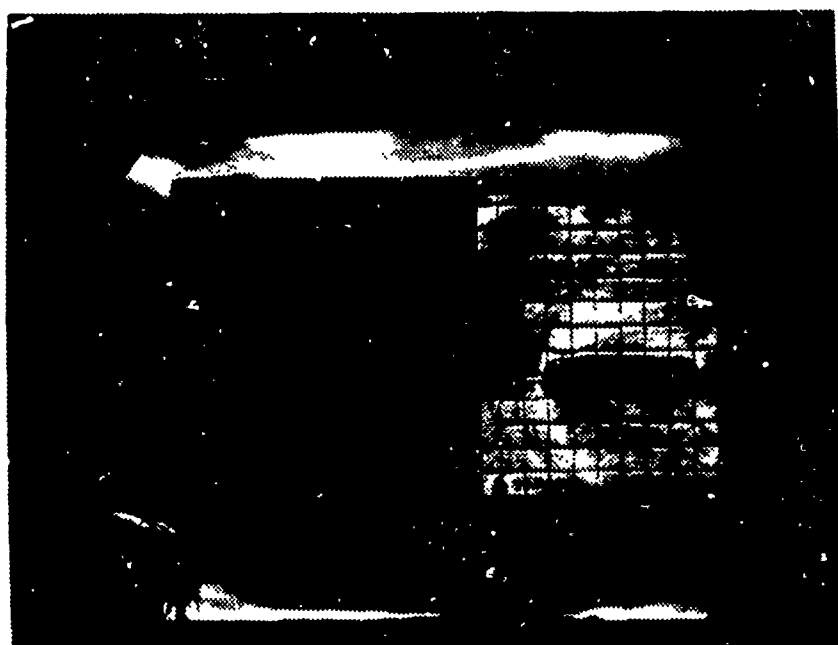


Figure 24. Interferogram Obtained in the Total Flow Method with the Clear Plexiglas Fin Model at 0° Rotation, Mach 2.84 and a .0045 Vertical Translation of the Diffuser Plate Parallel to the Test Section



Reproduced from
best available copy.

Figure 25(a). Illustration of the Shock Network Around the Fin at Mach 2.84 with a 90° Model Rotation Angle Using a Horizontal Knife Edge Schlieren System



Reproduced from
best available copy.

Figure 25(l). Illustration of the Shock Network Around the Fin at Mach 2.84 with a 90° Model Rotation Angle Using a Vertical knife Edge Schlieren System



Reproduced from
best available copy.

Figure 26. Illustration of the Model Flow Network at Mach 2.84, 0°
Model Rotation and a Plate Vibration of $\pm .05$ Angle of
Attack Using a Schlieren System



Reproduced from
best available copy.

Figure 27. Illustration of the Model Flow Network at Mach 2.84, 0°
Model Rotation and No Plate Vibration Using a Schlieren
System

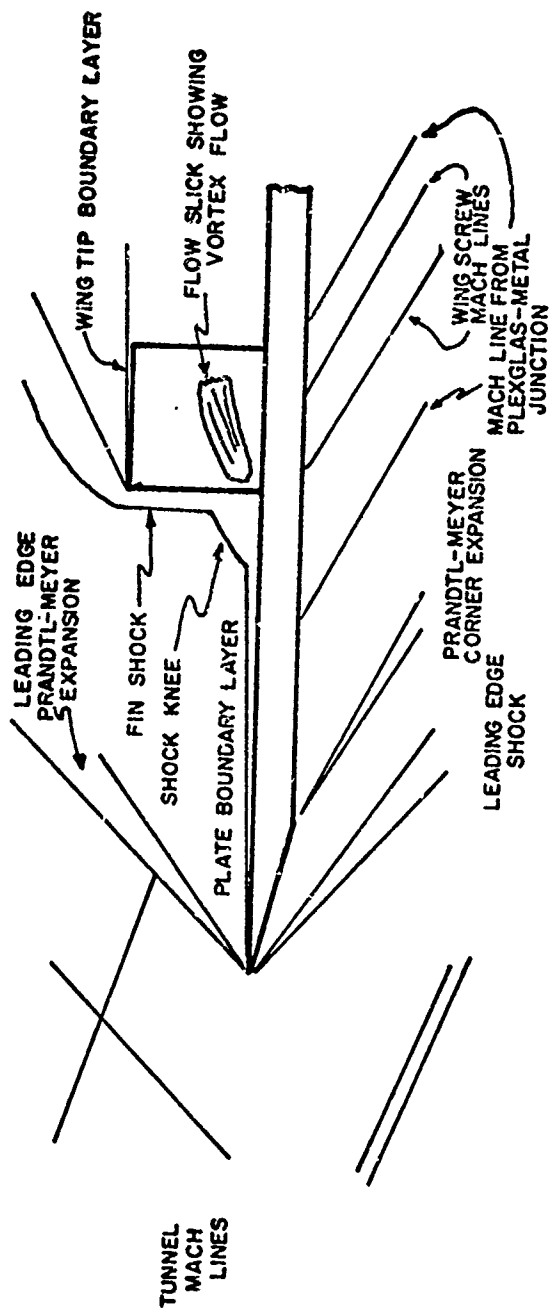


Figure 28. Schematic of the Flow Observed in the Schlieren Photographs

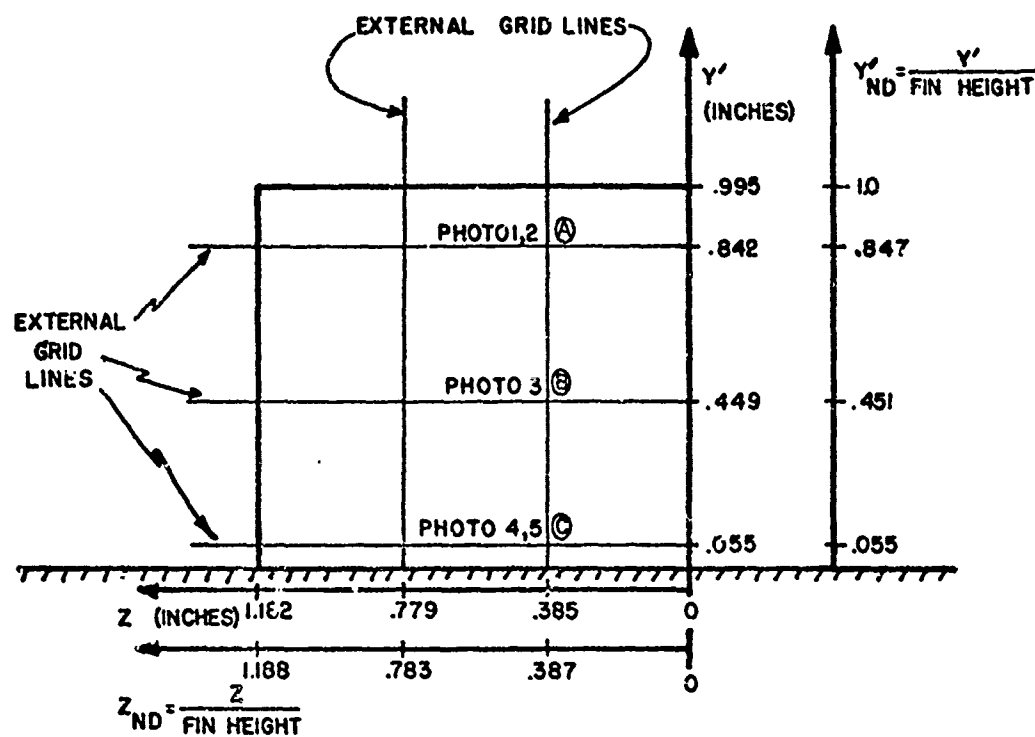


Figure 29. Schematic of the Fin at 0° Rotation Showing the Locations of the External Grid Lines and of the Interferogram Photographic Points

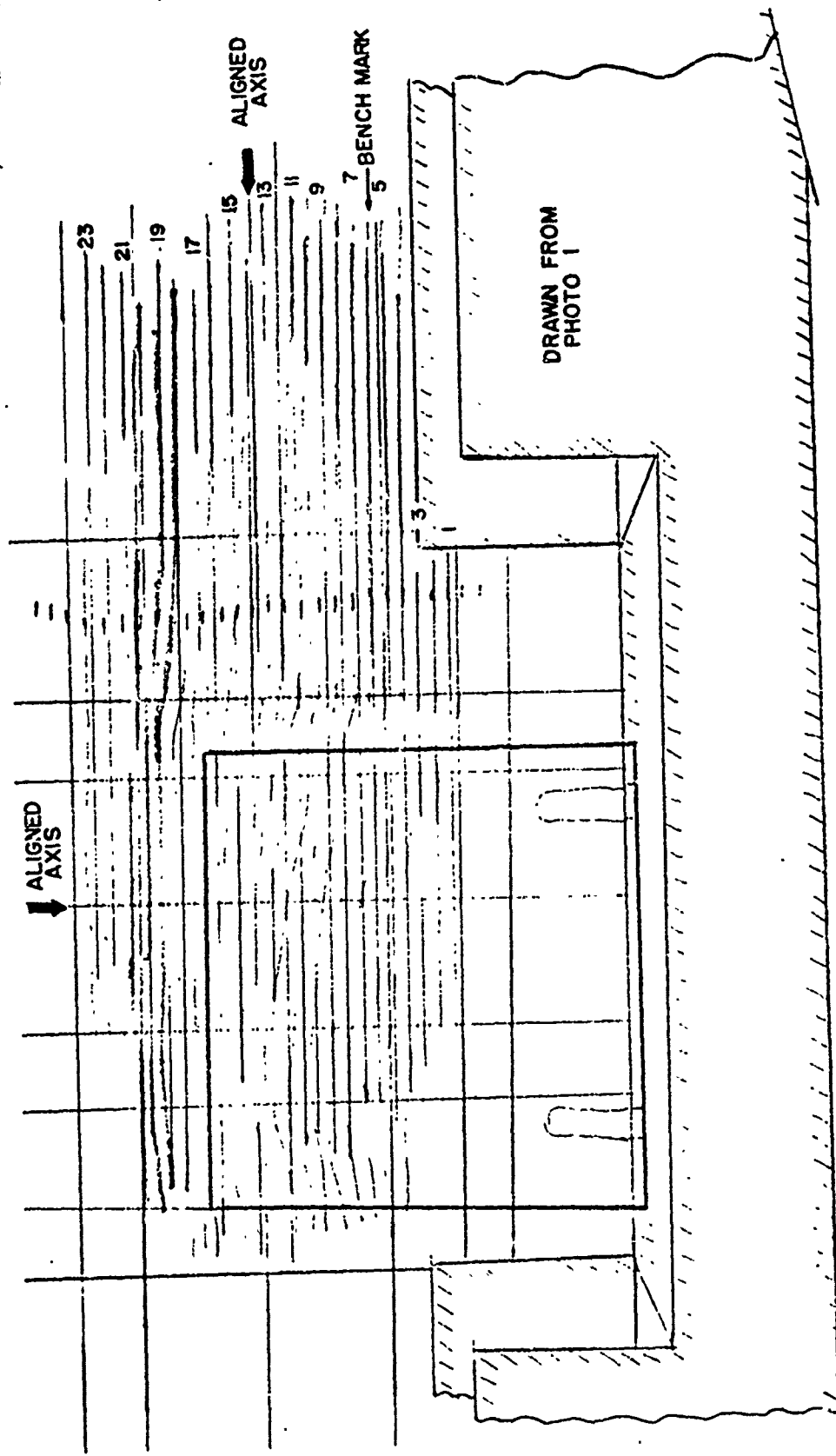


Figure 30. Actual Drawing and Data Reduction of Interferogram Photograph 1 Aligned at $Z = 0.387$,
 $y' = 0.847$ for Mach 2.84 and 0° Model Rotation Angle

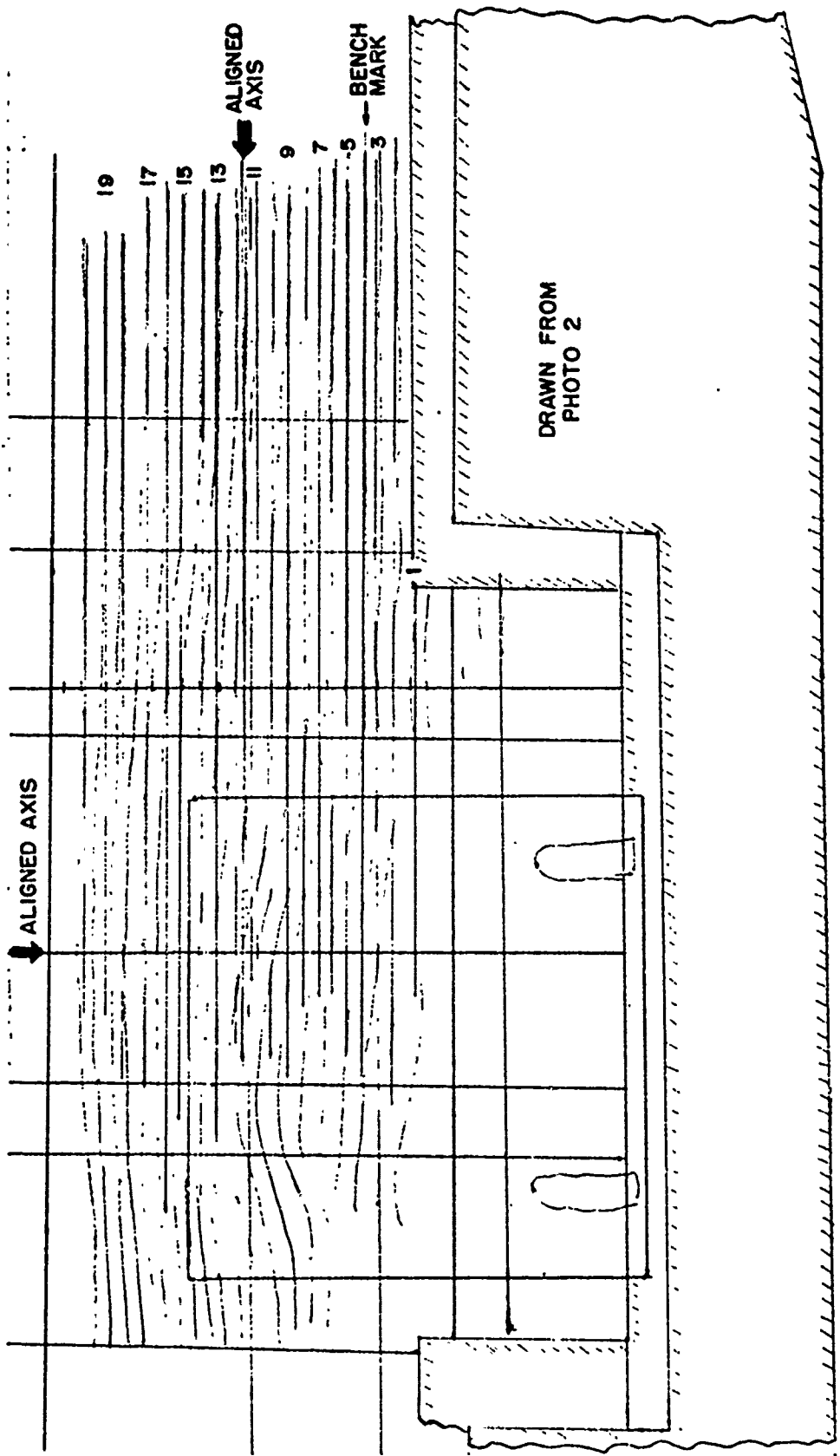


Figure 31. Actual Drawing and Data Reduction of Interferogram Photograph 2 Aligned at $Z = 0.387$,
 $\gamma_i = 0.847$ for Mach 2.84 and 0° Model Rotation Angle

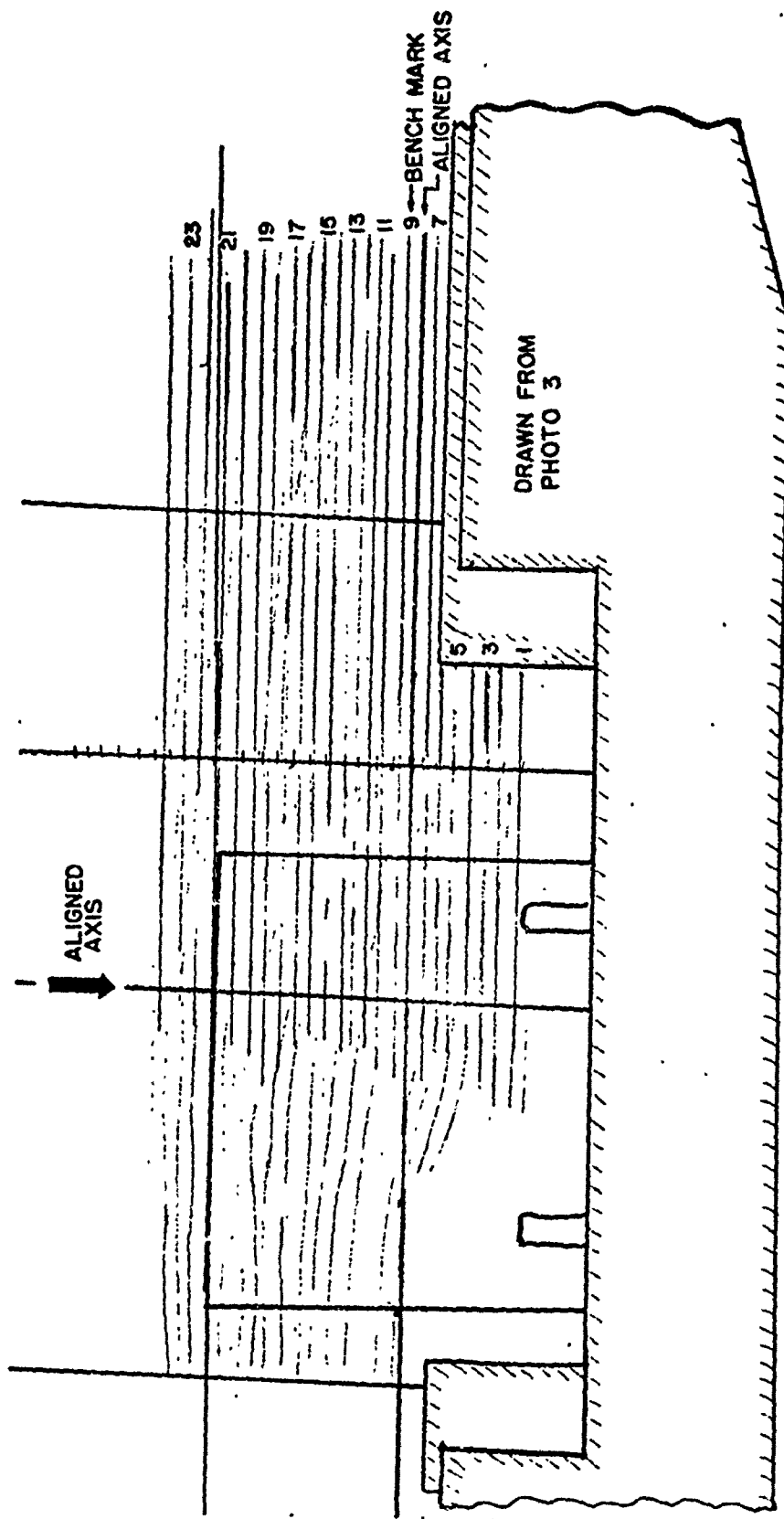


Figure 32. Actual Drawing and Data Reduction of Interferogram Photograph 3 Aligned at $z = 0.381$,
 $y_1 = 0.451$ for Nach 2.84 and 0° Model Rotation Angle

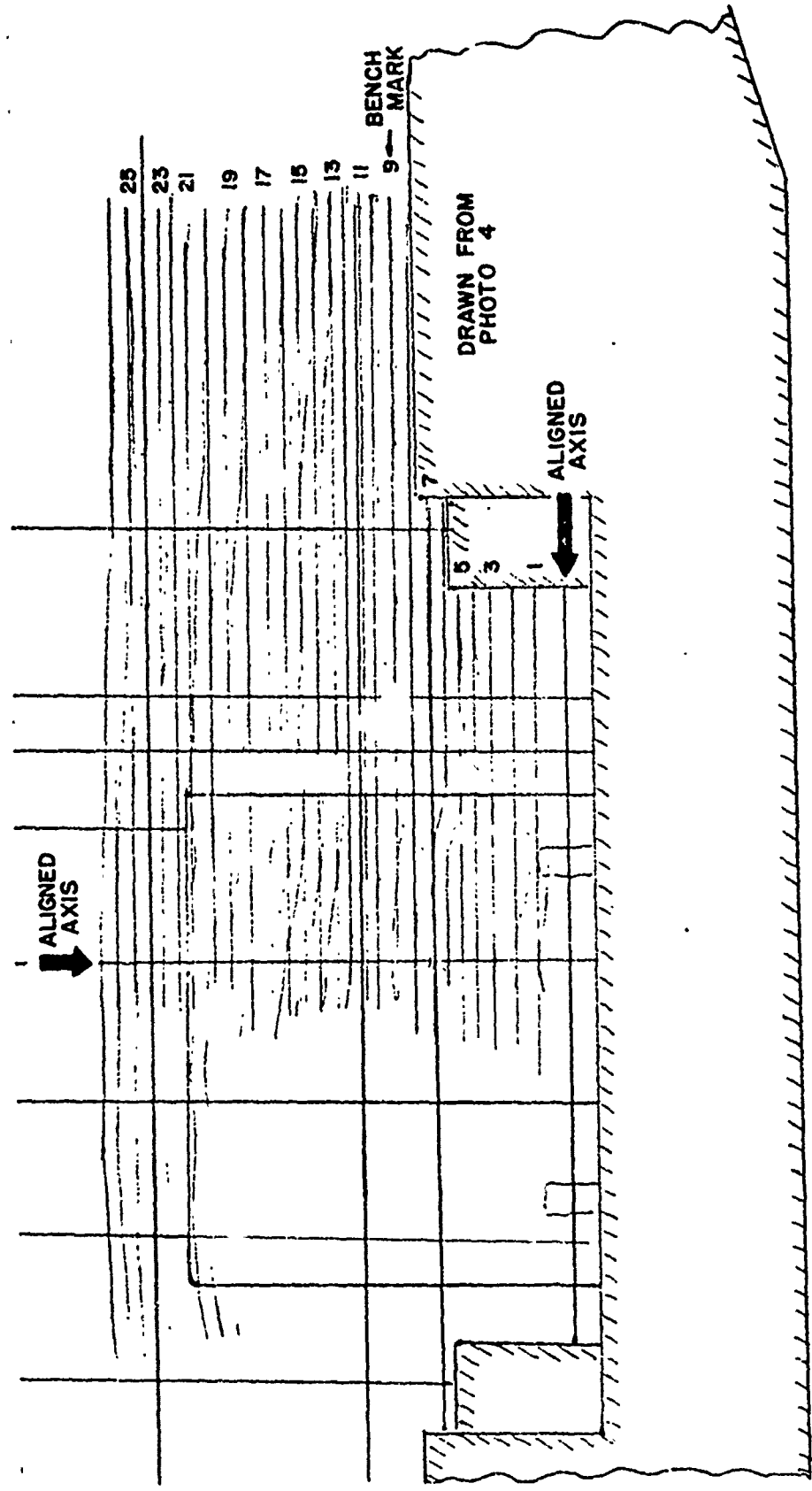


Figure 33. Actual Drawing and Data Reduction of Interferogram Photograph 4 Aligned at $Z = 0.387$,
 $\gamma' = 0.055$ for Mach 2.84 and 0° Model Rotation Angle

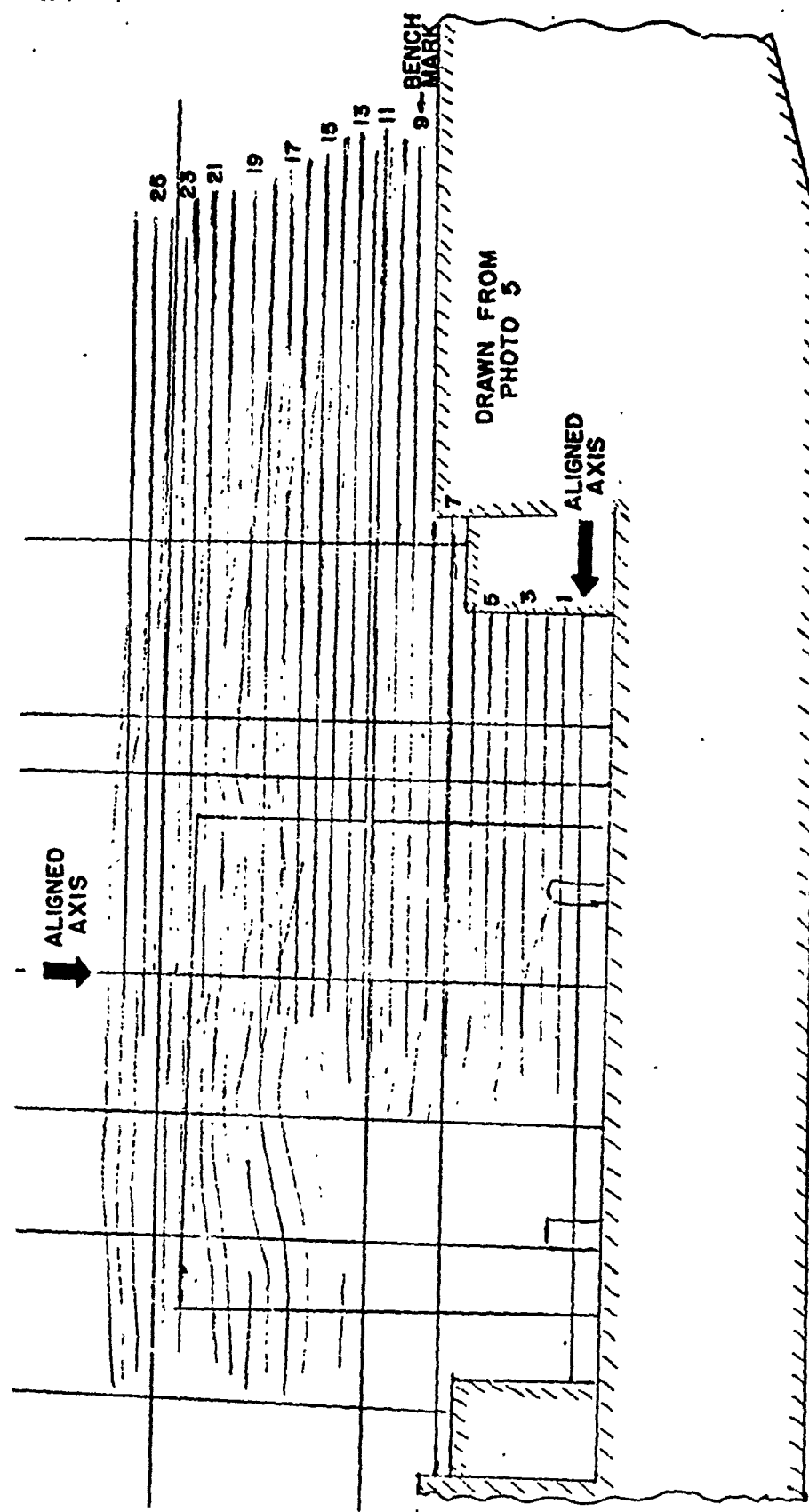


Figure 34. Actual Drawing and Data Reduction of Interferogram Photograph 5 Aligned at $z = 0.387$,
 $y_1 = 0.055$ for Mach 2.84 and 0° Model Rotation Angle

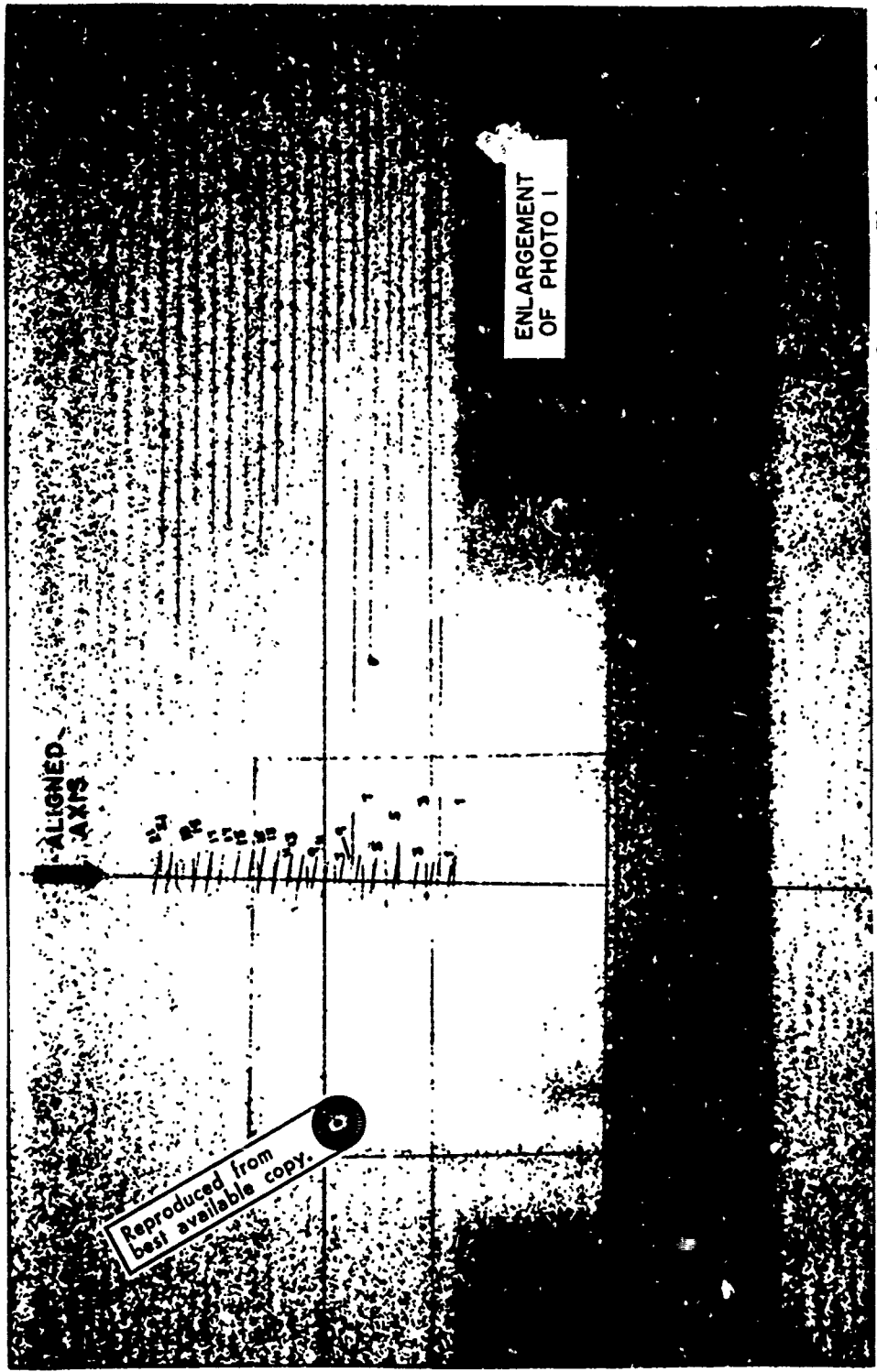


Figure 35. Actual Enlarged Photograph Used for the Data Reduction of Interferogram Photograph: 1
Aligned at $Z = 0.387$, $Y^* = 0.847$ for Mach 2.84 and 6° Model Rotation Angle

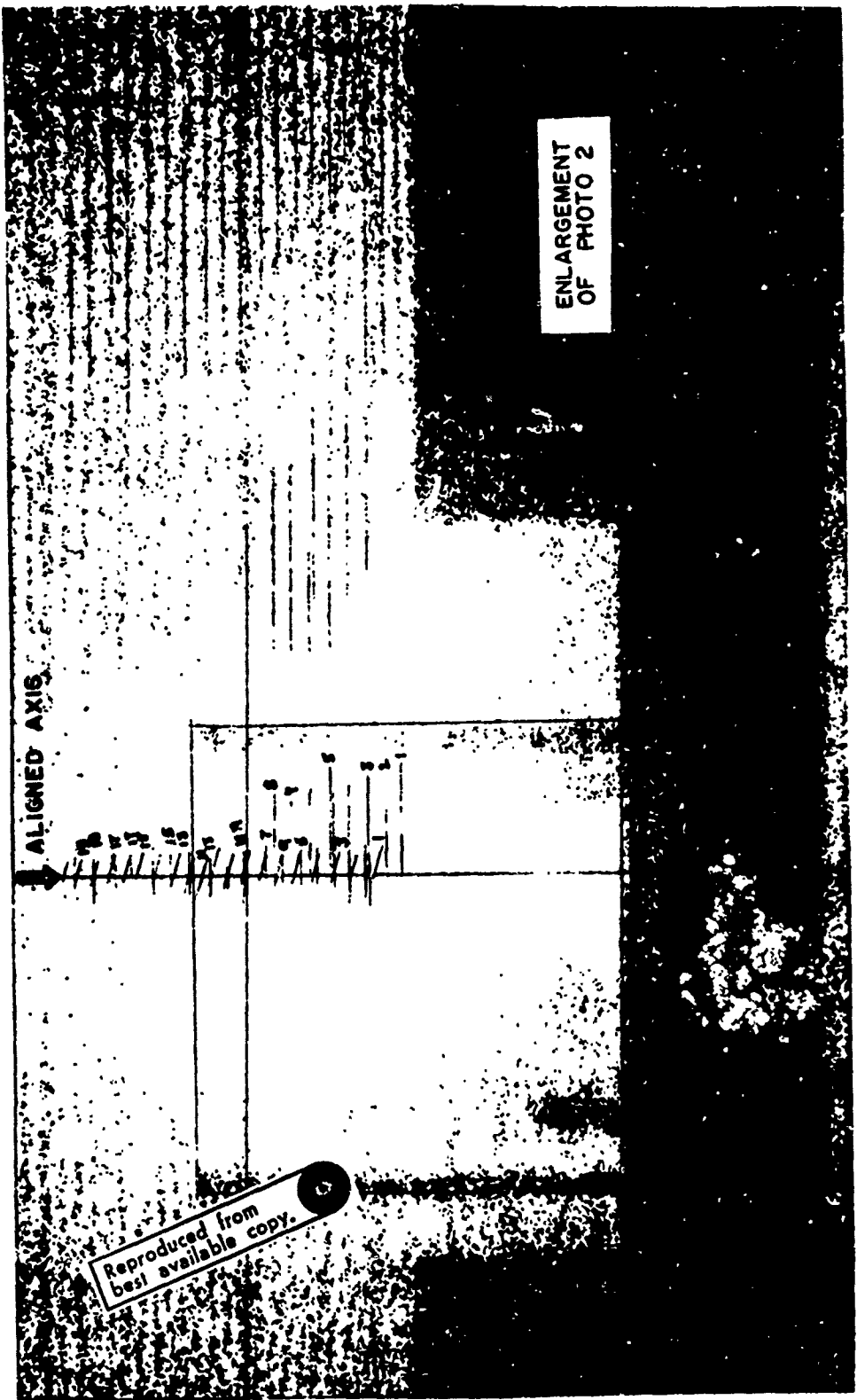


Figure 36. Actual Enlarged Photograph Used for the Data Reduction of Interferogram Photograph 2
Aligned at $z = 0.387$, $y' = 0.847$ for Mach 2.84 and 0° Model Rotation Angle

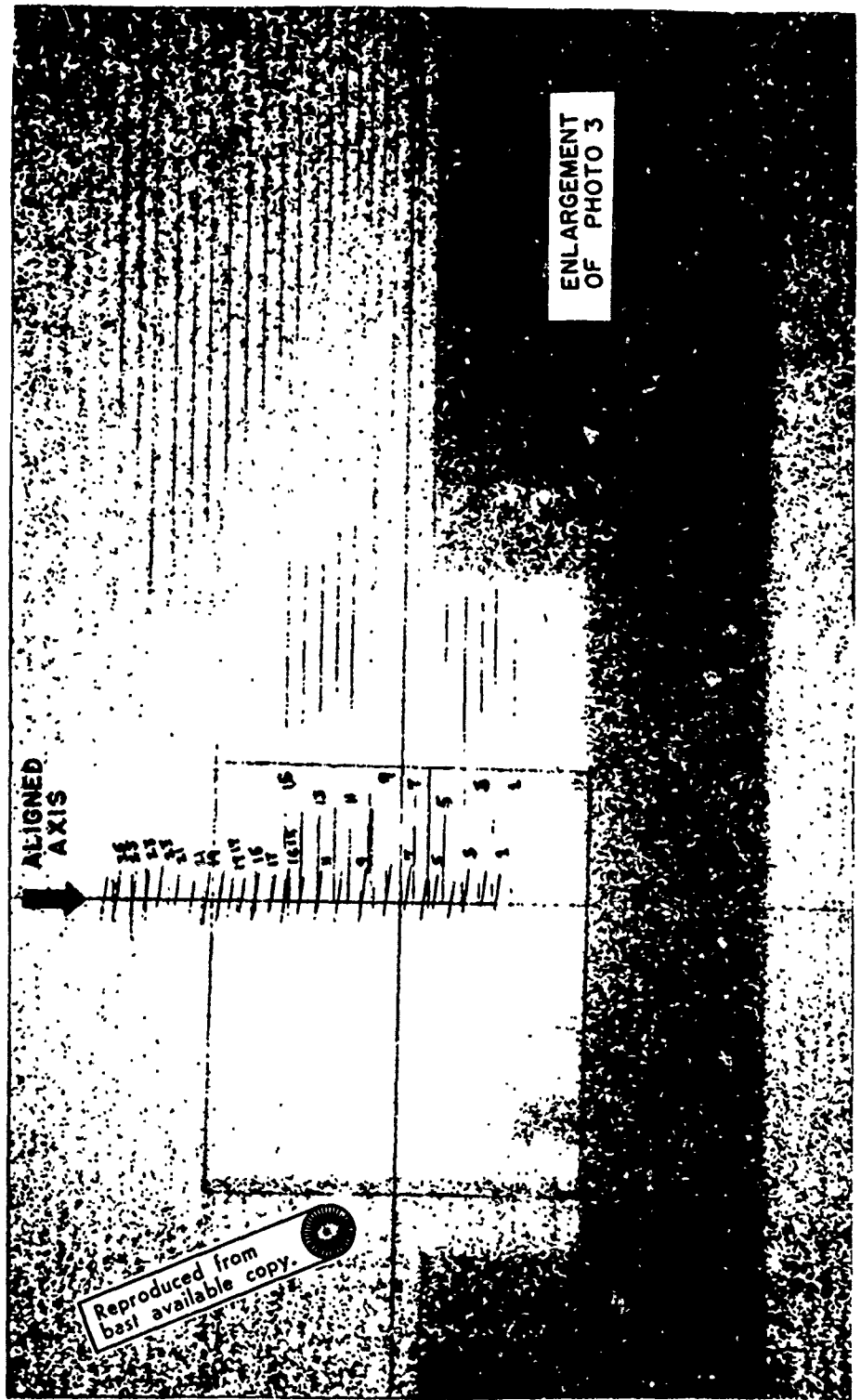


Figure 37. Actual Enlarged Photograph Used for the Data Reduction of Interferogram Photograph 3
Aligned at $Z = 0.387$, $y' = 0.451$ for Mach 2.84 and 0 Model Rotation Angle

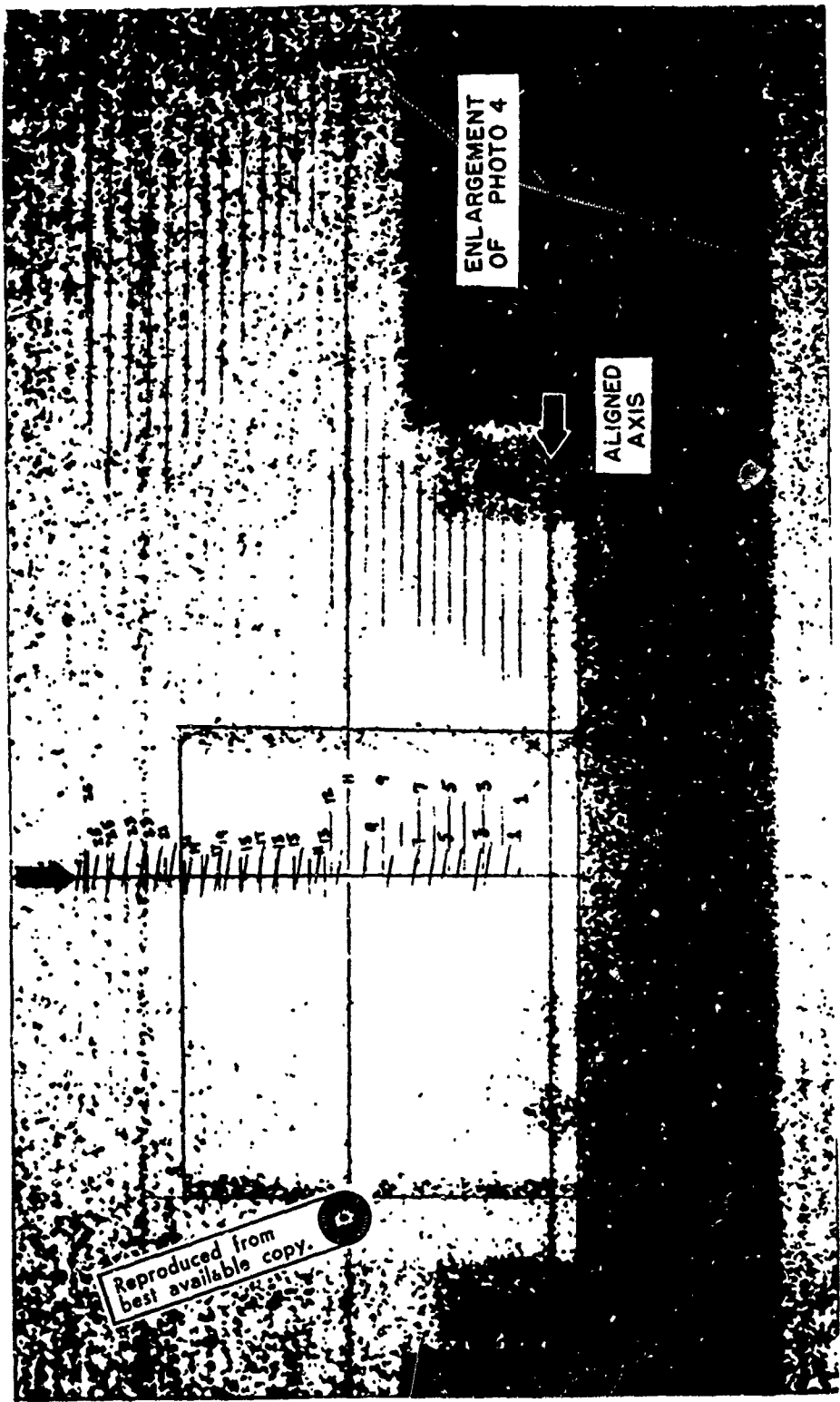


Figure 38. Actual Enlarged Photograph Used for the Data Reduction of Interferogram Photograph 4
Aligned at $Z = 0.387$, $y' = 0.055$ for Mach 2.84 and 0° Model Rotation Angle

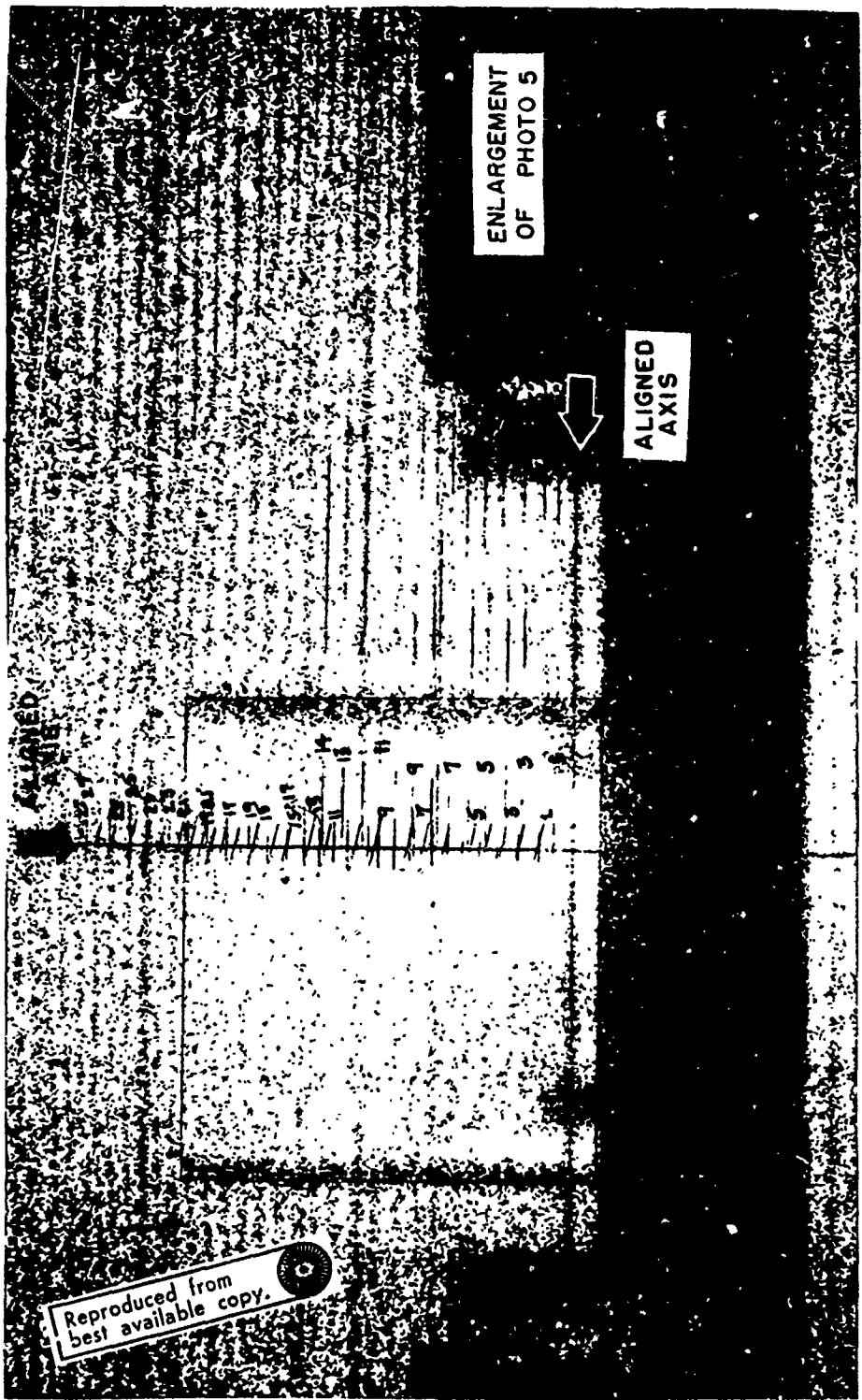


Figure 39. Actual Enlarged Photograph Used for the Data Reduction of Interferogram Photograph 5
Aligned at $Z = 0.387$, $Y' = 0.055$ for Mach 2.84 and 0° Model Rotation Angle

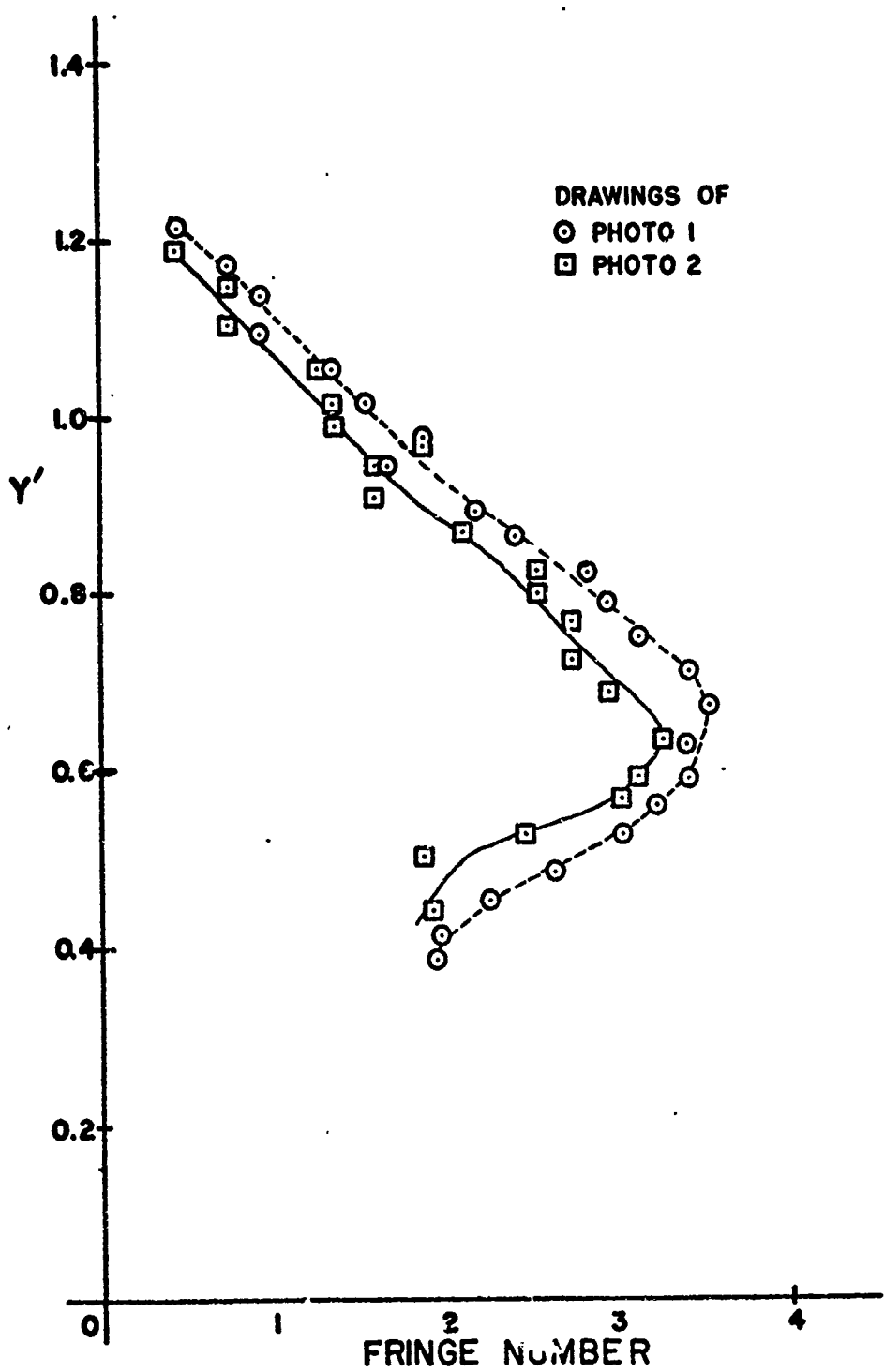


Figure 40. Comparison of Fringe Data Obtained from Drawings of Interferogram Photographs 1 and 2 Aligned at $Y' = 0.847$

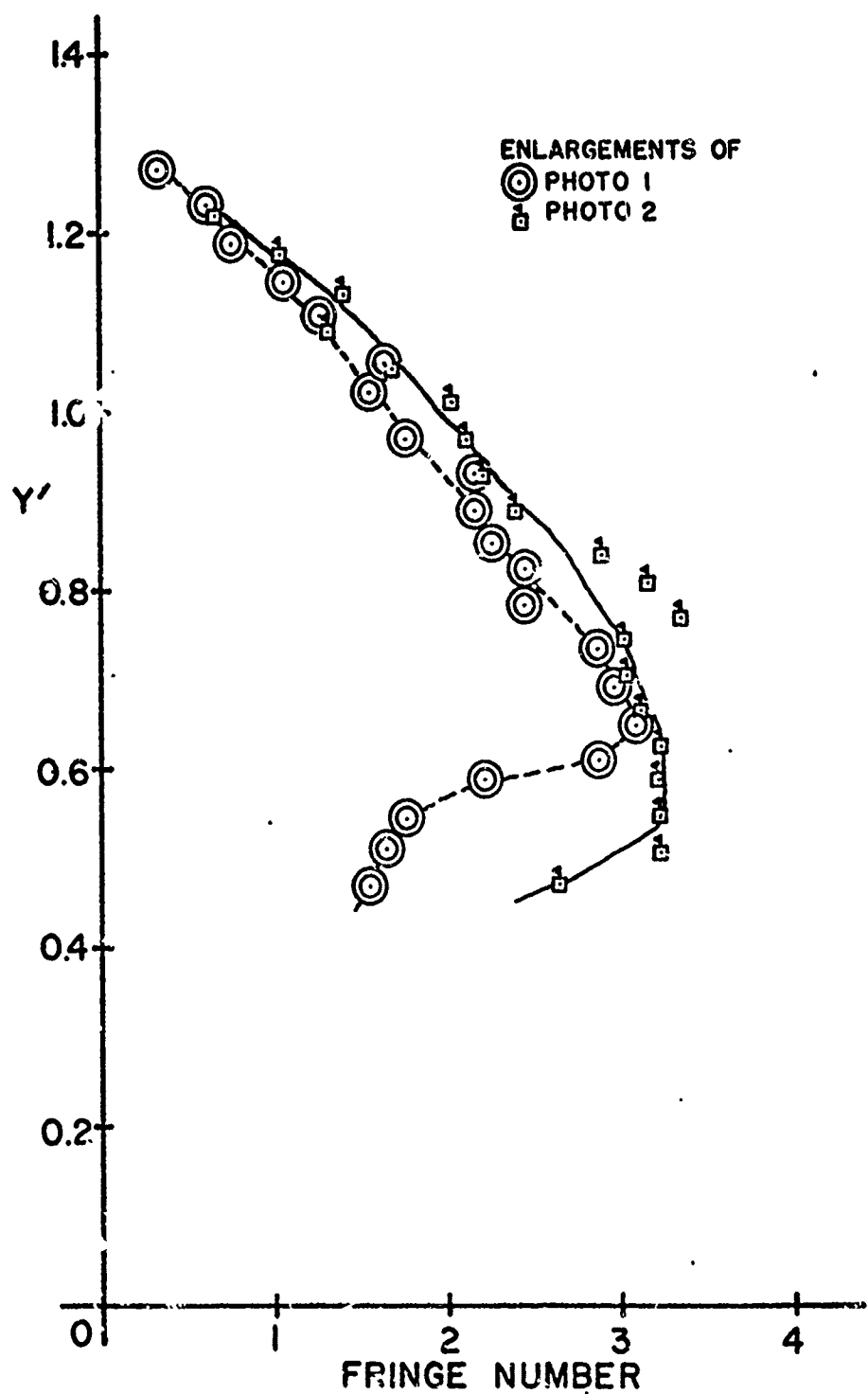


Figure 41. Comparison of Fringe Data Obtained from Photographic Enlargements of Interferogram Photographs 1 and 2 Aligned at $Y' = 0.847$

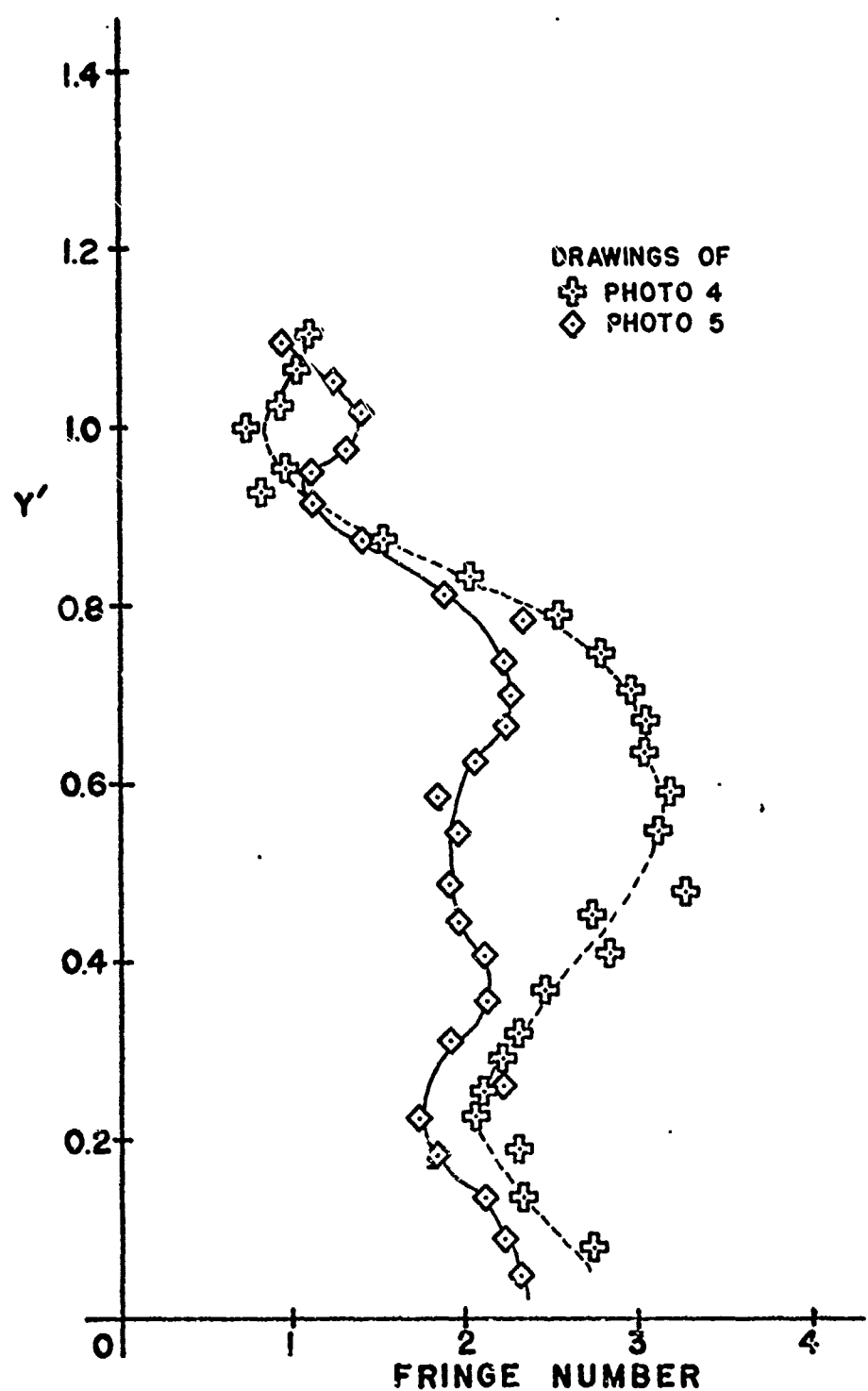


Figure 42. Comparison of Fringe Data Obtained from Drawings of Interferogram Photographs 4 and 5 Aligned at $Y' = 0.055$

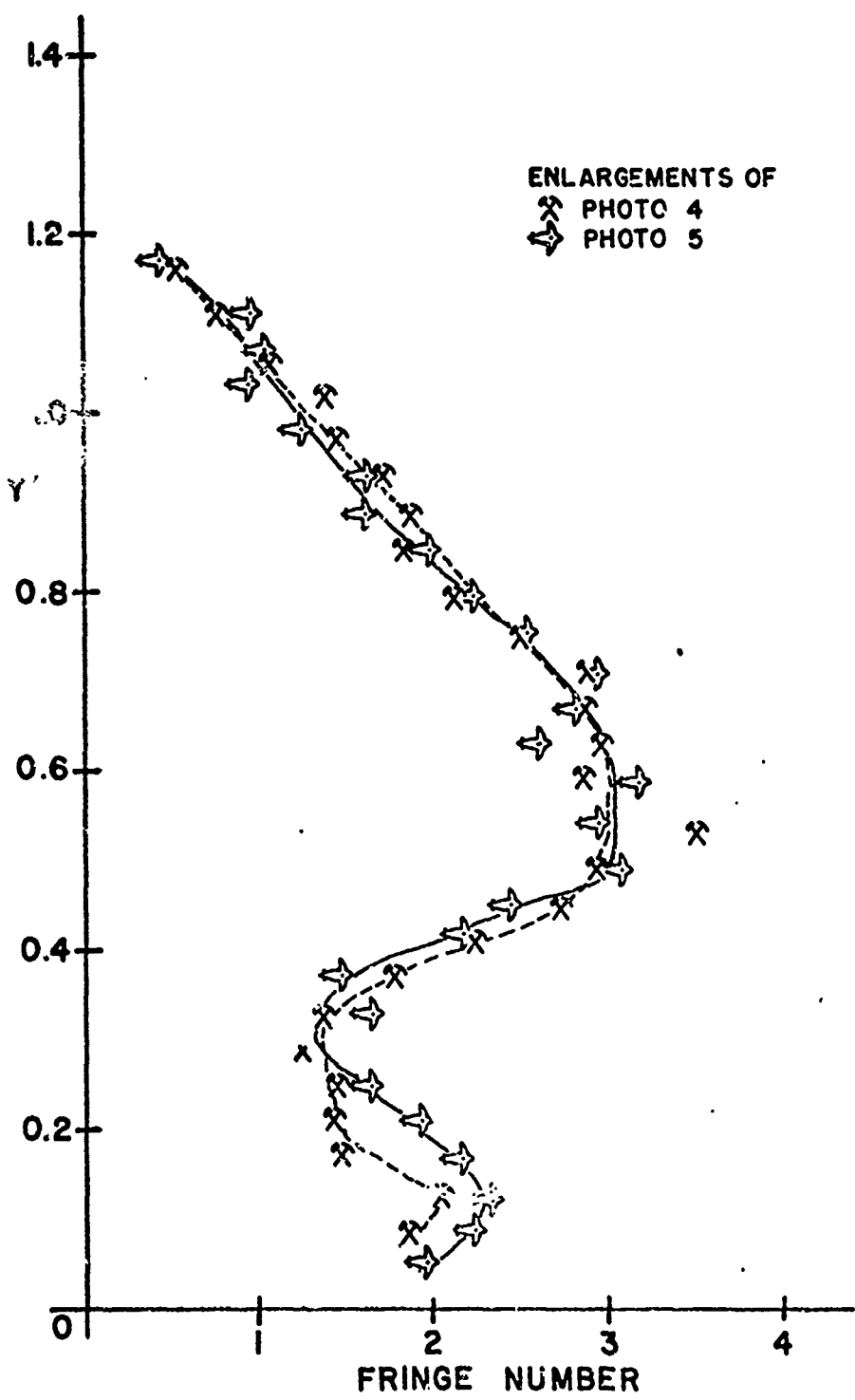


Figure 43. Comparison of Fringe Data Obtained from Photographic Enlargements of Interferogram Photographs 4 and 5 Aligned at $Y' = 0.055$

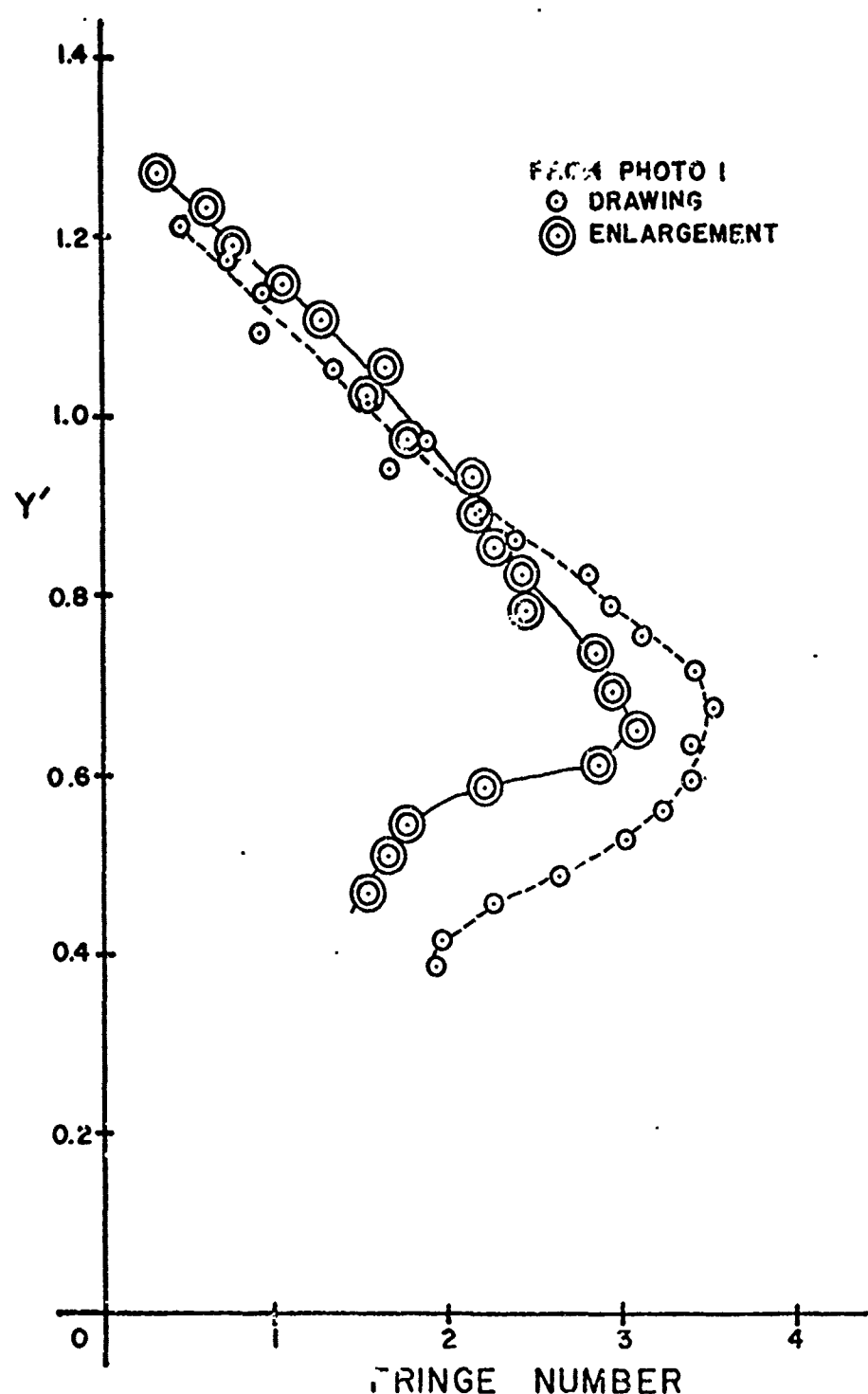


Figure 44. Comparison of Fringe Data Obtained from the Drawing and Photographic Enlargement of Interferogram Photograph 1 Aligned at $Y' = 0.847$

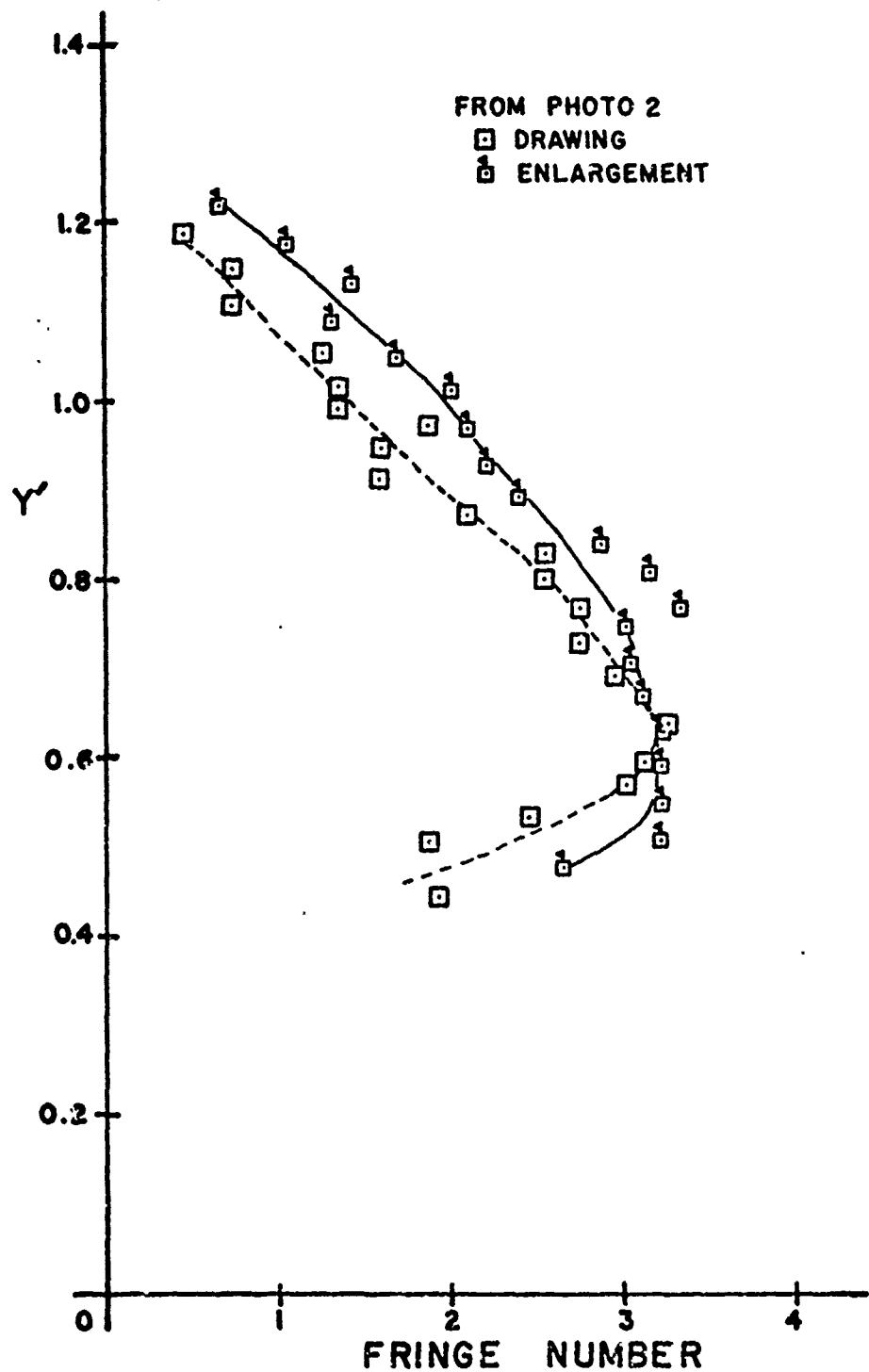


Figure 45. Comparison of Fringe Data Obtained from the Drawing and Photographic Enlargement of Interferogram Photograph 2 Aligned at $Y' = 0.847$

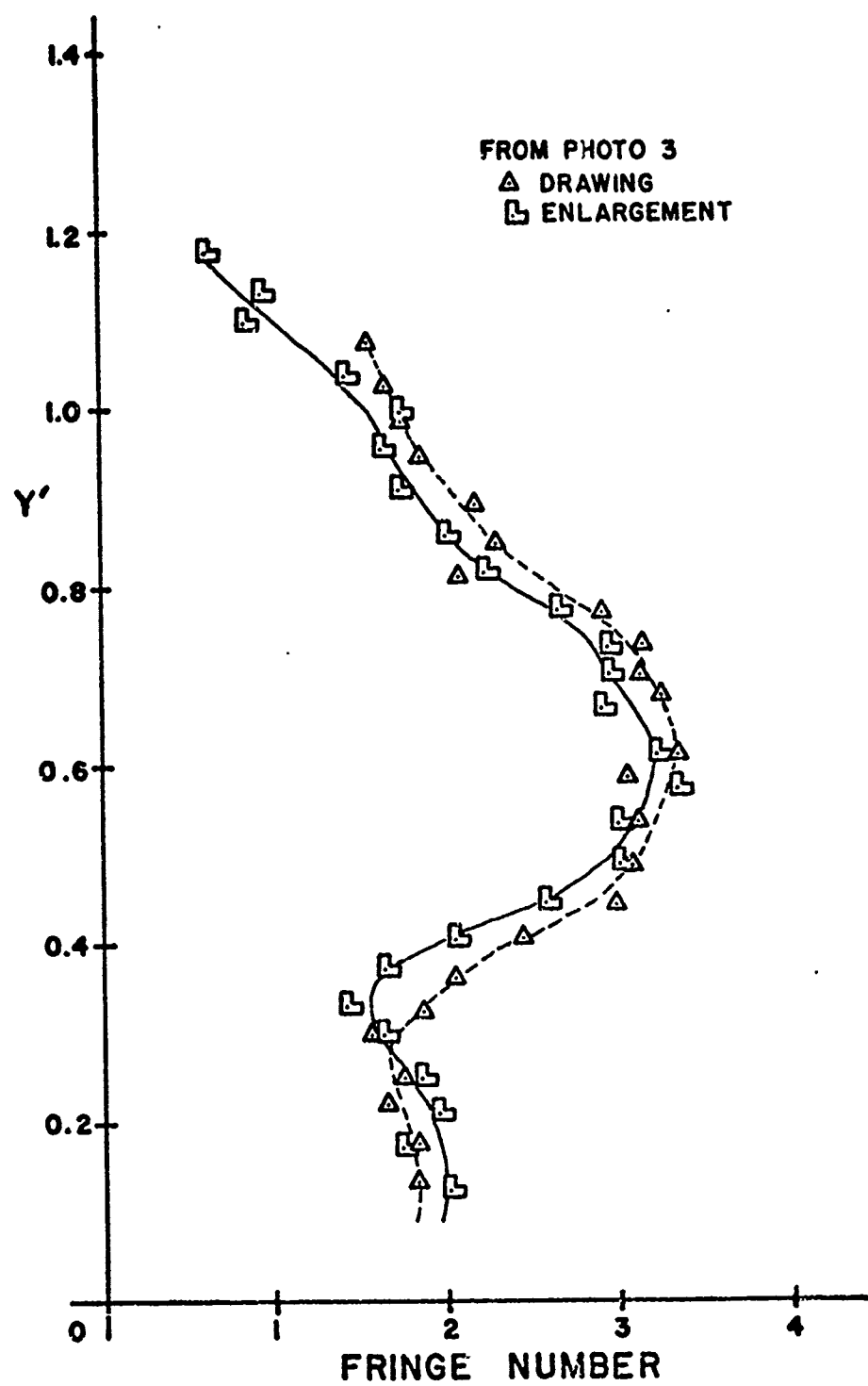


Figure 46. Comparison of Fringe Data Obtained from the Drawing and Photographic Enlargement of Interferogram Photograph 3 Aligned at $Y' = 0.451$

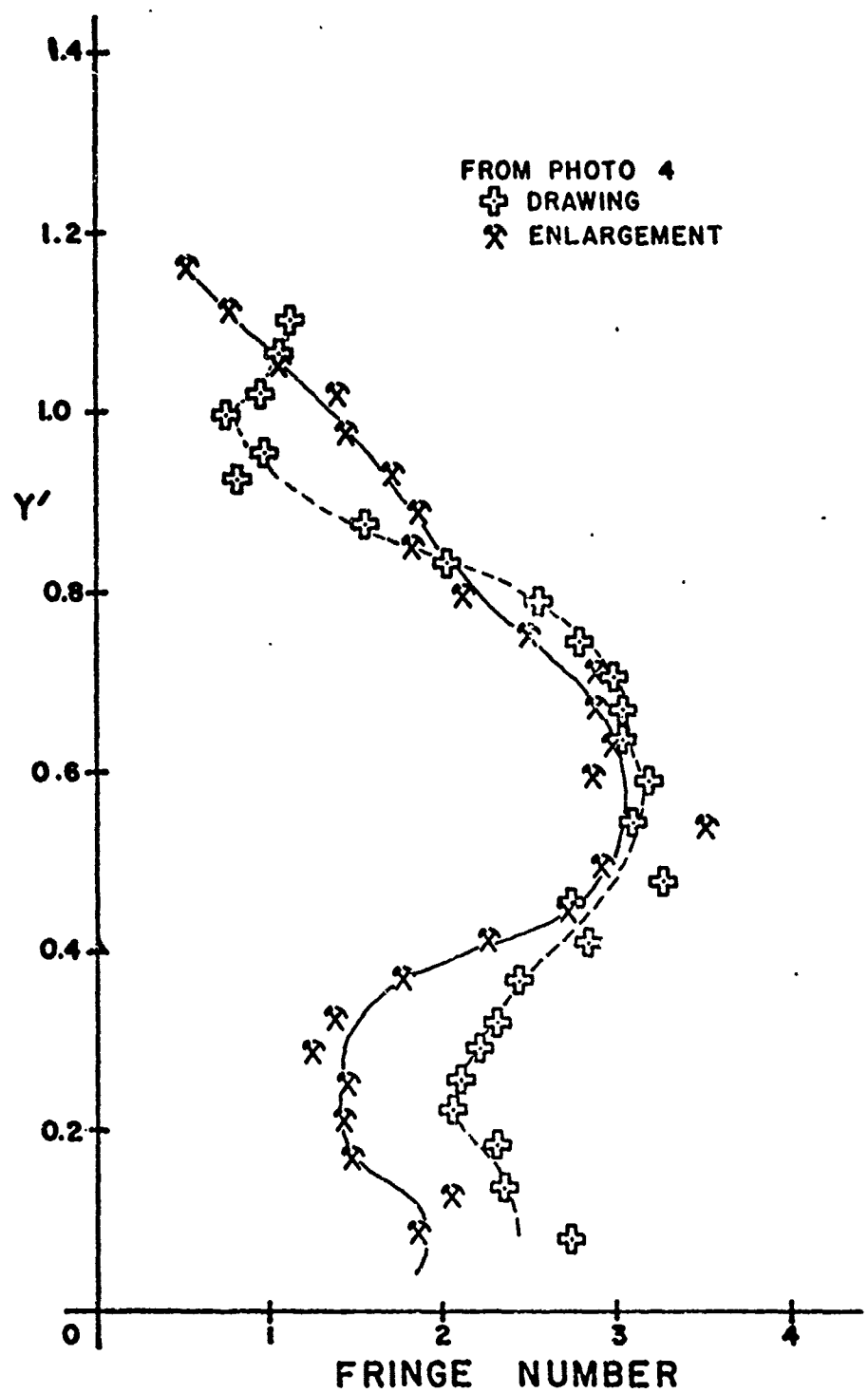


Figure 47. Comparison of Fringe Data Obtained from the Drawing and Photographic Enlargement of Interferogram Photograph 4 Aligned at $Y' = 0.055$

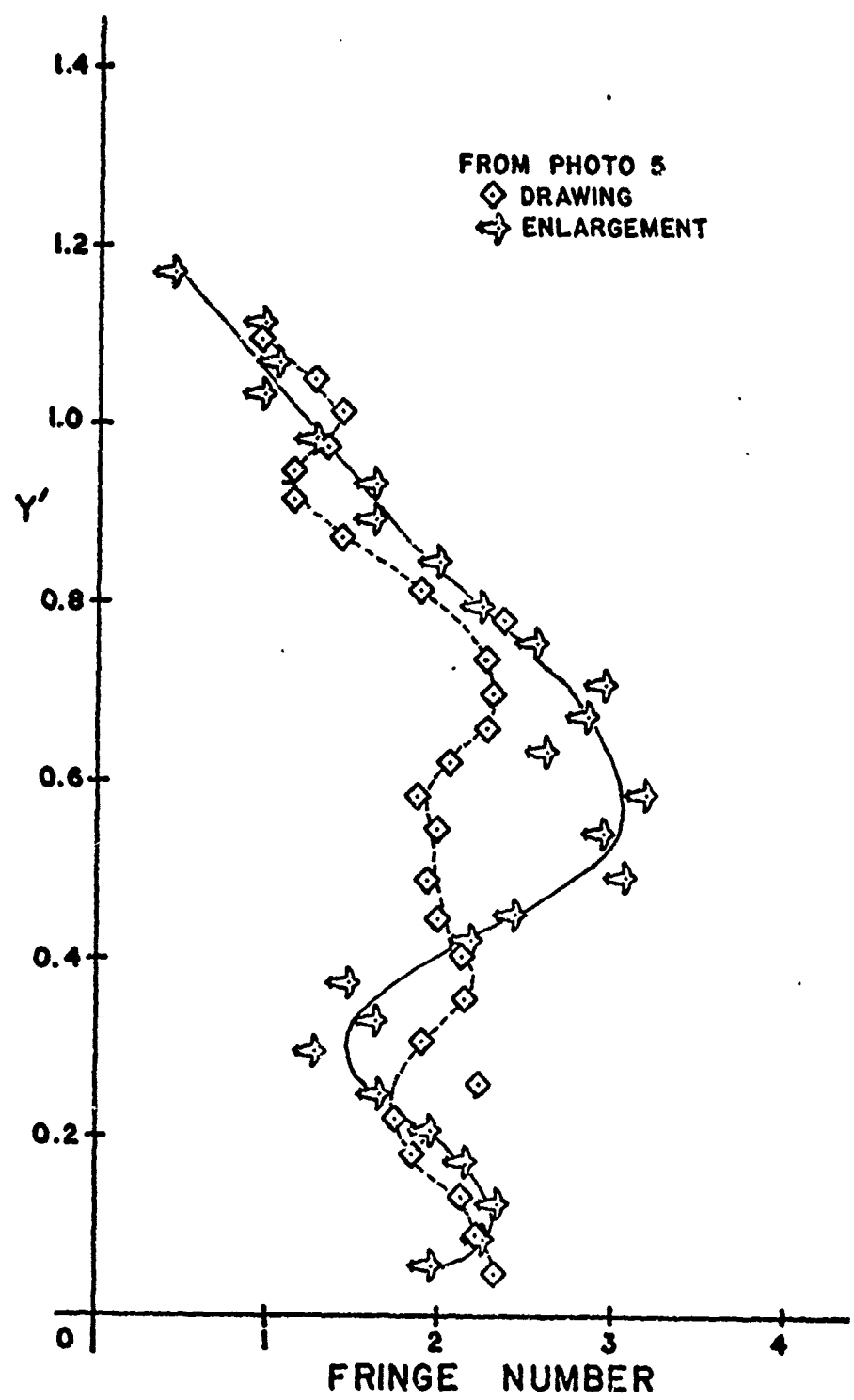


Figure 42. Comparison of Fringe Data Obtained from the Drawing and Photographic Enlargement of Interferogram Photograph 5 Aligned at $Y' = 0.055$

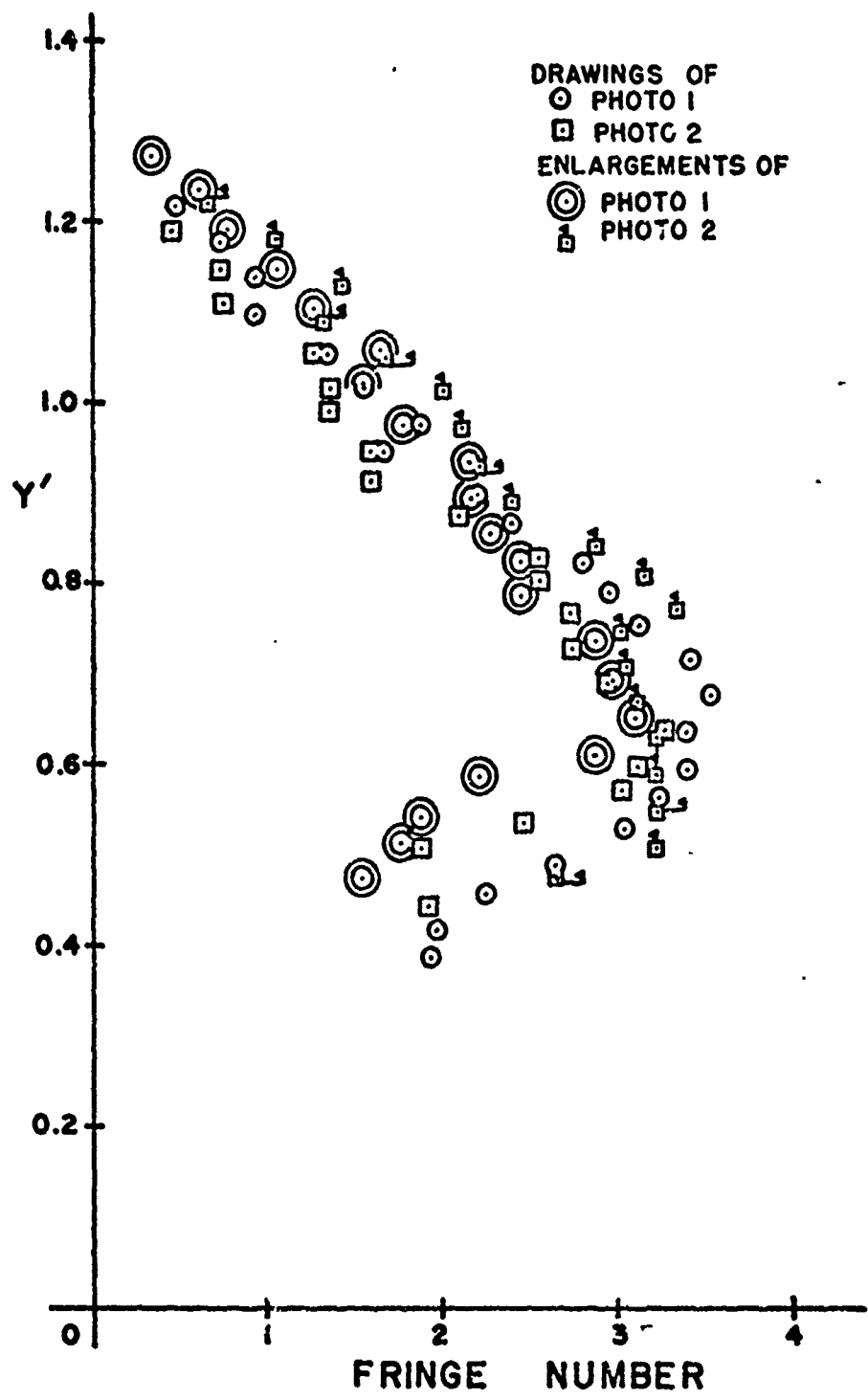


Figure 49. Comparison of Fringe Data Obtained from the Drawings and Photographic Enlargements of Interferogram Photographs 1 and 2 Aligned at $Y' = 0.847$

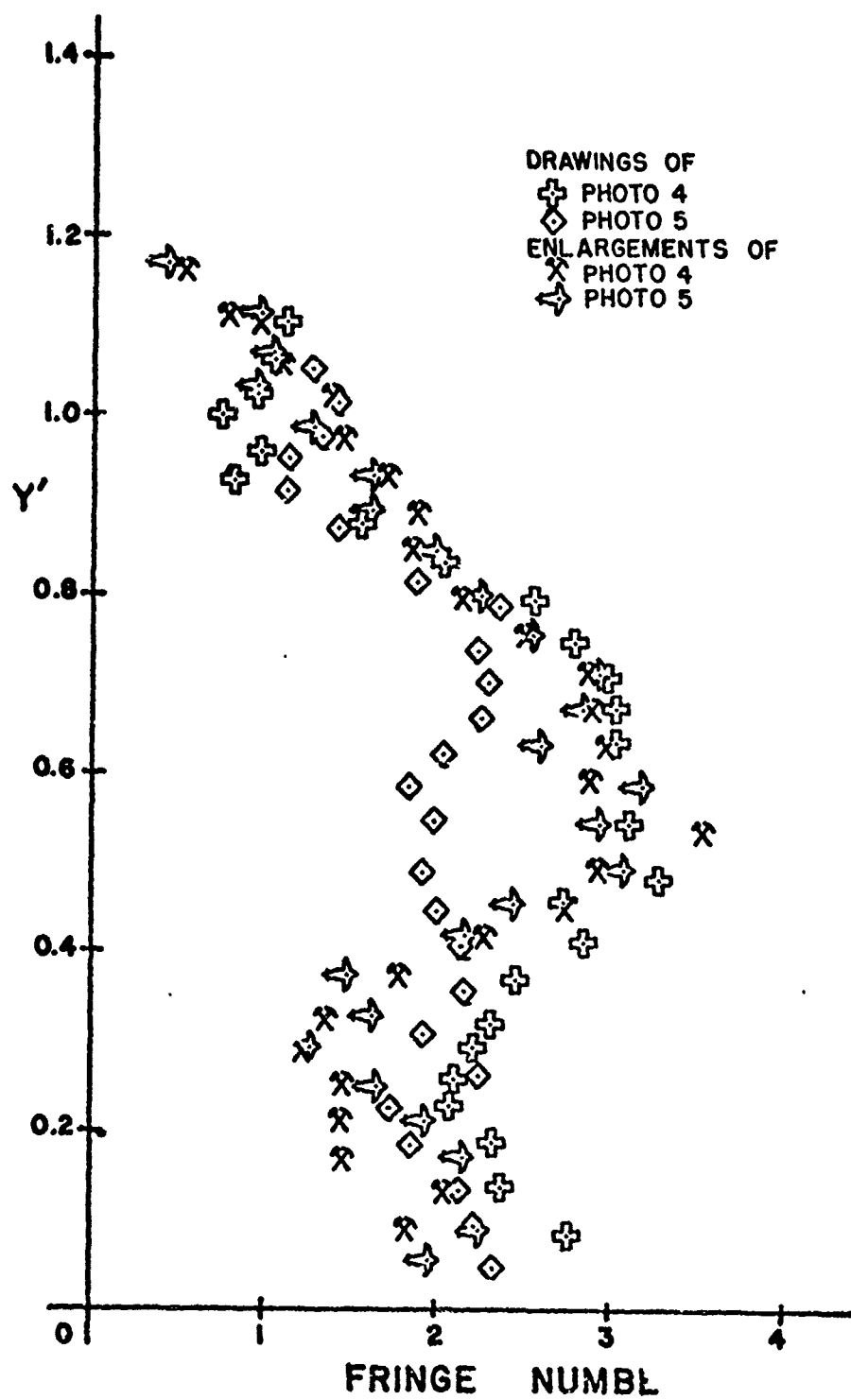


Figure 50. Comparison of Fringe Data Obtained from the Drawings and Photographic Enlargements of Interferogram Photographs 4 and 5 Aligned at $Y' = 0.055$

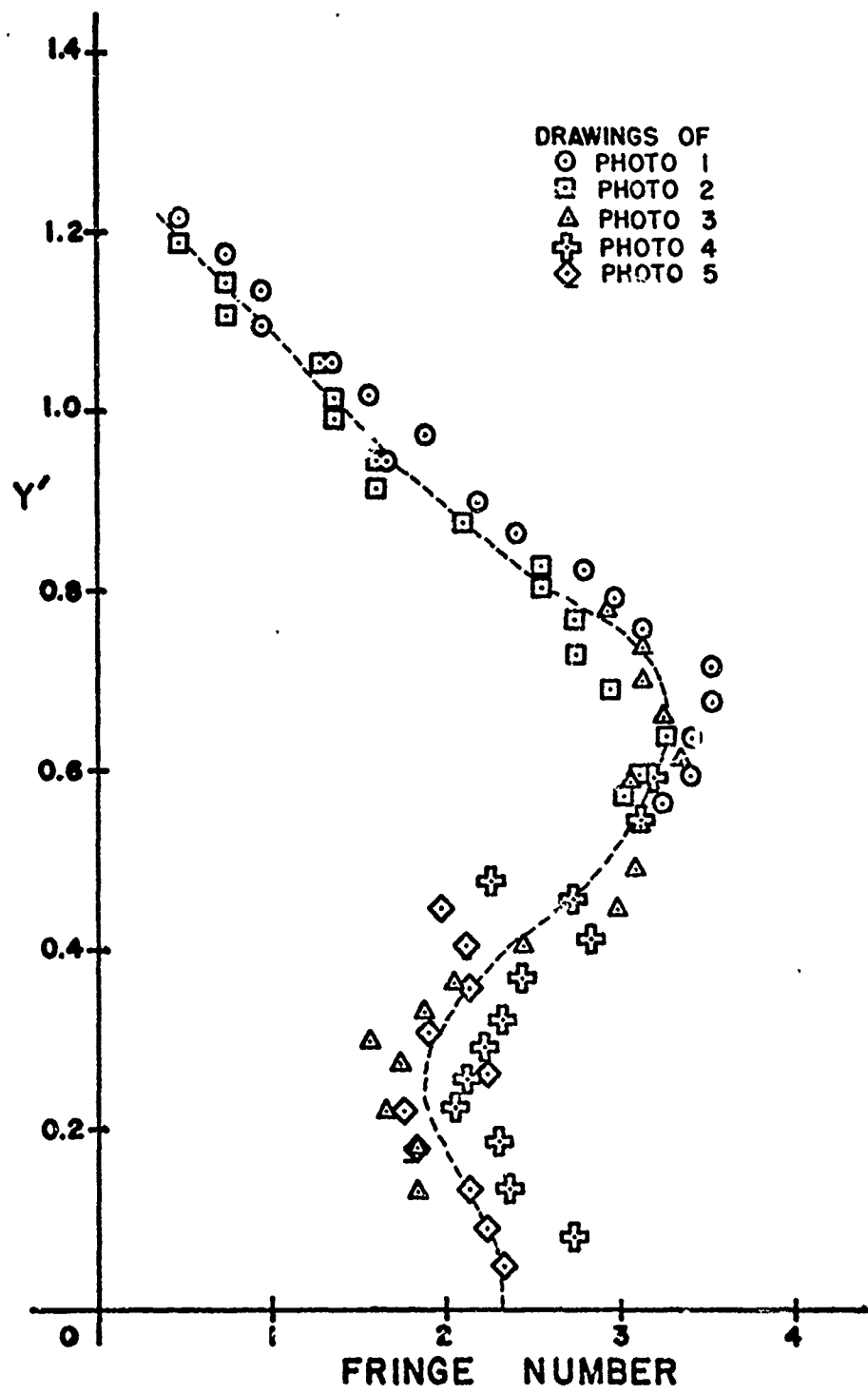


Figure 51. Fringe Number Across the Fin in the $Z = 0.387$ Plane for $3^\circ \alpha$, Mach 2.84 as Determined from the Drawings of the Interferogram Photographs

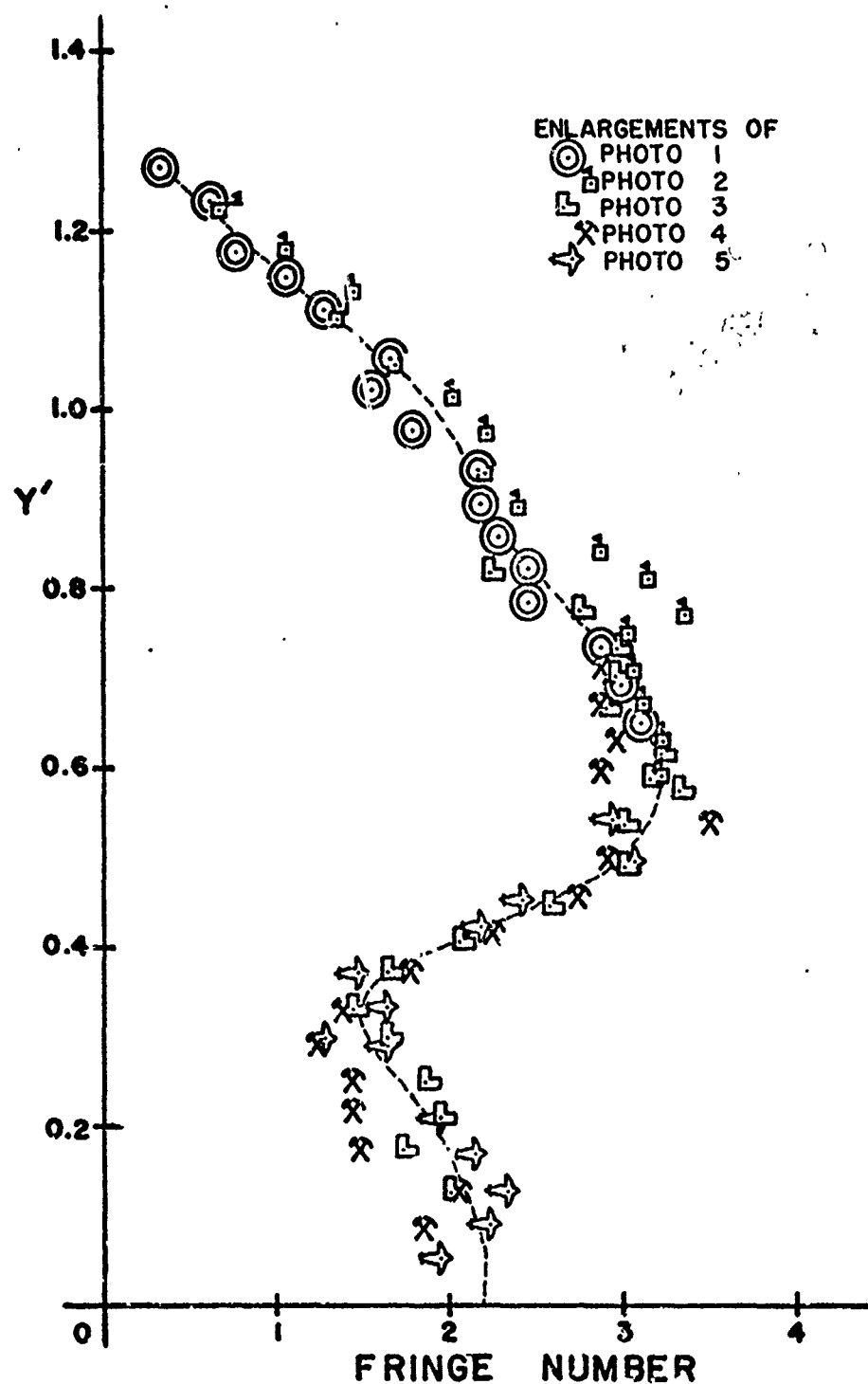


Figure 52. Fringe Number Across the Fin in the $Z = 0.387$ Plane for $\delta = 0^\circ$, Mach 2.84 as Determined from the Photographic Enlargements of the Interferogram Photographs

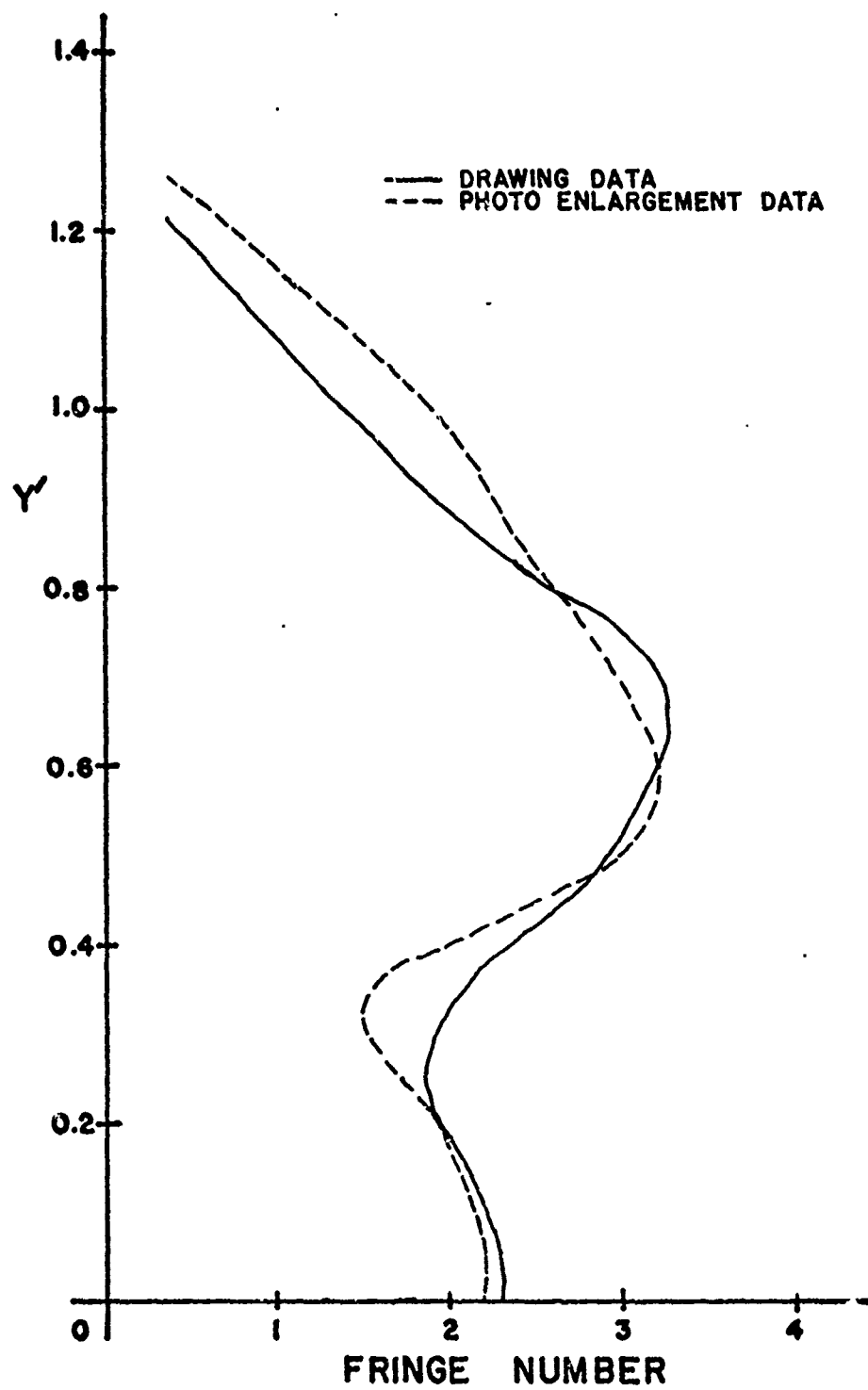


Figure 53. Comparison of the Fringe Numbers Across the Fin in the $Z = 0.387$ Plane for $\xi = 0^\circ$, Mach 2.84 as Determined from the Drawings and Photographic Enlargements of the Interferogram Photographs

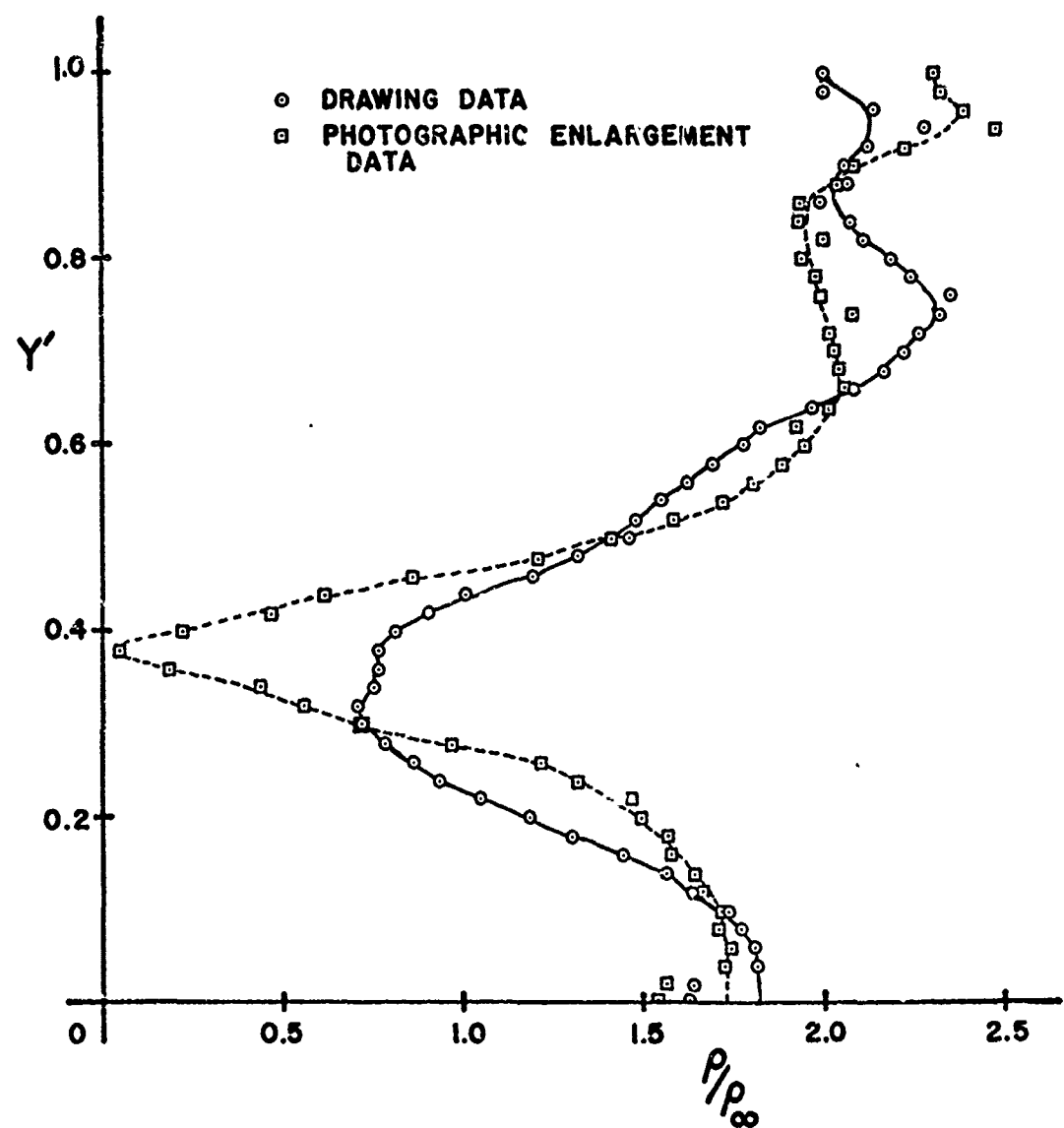


Figure 5'. Comparison of the Density Distributions Calculated by HOLOVIK for an Axisymmetric Case

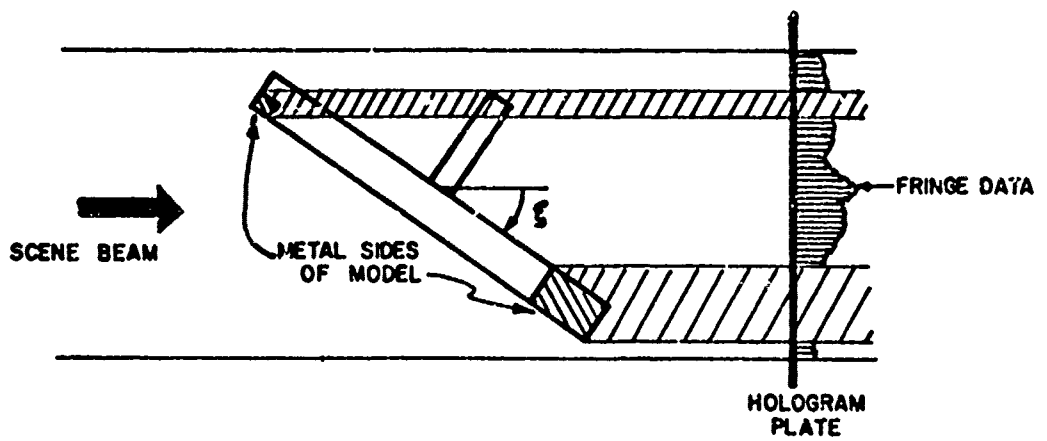


Figure 55. Schematic of the Model Center Section Rotated to Illustrate the Loss of Fringe Information Due to Model Shadows on the Hologram

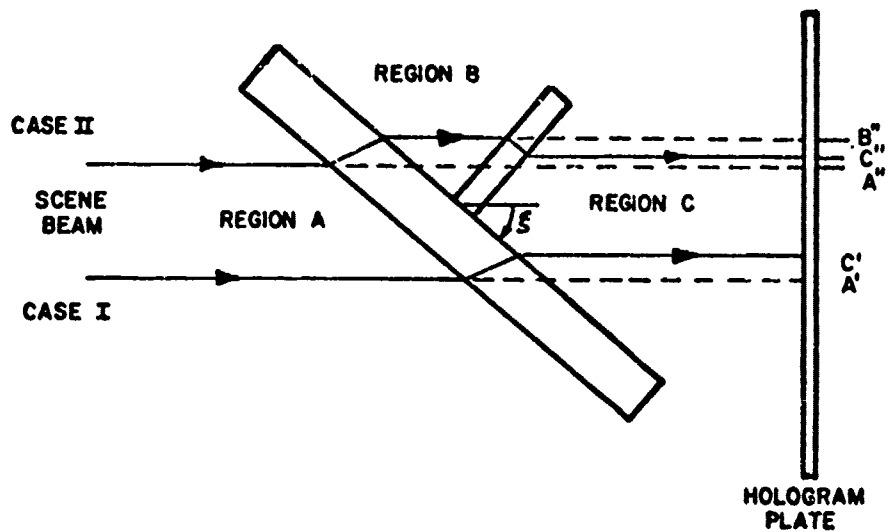


Figure 56. Schematic Illustrating the Problem of Different Fringe Information Being Superimposed on One Beam Caused by the Model Plastic.

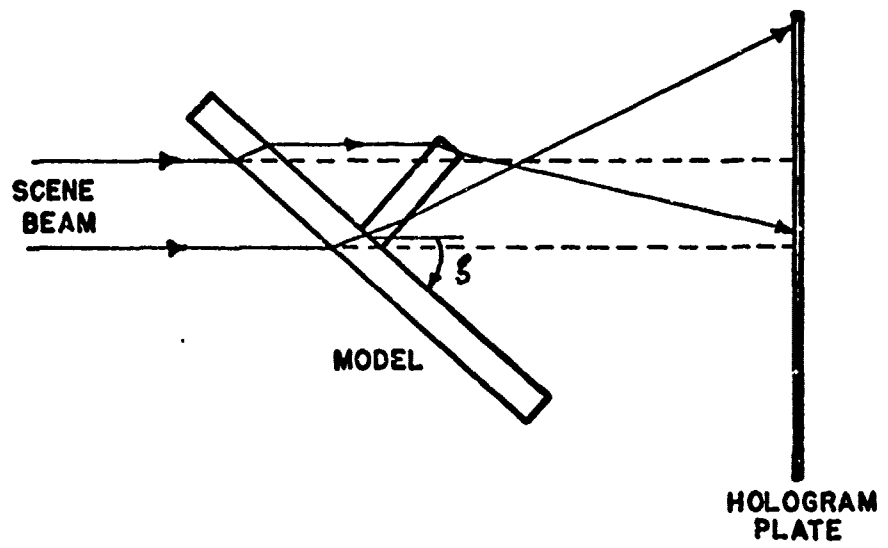


Figure 52. Schematic Illustrating the Scene Beam Refraction in the Fin Root and Tip Areas

Wing height = 2.52 inches

Wing length = 2.92 inches

Average fringe interval = .1036 inches

Table I. Tabulation of Fringe Shift Data Taken From the Drawing of Photo 4

Line No.	Distance Above Aligned Plane		$\Theta + .055$	Fringe Location (inches)	Fringe Change $f = \Theta - \Theta_0$	Fringe Number $R = \frac{f}{h}$	Amount of 1.1 Fringe Correction Required	Corrected Values
	Measured (inches)	Normalized wing height						
1	.190	.075	.071	.126	.360	.170	1.641	.081
2	.330	.131	.124	.179	.460	.130	1.255	.134
3	.465	.185	.176	.221	.590	.125	1.208	.186
4	.570	.226	.215	.270	.710	.100	1.1	2.31
5	.660	.262	.249	.304	.765	.105	1.013	.225
6	.745	.296	.281	.336	.860	.115	1.110	.254
7	.825	.327	.311	.366	.950	.125	1.208	.291
8	.950	.377	.358	.413	1.090	.140	1.352	.321
9	1.060	.421	.400	.455	1.240	.180	1.737	.368
10	1.180	.468	.445	.500	1.350	.170	1.641	.410
11	1.245	.494	.469	.524	1.500	.255	2.172	.455
12	1.350	.536	.509	.564	-	.160	.547	2.76
13	1.430	.567	.539	.594	1.750	.320	3.090	.543
14	1.513	.609	.579	.634	1.850	.315	3.061	.590
15	1.625	.649	.617	.672	1.940	.315	3.041	.634
16	1.720	.683	.649	.704	2.030	.310	2.994	.672
17	1.830	.726	.690	.745	2.120	.290	2.800	.704
18	1.955	.776	.737	.792	2.220	.265	2.560	.745
19	2.080	.825	.783	.838	2.290	.210	2.028	.792
20	2.180	.865	.821	.876	2.340	.160	1.545	2.56
21	2.315	.919	.872	.927	2.400	.085	.876	3.03
22	2.400	.952	.904	.959	2.500	.200	.927	.876
23	2.500	.992	.942	.997	2.580	.086	.772	.927
24	2.570	1.020	.969	1.024	2.670	.100	.965	.997
25	2.680	1.063	1.009	1.064	2.790	.110	1.062	.97
26	2.780	1.103	1.046	1.103	2.885	.115	1.110	1.064
								1.11

Line No.	Distance Above Aligned Plane Measured (inches) ①	Corrected to Free Stream (inches) ②	Normalized (wing height) ③	Corrected Distance from Tables ④		Y' = ① + .055	Fringe Location (inches) ⑤	Fringe Change f = ④ - ⑤	Fringe Number g = $\frac{f}{b}$
				①	③				
1	.190*	.076	.032	.030	.085	.270	.194	.1867	2.050
2	.290	.176	.073	.069	.124	.390	.214	.1482	1.434
3	.410*	.296	.123	.117	.172	.450	.154	.149	1.434
4	.525*	.411	.171	.162	.217	.560	.149	.149	1.242
5	.615*	.501	.208	.198	.253	.650	.129	.129	1.386
6	.710*	.596	.247	.235	.290	.725	.144	.184	1.771
7	.800*	.686	.285	.271	.326	.830	.234	.234	2.252
8	.910*	.796	.330	.314	.369	.980	.284	.284	2.738
9	1.020*	.906	.376	.357	.412	1.140	.304	.304	3.503
10	1.120*	1.006	.417	.396	.451	1.290	.364	.364	2.887
11	1.230*	1.116	.463	.440	.495	1.420	.300	.300	2.984
12	1.330*	1.216	.505	.480	.535	1.580	.360	.360	2.502
13	1.370	1.370	.568	.540	.595	1.670	.310	.310	2.117
14	1.460	1.460	.606	.576	.631	1.770	.220	.220	2.887
15	1.560	1.560	.647	.615	.670	1.860	.190	.190	1.829
16	1.660	1.660	.689	.655	.710	1.960	.195	.195	1.877
17	1.760	1.760	.730	.694	.749	2.020	.260	.260	1.704
18	1.880	1.880	.780	.741	.796	2.100	.150	.150	1.444
19	2.000	2.000	.830	.788	.843	2.190	.109	.109	1.396
20	2.110	2.110	.876	.832	.887	2.305	.110	.110	1.059
21	2.220	2.220	.921	.875	.930	2.390	.060	.060	.770
22	2.330	2.330	.967	.919	.974	2.480	.055	.055	.529
23	2.445	2.445	1.015	.964	1.019	2.590	.145	.145	1.059
24	2.570	2.570	1.066	1.013	1.068	2.680	.060	.060	1.059
25	2.680	2.680	1.112	1.056	1.111	2.760	.055	.055	1.059
26	2.805	2.805	1.164	1.106	1.161	2.860	.055	.055	1.059

* Locations to be corrected to free stream conditions
 Table II. Tabulation of Fringe Shift Data Taken From the Photographic Enlargement of Photo 4

APPENDIX A

REDUCTION OF AN INTERFEROGRAM TO OBTAIN FRINGE SHIFT DATA

The fringe shift reduction process was accomplished using two techniques. The first involved projecting the interferogram negative onto a sheet of white paper using a photo-enlarger. The light fringes offered the best contrast and were therefore traced out in Figures 30-34. In each drawing it was necessary to begin tracing the fringes above the fin and work towards the fin root since the transition across the fin tip determined the correct connection of the fringes across the fin leading edge shock. In order to determine the fringe change, one fringe line in the free stream region forward of the fin which appeared the straightest and paralleled the majority of other fringe lines was selected. A straight line, called the fringe reference line, was drawn over its centerline and extended to cross the y' axis. The remaining reference lines were then drawn parallel to the first and along the centerlines of the remaining free stream fringes. In reducing the drawings it was not realized until later that the free stream fringe patterns before and after the plate leading edge Prandtl-Meyer expansion differed considerably. This effect was taken into account later.

A ruler scaled to 0.01 inches was then placed along the y' axis and the distances of the fringes and reference lines above and below the aligned y' plane were then recorded in Table I for Photograph 4. The fin width and length were then measured and the average values were recorded. The average fringe interval was determined by measuring the distance between the first and last fringes used and dividing by the number of intervals. The fringe change was found by subtracting the fringe crossing

point. The fringe number was calculated by dividing the change by the average fringe interval. The reference line location was then normalized with respect to the measured fin height. Since the actual fin height was very close to one inch, the above number was considered to be the number of inches above or below the aligned plane. Thus the table computing the tunnel wall and grid refraction displacements in Appendix B could be entered to determine the actual reference line location with respect to the aligned plane of the drawing (see Figure 29). The locations were then converted to the y' axis system by adding the normalized location of the aligned plane. After realizing that not all the reference lines were referenced to the free stream density forward of the plate leading edge, the enlarged photographs (Figures 35-39) were checked against the drawings. It was found that the Prandtl-Meyer expansion caused a fringe number change of approximately 1.1. Consequently each reference line in the drawing was compared with the enlarged photograph and an appropriate percentage of the 1.1 fringe number was used as a correction (see Table I). The calculated fringe numbers had the correction fringe number added to them while the y' locations were corrected by

$$y'^{\text{corr}} = y'^{\text{orig}} - \frac{(1.1 \text{ Fringe no.}) \times (\text{Fringe Interval})}{(\text{Fin Height})} \quad (\text{A-1})$$

The second reduction technique was to use enlarged photographs made from the interferogram negatives to obtain the fringe change. The fringe lines were first traced over lightly with a pencil and then verified against the other photographs to ensure correct tracing. A datum fringe reference line was chosen as before and drawn. The remaining reference lines for the upper free stream fringe lines forward of the Prandtl-Meyer expansion were then drawn parallel to the datum. When it became impossible

to use fringe lines forward of the expansion, the reference lines were then drawn along the centerline of the fringes between the expansion and the fin. The same ruler was used to obtain the fringe crossing points, the reference crossing points, fin measurements, and the average fringe interval and they were recorded in Table 2. The reference line crossing points were then corrected to free stream conditions, using a 1.1 Fringe number correction for those referenced to the pattern between the expansion and fin leading edge. The fringe number and reference fin locations were calculated as before. This method was considered more accurate because the reference lines and fringe lines could easily be rechecked for accuracy and corrected in the event that a fringe line was traced incorrectly or a reference line was misaligned. The accuracy was directly proportional to the hologram resolution which was not true for the drawings since the reference lines are drawn parallel to hand-drawn fringe lines.

APPENDIX B

CALCULATION OF TUNNEL WALL AND GRID PLASTIC REFRACTION CORRECTION

In the interferogram photographs used to obtain the fringe change, every point off the alignment axis will be slightly distorted due to the plastic tunnel wall and grid. This effect is illustrated in Figure 19. From Snells Law of Refraction, the angles of incidence and refraction are related by

$$\sin \alpha = n \sin \beta \quad (B-1)$$

where n is the index of refraction between plastic and air. Then can be written

$$\beta = \sin^{-1} \left(\frac{\sin \alpha}{n} \right) \quad (B-2)$$

Since the tunnel wall and grid have the same index of refraction, they can be considered on material with thickness $t = ab$ in Figure 19. Then consider the height bd which can be written

$$bd = t \tan \alpha \quad (B-3)$$

The beam displacement, Δy , is then

$$\Delta Y = bd - bc = t \tan \alpha - t \tan \beta \quad (B-4)$$

but $\tan \alpha$ is

$$\tan \alpha = \frac{y_{\text{observed}}}{L} \quad (B-5)$$

Combining Equation (B-2), (B-4), and (B-5) the beam displacement becomes

$$\Delta Y = t \left[\frac{y_{\text{observed}}}{L} - \tan \left[\sin^{-1} \left(\frac{\sin \alpha}{n} \right) \right] \right] \quad (B-6)$$

The true location of the observed point is then

$$y_{\text{true}} = y_{\text{observed}} - \Delta Y \quad (B-7)$$

A FORTRAN computer program was written to generate a table giving the true locations versus the observed locations. In the program the constants and variables from the above equations were defined as

$$\begin{aligned}Y_{\text{observed}} &= Y \\Y_{\text{true}} &= Y_{\text{TRUE}} \\\Delta Y &= DY \\&= ALFA \\L &= L \\n &= N\end{aligned}$$

Since the computer cannot calculate Equations (B-2) and (B-6) as written, they were constructed by parts using such letters as AA, AB, etc. The program and tables are included in the next few pages.

THE FOLLOWING TABLE IS TO ACCOUNT FOR THE PARALLAX
ERROR IN VIEWING THE MODEL THROUGH GLASS WALLS AT
ANY OTHER POINT THAN AT THE ALIGNMENT POINT. INPUT
PARAMETERS ARE:

- (1) L = 15.000 INCHES
- (2) N = 1.500 INCHES
- (3) T = 2.250 INCHES

OBSERVED DISTANCE (INCHES)	TRUE DISTANCE (INCHES)	ERROR (INCHES)	RAY ANGLE (DEGREES)
0.0	0.0	0.0	0.0
0.0020	0.0019	0.000100	0.0076
0.0040	0.0038	0.000200	0.0153
0.0060	0.0057	0.000300	0.0229
0.0080	0.0076	0.000400	0.0306
0.0100	0.0095	0.000500	0.0382
0.0120	0.0114	0.000600	0.0458
0.0140	0.0133	0.000700	0.0535
0.0160	0.0152	0.000800	0.0611
0.0180	0.0171	0.000900	0.0688
0.0200	0.0190	0.001000	0.0764
0.0220	0.0209	0.001100	0.0840
0.0240	0.0228	0.001200	0.0917
0.0260	0.0247	0.001300	0.0993
0.0280	0.0266	0.001400	0.1070
0.0300	0.0285	0.001500	0.1146
0.0320	0.0304	0.001600	0.1222
0.0340	0.0323	0.001700	0.1299
0.0360	0.0342	0.001800	0.1375
0.0380	0.0361	0.001900	0.1451
0.0400	0.0380	0.002000	0.1528
0.0420	0.0399	0.002100	0.1604
0.0440	0.0418	0.002200	0.1681
0.0460	0.0437	0.002300	0.1757
0.0480	0.0456	0.002400	0.1833
0.0500	0.0475	0.002500	0.1910
0.0520	0.0494	0.002600	0.1986
0.0540	0.0513	0.002700	0.2063
0.0560	0.0532	0.002800	0.2139
0.0580	0.0551	0.002900	0.2215
0.0600	0.0570	0.003000	0.2292
0.0620	0.0589	0.003100	0.2368
0.0640	0.0608	0.003200	0.2445
0.0660	0.0627	0.003300	0.2521
0.0680	0.0646	0.003400	0.2597
0.0700	0.0665	0.003500	0.2674
0.0720	0.0684	0.003600	0.2750
0.0740	0.0703	0.003700	0.2827
0.0760	0.0722	0.003800	0.2903
0.0780	0.0741	0.003900	0.2979
0.0800	0.0760	0.004000	0.3056
0.0820	0.0779	0.004100	0.3132
0.0840	0.0798	0.004200	0.3209
0.0860	0.0817	0.004300	0.3285
0.0880	0.0836	0.004400	0.3361
0.0900	0.0855	0.004500	0.3438
0.0920	0.0874	0.004600	0.3514
0.0940	0.0893	0.004700	0.3590
0.0960	0.0912	0.004800	0.3667
0.0980	0.0931	0.004900	0.3743
0.1000	0.0950	0.005000	0.3820
0.1020	0.0969	0.005100	0.3896
0.1040	0.0988	0.005200	0.3972
0.1060	0.1007	0.005300	0.4049
0.1080	0.1026	0.005400	0.4125
0.1100	0.1045	0.005500	0.4202
0.1120	0.1064	0.005600	0.4278
0.1140	0.1083	0.005700	0.4354
0.1160	0.1102	0.005800	0.4431
0.1180	0.1121	0.005900	0.4507

OBSERVED DISTANCE (INCHES)	TRUE DISTANCE (INCHES)	ERROR (INCHES)	RAY ANGLE (DEGREES)
0.1200	0.1140	0.006000	0.4584
0.1220	0.1159	0.006100	0.4660
0.1240	0.1178	0.006200	0.4736
0.1260	0.1197	0.006300	0.4813
0.1280	0.1216	0.006400	0.4889
0.1300	0.1235	0.006500	0.4966
0.1320	0.1254	0.006600	0.5042
0.1340	0.1273	0.006700	0.5118
0.1360	0.1292	0.006800	0.5195
0.1380	0.1311	0.006900	0.5271
0.1400	0.1330	0.007000	0.5347
0.1420	0.1349	0.007100	0.5424
0.1440	0.1368	0.007200	0.5500
0.1460	0.1387	0.007300	0.5577
0.1480	0.1406	0.007400	0.5653
0.1500	0.1425	0.007500	0.5729
0.1520	0.1444	0.007600	0.5806
0.1540	0.1463	0.007700	0.5882
0.1560	0.1482	0.007800	0.5959
0.1580	0.1501	0.007901	0.6035
0.1600	0.1520	0.008001	0.6111
0.1620	0.1539	0.008101	0.6188
0.1640	0.1558	0.008201	0.6264
0.1660	0.1577	0.008301	0.6340
0.1680	0.1596	0.008401	0.6417
0.1700	0.1615	0.008501	0.6493
0.1720	0.1634	0.008601	0.6570
0.1740	0.1653	0.008701	0.6646
0.1760	0.1672	0.008801	0.6722
0.1780	0.1691	0.008901	0.6799
0.1800	0.1710	0.009001	0.6875
0.1820	0.1729	0.009101	0.6952
0.1840	0.1748	0.009201	0.7028
0.1860	0.1767	0.009301	0.7104
0.1880	0.1786	0.009401	0.7181
0.1900	0.1805	0.009501	0.7257
0.1920	0.1824	0.009601	0.7333
0.1940	0.1843	0.009701	0.7410
0.1960	0.1862	0.009801	0.7486
0.1980	0.1881	0.009901	0.7563
0.2000	0.1900	0.010001	0.7639
0.2020	0.1919	0.010101	0.7715
0.2040	0.1938	0.010201	0.7792
0.2060	0.1957	0.010301	0.7868
0.2080	0.1976	0.010401	0.7944
0.2100	0.1995	0.010501	0.8021
0.2120	0.2014	0.010601	0.8097
0.2140	0.2033	0.010701	0.8174
0.2160	0.2052	0.010801	0.8250
0.2180	0.2071	0.010901	0.8326
0.2200	0.2090	0.011001	0.8403
0.2220	0.2109	0.011101	0.8479
0.2240	0.2128	0.011201	0.8556
0.2260	0.2147	0.011301	0.8632
0.2280	0.2166	0.011401	0.8708
0.2300	0.2185	0.011502	0.8785
0.2320	0.2204	0.011602	0.8861
0.2340	0.2223	0.011702	0.8937
0.2360	0.2242	0.011802	0.9014
0.2380	0.2261	0.011902	0.9090

OBSERVED DISTANCE (INCHES)	TRUE DISTANCE (INCHES)	ERROR (INCHES)	RAY ANGLE (DEGREES)
0.2400	0.2280	0.012002	0.9167
0.2420	0.2299	0.012102	0.9243
0.2440	0.2318	0.012202	0.9319
0.2460	0.2337	0.012302	0.9396
0.2480	0.2356	0.012402	0.9472
0.2500	0.2375	0.012502	0.9548
0.2520	0.2394	0.012602	0.9625
0.2540	0.2413	0.012702	0.9701
0.2560	0.2432	0.012802	0.9778
0.2580	0.2451	0.012902	0.9854
0.2600	0.2470	0.013002	0.9930
0.2620	0.2489	0.013102	1.0007
0.2640	0.2508	0.013202	1.0083
0.2660	0.2527	0.013302	1.0159
0.2680	0.2546	0.013402	1.0236
0.2700	0.2565	0.013502	1.0312
0.2720	0.2584	0.013602	1.0388
0.2740	0.2603	0.013703	1.0465
0.2760	0.2622	0.013803	1.0541
0.2780	0.2641	0.013903	1.0618
0.2800	0.2660	0.014003	1.0694
0.2820	0.2679	0.014103	1.0770
0.2840	0.2698	0.014203	1.0847
0.2860	0.2717	0.014303	1.0923
0.2880	0.2736	0.014403	1.0999
0.2900	0.2755	0.014503	1.1076
0.2920	0.2774	0.014603	1.1152
0.2940	0.2793	0.014703	1.1229
0.2950	0.2812	0.014803	1.1305
0.2980	0.2831	0.014903	1.1381
0.3000	0.2850	0.015003	1.1458
0.3020	0.2869	0.015103	1.1534
0.3040	0.2888	0.015203	1.1610
0.3060	0.2907	0.015304	1.1687
0.3080	0.2926	0.015404	1.1763
0.3100	0.2945	0.015504	1.1839
0.3120	0.2964	0.015604	1.1916
0.3140	0.2983	0.015704	1.1992
0.3160	0.3002	0.015804	1.2069
0.3180	0.3021	0.015904	1.2145
0.3200	0.3040	0.016004	1.2221
0.3220	0.3059	0.016104	1.2298
0.3240	0.3078	0.016204	1.2374
0.3260	0.3097	0.016304	1.2450
0.3280	0.3116	0.016404	1.2527
0.3300	0.3135	0.016504	1.2603
0.3320	0.3154	0.016605	1.2679
0.3340	0.3173	0.016705	1.2756
0.3360	0.3192	0.016805	1.2832
0.3380	0.3211	0.016905	1.2908
0.3400	0.3230	0.017005	1.2985
0.3420	0.3249	0.017105	1.3061
0.3440	0.3268	0.017205	1.3138
0.3460	0.3287	0.017305	1.3214
0.3480	0.3306	0.017405	1.3290
0.3500	0.3325	0.017505	1.3367
0.3520	0.3344	0.017605	1.3443
0.3540	0.3363	0.017705	1.3519
0.3560	0.3382	0.017806	1.3596
0.3580	0.3401	0.017906	1.3672

OBSERVED DISTANCE (INCHES)	TRUE DISTANCE (INCHES)	ERROR (INCHES)	RAY ANGLE (DEGREES)
0.3600	0.3420	0.018006	1.3748
0.3620	0.3439	0.018106	1.3825
0.3640	0.3458	0.018206	1.3901
0.3660	0.3477	0.018306	1.3977
0.3680	0.3496	0.018406	1.4054
0.3700	0.3515	0.018506	1.4130
0.3720	0.3534	0.018606	1.4206
0.3740	0.3553	0.018706	1.4283
0.3760	0.3572	0.018807	1.4359
0.3780	0.3591	0.018907	1.4435
0.3800	0.3610	0.019007	1.4512
0.3820	0.3629	0.019107	1.4588
0.3840	0.3648	0.019207	1.4665
0.3860	0.3667	0.019307	1.4741
0.3880	0.3686	0.019407	1.4817
0.3900	0.3705	0.019507	1.4894
0.3920	0.3724	0.019607	1.4970
0.3940	0.3743	0.019708	1.5046
0.3960	0.3762	0.019808	1.5123
0.3980	0.3781	0.019908	1.5199
0.4000	0.3800	0.020008	1.5275
0.4020	0.3819	0.020108	1.5352
0.4040	0.3838	0.020208	1.5428
0.4060	0.3857	0.020308	1.5504
0.4080	0.3876	0.020408	1.5581
0.4100	0.3895	0.020509	1.5657
0.4120	0.3914	0.020609	1.5733
0.4140	0.3933	0.020709	1.5810
0.4160	0.3952	0.020809	1.5886
0.4180	0.3971	0.020909	1.5962
0.4200	0.3990	0.021009	1.6039
0.4220	0.4009	0.021109	1.6115
0.4240	0.4028	0.021209	1.6191
0.4260	0.4047	0.021310	1.6268
0.4280	0.4066	0.021410	1.6344
0.4300	0.4085	0.021510	1.6420
0.4320	0.4104	0.021610	1.6497
0.4340	0.4123	0.021710	1.6573
0.4360	0.4142	0.021810	1.6649
0.4380	0.4161	0.021910	1.6726
0.4400	0.4180	0.022011	1.6802
0.4420	0.4199	0.022111	1.6878
0.4440	0.4218	0.022211	1.6955
0.4460	0.4237	0.022311	1.7031
0.4480	0.4256	0.022411	1.7107
0.4500	0.4275	0.022511	1.7184
0.4520	0.4294	0.022611	1.7260
0.4540	0.4313	0.022712	1.7336
0.4560	0.4332	0.022812	1.7413
0.4580	0.4351	0.022912	1.7489
0.4600	0.4370	0.023012	1.7565
0.4620	0.4389	0.023112	1.7642
0.4640	0.4408	0.023212	1.7718
0.4660	0.4427	0.023312	1.7794
0.4680	0.4446	0.023413	1.7870
0.4700	0.4465	0.023513	1.7947
0.4720	0.4484	0.023613	1.8023
0.4740	0.4503	0.023713	1.8099
0.4760	0.4522	0.023813	1.8176
0.4780	0.4541	0.023913	1.8252

OBSERVED DISTANCE (INCHES)	TRUE DISTANCE (INCHES)	ERROR (INCHES)	RAY ANGLE (DEGREES)
0.4800	0.4560	0.024014	1.8328
0.4820	0.4579	0.024114	1.8405
0.4840	0.4598	0.024214	1.8481
0.4860	0.4617	0.024314	1.8557
0.4880	0.4636	0.024414	1.8634
0.4900	0.4655	0.024515	1.8710
0.4920	0.4674	0.024615	1.8786
0.4940	0.4693	0.024715	1.8863
0.4960	0.4712	0.024815	1.8939
0.4980	0.4731	0.024915	1.9015
0.5000	0.4750	0.025015	1.9092
0.5020	0.4769	0.025116	1.9168
0.5040	0.4788	0.025216	1.9244
0.5060	0.4807	0.025316	1.9320
0.5080	0.4826	0.025416	1.9397
0.5100	0.4845	0.025516	1.9473
0.5120	0.4864	0.025617	1.9549
0.5140	0.4883	0.025717	1.9626
0.5160	0.4902	0.025817	1.9702
0.5180	0.4921	0.025917	1.9778
0.5200	0.4940	0.026017	1.9855
0.5220	0.4959	0.026118	1.9931
0.5240	0.4978	0.026218	2.0007
0.5260	0.4997	0.026318	2.0083
0.5280	0.5016	0.026418	2.0160
0.5300	0.5035	0.026518	2.0236
0.5320	0.5054	0.026619	2.0312
0.5340	0.5073	0.026719	2.0389
0.5360	0.5092	0.026819	2.0465
0.5380	0.5111	0.026919	2.0541
0.5400	0.5130	0.027019	2.0618
0.5420	0.5149	0.027120	2.0694
0.5440	0.5168	0.027220	2.0770
0.5460	0.5187	0.027320	2.0846
0.5480	0.5206	0.027420	2.0923
0.5500	0.5225	0.027521	2.0999
0.5520	0.5244	0.027621	2.1075
0.5540	0.5263	0.027721	2.1152
0.5560	0.5282	0.027821	2.1228
0.5580	0.5301	0.027921	2.1304
0.5600	0.5320	0.028022	2.1380
0.5620	0.5339	0.028122	2.1457
0.5640	0.5358	0.028222	2.1533
0.5660	0.5377	0.028322	2.1609
0.5680	0.5396	0.028423	2.1686
0.5700	0.5415	0.028523	2.1762
0.5720	0.5434	0.028623	2.1838
0.5740	0.5453	0.028723	2.1914
0.5760	0.5472	0.028824	2.1991
0.5780	0.5491	0.028924	2.2067
0.5800	0.5510	0.029024	2.2143
0.5820	0.5529	0.029124	2.2220
0.5840	0.5548	0.029225	2.2296
0.5860	0.5567	0.029325	2.2372
0.5880	0.5586	0.029425	2.2448
0.5900	0.5605	0.029525	2.2525
0.5920	0.5624	0.029625	2.2601
0.5940	0.5643	0.029726	2.2677
0.5960	0.5662	0.029826	2.2754
0.5980	0.5681	0.029926	2.2830

OBSERVED DISTANCE (INCHES)	TRUE DISTANCE (INCHES)	ERROR (INCHES)	RAY ANGLE (DEGREES)
0.6000	0.5700	0.030027	2.2906
0.6020	0.5719	0.030127	2.2982
0.6040	0.5738	0.030227	2.3059
0.6060	0.5757	0.030327	2.3135
0.6080	0.5776	0.030428	2.3211
0.6100	0.5795	0.030528	2.3287
0.6120	0.5814	0.030628	2.3364
0.6140	0.5833	0.030729	2.3440
0.6160	0.5852	0.030829	2.3516
0.6180	0.5871	0.030929	2.3593
0.6200	0.5890	0.031029	2.3669
0.6220	0.5909	0.031130	2.3745
0.6240	0.5928	0.031230	2.3821
0.6260	0.5947	0.031330	2.3898
0.6280	0.5966	0.031431	2.3974
0.6300	0.5985	0.031531	2.4050
0.6320	0.6004	0.031631	2.4126
0.634	0.6023	0.031731	2.4203
0.6360	0.6042	0.031832	2.4279
0.6380	0.6061	0.031932	2.4355
0.6400	0.6080	0.032032	2.4431
0.6420	0.6099	0.032133	2.4508
0.6440	0.6118	0.032233	2.4584
0.6460	0.6137	0.032333	2.4660
0.6480	0.6156	0.032434	2.4736
0.6500	0.6175	0.032534	2.4813
0.6520	0.6194	0.032634	2.4889
0.6540	0.6213	0.032735	2.4965
0.6560	0.6232	0.032835	2.5041
0.6580	0.6251	0.032935	2.5118
0.6600	0.6270	0.033035	2.5194
0.6620	0.6289	0.033136	2.5270
0.6640	0.6308	0.033231	2.5346
0.6660	0.6327	0.033336	2.5423
0.6680	0.6346	0.033437	2.5499
0.6700	0.6365	0.033537	2.5575
0.6720	0.6384	0.033637	2.5651
0.6740	0.6403	0.033738	2.5728
0.6760	0.6422	0.033838	2.5804
0.6780	0.6441	0.033938	2.5880
0.6800	0.6460	0.034039	2.5956
0.6820	0.6479	0.034139	2.6033
0.6840	0.6498	0.034239	2.6109
0.6860	0.6517	0.034340	2.6185
0.6880	0.6536	0.034440	2.6261
0.6900	0.6555	0.034541	2.6337
0.6920	0.6574	0.034641	2.6414
0.6940	0.6593	0.034741	2.6490
0.6960	0.6612	0.034842	2.6566
0.6980	0.6631	0.034942	2.6642
0.7000	0.6650	0.035042	2.6719
0.7020	0.6669	0.035143	2.6795
0.7040	0.6688	0.035243	2.6871
0.7060	0.6707	0.035343	2.6947
0.7080	0.6726	0.035444	2.7024
0.7100	0.6745	0.035544	2.7100
0.7120	0.6764	0.035645	2.7176
0.7140	0.6783	0.035745	2.7252
0.7160	0.6802	0.035845	2.7328
0.7180	0.6821	0.035946	2.7405

OBSERVED DISTANCE (INCHES)	TRUE DISTANCE (INCHES)	ERROR (INCHES)	RAY ANGLE (DEGREES)
0.7200	0.6840	0.036046	2.7481
0.7220	0.6859	0.036146	2.7557
0.7240	0.6878	0.036247	2.7633
0.7260	0.6897	0.036347	2.7710
0.7280	0.6916	0.036448	2.7786
0.7300	0.6935	0.036548	2.7862
0.7320	0.6954	0.036648	2.7938
0.7340	0.6973	0.036749	2.8014
0.7360	0.6992	0.036849	2.8091
0.7380	0.7011	0.036950	2.8167
0.7400	0.7029	0.037050	2.8243
0.7420	0.7048	0.037150	2.8319
0.7440	0.7067	0.037251	2.8395
0.7460	0.7086	0.037351	2.8472
0.7480	0.7105	0.037452	2.8548
0.7500	0.7124	0.037552	2.8624
0.7520	0.7143	0.037652	2.8700
0.7540	0.7162	0.037753	2.8776
0.7560	0.7181	0.037853	2.8853
0.7580	0.7200	0.037954	2.8929
0.7600	0.7219	0.038054	2.9005
0.7620	0.7238	0.038155	2.9081
0.7640	0.7257	0.038255	2.9157
0.7660	0.7276	0.038355	2.9234
0.7680	0.7295	0.038456	2.9310
0.7700	0.7314	0.038556	2.9386
0.7720	0.7333	0.038657	2.9462
0.7740	0.7352	0.038757	2.9538
0.7760	0.7371	0.038858	2.9615
0.7780	0.7390	0.038958	2.9691
0.7800	0.7409	0.039059	2.9767
0.7820	0.7428	0.039159	2.9843
0.7840	0.7447	0.039259	2.9919
0.7860	0.7466	0.039360	2.9996
0.7880	0.7485	0.039460	3.0072
0.7900	0.7504	0.039561	3.0148
0.7920	0.7523	0.039661	3.0224
0.7940	0.7542	0.039762	3.0300
0.7960	0.7561	0.039862	3.0376
0.7980	0.7580	0.039963	3.0453
0.8000	0.7599	0.040063	3.0529
0.8020	0.7618	0.040164	3.0605
0.8040	0.7637	0.040264	3.0681
0.8060	0.7656	0.040365	3.0757
0.8080	0.7675	0.040465	3.0834
0.8100	0.7694	0.040566	3.0910
0.8120	0.7713	0.040666	3.0986
0.8140	0.7732	0.040767	3.1062
0.8160	0.7751	0.040867	3.1138
0.8180	0.7770	0.040968	3.1214
0.8200	0.7789	0.041068	3.1291
0.8220	0.7808	0.041169	3.1367
0.8240	0.7827	0.041269	3.1443
0.8260	0.7846	0.041369	3.1519
0.8280	0.7865	0.041470	3.1595
0.8300	0.7884	0.041570	3.1671
0.8320	0.7903	0.041671	3.1748
0.8340	0.7922	0.041772	3.1824
0.8360	0.7941	0.041872	3.1900
0.8380	0.7960	0.041973	3.1976

OBSERVED DISTANCE (INCHES)	TRUE DISTANCE (INCHES)	ERROR (INCHES)	RAY ANGLE (DEGREES)
0.8400	0.7979	0.042073	3.2052
0.8420	0.7998	0.042174	3.2128
0.8440	0.8017	0.042274	3.2204
0.8460	0.8036	0.042375	3.2281
0.8480	0.8055	0.042475	3.2357
0.8500	0.8074	0.042576	3.2433
0.8520	0.8093	0.042676	3.2509
0.8540	0.8112	0.042777	3.2585
0.8560	0.8131	0.042877	3.2661
0.8580	0.8150	0.042978	3.2738
0.8600	0.8169	0.043078	3.2814
0.8620	0.8188	0.043179	3.2890
0.8640	0.8207	0.043280	3.2966
0.8660	0.8226	0.043380	3.3042
0.8680	0.8245	0.043481	3.3118
0.8700	0.8264	0.043581	3.3194
0.8720	0.8283	0.043682	3.3270
0.8740	0.8302	0.043782	3.3347
0.8760	0.8321	0.043883	3.3423
0.8780	0.8340	0.043983	3.3499
0.8800	0.8359	0.044084	3.3575
0.8820	0.8378	0.044185	3.3651
0.8840	0.8397	0.044285	3.3727
0.8860	0.8416	0.044386	3.3803
0.8880	0.8435	0.044486	3.3880
0.8900	0.8454	0.044587	3.3956
0.8920	0.8473	0.044688	3.4032
0.8940	0.8492	0.044788	3.4108
0.8960	0.8511	0.044889	3.4184
0.8980	0.8530	0.044989	3.4260
0.9000	0.8549	0.045090	3.4336
0.9020	0.8568	0.045190	3.4412
0.9040	0.8587	0.045291	3.4489
0.9060	0.8606	0.045392	3.4565
0.9080	0.8625	0.045492	3.4541
0.9100	0.8644	0.045593	3.4717
0.9120	0.8663	0.045693	3.4793
0.9140	0.8682	0.045794	3.4869
0.9160	0.8701	0.045895	3.4945
0.9180	0.8720	0.045995	3.5021
0.9200	0.8739	0.046096	3.5097
0.9220	0.8758	0.046197	3.5174
0.9240	0.8777	0.046297	3.5250
0.9260	0.8796	0.046398	3.5326
0.9280	0.8815	0.046499	3.5402
0.9300	0.8834	0.046599	3.5478
0.9320	0.8853	0.046700	3.5554
0.9340	0.8872	0.046800	3.5630
0.9360	0.8891	0.046901	3.5706
0.9380	0.8910	0.047002	3.5782
0.9400	0.8929	0.047102	3.5858
0.9420	0.8948	0.047203	3.5935
0.9440	0.8967	0.047304	3.6011
0.9460	0.8986	0.047404	3.6087
0.9480	0.9005	0.047505	3.6163
0.9500	0.9024	0.047606	3.6239
0.9520	0.9043	0.047706	3.6315
0.9540	0.9062	0.047807	3.6391
0.9560	0.9081	0.047908	3.6467
0.9580	0.9100	0.048009	3.6543

OBSERVED DISTANCE (INCHES)	TRUE DISTANCE (INCHES)	ERROR (INCHES)	RAY ANGLE (DEGREES)
0.9600	0.9119	0.048109	3.6619
0.9620	0.9138	0.048210	3.6695
0.9640	0.9157	0.048310	3.6771
0.9660	0.9176	0.048411	3.6848
0.9680	0.9195	0.048512	3.6924
0.9700	0.9214	0.048613	3.7000
0.9720	0.9233	0.048713	3.7076
0.9740	0.9252	0.048814	3.7152
0.9760	0.9271	0.048915	3.7228
0.9780	0.9290	0.049015	3.7304
0.9800	0.9309	0.049116	3.7380
0.9820	0.9328	0.049217	3.7456
0.9840	0.9347	0.049318	3.7532
0.9860	0.9366	0.049418	3.7608
0.9880	0.9385	0.049519	3.7684
0.9900	0.9404	0.049620	3.7760
0.9920	0.9423	0.049720	3.7836
0.9940	0.9442	0.049821	3.7913
0.9960	0.9461	0.049922	3.7989
0.9980	0.9480	0.050023	3.8065
1.0000	0.9499	0.050123	3.8141
1.0020	0.9518	0.050224	3.8217
1.0040	0.9537	0.050325	3.8293
1.0060	0.9556	0.050426	3.8369
1.0080	0.9575	0.050526	3.8445
1.0100	0.9594	0.050627	3.8521
1.0120	0.9613	0.050728	3.8597
1.0140	0.9632	0.050829	3.8673
1.0160	0.9651	0.050929	3.8749
1.0180	0.9670	0.051030	3.8825
1.0200	0.9689	0.051131	3.8901
1.0220	0.9708	0.051232	3.8977
1.0240	0.9727	0.051332	3.9053
1.0260	0.9746	0.051433	3.9129
1.0280	0.9765	0.051534	3.9205
1.0300	0.9784	0.051635	3.9281
1.0320	0.9803	0.051735	3.9357
1.0340	0.9822	0.051836	3.9433
1.0360	0.9841	0.051937	3.9509
1.0380	0.9860	0.052038	3.9586
1.0400	0.9879	0.052139	3.9662
1.0420	0.9898	0.052240	3.9738
1.0440	0.9917	0.052340	3.9814
1.0460	0.9936	0.052441	3.9890
1.0480	0.9955	0.052542	3.9966
1.0500	0.9974	0.052643	4.0042
1.0520	0.9993	0.052743	4.0118
1.0540	1.0012	0.052844	4.0194
1.0560	1.0031	0.052945	4.0270
1.0580	1.0050	0.053046	4.0346
1.0600	1.0069	0.053147	4.0422
1.0620	1.0088	0.053248	4.0498
1.0640	1.0107	0.053348	4.0574
1.0660	1.0125	0.053449	4.0650
1.0680	1.0144	0.053550	4.0726
1.0700	1.0163	0.053651	4.0802
1.0720	1.0182	0.053752	4.0878
1.0740	1.0201	0.053853	4.0954
1.0760	1.0220	0.053953	4.1030
1.0780	1.0239	0.054054	4.1106

OBSERVED DISTANCE (INCHES)	TRUE DISTANCE (INCHES)	ERROR (INCHES)	RAY ANGLE (DEGREES)
1.0800	1.0258	0.054155	4.1182
1.0820	1.0277	0.054256	4.1258
1.0840	1.0296	0.054357	4.1334
1.0860	1.0315	0.054458	4.1410
1.0880	1.0334	0.054559	4.1486
1.0900	1.0353	0.054660	4.1562
1.0920	1.0372	0.054760	4.1638
1.0940	1.0391	0.054861	4.1714
1.0960	1.0410	0.054962	4.1790
1.0980	1.0429	0.055063	4.1866
1.1000	1.0448		
1.1020	1.0467	0.055164	4.1942
1.1040	1.0486	0.055265	4.2018
1.1060	1.0505	0.055366	4.2094
1.1080	1.0524	0.055467	4.2170
1.1100	1.0543	0.055568	4.2246
1.1120	1.0562	0.055668	4.2322
1.1140	1.0581	0.055769	4.2398
1.1160	1.0600	0.055870	4.2474
1.1180	1.0619	0.055971	4.2550
		0.056072	4.2626
1.1200	1.0638	0.056173	4.2702
1.1220	1.0657	0.056274	4.2778
1.1240	1.0676	0.056375	4.2854
1.1260	1.0695	0.056476	4.2929
1.1280	1.0714	0.056577	4.3005
1.1300	1.0733	0.056678	4.3081
1.1320	1.0752	0.056779	4.3157
1.1340	1.0771	0.056880	4.3233
1.1360	1.0790	0.056981	4.3309
1.1380	1.0809	0.057082	4.3385
1.1400	1.0828	0.057183	4.3461
1.1420	1.0847	0.057284	4.3537
1.1440	1.0866	0.057385	4.3613
1.1460	1.0885	0.057486	4.3689
1.1480	1.0904	0.057586	4.3765
1.1500	1.0923	0.057687	4.3841
1.1520	1.0942	0.057788	4.3917
1.1540	1.0961	0.057889	4.3993
1.1560	1.0980	0.057990	4.4069
1.1580	1.0999	0.058091	4.4145
1.1600	1.1018	0.058192	4.4221
1.1620	1.1037	0.058293	4.4297
1.1640	1.1056	0.058394	4.4373
1.1660	1.1075	0.058495	4.4448
1.1680	1.1094	0.058596	4.4524
1.1700	1.1113	0.058697	4.4600
1.1720	1.1132	0.058798	4.4676
1.1740	1.1151	0.058899	4.4752
1.1760	1.1170	0.058900	4.4828
1.1780	1.1189	0.059101	4.4904
1.1800	1.1208	0.059202	4.4980
1.1820	1.1227	0.059303	4.5056
1.1840	1.1246	0.059404	4.5132
1.1860	1.1265	0.059506	4.5208
1.1880	1.1284	0.059607	4.5284
1.1900	1.1303	0.059708	4.5360
1.1920	1.1322	0.059809	4.5436
1.1940	1.1341	0.059910	4.5511
1.1960	1.1360	0.060011	4.5587
1.1980	1.1379	0.060112	4.5663

OBSERVED DISTANCE (INCHES)	TRUE DISTANCE (INCHES)	ERROR (INCHES)	RAY ANGLE (DEGREES)
1.2000	1.1398	0.060213	4.5739
1.2020	1.1417	0.060314	4.5815
1.2040	1.1436	0.060415	4.5891
1.2060	1.1455	0.060516	4.5967
1.2080	1.1474	0.060617	4.6043
1.2100	1.1493	0.060718	4.6119
1.2120	1.1512	0.060819	4.6195
1.2140	1.1531	0.060920	4.6270
1.2160	1.1550	0.061021	4.6346
1.2180	1.1569	0.061123	4.6422
1.2200	1.1588	0.061224	4.6498
1.2220	1.1607	0.061325	4.6574
1.2240	1.1626	0.061426	4.6650
1.2260	1.1645	0.061527	4.6726
1.2280	1.1664	0.061628	4.6802
1.2300	1.1683	0.061729	4.6878
1.2320	1.1702	0.061830	4.6954
1.2340	1.1721	0.061931	4.7029
1.2360	1.1740	0.062032	4.7105
1.2380	1.1759	0.062134	4.7181
1.2400	1.1778	0.062235	4.7257
1.2420	1.1797	0.062336	4.7333
1.2440	1.1816	0.062437	4.7409
1.2460	1.1835	0.062538	4.7485
1.2480	1.1854	0.062639	4.7560
1.2500	1.1873	0.062740	4.7636
1.2520	1.1892	0.062842	4.7712
1.2540	1.1911	0.062943	4.7788
1.2560	1.1930	0.063044	4.7864
1.2580	1.1949	0.063145	4.7940
1.2600	1.1968	0.063246	4.8016
1.2620	1.1987	0.063348	4.8092
1.2640	1.2006	0.063448	4.8167
1.2660	1.2024	0.063550	4.8242
1.2680	1.2043	0.063651	4.8319
1.2700	1.2062	0.063752	4.8395
1.2720	1.2081	0.063854	4.8471
1.2740	1.2100	0.063955	4.8547
1.2760	1.2119	0.064056	4.8622
1.2780	1.2138	0.064157	4.8698
1.2800	1.2157	0.064258	4.8774
1.2820	1.2176	0.064360	4.8850
1.2840	1.2195	0.064461	4.8926
1.2860	1.2214	0.064562	4.9002
1.2880	1.2233	0.064663	4.9078
1.2900	1.2252	0.064764	4.9153
1.2920	1.2271	0.064865	4.9229
1.2940	1.2290	0.064967	4.9305
1.2960	1.2309	0.065068	4.9381
1.2980	1.2328	0.065169	4.9457
1.3000	1.2347	0.065270	4.9533
1.3020	1.2366	0.065372	4.9608
1.3040	1.2385	0.065473	4.9684
1.3060	1.2404	0.065574	4.9760
1.3080	1.2423	0.065675	4.9836
1.3100	1.2442	0.065777	4.9912
1.3120	1.2461	0.065878	4.9987
1.3140	1.2480	0.065979	5.0063
1.3160	1.2499	0.066081	5.0139
1.3180	1.2518	0.066182	5.0215

OBSERVED DISTANCE (INCHES)	TRUE DISTANCE (INCHES)	ERROR (INCHES)	RAY ANGLE (DEGREES)
1.3200	1.2537	0.066283	5.0291
1.3220	1.2556	0.066384	5.0366
1.3240	1.2575	0.066486	5.0442
1.3260	1.2594	0.066587	5.0518
1.3280	1.2613	0.066688	5.0594
1.3300	1.2632	0.066789	5.0670
1.3320	1.2651	0.066891	5.0745
1.3340	1.2670	0.066992	5.0821
1.3360	1.2689	0.067093	5.0897
1.3380	1.2708	0.067195	5.0973
1.3400	1.2727	0.067296	5.1049
1.3420	1.2746	0.067398	5.1124
1.3440	1.2765	0.067499	5.1200
1.3460	1.2784	0.067600	5.1276
1.3480	1.2803	0.067701	5.1352
1.3500	1.2822	0.067803	5.1428
1.3520	1.2841	0.067904	5.1503
1.3540	1.2860	0.068005	5.1579
1.3560	1.2879	0.068107	5.1655
1.3580	1.2898	0.068208	5.1731
1.3600	1.2917	0.068309	5.1806
1.3620	1.2936	0.068411	5.1882
1.3640	1.2955	0.068512	5.1958
1.3660	1.2974	0.068614	5.2034
1.3680	1.2993	0.068715	5.2110
1.3700	1.3012	0.068816	5.2185
1.3720	1.3031	0.068918	5.2261
1.3740	1.3050	0.069019	5.2337
1.3760	1.3069	0.069121	5.2413
1.3780	1.3088	0.069222	5.2488
1.3800	1.3107	0.069323	5.2564
1.3820	1.3126	0.069425	5.2640
1.3840	1.3145	0.069526	5.2716
1.3860	1.3164	0.069628	5.2791
1.3880	1.3183	0.069729	5.2867
1.3900	1.3202	0.069830	5.2943
1.3920	1.3221	0.069932	5.3019
1.3940	1.3240	0.070033	5.3094
1.3960	1.3259	0.070135	5.3170
1.3980	1.3278	0.070236	5.3246
1.4000	1.3297	0.070338	5.3322
1.4020	1.3316	0.070439	5.3397
1.4040	1.3335	0.070540	5.3473
1.4060	1.3354	0.070642	5.3549
1.4080	1.3373	0.070743	5.3624
1.4100	1.3392	0.070845	5.3700
1.4120	1.3411	0.070946	5.3776
1.4140	1.3430	0.071048	5.3852
1.4160	1.3448	0.071149	5.3927
1.4180	1.3467	0.071251	5.4003
1.4200	1.3486	0.071352	5.4079
1.4220	1.3505	0.071454	5.4154
1.4240	1.3524	0.071555	5.4230
1.4260	1.3543	0.071657	5.4306
1.4280	1.3562	0.071758	5.4382
1.4300	1.3581	0.071860	5.4457
1.4320	1.3600	0.071961	5.4533
1.4340	1.3619	0.072063	5.4609
1.4360	1.3638	0.072164	5.4684
1.4380	1.3657	0.072266	5.4760

OBSERVED DISTANCE (INCHES)	TRUE DISTANCE (INCHES)	ERROR (INCHES)	RAY ANGLE (DEGREES)
1.4400	1.3676	0.072367	5.4836
1.4420	1.3695	0.072469	5.4912
1.4440	1.3714	0.072571	5.4987
1.4460	1.3733	0.072672	5.5063
1.4480	1.3752	0.072774	5.5139
1.4500	1.3771	0.072875	5.5214
1.4520	1.3790	0.072977	5.5290
1.4540	1.3809	0.073078	5.5366
1.4560	1.3828	0.073180	5.5441
1.4580	1.3847	0.073281	5.5517
1.4600	1.3866	0.073383	5.5593
1.4620	1.3885	0.073484	5.5668
1.4640	1.3904	0.073586	5.5744
1.4660	1.3923	0.073687	5.5820
1.4680	1.3942	0.073789	5.5895
1.4700	1.3961	0.073891	5.5971
1.4720	1.3980	0.073992	5.6047
1.4740	1.3999	0.074094	5.6122
1.4760	1.4018	0.074196	5.6198
1.4780	1.4037	0.074297	5.6274
1.4800	1.4056	0.074399	5.6349
1.4820	1.4075	0.074500	5.6425
1.4840	1.4094	0.074602	5.6501
1.4860	1.4113	0.074704	5.6576
1.4880	1.4132	0.074805	5.6652
1.4900	1.4151	0.074907	5.6728
1.4920	1.4170	0.075009	5.6803
1.4940	1.4189	0.075110	5.6879
1.4960	1.4208	0.075212	5.6955
1.4980	1.4227	0.075314	5.7030
1.5000	1.4246	0.075415	5.7106
1.5020	1.4265	0.075517	5.7182
1.5040	1.4284	0.075618	5.7257
1.5060	1.4303	0.075720	5.7333
1.5080	1.4322	0.075822	5.7408
1.5100	1.4341	0.075923	5.7484
1.5120	1.4360	0.075025	5.7560
1.5140	1.4379	0.076127	5.7635
1.5160	1.4398	0.076229	5.7711
1.5180	1.4417	0.076330	5.7787
1.5200	1.4436	0.076432	5.7862
1.5220	1.4455	0.076534	5.7938
1.5240	1.4474	0.076635	5.8013
1.5260	1.4493	0.076737	5.8089
1.5280	1.4512	0.076839	5.8165
1.5300	1.4531	0.076940	5.8240
1.5320	1.4550	0.077042	5.8316
1.5340	1.4569	0.077144	5.8391
1.5360	1.4588	0.077246	5.8467
1.5380	1.4607	0.077347	5.8543
1.5400	1.4625	0.077449	5.8618
1.5420	1.4644	0.077551	5.8694
1.5440	1.4663	0.077653	5.8769
1.5460	1.4682	0.077754	5.8845
1.5480	1.4701	0.077856	5.8921
1.5500	1.4720	0.077958	5.8996
1.5520	1.4739	0.078060	5.9072
1.5540	1.4758	0.078161	5.9147
1.5560	1.4777	0.078263	5.9223
1.5580	1.4796	0.076365	5.9299

OBSERVED DISTANCE (INCHES)	TRUE DISTANCE (INCHES)	ERROR (INCHES)	RAY ANGLE (DEGREES)
1.5600	1.4815	0.078467	5.9374
1.5620	1.4834	0.078568	5.9450
1.5640	1.4853	0.078670	5.9525
1.5660	1.4872	0.078772	5.9601
1.5680	1.4891	0.078874	5.9676
1.5700	1.4910	0.078976	5.9752
1.5720	1.4929	0.079078	5.9827
1.5740	1.4948	0.079179	5.9903
1.5760	1.4967	0.079281	5.9979
1.5780	1.4986	0.079383	6.0054
1.5800	1.5005	0.079485	6.0130
1.5820	1.5024	0.079587	6.0205
1.5840	1.5043	0.079689	6.0281
1.5860	1.5062	0.079790	6.0356
1.5880	1.5081	0.079892	6.0432
1.5900	1.5100	0.079994	6.0508
1.5920	1.5119	0.080096	6.0583
1.5940	1.5138	0.080198	6.0659
1.5960	1.5157	0.080300	6.0734
1.5980	1.5176	0.080402	6.0810
1.6000	1.5195	0.080503	6.0885
1.6020	1.5214	0.080605	6.0961
1.6040	1.5233	0.080707	6.1036
1.6060	1.5252	0.080809	6.1112
1.6080	1.5271	0.080911	6.1187
1.6100	1.5290	0.081013	6.1263
1.6120	1.5309	0.081115	6.1338
1.6140	1.5328	0.081217	6.1414
1.6160	1.5347	0.081319	6.1489
1.6180	1.5366	0.081421	6.1565
1.6200	1.5385	0.081523	6.1640
1.6220	1.5404	0.081624	6.1716
1.6240	1.5423	0.081726	6.1791
1.6260	1.5442	0.081828	6.1867
1.6280	1.5461	0.081930	6.1942
1.6300	1.5480	0.082032	6.2018
1.6320	1.5499	0.082134	6.2093
1.6340	1.5518	0.082236	6.2169
1.6360	1.5537	0.082338	6.2244
1.6380	1.5556	0.082440	6.2320
1.6400	1.5575	0.082542	6.2395
1.6420	1.5594	0.082644	6.2471
1.6440	1.5613	0.082746	6.2546
1.6460	1.5632	0.082848	6.2622
1.6480	1.5650	0.082950	6.2697
1.6500	1.5669	0.083052	6.2773
1.6520	1.5688	0.083154	6.2848
1.6540	1.5707	0.083256	6.2924
1.6560	1.5726	0.083358	6.2999
1.6580	1.5745	0.083460	6.3075
1.6600	1.5764	0.083562	6.3150
1.6620	1.5783	0.083664	6.3226
1.6640	1.5802	0.083766	6.3301
1.6660	1.5821	0.083868	6.3377
1.6680	1.5840	0.083970	6.3452
1.6700	1.5859	0.084072	6.3528
1.6720	1.5878	0.084174	6.3603
1.6740	1.5897	0.084276	6.3679
1.6760	1.5916	0.084378	6.3754
1.6780	1.5935	0.084480	6.3829

OBSERVED DISTANCE (INCHES)	TRUE DISTANCE (INCHES)	ERROR (INCHES)	RAY ANGLE (DEGREES)
1.6800	1.5954	0.034583	6.3905
1.6820	1.5973	0.094685	6.3980
1.6840	1.5992	0.084787	6.4056
1.6860	1.6011	0.084889	6.4131
1.6880	1.6030	0.084991	6.4207
1.6900	1.6049	0.085093	6.4282
1.6920	1.6068	0.085195	6.4358
1.6940	1.6087	0.085297	6.4433
1.6960	1.6106	0.085399	6.4508
1.6980	1.6125	0.085501	6.4584
1.7000	1.6144	0.085603	6.4659
1.7020	1.6163	0.085706	6.4735
1.7040	1.6182	0.085808	6.4810
1.7060	1.6201	0.085910	6.4886
1.7080	1.6220	0.086012	6.4961
1.7100	1.6239	0.086114	6.5036
1.7120	1.6258	0.086216	6.5112
1.7140	1.6277	0.086318	6.5187
1.7160	1.6296	0.086421	6.5263
1.7180	1.6315	0.086523	6.5338
1.7200	1.6334	0.086625	6.5413
1.7220	1.6353	0.086727	6.5489
1.7240	1.6372	0.086829	6.5564
1.7260	1.6391	0.086932	6.5640
1.7280	1.6410	0.087034	6.5715
1.7300	1.6429	0.087136	6.5790
1.7320	1.6448	0.087238	6.5866
1.7340	1.6467	0.087340	6.5941
1.7360	1.6486	0.087443	6.6017
1.7380	1.6505	0.087545	6.6092
1.7400	1.6524	0.087647	6.6167
1.7420	1.6543	0.087749	6.6243
1.7440	1.6561	0.087851	6.6318
1.7460	1.6580	0.087954	6.6393
1.7480	1.6599	0.088056	6.6469
1.7500	1.6618	0.088158	6.6544
1.7520	1.6637	0.088260	6.6620
1.7540	1.6656	0.088363	6.6695
1.7560	1.6675	0.088465	6.6770
1.7580	1.6694	0.088567	6.5846
1.7600	1.6713	0.088669	6.6921
1.7620	1.6732	0.088772	6.6996
1.7640	1.6751	0.088874	6.7072
1.7660	1.6770	0.088976	6.7147
1.7680	1.6789	0.089079	6.7222
1.7700	1.6808	0.089181	6.7298
1.7720	1.6827	0.089283	6.7373
1.7740	1.6846	0.089385	6.7448
1.7760	1.6865	0.089488	6.7524
1.7780	1.6884	0.089590	6.7599
1.7800	1.6903	0.089692	6.7674
1.7820	1.6922	0.089795	6.7750
1.7840	1.6941	0.089897	6.7825
1.7860	1.6960	0.089999	6.7900
1.7880	1.6979	0.090102	6.7976
1.7900	1.6998	0.090204	6.8051
1.7920	1.7017	0.090306	6.8126
1.7940	1.7036	0.090409	6.8202
1.7960	1.7055	0.090511	6.8277
1.7980	1.7074	0.090613	6.8352

OBSERVED DISTANCE (INCHES)	TRUE DISTANCE (INCHES)	ERROR (INCHES)	RAY ANGLE (DEGREES)
1.8000	1.7093	0.090716	6.8428
1.8020	1.7112	0.090818	6.8503
1.8040	1.7131	0.090921	6.8578
1.8060	1.7150	0.091023	6.8654
1.8080	1.7169	0.091125	6.8729
1.8100	1.7188	0.091228	6.8804
1.8120	1.7207	0.091330	6.8879
1.8140	1.7226	0.091433	6.8955
1.8160	1.7245	0.091535	6.9030
1.8180	1.7264	0.091637	6.9105
1.8200	1.7283	0.091740	6.9181
1.8220	1.7302	0.091842	6.9256
1.8240	1.7321	0.091945	6.9331
1.8260	1.7340	0.092047	6.9406
1.8280	1.7358	0.092150	6.9482
1.8300	1.7377	0.092252	6.9557
1.8320	1.7396	0.092355	6.9632
1.8340	1.7415	0.092457	6.9708
1.8360	1.7434	0.092559	6.9783
1.8380	1.7453	0.092662	6.9858
1.8400	1.7472	0.092764	6.9933
1.8420	1.7491	0.092867	7.0009
1.8440	1.7510	0.092969	7.0084
1.8460	1.7529	0.093072	7.0159
1.8480	1.7548	0.093174	7.0244
1.8500	1.7567	0.093277	7.0340
1.8520	1.7586	0.093379	7.0385
1.8540	1.7605	0.093482	7.0460
1.8560	1.7624	0.093584	7.0535
1.8580	1.7643	0.093687	7.0611
1.8600	1.7662	0.093790	7.0686
1.8620	1.7681	0.093892	7.0761
1.8640	1.7700	0.093995	7.0836
1.8660	1.7719	0.094097	7.0912
1.8680	1.7738	0.094200	7.0987
1.8700	1.7757	0.094302	7.1062
1.8720	1.7776	0.094405	7.1137
1.8740	1.7795	0.094507	7.1213
1.8760	1.7814	0.094610	7.1288
1.8780	1.7833	0.094713	7.1363
1.8800	1.7852	0.094815	7.1438
1.8820	1.7871	0.094918	7.1513
1.8840	1.7890	0.095020	7.1589
1.8860	1.7909	0.095123	7.1664
1.8880	1.7928	0.095226	7.1739
1.8900	1.7947	0.095328	7.1814
1.8920	1.7966	0.095431	7.1889
1.8940	1.7985	0.095533	7.1965
1.8960	1.8004	0.095636	7.2040
1.8980	1.8023	0.095739	7.2115
1.9000	1.8042	0.095841	7.2190
1.9020	1.8061	0.095944	7.2265
1.9040	1.8080	0.096047	7.2340
1.9060	1.8098	0.096149	7.2416
1.9080	1.8117	0.096252	7.2491
1.9100	1.8136	0.096355	7.2566
1.9120	1.8155	0.096457	7.2641
1.9140	1.8174	0.096560	7.2716
1.9160	1.8193	0.096663	7.2792
1.9180	1.8212	0.096765	7.2867

OBSERVED DISTANCE (INCHES)	TRUE DISTANCE (INCHES)	ERROR (INCHES)	RAY ANGLE (DEGREES)
1.9200	1.8231	0.096868	7.2942
1.9220	1.8250	0.096971	7.3017
1.9240	1.8269	0.097073	7.3092
1.9260	1.8288	0.097176	7.3167
1.9280	1.8307	0.097279	7.3242
1.9300	1.8326	0.097382	7.3318
1.9320	1.8345	0.097484	7.3393
1.9340	1.8364	0.097587	7.3468
1.9360	1.8383	0.097690	7.3543
1.9380	1.8402	0.097793	7.3618
1.9400	1.8421	0.097895	7.3693
1.9420	1.8440	0.097998	7.3769
1.9440	1.8459	0.098101	7.3844
1.9460	1.8478	0.098204	7.3919
1.9480	1.8497	0.098306	7.3994
1.9500	1.8516	0.098409	7.4069
1.9520	1.8535	0.098512	7.4144
1.9540	1.8554	0.098615	7.4219
1.9560	1.8573	0.098718	7.4294
1.9580	1.8592	0.098820	7.4370
1.9600	1.8611	0.098923	7.4445
1.9620	1.8630	0.099026	7.4520
1.9640	1.8649	0.099129	7.4595
1.9660	1.8668	0.099232	7.4670
1.9680	1.8687	0.099335	7.4745
1.9700	1.8706	0.099437	7.4820
1.9720	1.8725	0.099540	7.4895
1.9740	1.8744	0.099643	7.4970
1.9760	1.8763	0.099746	7.5045
1.9780	1.8782	0.099849	7.5121
1.9800	1.8800	0.099952	7.5196
1.9820	1.8819	0.100054	7.5271
1.9840	1.8838	0.100157	7.5346
1.9860	1.8857	0.100260	7.5421
1.9880	1.8876	0.100363	7.5496
1.9900	1.8895	0.100466	7.5571
1.9920	1.8914	0.100569	7.5646
1.9940	1.8933	0.100672	7.5721
1.9960	1.8952	0.100775	7.5796
1.9980	1.8971	0.100878	7.5871
2.0000	1.8990	0.100981	7.5946
2.0020	1.9009	0.101084	7.6021
2.0040	1.9028	0.101186	7.6096
2.0060	1.9047	0.101289	7.6172
2.0080	1.9066	0.101392	7.6247
2.0100	1.9085	0.101495	7.6322
2.0120	1.9104	0.101599	7.6397
2.0140	1.9123	0.101701	7.6472
2.0160	1.9142	0.101804	7.6547
2.0180	1.9161	0.101907	7.6622
2.0200	1.9180	0.102010	7.6697
2.0220	1.9199	0.102113	7.6772
2.0240	1.9218	0.102216	7.6847
2.0260	1.9237	0.102319	7.6922
2.0280	1.9256	0.102422	7.6997
2.0300	1.9275	0.102525	7.7072
2.0320	1.9294	0.102628	7.7147
2.0340	1.9313	0.102731	7.7222
2.0360	1.9332	0.102834	7.7297
2.0380	1.9351	0.102937	7.7372

OBSERVED DISTANCE (INCHES)	TRUE DISTANCE (INCHES)	ERROR (INCHES)	RAY ANGLE (DEGREES)
2.0400	1.9370	0.103040	7.7447
2.0420	1.9389	0.103143	7.7522
2.0440	1.9408	0.103246	7.7597
2.0460	1.9426	0.103349	7.7672
2.0480	1.9445	0.103453	7.7747
2.0500	1.9464	0.103556	7.7822
2.0520	1.9483	0.103659	7.7897
2.0540	1.9502	0.103762	7.7972
2.0560	1.9521	0.103865	7.8047
2.0580	1.9540	0.103968	7.8122
2.0600	1.9559	0.104071	7.8197
2.0620	1.9578	0.104174	7.8272
2.0640	1.9597	0.104277	7.8347
2.0660	1.9616	0.104380	7.8422
2.0680	1.9635	0.104483	7.8497
2.0700	1.9654	0.104587	7.8572
2.0720	1.9673	0.104690	7.8647
2.0740	1.9692	0.104793	7.8722
2.0760	1.9711	0.104896	7.8797
2.0780	1.9730	0.104999	7.8872
2.0800	1.9749	0.105102	7.8947
2.0820	1.9768	0.105205	7.9022
2.0840	1.9787	0.105309	7.9097
2.0860	1.9806	0.105412	7.9172
2.0880	1.9825	0.105515	7.9246
2.0900	1.9844	0.105618	7.9321
2.0920	1.9863	0.105721	7.9396
2.0940	1.9882	0.105825	7.9471
2.0960	1.9901	0.105928	7.9546
2.0980	1.9920	0.106031	7.9621
2.1000	1.9939	0.106134	7.9696
2.1020	1.9958	0.106238	7.9771
2.1040	1.9977	0.106341	7.9846
2.1060	1.9996	0.106444	7.9921
2.1080	2.0015	0.106547	7.9996
2.1100	2.0033	0.106650	8.0071
2.1120	2.0052	0.106754	8.0146
2.1140	2.0071	0.106857	8.0220
2.1160	2.0090	0.106960	8.0295
2.1180	2.0109	0.107064	8.0370
2.1200	2.0128	0.107167	8.0445
2.1220	2.0147	0.107270	8.0520
2.1240	2.0166	0.107374	8.0595
2.1260	2.0185	0.107477	8.0670
2.1280	2.0204	0.107580	8.0745
2.1300	2.0223	0.107683	8.0820
2.1320	2.0242	0.107787	8.0894
2.1340	2.0261	0.107890	8.0969
2.1360	2.0280	0.107993	8.1044
2.1380	2.0299	0.108097	8.1119
2.1400	2.0318	0.108200	8.1194
2.1420	2.0337	0.108303	8.1269
2.1440	2.0356	0.108407	8.1344
2.1460	2.0375	0.108510	8.1419
2.1480	2.0394	0.108613	8.1493
2.1500	2.0413	0.108717	8.1568
2.1520	2.0432	0.108820	8.1643
2.1540	2.0451	0.108924	8.1718
2.1560	2.0470	0.109027	8.1793
2.1580	2.0489	0.109131	8.1868

OBSERVED DISTANCE (INCHES)	TRUE DISTANCE (INCHES)	ERROR (INCHES)	RAY ANGLE (DEGREES)
2.1600	2.0508	0.109234	8.1943
2.1620	2.0527	0.109337	8.2017
2.1640	2.0546	0.109441	8.2092
2.1660	2.0565	0.109544	8.2157
2.1680	2.0584	0.109647	8.2242
2.1700	2.0602	0.109751	8.2317
2.1720	2.0621	0.109854	8.2392
2.1740	2.0640	0.109958	8.2466
2.1760	2.0659	0.110061	8.2541
2.1780	2.0678	0.110165	8.2616
2.1800	2.0697	0.110268	8.2691
2.1820	2.0716	0.110372	8.2766
2.1840	2.0735	0.110475	8.2840
2.1860	2.0754	0.110579	8.2915
2.1880	2.0773	0.110682	8.2990
2.1900	2.0792	0.110786	8.3065
2.1920	2.0811	0.110889	8.3140
2.1940	2.0830	0.110993	8.3214
2.1960	2.0849	0.111096	8.3289
2.1980	2.0868	0.111200	8.3364
2.2000	2.0887	0.111303	8.3439
2.2020	2.0906	0.111407	8.3514
2.2040	2.0925	0.111510	8.3588
2.2060	2.0944	0.111614	8.3663
2.2080	2.0963	0.111717	8.3738
2.2100	2.0982	0.111821	8.3813
2.2120	2.1001	0.111924	8.3887
2.2140	2.1020	0.112028	8.3962
2.2160	2.1039	0.112131	8.4037
2.2180	2.1058	0.112235	8.4112
2.2200	2.1077	0.112339	8.4187
2.2220	2.1096	0.112442	8.4261
2.2240	2.1115	0.112546	8.4336
2.2260	2.1133	0.112650	8.4411
2.2280	2.1152	0.112753	8.4486
2.2300	2.1171	0.112857	8.4560
2.2320	2.1190	0.112960	8.4635
2.2340	2.1209	0.113064	8.4710
2.2360	2.1228	0.113168	8.4784
2.2380	2.1247	0.113271	8.4859
2.2400	2.1266	0.113375	8.4934
2.2420	2.1285	0.113479	8.5009
2.2440	2.1304	0.113582	8.5083
2.2460	2.1323	0.113686	8.5158
2.2480	2.1342	0.113790	8.5233
2.2500	2.1361	0.113893	8.5308
2.2520	2.1380	0.113997	8.5382
2.2540	2.1399	0.114101	8.5457
2.2560	2.1418	0.114205	8.5532
2.2580	2.1437	0.114308	8.5606
2.2600	2.1456	0.114412	8.5681
2.2620	2.1475	0.114516	8.5756
2.2640	2.1494	0.114620	8.5830
2.2660	2.1513	0.114723	8.5905
2.2680	2.1532	0.114827	8.5980
2.2700	2.1551	0.114931	8.6055
2.2720	2.1570	0.115034	8.6129
2.2740	2.1589	0.115138	8.6204
2.2760	2.1608	0.115242	8.6279
2.2780	2.1627	0.115346	8.6353

OBSERVED DISTANCE (INCHES)	TRUE DISTANCE (INCHES)	ERROR (INCHES)	RAY ANGLE (DEGREES)
2.2800	2.1645	0.115450	8.6428
2.2820	2.1664	0.115553	8.6503
2.2840	2.1683	0.115657	8.6577
2.2860	2.1702	0.115761	8.6652
2.2880	2.1721	0.115865	8.6727
2.2900	2.1740	0.115969	8.6801
2.2920	2.1759	0.116072	8.6876
2.2940	2.1778	0.116176	8.6951
2.2960	2.1797	0.116280	8.7025
2.2980	2.1816	0.116384	8.7100
2.3000	2.1835	0.116488	8.7174
2.3020	2.1854	0.116592	8.7249
2.3040	2.1873	0.116695	8.7324
2.3060	2.1892	0.116799	8.7398
2.3080	2.1911	0.116903	8.7473
2.3100	2.1930	0.117007	8.7548
2.3120	2.1949	0.117111	8.7622
2.3140	2.1968	0.117215	8.7697
2.3160	2.1987	0.117319	8.7772
2.3180	2.2006	0.117423	8.7846
2.3200	2.2025	0.117527	8.7921
2.3220	2.2044	0.117631	8.7995
2.3240	2.2063	0.117735	8.8070
2.3260	2.2082	0.117839	8.8145
2.3280	2.2101	0.117942	8.8219
2.3300	2.2120	0.118046	8.8294
2.3320	2.2138	0.118150	8.8368
2.3340	2.2157	0.118254	8.8443
2.3360	2.2176	0.118358	8.8518
2.3380	2.2195	0.118462	8.8592
2.3400	2.2214	0.118566	8.8667
2.3420	2.2233	0.118670	8.8741
2.3440	2.2252	0.118774	8.8816
2.3460	2.2271	0.118878	8.8890
2.3480	2.2290	0.118982	8.8965
2.3500	2.2309	0.119086	8.9040
2.3520	2.2328	0.119190	8.9114
2.3540	2.2347	0.119294	8.9189
2.3560	2.2366	0.119398	8.9263
2.3580	2.2385	0.119502	8.9338
2.3600	2.2404	0.119606	8.9412
2.3620	2.2423	0.119711	8.9487
2.3640	2.2442	0.119815	8.9561
2.3660	2.2461	0.119919	8.9636
2.3680	2.2480	0.120023	8.9711
2.3700	2.2499	0.120127	8.9785
2.3720	2.2518	0.120231	8.9860
2.3740	2.2537	0.120335	8.9934
2.3760	2.2556	0.120439	9.0009
2.3780	2.2575	0.120543	9.0083
2.3800	2.2594	0.120647	9.0158
2.3820	2.2612	0.120751	9.0232
2.3840	2.2631	0.120856	9.0307
2.3860	2.2650	0.120960	9.0381
2.3880	2.2669	0.121064	9.0456
2.3900	2.2688	0.121168	9.0530
2.3920	2.2707	0.121272	9.0605
2.3940	2.2726	0.121376	9.0679
2.3960	2.2745	0.121480	9.0754
2.3980	2.2764	0.121585	9.0828

OBSERVED DISTANCE (INCHES)	TRUE DISTANCE (INCHES)	ERROR (INCHES)	RAY ANGLE (DEGREES)
2.4000	2.2783	0.121689	9.0903
2.4020	2.2802	0.121793	9.0977
2.4040	2.2821	0.121897	9.1052
2.4060	2.2840	0.122001	9.1126
2.4080	2.2859	0.122106	9.1201
2.4100	2.2878	0.122210	9.1275
2.4120	2.2897	0.122314	9.1350
2.4140	2.2916	0.122418	9.1424
2.4160	2.2935	0.122523	9.1498
2.4180	2.2954	0.122627	9.1573
2.4200	2.2973	0.122731	9.1647
2.4220	2.2992	0.122835	9.1722
2.4240	2.3011	0.122940	9.1796
2.4260	2.3030	0.123044	9.1871
2.4280	2.3049	0.123148	9.1945
2.4300	2.3067	0.123253	9.2020
2.4320	2.3086	0.123357	9.2094
2.4340	2.3105	0.123461	9.2168
2.4360	2.3124	0.123565	9.2243
2.4380	2.3143	0.123670	9.2317
2.4400	2.3162	0.123774	9.2392
2.4420	2.3181	0.123879	9.2466
2.4440	2.3200	0.123983	9.2541
2.4460	2.3219	0.124087	9.2615
2.4480	2.3238	0.124191	9.2689
2.4500	2.3257	0.124296	9.2764
2.4520	2.3276	0.124400	9.2838
2.4540	2.3295	0.124505	9.2913
2.4560	2.3314	0.124609	9.2987
2.4580	2.3333	0.124713	9.3061
2.4600	2.3352	0.124818	9.3136
2.4620	2.3371	0.124922	9.3210
2.4640	2.3390	0.125027	9.3285
2.4660	2.3409	0.125131	9.3359
2.4680	2.3428	0.125235	9.3433
2.4700	2.3447	0.125340	9.3508
2.4720	2.3466	0.125444	9.3582
2.4740	2.3484	0.125549	9.3657
2.4760	2.3503	0.125653	9.3731
2.4780	2.3522	0.125758	9.3805
2.4800	2.3541	0.125862	9.3880
2.4820	2.3560	0.125967	9.3954
2.4840	2.3579	0.126071	9.4028
2.4860	2.3598	0.126176	9.4103
2.4880	2.3617	0.126280	9.4177
2.4900	2.3636	0.126385	9.4251
2.4920	2.3655	0.126489	9.4326
2.4940	2.3674	0.126594	9.4400
2.4960	2.3693	0.126698	9.4474
2.4980	2.3712	0.126803	9.4549
2.5000	2.3731	0.126907	9.4623

APPENDIX C

APPLICATION OF COMPUTER PROGRAM "HOLOFER"

The computer program is an adptation of the inversion first proposed by C. D. Maldonado [9, 10, 11] and is designed to invert fringe numbers across a field to the density field. It can be operated in three different modes as described below:

(a) Mode 1

Mode 1 is utilized as a self-test of the computer program. It can either generate its own input density field using Subroutine FUNCT or read in a density field through Subroutine FREAD. The program then generates the fringe array and inverts the array back to the original density field. This mode was utilized in the present investigation to determine the value of the scale factor, α , required to obtain the correct density across the fin.

(b) Mode 2

This mode reads in irregularly spaced fringe data and generates the fringe array at regular intervals across the field using Subroutine SHEET. By specifying NCODE = 1, the fringe array can be generated by one of the functions in Subroutine FUNCT. Mode 2 was not utilized .

(c) Mode 3

Mode 3 reads in the fringe data at regularly spaced intervals and inverts the array to density data across the field. The Subroutine GARRAY calls Subroutine READ to read in the fringe data. The first two cards preceding the fringe data provide the program with the fringe field size, location, and symmetry.

The following parameters were used in considering the symmetric field case:

<u>PARAMETER</u>	<u>INPUT</u>
NOF	Run Number
IMAX	201
JMAX	1
ISYM	101
JSYM	1
IMS	2
JMS	100
Z	0.387
XO	0.0
YO	0.0
PHISYM	.0.0

References [3] and [12] contain further details and applications of the computer program. A print-out of the program is included in the next few pages of this appendix.


```

NPTS=AR(15)
NLINS=AR(16)
SD=AR(18)
PHI2=AR(19)
DELPHI=AR(20)
DZERO=AR(21)
YPRNG=AR(22)
XPRNG=AR(23)
NAF=AR(24)
IPT=AR(25)
LPT=AR(26)
BND=AR(27)
A=AR(28)
B=AR(29)
C=AR(30)
D=AR(31)
E=AR(32)
F=AR(33)
G=AR(34)
H=AR(35)
I=AR(36)
J=AR(37)
K=AR(38)
L=AR(39)
M=AR(40)
N=AR(41)
Q=AR(42)
WRITE(6,90)
WRITE(6,91)
WRITE(6,92)
WRITE(6,93)
WRITE(6,94)
WRITE(6,95)
WRITE(6,96)
WRITE(6,97)
WRITEM(6,98)
(LST I=1,75)
(LST I=1,76)
(LST I=1,77)
(LST I=1,78)
(LST I=1,79)
(LST I=1,80)
(LST I=1,81)
(LST I=1,82)
(LST I=1,83)
(LST I=1,84)
(LST I=1,85)
(LST I=1,86)
(LST I=1,87)
(LST I=1,88)
(LST I=1,89)
(LST I=1,90)
(LST I=1,91)
(LST I=1,92)
(LST I=1,93)
(LST I=1,94)
(LST I=1,95)
(LST I=1,96)
(LST I=1,97)
(LST I=1,98)
FORMAT(//,/* THE INPUT PARAMETER FOR THIS RUN ARE : */)
90 FORMAT(5X,/* JMAX/2 * KLIMIT * MLIMIT * KEXTRA */
91 1* MEXTRA /* 3X,6F10.0 */
92 1* FORMAT(5X,/* ALPHA /* SIZE /* EPS /* RHO-INF /* LAMBDA */
93 1* BETA /* 3X,2F10.3 /* F11.6 /* POINTS /* F9.1 /* F11.6 /* SYM.
94 1* STD DEV /* 2X,5F10.0 /* F10.3 /* PHIZERO /* DELPHI /* YPZERO /* YPRANGE */
95 1* XPRANGE /* 4X,6F10.3 /* TST FUN /* ADD FUN /* GARRAY /* GRAPH /* LIN PRT */
1* MAP BND /* 2X,6F10.0 /* DIAGNOS /* XPZERO /* SET00360 /* SET00340 /* SET00310 /* SET00400

```

```

96 FORMAT (/5X,'*',A,5F10.3)*      B   *   C   *   D   *   E
97 FORMAT (/5X,'*',S,5F10.3)*      T   *   U   *   V   *   W
98 FORMAT (/3X,75A1)               WRITE (6,89) (AR(I),I=1,42)
NNN=2
IF (MODE.LT.0) NNN=1
IF (MODE.GT.5) MODE=MODE-10
NGP=0
IF (KLIMIT.LT.KEXTRA) KEXTRA=KLIMIT
IF (MLIMIT.LT.MEXTRA) MEXTRA=MLIMIT
IF (IPTR.LT.O) NGP=IPTR
IF (IPTR.LT.O) IPT=-IPTR
JSYM=2*I-(FLOAT(JSYM)/2.-FLOAT(JSYM/2))*2
IF (JSYM.EQ.0) JSYM=1
IF (JSYM.GT.JMAX) JSYM=2
IF (JSYM.EQ.1) JMAX=(JMAX+1)/2)*2
RJMX=JMAX
MSYM=JSYM
IF CU((MSYM.EQ.0).OR.(MSYM.GT.JMAX)) MSYM=1
IF ((JSYM.GT.JMAX).OR.(JSYM.EQ.0)) FCU=JMAX
QSYM=FCU/RJMX
IM= (IMAX+ISYM-1)/ISYM
JHS=(JMAX
IF (JSYM.EQ.1) JMS=(JMAX/2+1)/2
IF (JSYM.EQ.0) JMS=JMAX/2
MODE=ABS(AR(13))
XO=0.
ZD=0.
PHISYM=0.
HS=SIZE/2.
RHOS=1.286
BOTS=NPTS
RPTS=NPTS
XPR=0.
IF (NPTS.GT.1) XPR=XPRNG/(RPTS-1.)/2.
XPM=-XPR
PIE=3.141592653589793
MONE=1
FORMAT (6.58, IMAX,JMAX,IMS,JMS,ISYM,JSYM,MSYM,QSYM,FCU,
        FORMAT (3X,1MAX,JMAX,IMS,JMS,ISYM,JSYM,MSYM,QSYM,FCU,
        NTWO=2
IX=IMAX+JMAX

```

```

NF=IN1
IF ((MODE.EQ.1).AND.(NOF.EQ.8)) CALL FREAD (NO,RO,NF,ZD) 6,69)
IF (Z=ZD
IF (DGN.GE.1.) WRITE (6,68)
CALL GARRAY (G,GA,NOF,DGN,MONE,XO,YO,PHISYM)
LM=1 ((LPT.EQ.0).AND.(BND.EQ.0)) LM=0
I JMX=IMAX+1
I JMX=IMAX+1
I JMX=IMAX*JMAX
NBD=1
IF (JSYM.EQ.0) NBD=2
KBD=15
DO 15 IJ=1,I JMX
GA(IJ)=0 GO TO 16
IF (NAF.EQ.0) GO TO 16
NF=IN2
IF ((NAF.EQ.8).AND.(DGN.GE.1.)) WRITE (6,69)
IF ((NAF.EQ.8)) CALL FREAD (NA,RA,NF,ZD)
MST=MODE
MODE=MST
IF (DGN.GE.1.) WRITE (6,68)
IF (NAF.NE.0) CALL GARRAY (GA,G,NAF,DGN,NTWO,XO,YO,PHISYM)
DO 6 IJ=1,I JMX
G(IJ)=G(IJ)+GA(IJ)
RLINS=NLINS
IF (NAF.EQ.8) WRITE (6,88) NA,(RA(L)),L=1,NA
IF (NOF.EQ.8) WRITE (6,87) NO,(RO(I)),I=1,NO
IF (LM.EQ.0) GO TO 14
RB(1)=-1
DO 1 I=2,7
RB(I)=RB(I-1)+.5
TPIE=2.*PIE
MPIE=-PIE
DYP=0.
DXP=0.
IF (NL INS.GT.1) DYP=YPRNG/(RLINS-1.)
IF (NP TS.GT.1) DXP=XPRNG/(RPTS-1.)
IF ((DGN.GE.1.) AND (NNN.EQ.2)) WRITE (6,64)
IF (NNN.EQ.2) CALL BDGEN (G,H,SCF,DGN,NBD,BDA,KBD)
DO 5 J=1,NLINS
IF (DGN.GE.1.) WRITE (6,67) J
RJM=J-1
PHI=PHI*Z+DELPHI*RJM
YD=(PHI+YD)*PIE/180.
PSI=(PHI+90.)*PIE/180.
1

```

```

TAU=PSI-PHI*SYM
IF(LPT.EQ.0) GO TO 9
IF(LLPT.GT.1) WRITE(6,78) (ST,I=1,124)
IF(LLCMS.EQ.1) WRITE(6,74) (ST,I=1,95)
IF(LLCMS.EQ.1).AND.(LPT.GT.1) READ(5,79) ZZ
WRITE(6,85) Z, PHI, YP(J)
WRITE(6,76) MODE*EQ.1) WRITE(6,83) (RB(I),I=1,7)
IF(MODE.GT.1) WRITE(6,80) (RB(I),I=1,13)
WRITE(6,81) (DH,I=1,54), (PL,II=1,13)
IC=0 DO 3 I=1,10PTS
RIM=(-1,0,0)
THEO(I,J)=0.
CA(I,J)=0.
FERR(I,J)=0.
CALC(I,J)=XPZERC+DXP*RIM
XP(I)=XP(XP(I))
XP(I)=ABS(XP(I)*LT(I)*E-10) XP(I)=0.
IF(XP(I)*LT(I)*E-10) XP(I)*#2+YP(J)*#2)/HS
RS=SQR(S*GT(I)*#2+YP(J)*#2)
IF(RS.GT.1) GO TO 13
HT=ATAN(YP(J),XP(I))
IF(XP(I)*EQ.0.) HT=0.
SIG=TAU-PIE/2.+TH
IF(SIG.GT.PIE) SIG=SIG-TPIE
IF(SIG.LT.MPIE) SIG=SIG+TPIE
SIGI=R*S*COS(SIG)
IF(DGN.EQ.1) WRITE(6,44) SIG
FORMAT('1.SIG=,E10.3')
YS=R*S*SIN(SIG)
IF(DGN.EQ.5) WRITE(6,57) PHI, PSI, TAU, TH, SIG, SIGI, XS, YS
57 RI=I
F=0 IF(DGN.EQ.2) WRITE(6,66) I
CALL(FUNCT,(XS,YS,NAF,DGN,NTWO)
IF(MODE.EQ.1) CALL FUNCT((XS,YS,F,NOF,DGN,MONE)
THEO(I,J)=F
IF(NNN.EQ.2) REWIND 3
IF(NNN.EQ.3) CALL FIELD3 (RS, SIGI, SOLN,NBD, BDA, DGN, KBD)
IF(NNN.EQ.4) CALL FIELD2 (RS, SIGI, SOLN,G, H, SCF, DGN)
CA(I)=SOLN/BDX/H
CALC(I,J)=CA(I)-FA(I,J)

```

RHO(I)=RHOINF*(CALC(I,J)+1.)

ERR(I)=CALC(I,J)

IF (IMODE.EQ.1) ERR(I)=(CALC(I,J)-THEO(I,J))

IF (IMODE.GT.1) THEO(I,J)=FA(I,J)

IF (LPY.EQ.0) GO TO 3

LC=0

TL(L)=BL

IF (XP(I).GT.XPM).AND.(XP(I).LT.XPR)) TTL=1.

IF (IC.EQ.5) IC=0

IF (IC.EQ.0) TL(1)=PL

DO 2 L=2,62

IF ((I.EQ.1).OR.(TTL.EQ.1).OR.(I.EQ.NPTS)) TL(L)=PL

IF ((LC.EQ.10).AND.(LC.EQ.0).AND.(LC.EQ.0)) TL(L)=PL

IF (LC=LC+1) PL

TL(22)=PL

TL(62)=PL

IC=IC+1

RLW=(CA(I)+1.)*20.+2.5

LW=RLW

IF (LW.GT.62) LW=62

IF (LW.LT.2) LW=2

TL(LW)=SC

RLY=(FA(I,J)+1.)*20.+2.5

LY=RLY

IF (LY.LT.62) LY=62

IF (NAFE.NE.0) TL(LY)=ST

RLX=(THEO(I,J)+1.)*20.+2.5

LX=RLX

IF (LX.GT.62) LX=62

IF (LX.LE.2) LX=2

IF (CALC(I,J)+1.)*20.+2.5

RLZ=RLZ

IF (LZ.GT.62) LZ=62

IF (LZ.LE.2) LZ=2

TL(L)=EX

WRITE(6,82) MOUT, KOUT, INDEX, THEO(I,J), CALC(I,J), RHO(I),

1XP(I)*(TL(L),L=1,62)

IF ((NPTS.LE.20).AND.(I.NE.NPTS)) WRITE(6,79)

CONTINUE

IF (LPY.NE.0) WRITE(6,81) (DH,I=1,54), (PL,I=1,13)

TMAX=0.

TMIN=0.

13

2

3

```

IE=0.
IE=0.
DO=4  I=1,NPTS
TH=THEO(I,J)
IF (TH.GT.TMAX) TMAX=TH
IF ((TH.LT.TMIN) TMIN=TH
IF (ABS(CALC(I,J)-TH)<ER)
BE=ER
IE=I
CONTINUE
CTM=RHOINF*(CALC(IE,J)-THEO(IE,J))
IF (CTM.NE.0.) BE=(CALC(IE,J)-THEO(IE,J))*100/CTM
WRITE(6,75) EB,XP(IE),BE
IF ((MOD.EQ.1).AND.(LPT.NE.0.)) YP(J)=PHI
IF (DELPHI.NE.0.)
CONTINUE
IF (BND.EQ.0.) GO TO 14
IF (LPT.EQ.1) WRITE(6,78) (ST,I=1,124)
IF (LPT.GT.1) WRITE(6,74) (ST,I=1,95)
IF (CMS.EQ.1) AND.(LPT.GT.1) READ(5,79) ZZ
IF (DGN.EQ.1) WRITE(6,63)
CALL (NPTS,NLINS,CALC,NOF,Z,BND)
NAO=10*NOD+NAF
IF (NAO.EQ.1) GO TO 10
IF ((NGP.EQ.3).AND.(GPUNCH(Z,XO,YO,PHISYM,NAO,IMAX,JMAX,G)
DO(7,I,J=1,1-JM) CALL GPUNCH(Z,XO,YO,PHISYM,NAO,IMAX,JMAX,G)
G(1,I)=G(I,J)-GA(I,J)
IF (IPT.EQ.0) GO TO 11
IF ((IPT.EQ.1).OR.(IPT.EQ.3)) WRITE(6,78) (ST,I=1,124)
IF ((IPT.EQ.2).OR.(IPT.EQ.4)) WRITE(6,74) (ST,I=1,95)
IF (AND.(CMS.EQ.1).OR.(IPT.EQ.2).OR.(IPT.EQ.4)) READ(5,79) ZZ
CALL GPRINT(1,G,MONE)
IF (NGP.EQ.3) CALL GPUNCH(Z,XO,YO,PHISYM,NOF,IMAX,JMAX,G)
IF (IPT.EQ.3) WRITE(6,78) (ST,I=1,124)
IF (IPT.EQ.4) WRITE(6,74) (ST,I=1,95)
IF (AND.(CMS.EQ.1).OR.(IPT.EQ.4)) READ(5,79) ZZ
IF (IPT.EQ.3) CALL CPRINT(GA,NTWO)
IF (IPT.EQ.0) GO TO 12
IF ((KPT.EEQ.1).OR.(KPT.EEQ.2).OR.(KPT.EEQ.4)) WRITE(6,78) (ST,I=1,124)
IF ((CMS.EEQ.1).OR.(KPT.EEQ.2).OR.(KPT.EEQ.4)) WRITE(6,74) (ST,I=1,95)
IF (AND.(KPT.EEQ.1).OR.(KPT.EEQ.2).OR.(KPT.EEQ.4)) READ(5,79) ZZ
IF (DGN.EQ.1) WRITE(6,61)
CALL GPLQT(G,GA,JMS)
WRITE(6,78) (EX,I=1,124)
AGAIN=ST

```

4

5

10

11

12

```

IF (CMSINE=1.) READ'S,60) AGAIN
IF (AGAIN.EQ.BL) GO TO 20
FORMAT(6,7) WRITE(6,7)
FORMAT(1,7) 1 POINTS, / THE INPUT DATA FOR ADD-ON FUNCTION NO.8 (' ,13,
FORMAT(1,7) 1 POINTS, / THE INPUT DATA FOR THE TEST FUNCTION NO.8, (' ,13,
FORMAT(1,7) 1 POINTS, / 711F10.3/) 1 POINTS, / 711F10.3/
FORMAT(1,7) 1 POINTS, / THE INVERTED CROSS SECTION FOR: '1
FORMAT(1,7) 1 POINTS, / 10X, CM. / 10X, 'DEGREES' / 10X,
FORMAT(1,7) 1 POINTS, / F8.3, = ORIGINAL FUNCTION/
FORMAT(1,7) 1 POINTS, / F8.3, = 44X,0 = ORIGINAL FUNCTION/
FORMAT(1,7) 1 POINTS, / * ADD-ON FUNCTION, HIT SPACE AND RETURN.'1
FORMAT(1,7) 1 POINTS, / ADJUST PAGE, HIT SPACE AND RETURN.'1
FORMAT(1,7) 1 POINTS, / LIMIT MAX ORIGINAL ABS COMPUTED (MG/CC)'1,
FORMAT(1,7) 1 POINTS, / TERM FUNCTION ERROR FUNCTION DENSITY '1,6H X,F4.1,
FORMAT(1,7) 1 POINTS, / K TERM 6,2X, 'FUNCTION',5X, 'SUM',3X, 'FUNCTION DENSITY '1,
FORMAT(1,7) 1 POINTS, / 6F10.1 (2X,I2,1X,13,1X,14,1X,F9.4,2X,F7.3,1X,F9.4,1X,F7.3,
FORMAT(1,7) 1 POINTS, / 62A1 X,62A1 X,54A1,2X,A1,12(4X,A1)
FORMAT(1,7) 1 POINTS, / 3X,MAX,3X;ADD-ON'6X,'THE'4X,'DENSITY (MG/CC)'1/CAL033200
FORMAT(1,7) 1 POINTS, / K TERM 6,2X, 'FUNCTION',5X, 'SUM',3X, 'FUNCTION DENSITY '1,
FORMAT(1,7) 1 POINTS, / F4.1,6F10.1)
FORMAT(1,7) 1 POINTS, / IX,F10.3)
FORMAT(1,7) 1 POINTS, / IX,I24A1)
FORMAT(1,7) 1 POINTS, / IX,'FUNCTION = (RHO/RHC-INFINITY)-1.0',33X,' : = THE'
FORMAT(1,7) 1 POINTS, / INVERTED SUM,70X,'X = COMPUTED FUNCTION')
FORMAT(1,7) 1 POINTS, / LARGEST ERROR, '1, F8.6, GMS/CC: AT ' ,3HX' =, F6.3
FORMAT(1,7) 1 POINTS, / 4X F10.2A1, PERCENT: /, HIT SPACE, RETURN ' ,48A1)
FORMAT(1,7) 1 POINTS, / IX,47A1, PERCENT PAGE, HIT SPACE, RETURN ' ,48A1)
FORMAT(1,7) 1 POINTS, / CALL 'READY'
FORMAT(1,7) 1 POINTS, / LINE, '13, 'DO LOOP')
FORMAT(1,7) 1 POINTS, / FIELD, '13, 'CALL FUNCT')
FORMAT(1,7) 1 POINTS, / CALL FIELD')
FORMAT(1,7) 1 POINTS, / CALL BDGEN')
FORMAT(1,7) 1 POINTS, / CALL MAP')
FORMAT(1,7) 1 POINTS, / CALL GPUNCH')
FORMAT(1,7) 1 POINTS, / CALL GPOINT')
FORMAT(1,7) 1 POINTS, / STOP
END

```

COCOOO1.
C

```

SUBROUTINE BDGEN ( G, H, SCF, DGN, NBD, BDA, KBD)
C
C      BDGEN EVALUATES THE B AND D COEFFICIENTS FOR ALL M AND K, AND WRITES
C      THE ARRAY LINEARLY ON DISK.
C
COMMON /TAB/ JMAX,X,IIMX,JJMX,ALPHA,I SIZE,EPS,MODE,BOX,SD,IX,Z
COMMON /SYM/ ISYM,MSYM,JSYM,MSSYM,FCU,IIMS,JMS,QSYM
DIMENSION S(IIMX),H(IIMX,5),SCF(IIMX,6),BDA(KBD)
C
INITIALIZE THE VALUES:
INDEX=0
KL2=NBD*KLIMIT
REWIND 3
IIMX6=J'IMX*6
IIMX2=(IIMX+1)/2
PIFE=3*141592653589793
RIMP=KLIMIT+1
DX=2.*JMAX
RJMA=2.*PIE/FCU
INITIALIZE MODIFIED HERMITE POLYNOMIAL ARRAY: (5)=HM+2 STORED
(1)=H1, (2)=H2, (3)=ALPHA*X(1), (4)=HM+2 STORED, (5)=HM+1 STORED
DO 1 I=1,IIMX2
RI=I
RIN=IIMX-IL+1
T1H(IIM,3)=ALPHA*(RI*I*DX-DX-1.)
T1H(IIM,1)=2.*H(IIM,3)
T1H(IIM,2)=(H(IIM,3)*H(IIM,1)-1.)/3.
T1H(IIM,4)=-H(IIM,2)
T1H(IIM,5)=H(IIM,2)
T1H(IIM,6)=H(IIM,2)
T1H(IIM,7)=H(IIM,1)
SIGN=1.
INITIATE THE SIN/COS ARRAY:
DO 2 J=1,JJMX
RJM=J-1
SCF(J,1)=0.
SCF(J,2)=1.
SCF(J,3)=SIN(RJM*DXI-PIE/2.)
SCF(J,4)=COS(RJM*DXI-PIE/2.)
SCF(J,5)=0.
SCF(J,6)=0.
MSE=0
COMMENCE THE M LOOP:

```

```

DO 7 MP=1,MLIMIT
RM=M
SIGN=-SIGN
SIF(DGN.LE.-4) WRITE(6,88) SCF(1,1),SCF(2,1),SCF(1,2),SCF(2,2)
C TEST FOR SYMMETRY SKIPS:
TEST(MS.EQ.MSYM) MS=0
TOTAL=0.
MS=M+1
IF(MS.EQ.MSYM) MS=0
C COMMENT CKP=1,KLIMIT
DO 5 KP=1,KLIMIT
K=KP-1
PK=K
RK=K
INDEX=INDEX+1
CALL BD(M,K,1,G,H,SCF(3,89),JMX6)
IF(DGN.EQ.3.) WRITE(6,89) M,K,B,D
IF(DGN.LE.-2.) WRITE(6,88) H(1,1),H(1,2),H(1,4),H(1,5)
IF(DGN.LE.1.)
KK=K*NBD+1
K2=K*NBD
BDA(K2)=D
BDA(KK)=B
GENERATE=M+2*KP+1
ORDER=SQR(T(PK*(PK+RM)))*(ORDER
HB=2.*SQR((PK+1.)*(RM+PK+1.))/(ORDER+1.)/(ORDER+2.))
DO 5 I=1,IMX2
IM=IMX-I+1
I1=I+1
I2=I+2
I3=I+3
H(I1,I1)=2.*((H(I1,I3)*H(I1,2))-HA*H(I1,1))
H(I1,I2)=SIGN(H(I1,I1))*H(I1,I3)-(H(I1,I1)-ORDER*H(I1,2))
H(I1,I3)=HB*((H(I1,I3)*H(I1,2))-ORDER*H(I1,1))
ADVANCE THE SIN/COS ARRAY FOR THE NEXT M:
DO 3 J=1,JMX
IF(DGN.LE.-5) WRITE(6,87) SCF(J,NT),NT=1,6)
FORMAT(5E10.3)
STEMP=SCF(J,1)
SCF(J,1)=SCF(J,2)*SCF(J,1)*SCF(J,3)*SCF(J,4)
SCF(J,2)=SCF(J,1)*SCF(J,3)
SCF(J,3)=SCF(J,1)*SCF(J,2)-SCF(J,1)
SCF(J,4)=SCF(J,5)*SCF(J+1,1)-SCF(J,1)
SCF(J,5)=SCF(J+1,2)-SCF(J,2)
WRITE(3)(BDA(I),I=1,KBD)
IF(DGN.LE.-3) WRITE(6,88) (BDA(I),I=1,10)
RM=RM+1

```

6

```

C   REGENERATE THE HERMITE ARRAY FOR NEW M, K=0:
      DD? I=1 IMX2
      IM= IIMX-1+1
      H(I,I,2)=H((I,I,4)*SQRT(RM)/(RM+1.))
      H(I,I,1)=-SIGN*(H(I,I,1)
      H(I,I,2)=2.*SQRT(RM+1)*(H((I,I,3)*H((I,I,1)-(RM+1.)*H((I,I,2)))
      H(I,I,2)=(H((I,I,2)/(RM+2.)/(RM+3.))
      H(I,I,4)=H((I,I,2)
      FORMAT(7,14);*, K=' , i4, *, B=' , E10.4, *, D=' , E10.4)
      FORMAT(2X,10E10.3)
      RETURN
      END

      C0000002

C   SUBROUTINE FIELD (RS,SIG,SOLN,NBD,BDA,DGN,KBD)
C
C   FIELD EVALUATES THE VALUE OF THE FIELD FUNCTION AT A PARTICULAR
C   POINT DESIGNATED IN CYLINDRICAL COORDINATES, BY USING THE INVERSION
C   EQUATION OF MALDONADO. AL FIELD USES THE ARRAY OF B & D
C   COEFFICIENTS GENERATED IN SUBROUTINE BOGEN.
C
C   COMMON IMAX,IJMAX,JJMAX,IJTRA,MEXTRA,KLIMIT,MLIMIT,MOUT,MOUT,
C   /TAB,IINDEX,KEXTRA,MSYM,FCU,IMS,JMS,QSYM
C   COMMON /SYM/ ISYM,JSYM,MSYM,FCU,IMS,JMS,QSYM
C   DIMENSION BDA(KBD),STK(52),STM(52)
C
C   INITIALIZES THE VALUES:
C   INDEX=C
C   MTIME=0
C   KOUT=0
C   MOUT=0
C   KMAX=0
C   TOTAL=C*JM*6
C   JMAX6=J*JM*6
C   REWIND 3
C   AR=ALPHA*S
C   ARG=AR**2
C   EXPON=EXP(-ARG)
C   PIE=ALPHA/PIE/PIE
C   M=0
C   RM=M
C   RIMAX=IMAX
C   DX=2./RIMAX

```

```

RJMAX=JMAX
SIGN=1.
STK(1)=0.
STM(1)=0.
SMS=0.
CM1=SIN(SIG)
CMEP=COS(XTRA+1)
DO 16 MB=1,MEP
16 STM(MB)=0.
SFH=1.

MS=0
2 COMMENCE THE M LOOP:
SIGN=-SIGN
K=0
RK=K
RM=M
ARM=1.
IF (M.NE.0) ARM=ARM**M
KTIMER=0
KEP=KXTRA+1
DO 15 KB=1,KEP
15 STK(KB)=0.
SIGNK=-1.
C COMPUTE THE K=0 & K=1 ORDERS OF LAGUERRE POLYNOMIAL FOR GIVEN M:
PM=0.
P=SQRT((1./FM)
PP=(CRM+L*TARG)*SQRT((1./FM)/(RM+1.))
C TEST FOR SYMMETRY SKIPS:
TEST(MS.EQ.MSYM) MS=0
MS=MS+1
IF (MS.NE.1) GO TO 7 COEFFICIENTS FOR GIVEN M:
READ A LINE OF B & D COEFFICIENTS FOR GIVEN M:
READ (3) (BDA(I),I=1,KBD)
IF (DGN.LE.-6) WRITE (6,88) (BDA(I),I=1,10)
C COMMENCE THE K LOOP:
3 INDEX=INDEX+1
SIGNK=-SIGNK
C COMPUTE THE M,K SUMMATION TERM:
KK=K*NBD+1
B=BDA(KK)
D=0.
IF (NBD.EQ.2) D=BDA(KK+1)
BRAKE=B
IF (RM.EQ.0.) GO TO 4
BRAKE=B*CMS+D*SMS
ADD=SIGNK*BRAKE*P*ARM
4

```

```

TOTAL=TOTAL+ADD GO TO 5
IF (DGN.GT.-5) GO TO 5
STOT=TOTAL*EXPN*APP/BOX/SIZE
WRITE (6,89) M,K,STOT,ADD,BRAKET,P,ARM,B,CMS,D,T,SMS
89 WRITE (6,89) THE RELATIVE SIZE OF THE SERIES:
C ESTABLISH CHECK AS THE RELATIVE SIZE OF THE SERIES:
CHECK=ABS(ADD)
IF (TOTAL.GT.EPS) CHECK=ABS(ADD/TOTAL)
C ADVANCE THE K INDEX:
K=K+1
RK=K
DO 10 KA=1,KEXTRA
KB=KEXTRA-KA+1
STK(KB+1)=STK(KB)
10 STK(2)=TOTAL
ORDER=M+2*K+1
PM=P
P=PP
PP=PP*(ORDER-ARG)-PM*SQRT(RK*(RM+RK))
C SET K TIMER TO PROVIDE EXTRA K TERMS AFTER CHECK < EPS:
K TIMER=KTIMER+1
IF (K.GE.KLIMIT) GO TO 6
IF (CHECK.GE.EPS) K TIMER=0
IF (KTIMER.LE.KEXTRA) GO TO 3
GO TO 7
KOUT=KOUT+1
6 IF (KEXTRA.EQ.0) GO TO 7
TOTAL=0
DO 11 KA=1,KEXTRA
11 TOTAL=TOTAL+STK(KA+1)
RKX=KEXTRA
TOTAL=TOTAL/RKX
END OF K LOOP: ADVANCE M:
7 M=N+1
RM=N
STP=SMS
SMS=S4S*CM1+CMS*SM1
CMS=CM1*CM1-STP*SM1
IF (K.GT.KMAX) KMAX=K
FM=FM*RM
DO 12 MA=1,MEXTRA
MB=MEXTRA-MA+1
STM(MB+1)=STM(MB)
12 STM(2)=TOTAL
SET M TIMER FOR EXTRA M TERMS:
IF (MS.EQ.1) MTIMER=MTIMER+1
IF (JSYM.GT.JMAX) GO TO 9

```

```

13      IF (K.GT.KEXTRA) MTIMER=0
13      IF (M.GE.MLIMIT) GO TO 13
13      IF (MTIMER.LE.MEXTRA.EQ.0) GO TO 9
13      TOTAL=MEXTRA
14      TOTAL=TOTAL+STM(MA+1)
14      RMX=MEXTRA
14      TOTAL=TOTAL/RMX
14      END OF M LOOP: COMPUTE OUTPUT SOLN.
14      MOUT=M-1
14      IF (KOUT.EQ.0) KOUT=KMAX-1
14      SOLN=TOTAL*EXP(ON*APP/2.)
14      FORMAT ('M=',I4,'; K=',I4,'; SUBTOTAL = ',9E10.3)
14      RETURN
14      END
C000003
C

SUBROUTINE BD (M,K,G,H,SCF,B,D,JJMX6)
C
C BD EVALUATES THE FIRST (B) AND SECOND (D) COEFFICIENTS IN THE
C INVERSION EQUATION FOR A PARTICULAR SET OF INDEXES M & K.
C BD MAKES USE OF THE HERMITE POLYNOMIAL ARRAY GENERATED BY
C SUBROUTINE FIELD AS M & K ADVANCE.
C
COMMON /SYM/ IJMAX, IJMX, IJSYM, IJSYMX, FCU, IMX, Z
COMMON /SCF/ IJMX, IJSYM, IJSYMX, SCF(IJMX), H(IJMX)
DIMENSION G(IJMX), B(IJMX), D(IJMX)
PIE=3.141592653589793
B=0.
D=0.
RM=K
RK=K
RJMAX=JMAX
JJMX4=4*IJMX
DXI=2.*PIE/FCU
FORMAT(1X,I10,1)
IF (M.NE.0) GO TO 2
S=DXI
DO 1 J=1,JMAX
DO 1 I=1,IMAX
1 I=I+1
1 J=IJMX*(J-1)+1
20.0
SUB02400
SUB02410
SUB02420
SUB02430
SUB02440
SUB02450
SUB02460
SUB02470
SUB02480
SUB02490
SUB02500
SUB02510
SUB02520
SUB02530
SUB02540
SUB02550
SUB02560
SUB02570
SUB02580
SUB02590
SUB02600
SUB02610
SUB02620
SUB02630
SUB02640
SUB02650
SUB02660
SUB02670
SUB02680
SUB02690
SUB02700
SUB02710
SUB02720
SUB02730
SUB02740
SUB02750
SUB02760
SUB02770
SUB02780
SUB02790
SUB02800
SUB02810
SUB02820
SUB02830
SUB02840

```

```

1      DH=H(I,I)-H(I,I)
2      B=B+G(I,J)*S*DH
3      B=B*QSYM/2.
      RETURN
4      DO 5 J=1,JMAX
5      S=SCF(J,J)/RM
      DO 6 I=1,IMAX
6      I1=I+1
      IJ=I*MAX*(J-1)+I
      DH=H(I,I)-H(I,I)
      B=B+G(I,J)*S*DH
      B=B/2.
      RETURN
7      IF(M.NE.0) GO TO 6
8      S=DXI
      DO 9 J=1,JMAX
9      S=SCF(I,J)/RM
      DO 10 I=1,IMAX
10     I1=I+1
      IJ=I*MAX*(J-1)+I
      DH=H(I,I)-H(I,I)
      B=B+G(I,J)*S*DH
      B=B/2.
      RETURN
11     DO 12 J=1,JMAX
12     J2=J*S+J*JMX
      S=SCF(J,J2)/RM
      C=SCF(J,J2)/RM
      DO 13 I=1,IMAX
13     I1=I+1
      IJ=I*MAX*(J-1)+I
      DH=H(I,I)-H(I,I)
      B=B+G(I,J)*S*DH
      FORMAT(1,BD:,415,10F6.2)
      D=D-G(I,J)*C*DH
      RETURN
14     END
      C000004

```

SUBROUTINE FIELD2 (RS,SIG,SOL J,H,SCF,DGN)
 SUB02850
 SUB02860
 SUB02870
 SUB02880
 SUB02890
 SUB02910
 SUB02920
 SUB02930
 SUB02940
 SUB02950
 SUB02960
 SUB02970
 SUB02980
 SUB02990
 SUB03000
 SUB03010
 SUB03020
 SUB03030
 SUB03040
 SUB03050
 SUB03060
 SUB03070
 SUB03080
 SUB03090
 SUB03100
 SUB03110
 SUB03120
 SUB03130
 SUB03140
 SUB03150
 SUB03160
 SUB03170
 SUB03180
 SUB03190
 SUB03200
 SUB03210
 SUB03220
 SUB03230
 SUB03240
 SUB03250
 SUB03260
 SUB03270
 SUB03280
 SUB03290
 SUB03300

CC FIELD2 COMPUTES THE SAME INVERSION AS SUBROUTINE FIELD1 EXCEPT THAT
 CC THE COEFFICIENTS B AND D ARE COMPUTED INDIVIDUALLY AS USED BY
 CC CALLING BD. DISK STORAGE IS NOT REQUIRED BUT COMPUTING TIME IS
 CC MUCH GREATER. FIELD2 IS UTILIZED BY SPECIFYING A NEGATIVE MODE ON

THE INPUT PARAMETER. VALUE OF THE FIELD FUNCTION AT A PARTICULAR
 FIELD POINT DESIGNATED IN CYLINDRICAL COORDINATES BY USING THE INVERSION
 EQUATION OF MALDONADO, ET AL. FIELD CALLS SUBROUTINES BD & GARRAY.
 COMMON /TAB/ JMAX, JMAX, JMAX, ALPHA, EPS, MODE, BOX, SD, IX, Z
 COMMON /SYM/ ISYM, JSYM, MSYM, FCU, IJMS, QSYM
 DIMENSION G(IJMX), H(IJMX,5), SCF(IJMX,6)
 INITIALIZE THE VALUES:
 INDEX=0
 INTIMER=0
 KOUT=0
 KMAX=0
 KWMAX=0
 TOTAL=0
 JJMX6=JJMX*6
 JJMX2=(IJMX+1)/2
 AR=ALPHA*RS
 ARG=AR**2
 EXPON=EXP(-ARG)
 PIE=3.141592653589793
 APP=ALPHA/PIE
 NM=0
 RM=M
 RIMAX=IMAX
 DX=2./RIMAX
 RJMAX=JMAX
 OXI=2.*PIE/FCU
 INITIALIZE THE MODIFIED HERMITE POLYNOMIAL ARRAY: VECTORS:
 (1)=H1, (2)=H2, (3)=ALPHA*X(1), (4)=HM+2 STORED, (5)=HM+1 STORED
 DO 1 I=1,IJMX2
 RI=IJMX-I+1
 TI=IJMX-I+1
 H(I,I,3)=ALPHA*(RII*DX-DX-1.)
 H(I,I,3)=-H(I,I,3)
 H(I,I,2)=2.*H(I,I,3)
 H(I,I,2)=(H(I,I,3)*H(I,I,1)-1.)/3.
 H(I,I,1)=-H(I,I,2)
 H(I,I,2)=H(I,I,2)
 H(I,I,3)=H(I,I,2)
 H(I,I,4)=H(I,I,2)
 H(I,I,4)=H(I,I,1)
 SIGN=1.
 FN=1.
 C INITIATE THE SIN/COS ARRAY:
 SUB03310
 SUB03320
 SUB03330
 SUB03340
 SUB03350
 SUB03360
 SUB03370
 SUB03380
 SUB03390
 SUB03400
 SUB03410
 SUB03420
 SUB03430
 SUB03440
 SUB03450
 SUB03460
 SUB03470
 SUB03480
 SUB03490
 SUB03500
 SUB03510
 SUB03520
 SUB03530
 SUB03540
 SUB03550
 SUB03560
 SUB03570
 SUB03580
 SUB03590
 SUB03600
 SUB03610
 SUB03620
 SUB03630
 SUB03640
 SUB03650
 SUB03660
 SUB03670
 SUB03680
 SUB03690
 SUB03700
 SUB03710
 SUB03720
 SUB03730
 SUB03740
 SUB03750
 SUB03760
 SUB03770
 SUB03780

```

DO 11 J=1, JJMX
RJM=J-1
SCF(J,1)=0.
SCF(J,2)=1.
SCF(J,3)=SIN(RJM*DXI-PIE)
SCF(J,4)=COS(RJM*DXI-PIE)
SCF(J,5)=0.
SCF(J,6)=0.
11 MS=0
      COMMENCE THE M LOOP:
      K=K
      ARM=1.
      IF (M*NE.0) ARM=ARM***M
      K1MER=0
      SIGNK=-1
      COMPUTE THE K=0 & K=1 ORDERS OF LAGUERRE POLYNOMIAL FOR GIVEN M:
      PM=0.
      P=SQRT(1./FM)
      PP=(RM+1.-ARG)*SQRT((1./FM)/(RM+1.*M))
      ADVANCE THE SIN/COS ARRAY FOR NEW M:
      DO 12 J=1, JJMX
      SCF(J,1)=SCF(J,1)*SCF(J,1)+SCF(J,2)*SCF(J,3)
      SCF(J,2)=SCF(J,2)*SCF(J,1)-SCF(J,1)*SCF(J,3)
      DO 13 J=1, JJMX
      SCF(J,5)=SCF(J+1,1)-SCF(J,1)
      SCF(J,6)=SCF(J+1,2)-SCF(J,2)
      13 TEST FOR SYMMETRY SKIPS:
      IF (MS.EQ. MSYM) MS=0
      TOTAL=0.
      MS=MS+1
      IF (MS*NE.1) GO TO 7
      RMS=RJM*SIGNK
      CMS=COS(RJM)
      SMS=SIN(RJM)
      COMMENCE THE K LOOP:
      INDEX=INDEX+1
      SIGNK=-SIGNK
      CALL THE B & D COEFFICIENTS AND COMPUTE THE M,K SUMMATION TERM:
      3 CALL BD(M,K,GH,SCF18,D,JMX6)
      IF (DGN.LE.-2.) WRITE (6,89) M,K,B,D
      BRAKET=B
      IF (RM.EQ.0.) GO TO 4
      BRAKET=B*CMS+D*SMS
      ADD=SIGNK*BRAKET*p*ARM
      TOTAL=TOTAL+ADD
      4 ESTABLISH CHECK AS THE RELATIVE SIZE OF THE M,K TERM OF THE SERIES: SUB04260

```

```

C CHECK=ABS(ADD)
C IF (TOTAL.GT.EPS) CHECK=ABS(ADD/TOTAL)
C ADVANCE THE K INDEX:
K=K+1
RK=RK
ORDER=M+2*K+1
C GENERATE THE NEXT ORDER OF LAGUERRE POLYNOMIAL FOR NEW K:
PM=P
P=PP*(ORDER-ARG)-PM*SQRT(RK*(RM+RK))
PP=PP/SQRT((RK+1.)*(RM+RK+1.))
C GENERATE THE NEXT ORDER OF THE SET OF HERMITE POLYNOMIALS FOR NEW K:
HA=SQR(T(RK*(RK+RM))/ORDER)
HB=2.*SQRT((RK+1.)*(RM+RK+1.))/(ORDER+1.)/(ORDER+2.)
DO 5 IIMX=I+1,I+3
H(IIM1)=2.*H(IIM3)*H(II,2)-HA*H(II,1)
H(IIM2)=SIGN(H(IIM1))*H(IIM3)*H(II,1)-ORDER*H(IIM2)
5 SET K TIMER=KTIMER+1
IF (K.GE.KLIMITE) GO TO 6
IF (MTIMER.LE.KEXTRA) GO TO 2
IF (CHECK.GE.0) KTIMER=0
GO TO 7
END OF K LOOP: ADVANCE M AND COMPUTE NEW TOTAL:
M=M+1
KOUT=KOUT+1
IF (K.GT.KMAX) KMAX=X
RM=FM*RM
FM=FM*RM
C REGENERATE THE HERMITE ARRAY FOR NEW M, K=0:
DO 8 IIM=1,IIMX2
H(IIM1)=H(IIM4)*SQRT(RM)/(RM+1.)
H(IIM2)=H(IIM5)*(RM+2.)
H(IIM3)=-SIGN*H(IIM1)
H(IIM4)=2.*SQRT((RM+1.)*(H(IIM3)*H(IIM1)-(RM+1.)*(RM+3.)))
H(IIM5)=H(IIM2)/(RM+2.)
H(IIM6)=H(IIM1)
8 SET M TIMER FOR EXTRA M TERMS:
IF (MS.EQ.1) MTIMER=MTIMER+1
IF (JSYM.GT.JMAX) GO TO 9
IF (K.GT.KLIMIT) MTIMER=0
IF (M.GT.MLIMIT) GO TO 9
C END OF M LOOP: COMPUTE OUTPUT SOLN.

```

```

9      MOUT=M-1          KOUT=KMAX-1
     IF (KOUT.EQ.0)      KOUT=KMAX-1
     SOLN=TOTAL*EXPON*APP/2.
89    FORMAT (14,14,14,14)
     RETRN
     END
D=' , E10.4, ', B=' , E10.4, ', C=000005

```

SUBROUTINE GARRAY (G, GA, NOF, DGM, NUMB, XO, YO, PHISYM)
 GARRAY FILLS THE DATA ARRAY OVER AN ORTHOGONAL AREA WITH
 THE REGULAR DATA OBTAINED BY THE METHOD CORRESPONDING TO
 PARTICULAR MODE:

MODE 1	- DATA OBTAINED BY SAMPLING A KNOWN FUNCTION SUPPLIED IN SUBROUTINE FUNCT AND SAMPLED IN SUBROUTINE GOLF.
MODE 2	- DATA OBTAINED BY GENERATING A REGULAR ARRAY FROM IRREGULAR EXPERIMENTAL INPUT DATA READ IN. CALLS SUBROUTINE SHEET. (EXPERIMENTAL DATA MAY BE SIMULATED, SEE "SHEET")
MODE 3	- UTILIZES RAW DATA TAKEN AT THE PROPER INTERVALS AND GENERATES A REGULAR ARRAY FOR USE IN SUBROUTINE GOLF.

N 7E 3 - UTILIZES RAW DATA TAKEN AT THE PROPER INTERVAL,
OR PREVIOUSLY GENERATED AND READ DIRECTLY INTO THE
ARRAY. CALLS SUBROUTINE READ.

```

      DELR=SIZE/RIMX
      DELXI=2.*PIE/FCU
      IF (MODE.GT.1) GO TO 2
      DO 1 J=1,JMS
      RJ=J
      XI=(RJ-.5)*DELEXI-PIE
      J2=J+2*(JMS-J)
      J3=J+JMAX/2
      J4=J2+JMAX/2

```

```

DO 1 I=1,IMS
RI=I
I=IMAX+1-I
R=(RI-5)*DELR-HS
CALL GOLF(R,XI,GIJ,NOF,DGN,NUMB)
G(I,J)=GIJ
IF (ISYM.EQ.2) GO TO 1
IF (ISYM.EQ.2) GO TO 1
G(I,J3)=GIJ
IF (I,JSYM.EQ.0) GO TO 1
G(I,J2)=GIJ
G(I,J4)=GIJ
CONTINUE
GO TO 4
IF (MODE.EQ.2) GO TO 3
1   2   CALL SHEET (G,GA,X0,Y0,PHISYM,NOF)
      GO TO 4
      CALL READ (Z,X0,Y0,PHISYM,NOF,IMAX,JMAX,G)
      IF (DGN.EQ.2) WRITE (6,39)
      RETURN 10 GARRY RETURNS'
39  END
C000006
C

```

```

SUBROUTINE GOLF (R,XI,GIJ,NOF,DGN,NUMB)
C GOLF COMPUTES THE FUNCTION G(R,XI) FOR A PARTICULAR LINE OF SIGHT
C FROM A KNOWN FUNCTION CONTAINED IN SUBROUTINE FUNCT.
COMMON IMAX,JMAX,IIMX,JMX,ALPHA,SIZE,EPS,MODE,BOX,SD,IX,Z
ZERO=0.0
LMAX=IMAX*3
RLMAX=LMAX
DELXP=SIZE/RLMAX
SX1=SIN(XI)
CX1=COS(XI)
DELXS=DELXP*SX1
DELYS=DELXP*CX1
XP=DELXP*.5-SIZE/2.
XS=XP*CXI-R*SXI
YS=XP*SXI+R*CXI
GIJ=0.
DO 1 L=1,LMAX
RL=L
CALL FUNCT(XS,YS,F,NOF,DGN,NUMB)
GIJ=GIJ+F
1   39  FORMAT 10 GARRY RETURNS'
      39  END
C

```



```

1 IF (NOF.GT.1) GO TO 2
F=AA*EXP(-1.0*(R*HS/B8)**2)
GO TO 11

2. ADJUSTABLE RECTANGULAR STEP FUNCTION:
F=PP
IF ((ABS(XS-DD).LE.BB).AND.(ABS(YS-EE).LE.CC)) F=AA
GO TO 11

3. DISPLACABLE ELLIPTICAL GAUSSIAN:
IF (NOF.GT.3) GO TO 4
F=AA*EXP(-1.0*((XS-DD)/BB)**2+((YS-EE)/CC)**2)
GO TO 11

4. CONSTANT:
IF (NOF.GT.4) GO TO 5
F=AA
GO TO 11

5. ADJUSTABLE AND DISPLACABLE ELLIPTIC RAMP FUNCTION:
IF (NOF.GT.5) GO TO 6
RBC=SQRT((XS-DD)/BB)**2+((YS-EE)/CC)**2
F=0
IF (RBC.LT.1.) F=AA*((1.0-RBC)**PP)
GO TO 11

6. DISPLACABLE ELLIPTIC STEP FUNCTION:
IF (NOF.GT.6) GO TO 7
RBC=SQRT((XS-DD)/BB)**2+((YS-EE)/CC)**2
F=0
IF (RBC.LT.1.) F=AA
GO TO 11

7. CIRCULAR COSINE-SQUARED FUNCTION OF BB MAXIMA:
IF (NOF.GT.7) GO TO 8
F=AA*COS((2.*BB-1.)*PI*R/2.0)**2
GO TO 11

8. NUMERICAL FUNCTION: REQUIRES AN INPUT ARRAY READ IN BY
A SUBROUTINE FREAD: N FOLLOWED BY N POINT VALUES. (101 MAX)
A CONSTANT VALUE AA IS ADDED TO THE FUNCTION.
IF (NOF.GT.8) GO TO 9
IF (NUMB.LE.1) N=NO
IF (NUMB.GT.1) N=NA
NM=N-1
NM=N-2
RN=N

```

```

RI=R*(IRN-1)+1.
IR=INT(IR)
IR=IR-FLCAT(IR)
DI=(NUMB.LE.1) F=RO(IR)
IF (NUMB.GT.1) F=RA(IR)
IF ((IR.NE.N).AND.(NUMB.LE.1)) F=F+DI*(RO(IR+1)-RO(IR))
IF ((IR.NE.N).AND.(NUMB.GT.1)) F=F+DI*(RA(IR+1)-RA(IR))
F=F-AA+83
GO TO 11

C C C 9. SPECIAL FUNCTION: MAY BE WRITTEN FOR THE OCCASION AND
C C C INSERTED IN SUBROUTINE SPFUN
C C C IF (NPF.GT.9) GO TO 10
C C C CALL SPFUN (XS,YS,F)
C C C GO TO 11

C C C EQUATIONS NO. 10 AND BEYOND ARE SET TO ZERO.
C C C 10 F=0.

C C C 11 IF (DGN .GE. 4) WRITE (6,99) XS,YS,F
C C C 99 FORMAT (6,99) XS=1,YS=1,F8.3,*, F=1,F8.3)
C C C RETURN
C C C END
C C C 000008

C C C SUBROUTINE SPFUN (XS,YS,F)
C C C SPFUN IS A SPECIAL ROUTINE FOR EQN NO. 9. ANY FUNCTION MAY BE
C C C ENTERED.
C C C COMMON /EQPARA/A,B,C,D,E,P,Q,S,T,U,V,W,RO,RA,NO,NA,N1,N2
C C C DIMENSION RC(101),RA(101)
C C C F=0
C C C IF (ABS(XS).LE.B).AND.(ABS(YS).LE.C)) F=A
C C C RETURN
C C C END
C C C 000009

```

SUBROUTINE SHEET (G,D,XO,YO,PHISYM,NOF)
SHEET READS IRREGULARLY SPACED VALUES OF
OBTAINED FROM HOLOGRAPHIC INTERFEROGRAMS
DEFINED EITHER BY GRID INTERCEPT POSITION
ABOUT THE CENTER OF THE LABORATORY COORDINATE
SYSTEM. DATA MAY BE SIMULATED BY A FUN-
(POS.) RADIUS. DATA MAY BE SIMULATED BY
FOLLOWED BY A PERATURE POSITIONS FOR A FUN-

SUBROUTINE SHEET (G,D,XO,YO,PHISYM,NOF)

SHEET READS IRREGULARLY SPACED VALUES OF THE LINE INTEGRALS AS OBTAINED FROM HOLOGRAPHIC INTERFERograms. THE LINE INTEGRALS ARE DEFINED EITHER BY GRID INTERCEPT POSITIONS OR BY ANGLE AND RADIUS ABOUT THE CENTER OF THE LABORATORY COORDINATE SYSTEM. CENTER MUST BE ENTERED IN CONSECUTIVE ORDER FROM LOWEST (NEG.) TO HIGHEST (POS.) RADIUS. DATA MAY BE SIMULATED BY SPECIFYING NOCODE=1. SUBFUNCTION NUMBER IN *SUBFUNCNT*.

```

COMMON IMAXX,IIMX,JIMX,ISYM,MSYM,FCU,IMS,JMS,QSY,
COMMON /IO/CMS,IN1,IN2,IN4
DIMENSION XG(303),YD(303),YI(303),XY(303)
NAR=303
PIE=3.141592653589793
MPIE=-PIE
TPIE=2.*PIE
MPIT=PIE/2.
PIET=PIE/2.*PIE
      THE=1:J=1:IMAX
      DO 1 J=1:JMAX
      G11=1:J1=0.
      DO 2 I=1:NAR
      XG(I)=0.
      XYG(I)=0.
      YDG(I)=0.
      XRI=0.
      YRI=0.
      RR=0.
      IF (CMS*EQ.1.) REWIND 1
      READ (IN1,59) NOF,INCODE
      READ (IN1,58) ZM
      READ (IN1,59) JM
      RIMX=IMAX
      DR=SIZE/RIMX
      R=(DR-SIZE/2.*Y0**#2)
      RZ0=SQR(T(X0**#2+Y0**#2))
      GAN=SATANM(Y0,X0)
      BT=JSYM
      DAN=PIE*TP/BT
      HS=SIZE/2.
      C
      1
      2
      3
      4
      5
      6
      7
      8
      9
      10
      11
      12
      13
      14
      15
      16
      17
      18
      19
      20
      21
      22
      23
      24
      25
      26
      27
      28
      29
      30
      31
      32
      33
      34
      35
      36
      37
      38
      39
      40
      41
      42
      43
      44
      45
      46
      47
      48
      49
      50
      51
      52
      53
      54
      55
      56
      57
      58
      59
      60
      61
      62
      63
      64
      65
      66
      67
      68
      69
      70
      71
      72
      73
      74
      75
      76
      77
      78
      79
      80
      81
      82
      83
      84
      85
      86
      87
      88
      89
      90
      91
      92
      93
      94
      95
      96
      97
      98
      99
      100
      101
      102
      103
      104
      105
      106
      107
      108
      109
      110
      111
      112
      113
      114
      115
      116
      117
      118
      119
      120
      121
      122
      123
      124
      125
      126
      127
      128
      129
      130
      131
      132
      133
      134
      135
      136
      137
      138
      139
      140
      141
      142
      143
      144
      145
      146
      147
      148
      149
      150
      151
      152
      153
      154
      155
      156
      157
      158
      159
      160
      161
      162
      163
      164
      165
      166
      167
      168
      169
      170
      171
      172
      173
      174
      175
      176
      177
      178
      179
      180
      181
      182
      183
      184
      185
      186
      187
      188
      189
      190
      191
      192
      193
      194
      195
      196
      197
      198
      199
      200
      201
      202
      203
      204
      205
      206
      207
      208
      209
      210
      211
      212
      213
      214
      215
      216
      217
      218
      219
      220
      221
      222
      223
      224
      225
      226
      227
      228
      229
      230
      231
      232
      233
      234
      235
      236
      237
      238
      239
      240
      241
      242
      243
      244
      245
      246
      247
      248
      249
      250
      251
      252
      253
      254
      255
      256
      257
      258
      259
      260
      261
      262
      263
      264
      265
      266
      267
      268
      269
      270
      271
      272
      273
      274
      275
      276
      277
      278
      279
      280
      281
      282
      283
      284
      285
      286
      287
      288
      289
      290
      291
      292
      293
      294
      295
      296
      297
      298
      299
      300
      301
      302
      303
      304
      305
      306
      307
      308
      309
      310
      311
      312
      313
      314
      315
      316
      317
      318
      319
      320
      321
      322
      323
      324
      325
      326
      327
      328
      329
      330
      331
      332
      333
      334
      335
      336
      337
      338
      339
      340
      341
      342
      343
      344
      345
      346
      347
      348
      349
      350
      351
      352
      353
      354
      355
      356
      357
      358
      359
      360
      361
      362
      363
      364
      365
      366
      367
      368
      369
      370
      371
      372
      373
      374
      375
      376
      377
      378
      379
      380
      381
      382
      383
      384
      385
      386
      387
      388
      389
      390
      391
      392
      393
      394
      395
      396
      397
      398
      399
      400
      401
      402
      403
      404
      405
      406
      407
      408
      409
      410
      411
      412
      413
      414
      415
      416
      417
      418
      419
      420
      421
      422
      423
      424
      425
      426
      427
      428
      429
      430
      431
      432
      433
      434
      435
      436
      437
      438
      439
      440
      441
      442
      443
      444
      445
      446
      447
      448
      449
      450
      451
      452
      453
      454
      455
      456
      457
      458
      459
      460
      461
      462
      463
      464
      465
      466
      467
      468
      469
      470
      471
      472
      473
      474
      475
      476
      477
      478
      479
      480
      481
      482
      483
      484
      485
      486
      487
      488
      489
      490
      491
      492
      493
      494
      495
      496
      497
      498
      499
      500
      501
      502
      503
      504
      505
      506
      507
      508
      509
      510
      511
      512
      513
      514
      515
      516
      517
      518
      519
      520
      521
      522
      523
      524
      525
      526
      527
      528
      529
      530
      531
      532
      533
      534
      535
      536
      537
      538
      539
      540
      541
      542
      543
      544
      545
      546
      547
      548
      549
      550
      551
      552
      553
      554
      555
      556
      557
      558
      559
      560
      561
      562
      563
      564
      565
      566
      567
      568
      569
      570
      571
      572
      573
      574
      575
      576
      577
      578
      579
      580
      581
      582
      583
      584
      585
      586
      587
      588
      589
      590
      591
      592
      593
      594
      595
      596
      597
      598
      599
      600
      601
      602
      603
      604
      605
      606
      607
      608
      609
      610
      611
      612
      613
      614
      615
      616
      617
      618
      619
      620
      621
      622
      623
      624
      625
      626
      627
      628
      629
      630
      631
      632
      633
      634
      635
      636
      637
      638
      639
      640
      641
      642
      643
      644
      645
      646
      647
      648
      649
      650
      651
      652
      653
      654
      655
      656
      657
      658
      659
      660
      661
      662
      663
      664
      665
      666
      667
      668
      669
      670
      671
      672
      673
      674
      675
      676
      677
      678
      679
      680
      681
      682
      683
      684
      685
      686
      687
      688
      689
      690
      691
      692
      693
      694
      695
      696
      697
      698
      699
      700
      701
      702
      703
      704
      705
      706
      707
      708
      709
      710
      711
      712
      713
      714
      715
      716
      717
      718
      719
      720
      721
      722
      723
      724
      725
      726
      727
      728
      729
      730
      731
      732
      733
      734
      735
      736
      737
      738
      739
      740
      741
      742
      743
      744
      745
      746
      747
      748
      749
      750
      751
      752
      753
      754
      755
      756
      757
      758
      759
      760
      761
      762
      763
      764
      765
      766
      767
      768
      769
      770
      771
      772
      773
      774
      775
      776
      777
      778
      779
      770
      771
      772
      773
      774
      775
      776
      777
      778
      779
      780
      781
      782
      783
      784
      785
      786
      787
      788
      789
      780
      781
      782
      783
      784
      785
      786
      787
      788
      789
      790
      791
      792
      793
      794
      795
      796
      797
      798
      799
      790
      791
      792
      793
      794
      795
      796
      797
      798
      799
      800
      801
      802
      803
      804
      805
      806
      807
      808
      809
      800
      801
      802
      803
      804
      805
      806
      807
      808
      809
      810
      811
      812
      813
      814
      815
      816
      817
      818
      819
      810
      811
      812
      813
      814
      815
      816
      817
      818
      819
      820
      821
      822
      823
      824
      825
      826
      827
      828
      829
      820
      821
      822
      823
      824
      825
      826
      827
      828
      829
      830
      831
      832
      833
      834
      835
      836
      837
      838
      839
      830
      831
      832
      833
      834
      835
      836
      837
      838
      839
      840
      841
      842
      843
      844
      845
      846
      847
      848
      849
      840
      841
      842
      843
      844
      845
      846
      847
      848
      849
      850
      851
      852
      853
      854
      855
      856
      857
      858
      859
      850
      851
      852
      853
      854
      855
      856
      857
      858
      859
      860
      861
      862
      863
      864
      865
      866
      867
      868
      869
      860
      861
      862
      863
      864
      865
      866
      867
      868
      869
      870
      871
      872
      873
      874
      875
      876
      877
      878
      879
      870
      871
      872
      873
      874
      875
      876
      877
      878
      879
      880
      881
      882
      883
      884
      885
      886
      887
      888
      889
      880
      881
      882
      883
      884
      885
      886
      887
      888
      889
      890
      891
      892
      893
      894
      895
      896
      897
      898
      899
      890
      891
      892
      893
      894
      895
      896
      897
      898
      899
      900
      901
      902
      903
      904
      905
      906
      907
      908
      909
      900
      901
      902
      903
      904
      905
      906
      907
      908
      909
      910
      911
      912
      913
      914
      915
      916
      917
      918
      919
      920
      921
      922
      923
      924
      925
      926
      927
      928
      929
      920
      921
      922
      923
      924
      925
      926
      927
      928
      929
      930
      931
      932
      933
      934
      935
      936
      937
      938
      939
      930
      931
      932
      933
      934
      935
      936
      937
      938
      939
      940
      941
      942
      943
      944
      945
      946
      947
      948
      949
      940
      941
      942
      943
      944
      945
      946
      947
      948
      949
      950
      951
      952
      953
      954
      955
      956
      957
      958
      959
      950
      951
      952
      953
      954
      955
      956
      957
      958
      959
      960
      961
      962
      963
      964
      965
      966
      967
      968
      969
      960
      961
      962
      963
      964
      965
      966
      967
      968
      969
      970
      971
      972
      973
      974
      975
      976
      977
      978
      979
      970
      971
      972
      973
      974
      975
      976
      977
      978
      979
      980
      981
      982
      983
      984
      985
      986
      987
      988
      989
      980
      981
      982
      983
      984
      985
      986
      987
      988
      989
      990
      991
      992
      993
      994
      995
      996
      997
      998
      999
      990
      991
      992
      993
      994
      995
      996
      997
      998
      999
      1000
      1001
      1002
      1003
      1004
      1005
      1006
      1007
      1008
      1009
      1000
      1001
      1002
      1003
      1004
      1005
      1006
      1007
      1008
      1009
      1010
      1011
      1012
      1013
      1014
      1015
      1016
      1017
      1018
      1019
      1020
      1021
      1022
      1023
      1024
      1025
      1026
      1027
      1028
      1029
      1020
      1021
      1022
      1023
      1024
      1025
      1026
      1027
      1028
      1029
      1030
      1031
      1032
      1033
      1034
      1035
      1036
      1037
      1038
      1039
      1030
      1031
      1032
      1033
      1034
      1035
      1036
      1037
      1038
      1039
      1040
      1041
      1042
      1043
      1044
      1045
      1046
      1047
      1048
      1049
      1040
      1041
      1042
      1043
      1044
      1045
      1046
      1047
      1048
      1049
      1050
      1051
      1052
      1053
      1054
      1055
      1056
      1057
      1058
      1059
      1050
      1051
      1052
      1053
      1054
      1055
      1056
      1057
      1058
      1059
      1060
      1061
      1062
      1063
      1064
      1065
      1066
      1067
      1068
      1069
      1060
      1061
      1062
      1063
      1064
      1065
      1066
      1067
      1068
      1069
      1070
      1071
      1072
      1073
      1074
      1075
      1076
      1077
      1078
      1079
      1070
      1071
      1072
      1073
      1074
      1075
      1076
      1077
      1078
      1079
      1080
      1081
      1082
      1083
      1084
      1085
      1086
      1087
      1088
      1089
      1080
      1081
      1082
      1083
      1084
      1085
      1086
      1087
      1088
      1089
      1090
      1091
      1092
      1093
      1094
      1095
      1096
      1097
      1098
      1099
      1090
      1091
      1092
      1093
      1094
      1095
      1096
      1097
      1098
      1099
      1100
      1101
      1102
      1103
      1104
      1105
      1106
      1107
      1108
      1109
      1100
      1101
      1102
      1103
      1104
      1105
      1106
      1107
      1108
      1109
      1110
      1111
      1112
      1113
      1114
      1115
      1116
      1117
      1118
      1119
      1110
      1111
      1112
      1113
      1114
      1115
      1116
      1117
      1118
      1119
      1120
      1121
      1122
      1123
      1124
      1125
      1126
      1127
      1128
      1129
      1120
      1121
      1122
      1123
      1124
      1125
      1126
      1127
      1128
      1129
      1130
      1131
      1132
      1133
      1134
      1135
      1136
      1137
      1138
      1139
      1130
      1131
      1132
      1133
      1134
      1135
      1136
      1137
      1138
      1139
      1140
      1141
      1142
      1143
      1144
      1145
      1146
      1147
      1148
      1149
      1140
      1141
      1142
      1143
      1144
      1145
      1146
      1147
      1148
      1149
      1150
      1151
      1152
      1153
      1154
      1155
      1156
      1157
      1158
      1159
      1150
      1151
      1152
      1153
      1154
      1155
      1156
      1157
      1158
      1159
      1160
      1161
      1162
      1163
      1164
      1165
      1166
      1167
      1168
      1169
      1160
      1161
      1162
      1163
      1164
      1165
      1166
      1167
      1168
      1169
      1170
      1171
      1172
      1173
      1174
      1175
      1176
      1177
      1178
      1179
      1170
      1171
      1172
      1173
      1174
      1175
      1176
      1177
      1178
      1179
      1180
      1181
      1182
      1183
      1184
      1185
      1186
      1187
      1188
      1189
      1180
      1181
      1182
      1183
      1184
      1185
      1186
      1187
      1188
      1189
      1190
      1191
      1192
      1193
      1194
      1195
      1196
      1197
      1198
      1199
      1190
      1191
      1192
      1193
      1194
      1195
      1196
      1197
      1198
      1199
      1200
      1201
      1202
      1203
      1204
      1205
      1206
      1207
      1208
      1209
      1200
      1201
      1202
      1203
      1204
      1205
      1206
      1207
      1208
      1209
      1210
      1211
      1212
      1213
      1214
      1215
      1216
      1217
      1218
      1219
      1210
      1211
      1212
      1213
      1214
      1215
      1216
      1217
      1218
      1219
      1220
      1221
      1222
      1223
      1224
      1225
      1226
      1227
      1228
      1229
      1220
      1221
      1222
      1223
      1224
      1225
      1226
      1227
      1228
      1229
      1230
      1231
      1232
      1233
      1234
      1235
      1236
      1237
      1238
      1239
      1230
      1231
      1232
      1233
      1234
      1235
      1236
      1237
      1238
      1239
      1240
      1241
      1242
      1243
      1244
      1245
      1246
      1247
      1248
      1249
      1240
      1241
      1242
      1243
      1244
      1245
      1246
      1247
      1248
      1249
      1250
      1251
      1252
      1253
      1254
      1255
      1256
      1257
      1258
      1259
      1250
      1251
      1252
      1253
      1254
      1255
      1256
      1257
      1258
      1259
      1260
      1261
      1262
      1263
      1264
      1265
      1266
      1267
      1268
      1269
      1260
      1261
      1262
      1263
      1264
      1265
      1266
      1267
      1268
      1269
      1270
      1271
      1272
      1273
      1274
      1275
      1276
      1277
      1278
      1279
      1270
      1271
      1272
      1273
      1274
      1275
      1276
      1277
      1278
      1279
      1280
      1281
      1282
      1283
      1284
      1285
      1286
      1287
      1288
      1289
      1280
      1281
      1282
      1283
      1284
      1285
      1286
      1287
      1288
      1289
      1290
      1291
      1292
      1293
      1294
      1295
      1296
      1297
      1298
      1299
      1290
      1291
      1292
      1293
      1294
      1295
      1296
      1297
      1298
      1299
      1300
      1301
      1302
      1303
      1304
      1305
      1306
      1307
      1308
      1309
      1300
      1301
      1302
      1303
      1304
      1305
      1306
      1307
      1308
      1309
      1310
      1311
      1312
      1313
      1314
      1315
      1316
      1317
      1318
      1319
      1310
      1311
      1312
      1313
      1314
      1315
      1316
      1317
      1318
      1319
      1320
      1321
      1322
      1323
      1324
      1325
      1326
      1327
      1328
      1329
      1320
      1321
      1322
      1323
      1324
      1325
      1326
      1327
      1328
      1329
      1330
      1331
      1332
      1333
      1334
      1335
      1336
      1337
      1338
      1339
      1330
      1331
      1332
      1333
```

```

MXY=1
IF((MXY.EQ.0.) OR.(XMN.NE.0.) OR.(YMX.NE.0.) OR.(YMN.NE.0.)) MXY=2
IF(XM1X=XO+HS
XM2X=YO+HS
XM3N=YO-HS
XMN=YO-HS
C COMMENT THE READ AND FILL LOOP:
DO 12 J=1, JM
READ (IN1,59) IM
MN=0
XH=0.
C READ THE LINES, DETERMINE CODE, CALCULATE RADIUS & ANGLE FOR CODE 1:
DO 5 I=1,IM
IF(NCODE.LE.0) READ (IN1,58) XD(I), YD(I), XG(I), YG(I), RR(I),
1 IF((NCODE.EQ.1) CALL SIM(XD(I), YD(I), XG(I), YG(I), MN, NOF, I, IM),
1 XY(I), XO(I), YO(I), EC(3.0), GO TO 5
1 IF((XY(I).EQ.0.0.) OR.((YD(I).NE.0.0.) AND.(XY(I).EQ.0.0.)) XY(I)=2.
1 IF((XY(I).NE.0.0.) OR.((YG(I).NE.0.0.) AND.(XY(I).EQ.0.0.)) XY(I)=1.
1 IF((XGR(I).NE.0.0.) OR.((XI(I).NE.0.0.) AND.(XY(I).NE.0.0.)) XY(I)=2.
1 IF((XY(I).EQ.0.0.) AND.(D(I,J).NE.0.0.)) XY(I)=1.
1 IF((XY(I).NE.1.0.) AND.(D(I,J).NE.0.0.)) XY(I)=2.
DEN=SQR(T((XG(I)-XD(I))**2+(YG(I)-YD(I))**2))
IF((X-.EQ.0.0.) EQ.4.0) GO TO 4
RR(I)=((XO-XC(I))*(YG(I)-YD(I)),(XG(I)-XD(I)))
XIM=(ATANM((YG(I)-YD(I))/DEN)
XIM=(X(I).EQ.1.0.) XIM=XI(I)
IF((X(I).EQ.2.0.) RR(I)=RR(I)+RZ0*SIN(GAM-XI(I)))
CONTINUE
C COMPUTE MAX AND MIN ANGLE INDEXES FOR APERTURE POSITION LOCATION:
DO 6 I=1,IM
IF((XY(I).NE.1.0.) OR.(XY(I).NE.2.0.)) GO TO 6
IF((XI(I).GT.XIM) XIM=XI(I)
IF((XI(I).LT.XIM) XM=I
IF((XI(I).LE.XIN) INT=I
CONTINUE
C DETERMINE APERTURE LOCATION:
LPR=0
XID=XI(INT)-XI(INT)
IF(ABS(XID).LT.:00001) LPR=1
XIH=(XI(INT)+XI(INT))/2.

```

```

RRH=10000.
XH=RRH*COS(XIH)
YH=RRH*SIN(XIH)
IF (LPR-EQ-1) GO TO 7
YTX=-RR*(INT)*SIN(XI(INT))-YO
YTN=-RR*(INT)*SIN(XI(INT))-YO
XTX=RR*(INT)*COS(XI(INT))-XO
XTN=RR*(INT)*COS(XI(INT))-XO
UA=TAN(XI(INT))
UC=TAN(XI(INT))
UB=YTX-UA*XTX
UD=YTN-UA*XTN
XH=(UD-UB)/(UA-UC)
YH=XH*UA+UB
RRH=SQRT((XH-X0)**2+(YH-Y0)**2)
XIH=ATANM(YH-Y0),(XH-X0)
CONTINUE
7  FILL THE ANGLE AND RADIUS FOR ANY CODE 3 OR 4 LINES:
DO 9 I=1,IM
IF (XY(I)*NE-3.) GO TO 8
BAS=SQRT(RRH**2-RR(I)**2)
XI(I)=XIH-ATANM(RR(I),BAS)
GO TO 9
8  XI(I)=ATANM(YH-YD(I),(XH-XD(I)))
RR(I)=RRH*SIN(XI(I)-XIH)
CONTINUE
9  ANGLES AND RADII ARE NOW FILLED FOR ALL POINTS IN THIS LINE.
VACATE THE SET OF VECTORS TO BE USED AS TEMPORARY STORAGE:
DO 10 I=1,IM
XD(I)=0.
YD(I)=0.
XG(I)=0.
YG(I)=RR(I)
XR(I)=D(I,J)
RR(I)=0.
D(I,J)=0.
DX(I)=C.
CONVERT THE LINE TO REGULAR RADII USING INTERPOLATION:
10 RR(I)=R+DR
CALL SPLINE(YG,XY,IM,RR(1),D(1,J))
DO 11 I=2,IMAX
RI=I=R+DR*R
RR(I)=SPLINN(YG,XY,IM,RR(1),D(1,J))
GENERATE THE VECTOR OF ANGLES FOR THIS COLUMN AND STORE IN G ARRAY:
11 DO 12 I=1,IMAX
BAS=SQRT(RRH**2-RR(I)**2)
G(I,J)=XIH-ATANM(RR(I),BAS)

```

```

12      YG(I,J)=XY(I)
C      XY(MNS)=0. NOW ALL REGULARLY FILLED OVER THE ANGLES.
C      NEXTO,I,23,I=1,MAX
C      EXPAND THE DATA TO 2 SETS TO ESTABLISH SMOOTH INTERPOLATION.
C      JYM3=3*I*JM
I=I-MAX+1-JYM3 GO TO 14
IF(JYM3=1)J=JMS
DO1=J+JMS
DO2=J2+JMS
DO3=J3+JMS
XXD(J2,J3)=D(I,J)
XXD(J3,J2)=G(I,J)-TPIE-PHISYM
XXG(J2,J3)=G(I,J)-PIE-PHISYM
XXG(J3,J2)=G(I,J)-PHISYM
13      XGO1=1
DO1=JMS+1-J
DO2=JMS+J-1
DO3=JMS+1-J
XXD(J1,J2)=D(I,J)
XXD(J2,J3)=G(I,J)-2.*((G(I,J)-PHISYM)-PIE-PHISYM
XXG(J1,J2)=G(I,J)-PIE-PHISYM
XXG(J2,J3)=G(I,J)+2.*((DAN+PHISYM-G(I,J))-PIE-PHISYM
14      CONTINUE
JYM2=2.*JMS
JP=JYM2
DO1=17,J=1,JM2
XXD(J)=XD(J+JP)
XXG(J)=XG(J+JP)
DO1=18,J=JMS,JM3
XD(J)=0.
15      XG(J)=0.
16      FIND THE SMALLEST ANGLE
17      XY(I)=1.
SA=XG(I)
DO1=19,J=1,JM2
IF(XG(J).GE-SA) GO TO 19
SA=XG(J)
XY(I)=J
CONTINUE
18
19

```

```

C FIND THE MAX ANGLE IN THE ROW:
      XY(JM2)=JM2
      SB=XG(JM2)
      DO 20 J=1,JM2
      IF ((XG(J).LE.SB) GO TO 20
      SB=XG(J)
      XY(JM2)=J
      CONTINUE
20   DESB=XG(JM2)
      J=2
      JS=XY(J-1)
      TS=0
      DO 22 J=1,JM2
      IF ((XG(J).LE.SA) GO TO 22
      SB=XG(J)
      XY(J)=J
      TS=1
      CONTINUE
22   UJF(JTS.EQ.0) J=2=JJ
      UJF(JJ+1.LE.JM2) GO TO 21
      DO 23 J=1,JM2
      JX=XY(J)
      YD(J)=XD(JX)
      INTERPOLATE:
      DXI(J)=DXI/2.*PIE/FCU
      CALL SPLINE(XG,YD,XI(J),G(I,J))
      DO 24 J=2,JMS
      XI(J)=XI(J-1)+DXI
      CALL SPLINE(XG,YD,JM2,XI(J),G(I,J))
      DO 25 J=1,JMS
      XI(J)=XI(J)
      XU=XMX
      IF (((XI.J.GE.0.).AND.(XI.J.LT.PI))) XU=XMN
      YU=YMN
      IF (((XI.J.GE.MPIT).AND.(XI.J.LT.PIT))) YU=YMX
      XL=XMN
      IF (((XI.J.GE.0.).AND.(XI.J.LT.PI))) XL=XMX
      YL=YMX
      IF (((XI.J.GE.MPIT).AND.(XI.J.LT.PIT))) YL=YMN
      SXIJ=SIN(XIJ)
      CXIJ=COS(XIJ)
      RMX=(XO-XL)*SXIJ-(YO-YL)*CXIJ
      RMN=(XO-XU)*SXIJ-(YO-YU)*CXIJ

```

```

DO 25 I=1,IMAX
IF (RR(I).LT.RMN) G(I,J)=0.
IF (RR(I).GT.RMX) G(I,J)=0.
C CONTINUE EXPAND SYMMETRY SECTOR TO AN ORTHOGONAL INTERVAL.
25 IF (ISYM=2) GO TO 27
DO 26 J=1,JMAX
J2=JMAX/2+J
J3=JMAX/2-J
J4=JMAX+1-J
DO 26 I=1,IMAX+1-IMAX
I1=IMAX+1-I
G(I,J2)=G(I,J)
G(I,J3)=G(I,J)
G(I,J4)=G(I,J)
26 G RETURN FOR EVEN SYMMETRY AVERAGE THE GARRAY COLUMNS.
27 IWS=(2*IMAX+1)/2
DO 28 J=1,IMAX
DO 28 I=1,IWS
I1=IMAX+1-I
GST=(G(I,J)+G(I,J))/2.
G(I,J)=GST
28 G RETURN
59 FORMAT (515)
58 FORMAT (10F7.3)
END
C000010
C
FUNCTION ATANM(Y,X)
C COMPUTES THE ARCTAN OF Y/X BETWEEN -P1 AND +P1.
C
C P1E=3.141592653589793
C P12=P1E/2
C ATANM=SIGN(P12,Y)
C IF(X.NE.0.) ATANM=ATAN(Y/X)
C IF(Y.GE.0.) RETURN
C IF(Y.GT.0.) ATANM=P1E+ATANM
C RETURN
C END
C000011

```

```

SUBROUTINE SIM (XD,YD,XG,YG,D,R,XI,XY,XO,YO,PS,XM,XN,I,IM,
 100,NF)
C SIMULATES THE FRINGE NUMBER DATA ONE WOULD OBTAIN FROM THE
C Holographic Interference Process FOR A KNOWN FUNCTION AS
C CONTAINED IN SUBROUTINE FUNCT. THE GRID BOX DIMENSIONS MUST
C EXCEED THE INVERSE CIRCLE SIZE, AND APERTURE POINTS SPECIFIED
C MUST FALL BETWEEN XI=-40 DEGREES, AND XI=+130 DEGREES.

COMMON IMAX,JMAX,IJMAX,ALF,SIZ,EPS,MOD,BOX,SD,IX,Z
COMMON /IO/CMS,I,N1,I,N2,IN4
READ (IN1,29) XH,YH
ZER=0.
RIM=IM
DX=(XM-XN)/(RIM-1.)
DY=(YM-YN)/(RIM-1.)
DX1=XM-(RIM-1.)*DX
Y1=YM-(RIM-1.)*DY
X1=ATAN((YH-Y1)*(XH-X1)-PS)
RRH=SQR((XH-XO)**2+(YH-YO)**2)
X10=ATAN((YH-YO)*(XH-XO)-PS)
R1=RRH*SIN((XH-X1)*PI)
IF ((I*GT;1).AND.(I*LT;IM)) GO TO 1
IF (ABS(R1).LT.SIZ/2.) R1=SIGN(SIZ/2.,R1)
XY=3.0
GO TO 2
1 CALL GOLF (R,XI,D,IR,ZER,ZER)
XD=XN
YD=YN
IF (XH.NE.X1) YD=Y1-(X1-XN)*(YH-Y1)/(XH-X1)
IF (YS.GE.YN) GO TO 2
YD=YN
IF (YH.NE.Y1) XD=X1-(Y1-YN)*(XH-X1)/(YH-Y1)
RETURN
2 FORMAT (10F7.3)
END
C000012
C
C SUBROUTINE FREAD (NO,RO,NF,ZZ)
C FREAD READS THE NUMERIC ARRAY WHICH IS USED FOR EQUATION 8 OF
C SUBROUTINE FUNCT FIRST CARD IS NUMBER OF POINTS (N.GE.1), OF
C FOLLOWED BY ONE POINT PER CARD.
C DIMENSION RO(101)

```

```

      READ (NF,89) NO,ZZ
      WRITE(6,80) NO,ZZ
      DO 10 I=1,NO
      READ(NF,88) RO(I)
      WRITE(6,88) RO(I)
      CONTINUE
      FORMAT(15,F9.3)
      10 FORMAT(F8.5)
      89 FORMAT(1X,15,F9.3)
      90 RETURN
      END
      C000013

      SUBROUTINE GPRINT (G, NUMB)
C   PRINTS THE DATA ARRAY 'G' WHICH WAS INPUT TO
C   THE PROGRAM IN SUBROUTINE GARRAY.
C
COMMON IMAX,JMAX,IJMX, JMX, ALPHA, SIZE, EPS, MODE, BOX, SD, IX, Z
DIMENSION G(IJMX)
DATA HYP, VERT/1H-1H/1H-1H/
IF (NUMB.EQ.1) WRITE(6,99) MODE,Z
IF (NUMB.EQ.2) WRITE(6,92) Z
JN2=JMAX/2
RIMAX=I MAX
RJMAX=J MAX
DX=SIZE/RIMAX
DXI=360./RJMAX
INTRVL SETS THE NUMBER OF TERMS PRINTED PER LINE. IF IT IS ALTERED,
ONE MUST ALSO REDIMENSION X AND ALTER FORMATS 98, 97, AND 95.
C   INTRVL=15
IT=1
IT=IB+1INTRVL-1
IF (IT.GT.I MAX) IT=IMAX
IBT=IT-IB+1 (I,I=IB,IT)
WRITE(6,98) (I,I=IB,IT)
DO 2 I=1:IBT
RI=IB-1+I
X(I)=-SIZE/2.+(RI-.5)*DX
L4=7*I:IT+1 (X(I),I=1:IBT)
WRITE(6,97) (X(I),I=1:IBT)
WRITE(6,96) (HYP,L=1,LN), VERT
JMH=JM2+1
DO 3 J=JMH, J MAX
      RJ=J
      SUB00100
      SUB00120
      SUB00140
      SUB00150
      SUB00160
      SUB00170
      SUB00180
      SUB00190
      SUB00200
      SUB00210
      SUB00220
      SUB00230
      SUB00240
      SUB00250
      SUB00260
      SUB00270
      SUB00280
      SUB00290
      SUB00300
      SUB00310
      SUB00320
      SUB00330
      SUB00340
      SUB00350
      SUB00360
      SUB00370
      SUB00380
      SUB00390
      SUB00400
      SUB00410
      SUB00420
      SUB00430
      SUB00440
      SUB00450
      SUB00460
      SUB00470
      SUB00480
      SUB00490
      SUB00500

```

```

X1=-180.0+DXI*(RJ-.5)
IGB=IJ-1
IGT=IGB-IB+IT
9 WRITE(6,95) J, XI, G(L), L=1,LM), VERT, IGT
1 IB=IB+INTRVL
2 ITOLD=IT
3 IT=IT+INTRVL
4 IF(ITOLD.LT.IMAX) GO TO 1
5 WRITE(6,93) THE ARRAY GF INPUT DATA (G), OBTAINED BY GARRAY,
6 FORMAT(1H1//1X, I=1,15F7.3)
7 FORMAT(11X, X=15F7.3)
8 FORMAT(2X,I3,F9.2,I15AI,15F7.3)
9 FORMAT(14X,I3,F9.2,I15AI,15F7.3)
10 FORMAT(1//5X)
11 FORMAT(1H1//) THE ADD-ON FUNCTION GARRAY FOR Z=' , F7.3, ' CM: '
12 RETURN
13 C000014
14 C
15 C SUBROUTINE GPUNCH (Z, XO, YO, PHS, NOF, IMX, JMX, G)
16 C GPUNCH PUNCHES OUT THE FIRST NON-SYMMETRIC PORTION OF GARRAY
17 C (OR WRITES IT ON FILE 7 IN CMS VERSION)
18 C COMMON /SYM/ ISM, JSM, MSM, FCU, IMS, JMS, QSM
19 C DIMENSION G(IMX, JMX)
20 C WRITE(7,39) ((G(I,J), I=1,IMS), J=1, JMS)
21 C 39 FORMAT(10F15)
22 C FORMAT(10F7.3)
23 C RETURN
24 C END
25 C000015
26 C
27 C SUBROUTINE READ (Z, XO, YO, PHISYM, NJF, IMAX, JMAX, G)
28 C READS THE NON-SYMMETRIC PORTION OF THE GARRAY AND EXPANDS IT TO AN
29 C ORTHOGONAL SET. NOTI. INSURE SUFFICIENT DIMENSIONS IN MAIN PROGRAM.
30 C COMMON /SYM/ ISYM, JSYM, MSYM, FCU, IMS, JMS, QSYM
31 C
32 C SUB00510
33 C SUB00520
34 C SUB00530
35 C SUB00550
36 C SUB00560
37 C SUB00570
38 C SUB00580
39 C SUB00590
40 C SUB00600
41 C SUB00610
42 C SUB00620
43 C SUB00630
44 C SUB00640
45 C SUB00650
46 C SUB00660
47 C SUB00670
48 C SUB00680
49 C SUB00690
50 C SUB00700
51 C SUB00710
52 C SUB00720
53 C SUB00730
54 C SUB00740
55 C SUB00750
56 C SUB00760
57 C SUB00770
58 C SUB00780
59 C SUB00790
60 C SUB00800
61 C SUB00810
62 C SUB00820
63 C SUB00830
64 C SUB00840
65 C SUB00850
66 C SUB00860
67 C SUB00870
68 C SUB00880
69 C SUB00890
70 C SUB00900
71 C SUB00910
72 C SUB00920
73 C SUB00930
74 C SUB00940

```

```

COMMON /IO/ CMS, IN1, IN2, IN4
DIMENSION G(I MAX, J MAX)
READ (IN1, 39) NOF, I MAX, J MAX, ISYM, JSYM, IMS, JMS
READ (IN1, 40) Z, X0, Y0, PHI SYM
DO 10 J=1, J MS
  READ (IN1, 37) (G(I, J), I=1, IMS)
  WRITE (J MAX, 37) NOF, Z, X0, Y0, PHI SYM, I MAX, J MAX, JSYM
  MSYM = JSYM
  IF ((JSYM .EQ. 0) .OR. (MSYM .GT. J MAX)) MSYM=1
  FCU = ISYM * JSYM * J MAX
  QSYM = FCU / R J MS
  DO 4 J=1, J MS
    IF (ISYM .EQ. 1) GO TO 2
    DO 1 I=1, IMS
      LI=I MAX+1-I
      GO TO 4
    1   LI=I MAX+1-I
      J2=J MAX/2+1-J
      J3=J MAX/2+J
      J4=J MAX+1-J
      DO 3 I=1, I MAX
        LI=I MAX+1-I
        G(I, J2)=G(I, J)
        G(I, J3)=G(I, J)
        G(I, J4)=G(I, J)
      3   CONTINUE
      4   FORMAT(10 I 5)
      38  FORMAT(4 F7.3)
      37  FORMAT(10 F7.3) MODE 3 READS G ARRAY DIRECTLY: NOF='14/' IMAX='F7.3' PHISYM='F7.3'; {1, X0='F7.3', J MAX='I4', JSYM='I4'}; {1, T(I)=BL/1H, DO 1 I=1, 24, T(I)=BL
      RETURN
END
C000016
C
SUBROUTINE MAP (IM, JM, A, N, Z, BAND)
C MAP CALLS SUBROUTINE MIMPII AND PLOTS A CONTOUR MAP OF THE ARRAY
C
C DIMENSION A(IM, JM), T(24)
C DATA BL/1H /
C DO 1 I=1, 24
C   T(I)=BL
C
SUB01000
SUB01010
SUB01020
SUB01030
SUB01040
SUB01050
SUB01060
SUB01070
SUB01080
SUB01090
SUB01100
SUB01110
SUB01120
SUB01130
SUB01140
SUB01150
SUB01160
SUB01170
SUB01180
SUB01190
SUB01200
SUB01210
SUB01220
SUB01230
SUB01240
SUB01250
SUB01260
SUB01270
SUB01280
SUB01290
SUB01300
SUB01310
SUB01320
SUB01330
SUB01340
SUB01350
SUB01360
SUB01370
SUB01380

```

```

ICON=1
IF(BAND.LT.0.) ICON=0
AMIN=0.
IJT=0
AZ=1.
WRITE(6,49) NZ
CALL TMPIL(A,IMJMT,BAND,AZ,SURFACE,IJT,ICON)
49 FORMAT (1H1/,A,THE FUNCTION NO. I3, ' Z=' F5.3//)
      RETURN
      END
C000017

SUBROUTINE GPLCT (G,GA,JMS)
C GPLCT PRINTS A ROUGH PLOT OF THE LINE INTEGRAL FUNCTIONS IN GARRAY.
COMMON IMAX, JMAX, IJMX, JSYM, ALPHA, SIZE, EPS, MODE, BOX, SD, IX, Z
COMMON /TAB2/ INDEX(7), JSYM, ISYM
COMMON /TAB2/ IPT, KPT, LPT, MPT, REST(5)
DIMENSION G(IMAX, JMAX), GA(IJMX, JMAX)
DIMENSION A(201), B(101), C(201), D(101)
JM=101
DATA BL, PL, ST, DH, EX/1H , 1H+, 1H*, 1H-, 1H/
JMS2=JMAX/2+1
IF(ISYM.EQ.2) JMS2=1
JMS3=JMS2+JMS-1
DO 8 J=JMS2, JMS3
WRITE(6,67) (ST, I=1, 120)
DO 1 I=1, IMAX
AI(I)=GA(I, J)
CI(I)=GA(I, J)
AS=5
BS=0
1 CALL INTERP (A, IMAX, AS, B, JM, BS)
CALL INTERP (C, IMAX, AS, D, JM, BS)
WRITE (6,69)
1
2 BIG=0.
SMALL=0.
DD 2 I=1, IMAX
IF(A(I).GT.BIG) BIG=A(I)
IF(C(I).GT.BIG) BIG=C(I)
IF(A(I).LT.SMALL) SMALL=A(I)
IF(C(I).LT.SMALL) SMALL=C(I)
RANGE=BIG-SMALL

```

```

RINK=RANGE/80.
TOP=BIG+RINK
CEN=BIG
BOT=BIG-RINK
KC=0
DO 7 K=1,41
  IC=0
  DO 6 I=1,1C1
    ROW(I)=BL
    IF((I.EQ.1).OR.((I.EQ.51).OR.(I.EQ.101)))ROW(I)=PL
    IF((K.EQ.1).OR.(K.EQ.41))ROW(I)=PL
    IF((TOP.GE.0).AND.(BOT.LE.0.))ROW(I)=DH
    IF((IC.EQ.5))GO TO 3
    GO TO 4
  IC=0
  IF((KC.EQ.10))ROW(I)=PL
  IF((KPT.EQ.2))GO TO 5
  4   IF((D(I).LE.TOP).AND.(D(I).GE.BOT)) ROW(I)=ST
  IF((B(I).LE.TOP).AND.(B(I).GE.BOT)) ROW(I)=EX
  KC=IC+1
  IF((KC.EQ.5))KC=0
  IF((KC.NE.0))WRITE(6,65) (ROW(I),I=1,101)
  IF((KC.EQ.0))WRITE(6,68) (CEN,(ROW(I),I=1,101))
  TOP=TOP-2.*RINK
  CEN=CEN-2.*RINK
  IC=BOT-2.*RINK
  KC=KC+1
  WRITE(6,69) (ST,I=1,120)
  69 FORMAT(1X,F8.3,1X,10,A1)
  68 FORMAT(1H,I8,12,A1,/)
  67 FORMAT(1H,I2,A1,/)
  66 FORMAT(10X,10IA1,/)
  65 FORMAT(10X,10IA1,/)
  RETURN
  END
  C000018
C
C SUBROUTINE INTERP (A,IM,AS,B,JM,BS)
C
C INTERP CONVERTS A REGULAR VECTOR A OF IM POINTS TO A REGULAR VECTOR
C B OF JM POINTS. OS=.5 FOR A VECTOR WITH POINTS DEFINED IN THE
C CENTER OF THE INTERVAL AS AND BS ARE THE % OF AN INTERVAL FROM THE
C EDGE OF THE FIELD TO THE FIRST POINT (.0 OR .5 FOR EDGE OR CENTER
C DEFINED POINTS)
C
C DIMENSION A(IM),B(JM)
C
SUB01850
SUB01860
SUB01870
SUB01880
SUB01890
SUB01900
SUB01910
SUB01920
SUB01930
SUB01940
SUB01950
SUB01960
SUB01970
SUB01980
SUB01990
SUB02000
SUB02010
SUB02020
SUB02030
SUB02040
SUB02050
SUB02060
SUB02070
SUB02080
SUB02090
SUB02100
SUB02110
SUB02120
SUB02130
SUB02140
SUB02150
SUB02160
SUB02170
SUB02180
SUB02190
SUB02200
SUB02210
SUB02220
SUB02230
SUB02240
SUB02250
SUB02260
SUB02270
SUB02280
SUB02290
SUB02300

```

```

RJM=IJ
RAT=(RJ)^1 + 2.*AS) / (RJM-1.+2.*BS)
DO 2 I=1,JM
  AI=I
  AI=RAT*(BI+BS)-AS
  IA=AI
  F=AI-FLOAT(IA)
  IF((IA-EQ.0).OR.(IA-EQ.JM)) GO TO 1
  B(I)=A(IA)+F*(A(IA+I)-A(IA))
  GO TO 2
  IF((IA-EQ.0).OR.(B(I)=A(1)*(F-AS)/(1.-AS)))
    IF((IA-EQ.JM).OR.(I=1))=A(JM)*F/(1.-AS)
  CONTINUE
  2 RETURN
END

```

C000019

SUBROUTINE SPLINE

PURPOSE PROVIDES INTERPOLATED VALUE USING "CUBIC SPLINE FITTING"

USAGE FIRST CALL TO SUBROUTINE:
 CALL SPLINE(X,Y,M,XINT,YINT)
 SUBSEQUENT CALLS:
 CALL SPLINN(X,Y,M,XINT,YINT)

DESCRIPTION OF PARAMETERS
 X: MONOTONICALLY INCREASING ABSCISSA ARRAY
 Y: ONE-FOR-ONE CORRESPONDING ORDINATE ARRAY
 M: NUMBER OF X AND Y VALUES SUPPLIED < OR = 300
 XINT: VALUE OF ABSCISSA FOR WHICH CORRESPONDING ORDINATE
 IS TO BE INTERPOLATED (OR EXTRAPOLATED)
 YINT: INTERPOLATED (OR EXTRAPOLATED) ORDINATE VALUE

REMARKS IF SPECIFIED X FALLS OUTSIDE OF RANGE, AN EXTRAPOLATED
 VALUE WILL BE SUPPLIED

SUBROUTINES AND FUNCTIONS SUBPROGRAMS REQUIRED
 SUBROUTINE SPLINE IS INCLUDED IN SUBROUTINE SPLIN PACKAGE

```

SUB02310
SUB02330
SUB02340
SUB02350
SUB02360
SUB02370
SUB02380
SUB02390
SUB02400
SUB02410
SUB02420
SUB02430
SUB02440
SUB02450
SUB02460
SUB02470
SPL00010
SPL00020
SPL00030
SPL00040
SPL00050
SPL00060
SPL00070
SPL00080
SPL00090
SPL00100
SPL001100
SPL00120
SPL00130
SPL00140
SPL00150
SPL00160
SPL00170
SPL00180
SPL00190
SPL00200
SPL00210
SPL00220
SPL00230
SPL00240
SPL00250
SPL00260
SPL00270
SPL00280
SPL00290
SPL00300
SPL00310

```

MATHEMATICAL METHOD
UPON FIRST ENTRY TO SPLINE A CALL IS MADE TO
DETERMINE THE COEFFICIENTS TO BE USED IN PERFORMING THE
INTERPOLATIONS. SEARCH FOR BRACKETING ABSISSA VALUES IS
ALWAYS MADE FROM THE REFERENCE LAST USED IN INTERPOLATING.

REFERENCE
PENNINGTON, RALPH H., "INTRODUCTORY COMPUTER METHODS AND
NUMERICAL ANALYSIS", THE MACMILLAN COMPANY, NEW YORK, 1965

```

SUBROUTINE SPLINE(X,Y,M,XINT,YINT)
DIMENSION X(M),Y(M),C(4,300)
CALL SPLICO(X,Y,M,C)
K=1
ENTRY SPLINN(X,Y,M,XINT,YINT)
IF(XINT-X(1))70,1,2
3   K=1
    GO TO 7
1   YINT=Y(1)
    RETURN
2   IF(XINT-X(K+1))6,4,5
4   YINT=Y(K+1)
    RETURN
5   K=K+1
    IF(M-K)71,71,3
71  K=M-1
    GO TO 7
6   YINT=Y(K)
    RETURN
12  K=K-1
    GO TO 6
7   PRINT 101,XINT=E18.9,32H, OUT OF RANGE FOR INTERPOLATION)
101 FORMAT(8H0,XINT=(X(K+1)-XINT)*(C(K+1)*2+C(3,K))
11  YINT=YINT+(XINT-X(K))*(C(2,K)*(XINT-X(K))*2+C(4,K))
    RETURN
END

```

CCCCCCCCCCCC

```

SUBROUTINE SPLICO(X,Y,C)
DIMENSION X(M),Y(M),C(4,300),D(300),P(300),E(300),A(300),B(300)
12(M=M-1
DO 2 K=1,M
  DO 3 K'=K+1,M
    X(K')=X(K)+X(K)
  P(K)=D(K)/6
  E(K)=-Y(K+1)-Y(K)/D(K)
  DO 3 K=2,M
    B(K)=E(K)-E(K-1)/D(2)
    A(1,3)=D(1)/D(2)
    A(2,3)=P(2)-P(1)*A(1,3)
    A(2,2)=2*(P(1)+P(2))-P(1)*A(1,2)
    A(2,3)=A(2,3)/A(2,2)
    DO 4 K=3,M
      A(K,2)=2.0*(P(K-1)+P(K))/P(K-1)-P(K-1)*A(K-1,3)
      B(K)=B(K)-P(K-1)*B(K-1)
      A(K,3)=P(K)/A(K-2)
      B(K)=B(K)/A(K-2)
      Q=D(M-2)/D(M-1)
      A(M,1)=1.0+Q+A(M-2,3)
      A(M,2)=-Q-A(M-1)*A(M-1,3)
      B(M)=B(M-2)-A(M-1)*B(M-1)
      Z(M)=B(M)/A(M,2)
      MN=M-2
      DO 6 I=1,MN
        K=M-I
        Z(K)=B(K)-A(K,3)*Z(K+1)
        Z(1)=-A(1,2)*Z(2)-A(1,3)*Z(3)
        DO 7 K=1,MN
          Q=1.0/(6.0*D(K))
          C(1,K)=Z(K)*Q
          C(2,K)=Z(K+1)*Q
          C(3,K)=Y(K)/D(K)-Z(K)*P(K)
          C(4,K)=Y(K+1)/D(K)-Z(K+1)*P(K)
        END
      6
      7
      RETURN
    END
  2
  3
  4
  5
  6
  7
END
C0000020
CCCCCCC
***** SUBROUTINE MTMP II *****
PURPOSE
MET00010
MET00030
MET00040
MET00050
MET00060

```

MET00070
 MET00080
 MET00090
 MET000100
 MET000110
 MET000120
 MET000130
 MET000140
 MET000150
 MET000160
 MET000170
 MET000180
 MET000190
 MET000200
 MET000210
 MET000220
 MET000230
 MET000240
 MET000250
 MET000260
 MET000270
 MET000280
 MET000290
 MET000300
 MET000310
 MET000320
 MET000330
 MET000340
 MET000350
 MET000360
 MET000370
 MET000380
 MET000390
 MET000400
 MET000410
 MET000420
 MET000430
 MET000440
 MET000450
 MET000460
 MET000470
 MET000480
 MET000490
 MET000500
 MET000510
 MET000520
 MET000530
 MET000540

MTMPII WILL PRODUCE ON THE PRINTER A CONTOUR MAP OF ANY SINGLE PRECISION TWO DIMENSIONAL ARRAY.

USAGE CALL MTMPII(Y,N,M,T,BND,AZ,BZ,AMIN,IJT,ICON)

DESCRIPTION OF PARAMETERS

- Y - THE ARRAY TO BE CONTOURED. DIMENSIONED Y(N,M).
- N - NUMBER OF ROWS IN Y.
- M - NUMBER OF COLUMNS IN Y.
- T - REAL*4 TYPE FOR THE CONTOURING. IF BND IS ZERO BND - A BANDWIDTH FOR THE CONTOURING AS FOLLOWS BND=(MAX(Y)-MIN(Y))/15.
- AZ - A LINEAR TRANSFORMATION MAYBE PERFORMED ON THE ARRAY FOLLOWING FORM AZ*Y+BZ IF AZ=0 THEN AZ WILL BE COMPUTED SUCH THAT MAX(AZ+MAX(Y)) MIN(Y) WILL BE LESS THAN 1, AND BZ WILL BE LEFT AS INPUT.
- BZ - SEE UNDER AZ WHICH CONTOURING WILL BEGIN. IF AMIN > MIN(Y) THEN AMIN WILL BE CALCULATED ALONG CONTOUR LEVEL FROM MIN(Y) AS DETERMINED BY COND.
- IJT - ABOVE IJT=0 AMIN WILL BE CALCULATED AS DESCRIBED IN IJTN.
- ICON - IF ICON=0 NO CONTOURING WILL BE DONE BUT THE ARRAY Y WILL BE PRINTED IN THE PLOT FORMAT.

REMARKS

MTMPII REQUIRES A PRINTER WITH 132 PRINT POSITIONS. IF NECESSARY THE MAP WILL BE SEGMENTED COLUMNWISE. SOME ROWS AND COLUMNS ARE NUMBERED ALONG THE EDGES. ONLY THREE SEGMENTS OF THE MAP MAYBE EASILY JOINED TOGETHER. THE SIGNIFICANT FIGURES WILL BE PRINTED AT EACH POINT. THE POSITION OF THE FIRST SIGNIFICANT POINT WILL BE DETERMINED BY MAX(Y), MIN(Y). THE PLOT WILL BE PRODUCED ON A 1 INCH BY 1 INCH GRID. IT WILL BE ASSUMED THAT THE SPACING BETWEEN POINTS IN BOTH DIRECTIONS IS THE SAME AND EQUAL FOR ALL POINTS.

SUBROUTINES REQUIRED
NONE

METHOD THE CONTOUR LEVELS ARE DETERMINED BY SIMPLE LINEAR


```

SM=SM/10.0
IF(SM<1.0)50,50,45
50 AHD=10.0*N$      50,45
      BND=BND/2.0
55 PRINT79
      PRINT6,T
      FORMAT(5X,124A4,'/')
6   PRINT57,AHD,BZ
      FORMAT(1H0,65HTHE FOLLOWING TRANSFORMATION WAS PERFORMED ON THE IN
      PUT MATRIX /5X,1H(E12.5,8H#Y(I,J)+E12.5,IH) //2X,73HAND THREE
      2 DIGITS TO THE RIGHT OF THE DECIMAL POINT ARE PRINTED IN THE MAP)
C
      PRINT54,YMAX,YMIN
      FORMAT(4X,5HMAX=,E15.7,5X,5HMIN=,E15.7)
54 IF((ICON)5,58,5
      PRINT1,BND
5  PRINT(2X,17HTHE BAND WIDTH IS,E12.5,6H UNITS //4X,14HCONTOUR LEVEL
11 LS
      I=0
      YTOP=A MIN
      IF(ABS(YMIN-YMAX)-100.0*BND)53,53,58
53 YB=YTOP
      YTOP=YTOP+BND
      I=I+1
      J=MOD(I,20)
      IF(YB-YMAX)59,58,58
59 PRINT61,YB,YTOP,I,J
      FORMAT(4X,E10.3,4H,10 ,E10.3,2H =,1X,A1)
61 GOTO53
      NCP=0
58 NCP=0
      PRINT70
      70 FORMAT(1H1)
      PRINT6,T
      NLIN=0
      NCP=NCP+1
      NCP = NCP + 13
      IF(NCP-M)80,80,75
73 NCP=M
75 CONTINUE
      J=-2
      NLIN=NLIN+1
      NLIN=N-NLINE+1
      SET UP HEADING
      IF((NCCP-1)85,85,90
85 J=-1
90 DO 100 I = 1,135

```

```

A(I)=BLK
B(I)=BLK
H(I)=BLK
100 CONTINUE
110 DO 160 L=NCCP, NCP
     J = J+8
120   KI=L
     IF(KI-100) 130, 120, 120
     LL=KI/100
     AI(J)=KG(LL+1)
     KI=KI-100*L
     GO TO 135
130   A(J)=KG(1)
     IF(KI-10) 150, 140, 140
     LL=KI/10
     AI(J)=KG(LL+1)
     KI=KI-10*LL
     GO TO 155
140   A(J)=KG(1)
     J=J+1
     A(J)=KG(KI+1)
155   A(J)=KG(KI+1)
     CONTINUE
160 C SETUP FIRST ROW OF ARRAY
     GO TO 260
170   NLINE=NLINE+1
     LINE=NLINE-NLINE+1
     IF(NLINE-N) 180, 180, 380
     DO 190 I=1, 135
     A(I)=BLK
     B(I)=BLK
     C(I)=BLK
     D(I)=BLK
     E(I)=BLK
     F(I)=BLK
     G(I)=BLK
     H(I)=BLK
190   CONTINUE
     IF(ICON) 195, 260, 195
195   NCY=NCCP-1
     J=4
     IF(NCY) 200, 200, 210
200   J=5
     NCY=NCY+1
210   IF(NCY-NCP) 220, 220, 260
     IF(NCY-N) 230, 260, 260
230   NLINE = NLINE - 1
     YD1 = Y(NLINE, NCY) - Y(NLINE+1, NCY)

```

```

YD2=Y*(NLINE+1)-Y*(NLINE+1)*YD1
TP(X(11))=Y*(NLINE+1)-Y*(NLINE+1)*YD1
TPM(X(11))=Y*(NLINE+1)-Y*(NLINE+1)*YD1
XMT(X(11))=Y*(NLINE+1)-Y*(NLINE+1)*YD1
BTX(X(11))=Y*(NLINE+1)-Y*(NLINE+1)*YD1
TP(X(10))=Y*(NLINE+1)-Y*(NLINE+1)*YD1
TPM(X(10))=Y*(NLINE+1)-Y*(NLINE+1)*YD1
XMT(X(10))=Y*(NLINE+1)-Y*(NLINE+1)*YD1
BTX(X(10))=Y*(NLINE+1)-Y*(NLINE+1)*YD1
NLINE=TP(X(10))-TP(X(11))
NLINE=TPM(X(10))-TPM(X(11))
NLINE=XMT(X(10))-XMT(X(11))
NLINE=BTX(X(10))-BTX(X(11))
D01=0.1*D1
D02=0.1*D2
D03=0.1*D3
D04=0.1*D4
D05=0.1*D5
D06=0.1*D6
D07=0.1*D7
D08=0.1*D8
D09=0.1*D9
D10=0.1*D10
D11=0.1*D11
D12=0.1*D12
D13=0.1*D13
D14=0.1*D14
D15=0.1*D15
D16=0.1*D16
D17=0.1*D17
CONTINUE
DO 250 I=1,10
J=I+1
I1=MOD(J,12)
I2=MOD(J,13)
I3=MOD(J,14)
I4=MOD(J,15)
I5=MOD(J,16)
I6=MOD(J,17)
I7=MOD(J,18)
I8=MOD(J,19)
I9=MOD(J,20)
I10=MOD(J,21)
I11=MOD(J,22)
I12=MOD(J,23)
I13=MOD(J,24)
I14=MOD(J,25)
I15=MOD(J,26)
I16=MOD(J,27)
I17=MOD(J,28)
I18=MOD(J,29)
I19=MOD(J,30)
I20=MOD(J,31)
I21=MOD(J,32)
I22=MOD(J,33)
I23=MOD(J,34)
I24=MOD(J,35)
I25=MOD(J,36)
I26=MOD(J,37)
I27=MOD(J,38)
I28=MOD(J,39)
I29=MOD(J,40)
I30=MOD(J,41)
I31=MOD(J,42)
I32=MOD(J,43)
I33=MOD(J,44)
I34=MOD(J,45)
I35=MOD(J,46)
I36=MOD(J,47)
I37=MOD(J,48)
I38=MOD(J,49)
I39=MOD(J,50)
I40=MOD(J,51)
I41=MOD(J,52)
I42=MOD(J,53)
I43=MOD(J,54)
I44=MOD(J,55)
I45=MOD(J,56)
I46=MOD(J,57)
I47=MOD(J,58)
I48=MOD(J,59)
I49=MOD(J,60)
I50=MOD(J,61)
I51=MOD(J,62)
I52=MOD(J,63)
I53=MOD(J,64)
I54=MOD(J,65)
I55=MOD(J,66)
I56=MOD(J,67)
I57=MOD(J,68)
I58=MOD(J,69)
I59=MOD(J,70)
I60=MOD(J,71)
I61=MOD(J,72)
I62=MOD(J,73)
I63=MOD(J,74)
I64=MOD(J,75)
I65=MOD(J,76)
I66=MOD(J,77)
I67=MOD(J,78)
I68=MOD(J,79)
I69=MOD(J,80)
I70=MOD(J,81)
I71=MOD(J,82)
I72=MOD(J,83)
I73=MOD(J,84)
I74=MOD(J,85)
I75=MOD(J,86)
I76=MOD(J,87)
I77=MOD(J,88)
I78=MOD(J,89)
I79=MOD(J,90)
I80=MOD(J,91)
I81=MOD(J,92)
I82=MOD(J,93)
I83=MOD(J,94)
I84=MOD(J,95)
I85=MOD(J,96)
I86=MOD(J,97)
I87=MOD(J,98)
I88=MOD(J,99)
I89=MOD(J,100)
I90=MOD(J,101)
I91=MOD(J,102)
I92=MOD(J,103)
I93=MOD(J,104)
I94=MOD(J,105)
I95=MOD(J,106)
I96=MOD(J,107)
I97=MOD(J,108)
I98=MOD(J,109)
I99=MOD(J,110)
I100=MOD(J,111)
I101=MOD(J,112)
I102=MOD(J,113)
I103=MOD(J,114)
I104=MOD(J,115)
I105=MOD(J,116)
I106=MOD(J,117)
I107=MOD(J,118)
I108=MOD(J,119)
I109=MOD(J,120)
I110=MOD(J,121)
I111=MOD(J,122)
I112=MOD(J,123)
I113=MOD(J,124)
I114=MOD(J,125)
I115=MOD(J,126)
I116=MOD(J,127)
I117=MOD(J,128)
I118=MOD(J,129)
I119=MOD(J,130)
I110=MOD(J,131)
I111=MOD(J,132)
I112=MOD(J,133)
I113=MOD(J,134)
I114=MOD(J,135)
I115=MOD(J,136)
I116=MOD(J,137)
I117=MOD(J,138)
I118=MOD(J,139)
I119=MOD(J,140)
I110=MOD(J,141)
I111=MOD(J,142)
I112=MOD(J,143)
I113=MOD(J,144)
I114=MOD(J,145)
I115=MOD(J,146)
I116=MOD(J,147)
I117=MOD(J,148)
I118=MOD(J,149)
I119=MOD(J,150)
I110=MOD(J,151)
I111=MOD(J,152)
I112=MOD(J,153)
I113=MOD(J,154)
I114=MOD(J,155)
I115=MOD(J,156)
I116=MOD(J,157)
I117=MOD(J,158)
I118=MOD(J,159)
I119=MOD(J,160)
I110=MOD(J,161)
I111=MOD(J,162)
I112=MOD(J,163)
I113=MOD(J,164)
I114=MOD(J,165)
I115=MOD(J,166)
I116=MOD(J,167)
I117=MOD(J,168)
I118=MOD(J,169)
I119=MOD(J,170)
I110=MOD(J,171)
I111=MOD(J,172)
I112=MOD(J,173)
I113=MOD(J,174)
I114=MOD(J,175)
I115=MOD(J,176)
I116=MOD(J,177)
I117=MOD(J,178)
I118=MOD(J,179)
I119=MOD(J,180)
I110=MOD(J,181)
I111=MOD(J,182)
I112=MOD(J,183)
I113=MOD(J,184)
I114=MOD(J,185)
I115=MOD(J,186)
I116=MOD(J,187)
I117=MOD(J,188)
I118=MOD(J,189)
I119=MOD(J,190)
I110=MOD(J,191)
I111=MOD(J,192)
I112=MOD(J,193)
I113=MOD(J,194)
I114=MOD(J,195)
I115=MOD(J,196)
I116=MOD(J,197)
I117=MOD(J,198)
I118=MOD(J,199)
I119=MOD(J,200)
I110=MOD(J,201)
I111=MOD(J,202)
I112=MOD(J,203)
I113=MOD(J,204)
I114=MOD(J,205)
I115=MOD(J,206)
I116=MOD(J,207)
I117=MOD(J,208)
I118=MOD(J,209)
I119=MOD(J,210)
I110=MOD(J,211)
I111=MOD(J,212)
I112=MOD(J,213)
I113=MOD(J,214)
I114=MOD(J,215)
I115=MOD(J,216)
I116=MOD(J,217)
I117=MOD(J,218)
I118=MOD(J,219)
I119=MOD(J,220)
I110=MOD(J,221)
I111=MOD(J,222)
I112=MOD(J,223)
I113=MOD(J,224)
I114=MOD(J,225)
I115=MOD(J,226)
I116=MOD(J,227)
I117=MOD(J,228)
I118=MOD(J,229)
I119=MOD(J,230)
I110=MOD(J,231)
I111=MOD(J,232)
I112=MOD(J,233)
I113=MOD(J,234)
I114=MOD(J,235)
I115=MOD(J,236)
I116=MOD(J,237)
I117=MOD(J,238)
I118=MOD(J,239)
I119=MOD(J,240)
I110=MOD(J,241)
I111=MOD(J,242)
I112=MOD(J,243)
I113=MOD(J,244)
I114=MOD(J,245)
I115=MOD(J,246)
I116=MOD(J,247)
I117=MOD(J,248)
I118=MOD(J,249)
I119=MOD(J,250)

```

240

```

250 CONTINUE
260 GO TO 210
      NCY=NCCP-1
265 J=-1
      IF(NCY) 265,265,270
270 GO TO 330
      NCY=NCY+1
270 IF(NCY-NCY) 280,280,310
280 J=J+7
      THLD=AHLD*Y(NLINE,NCY)+BZ
      IF(THLD) 285,290,290
285 H(J)=EMI
      GO TO 295
290 H(J)=EPL
      NUM=INT(ABS(THLD-INT(THLD))*1000.0+0.5)
295 NDS=100
      DO 300 KK=1,3
      J=J+1
      KI=NUM/NDS
      H(J)=KG(KI+1)
      NUM=NUM-KI*NDS
      NDS=NDS/10
300 CONTINUE
310 GO TO 270
      IF((NCP-M) 360,320,320
320 IF((J-127) 330,330,360
330 J=J+3
      KI=NLINE
      IF((KI-100) 340,335,335
335 LL=KI/100
      H(J)=KG(LL+1)
      KI=KI-100*LL
      GO TO 343
340 H(J)=KG(1)
343 J=J+1
      IF((KI-10) 350,345,345
345 LL=KI/100
      H(J)=KG(LL+1)
      KI=KI-10*LL
      GO TO 355
350 H(J)=KG(1)
      J=J+1
      H(J)=KG(KI+1)
      J=J-5
      IF((NCY-1) 270,270,360
360 IF((NLINE-1) 362,362,368
362 PRINT 370,(A(I),I=1,132),(B(IP1),IP1=1,132),(H(IP2),IP2=1,132)

```

```

368 GO TO 170
368 PRINT 370{A(1),I=1;132},{B(IP1),IP1=1;132},{C(IP5),IP5=1;132},
      {D(IP3),IP3=1;132},{E(IP4),IP4=1;132},{F(IP7),IP7=1;132},
      {G(IP6),IP6=1;132},{H(IP8),IP8=1;132}
370 FORWA(132A1)
370 GO TO 170
380 DO 390 I=1,135
      A(I)=BLK

```

```

368 PRINT 170 {A(I),I=1,132},{B(IP1),IP1=1,132},{C(IP2),IP2=1,132},
    1,{D(IP3),IP3=1,132},{E(IP4),IP4=1,132},{F(IP5),IP5=1,132},
    ?,{G(IP6),IP6=1,132},{H(IP7),IP7=1,132}
370 FOR I=1 TO 170
370 GO TO 170
380 DO 390 I=1,135
380 A(I)=BLK
380 B(I)=BLK
380 C(I)=BLK
380 D(I)=BLK
380 CONTINUE
390 J=-2
390 IF (NCCP-1) 395,395,400
395 DO -1 430 L=NCCP,NCP
400 J=+8
405 K1=L
405 IF (K1-100) 410,405,405
405 LL=K1/100
405 C(J)=KG(LL+1)
405 K1=K1-100*LL
405 GO TO 412
405 C(J)=KG(1)
412 J=J+1
412 IF (K1-10) 420,415,415
415 LL=K1/10
415 C(J)=KG(LL+1)
415 K1=K1-10*LL
415 GO TO 422
415 C(J)=KG(1)
420 C(J)=KG(K1+1)
420 CONTINUE
420 PRINT 370,{B(IP1),IP1=1,132},{C(IP2),IP2=1,132}
420 IF (NCP-M) 60,500,500
420 RETURN
500 END

```

0000021
.....
SUBROUTINE GAUSS
PURPOSE COMPUTES A NORMALLY DISTRIBUTED RANDOM NUMBER WITH A GIVEN
GAUS 10
GAUS 20
GAUS 300
GAUS 400
GAUS 500
GAUS 600
GAUS 700

MEAN AND STANDARD DEVIATION

USAGE
CALL GAUSS(IX,S,AM,V)

DESCRIPTION OF PARAMETERS
IX - IX MUST CONTAIN AN ODD INTEGER NUMBER WITH NINE OR LESS DIGITS ON THE FIRST ENTRY TO GAUSS. THEREAFTER IT WILL CONTAIN A UNIFORMLY DISTRIBUTED INTEGER RANDOM NUMBER GENERATED BY THE SUBROUTINE FOR USE ON THE NEXT ENTRY TO THE SUBROUTINE.
S - THE DESIRED STANDARD DEVIATION OF THE NORMAL DISTRIBUTION.
AM - THE DESIRED MEAN OF THE NORMAL DISTRIBUTION
V - THE VALUE OF THE COMPUTED NORMAL RANDOM VARIABLE

REMARKS
THIS SUBROUTINE USES RANDU WHICH IS MACHINE SPECIFIC
SUBROUTINES AND FUNCTION SUBPROGRAMS REQUIRED
RANDU

METHOD
USES 12 UNIFORM RANDOM NUMBERS TO COMPUTE NORMAL RANDOM NUMBERS BY CENTRAL LIMIT THEOREM. THE RESULT IS THEN ADJUSTED TO MATCH THE GIVEN MEAN AND STANDARD DEVIATION. THE UNIFORM RANDOM NUMBERS COMPUTED WITHIN THE SUBROUTINE ARE FOUND BY THE POWER RESIDUE METHOD.

SUBROUTINE GAUSS(IX,S,AM,V)
A=0
DO 50 I=1,12
CALL RANDU(IX,IY,Y)
IX=IY
A=A+Y
V=(A-6.0)*S+AM
RETURN
END

C0000022
CCCC

GAUS 80
GAUS 90
GAUS 100
GAUS 110
GAUS 120
GAUS 130
GAUS 140
GAUS 150
GAUS 160
GAUS 170
GAUS 180
GAUS 190
GAUS 200
GAUS 210
GAUS 220
GAUS 230
GAUS 240
GAUS 250
GAUS 260
GAUS 270
GAUS 280
GAUS 290
GAUS 300
GAUS 310
GAUS 320
GAUS 330
GAUS 340
GAUS 350
GAUS 360
GAUS 370
GAUS 380

GAUS 390
GAUS 400
GAUS 410
GAUS 420
GAUS 430
GAUS 440
GAUS 450
GAUS 460
GAUS 470

RAND 10
RAND 20
RAND 30

SUBROUTINE RANDU

PURPOSE COMPUTES UNIFORMLY DISTRIBUTED RANDOM REAL NUMBERS BETWEEN 0 AND 1.0 AND RANDOM INTEGERS BETWEEN INTEGER INPUT AS A NEW INTEGER AND REAL RANDOM NUMBER.

USAGE CALL RANDU(IX,IY,YFL)

DESCRIPTION OF PARAMETERS THIS MUST CONTAIN ANY ODD INTEGER NUMBER WITH NINE OR LESS DIGITS. AFTER THE FIRST ENTRY, IX SHOULD BE THE PREVIOUS VALUE OF IY COMPUTED BY THIS SUBROUTINE.

IY - AN INTEGER RANDOM NUMBER REQUIRED FOR THE NEXT ENTRY TO THIS SUBROUTINE. THE RANGE OF THIS NUMBER IS BETWEEN ZERO AND $2^{31} - 1$.
YFL - THE RESULTANT UNIFORMLY DISTRIBUTED, FLOATING POINT, RANDOM NUMBER IN THE RANGE 0 TO 1.0

REMARKS THIS SUBROUTINE IS SPECIFIC TO SYSTEM/360 AND WILL PRODUCE RESULTS WHICH ARE NOT REPEATING. THE REFERENCE SEEDS (65539) USED FOR THE FIRST ENTRY, RUN PROBLEMS AND PROBLEMS CONCERNING MARSAGLIA JACM 12, P. 83-89, DISCUSSES CONGRUENTIAL GENERATORS OF TWO TYPES: ONE BASED ON ONE PICKING FROM THE RAND TABLE AND ONE BENEFIT FINISH SOME CASES. 65549 HAS BEEN TABLED AS A SEED WHICH HAS BETTER STATISTICAL PROPERTIES FOR HIGH ORDER BITS OF THE SEEDS SHOULD BE CHOSEN IN ACCORDANCE WITH THE DISCUSSION GIVEN IN THE REFERENCE BELOW. ALSO, IT SHOULD BE NOTED THAT RANDOM NUMBERS ARE DESIRED AS ARE AVAILABLE FROM RANDU. THE RANDOM CHARACTERISTICS OF THESE FLOATING POINT DEVIATES ARE MODIFIED AND IN FACT THESE DEVIATES HAVE HIGH PROBABILITY OF HAVING A TRAILING LOW ORDER ZERO BIT IN THEIR FRACTIONAL PART.

SUBROUTINES AND FUNCTION SUBPROGRAMS REQUIRED
NONE

METHOD POWER RESIDUE METHOD DISCUSSED IN IBM MANUAL C20-8011.
RANDOM NUMBER GENERATION AND TESTING

RAND 40
RAND 500
RAND 600
RAND 700
RAND 800
RAND 900
RAND 1000
RAND 1100
RAND 1200
RAND 1300
RAND 1400
RAND 1500
RAND 1600
RAND 1700
RAND 1800
RAND 1900
RAND 2000
RAND 2100
RAND 2200
RAND 2300
RAND 2400
RAND 2500
RAND 2600
RAND 2700
RAND 2800
RAND 2900
RAND 3000
RAND 3100
RAND 3200
RAND 3300
RAND 3400
RAND 3500
RAND 3600
RAND 3700
RAND 3800
RAND 3900
RAND 4000
RAND 4100
RAND 4200
RAND 4300
RAND 4400
RAND 4500
RAND 4600
RAND 4700
RAND 4800
RAND 4900
RAND 500
RAND 510

C C

```
SUBROUTINE RANDU(IX,IY,YFL)
IY=IX*65539
IF(IY>616
 5 IY=IY+2147483647+1
 6 YFL=IY
    YFL=YFL*.4656613E-9
  RETURN
END
```

```
      RAND 520
      RAND 530
      RAND 540
      RAND 550
      RAND 560
      RAND 570
      RAND 580
      RAND 590
      RAND 600
```

BIBLIOGRAPHY

1. Caulfield, H. J. and Lee, Sun, The Applications of Holography, John Wiley and Sons, 1970.
2. Ellis, B. K. and Furey, R. J., Wing-Body Interactions at a Mach Number of 9.5., Naval Ship Research and Development Center Report 2564, Aerodynamics Laboratory Research and Development Report 1133, September 1967.
3. Jagota, R. C., The Application of Holographic Interferometry to the Determination of the Flow Field Around a Right Circular Cone at Angle of Attack, Aeronautical Engineer Thesis, Naval Postgraduate School, December 1970.
4. Jagota, R. C. and Collins, D. J., "Finite Fringe Holographic Interferometry Applied to a Right Circular Cone at Angle of Attack", to be published in Journal of Applied Mechanics.
5. Kaufman, L. G. II and Meckler, L., Pressure and Heat Transfer Measurements at Mach 5 and 8 for a Fin-Flat Plate Model, Technical Documentary Report No. ASD-TDR 63-235, April 1963.
6. Kaufman, L. G. II, Pressure Distributions and Oil Film Photographs for Mach 5 Flows Past Fins Mounted on a Flat Plate, Technical Documentary Report No. ASD-TDR-63-755, September 1963.
7. Landenberg, R. W., et. al., ed., Physical Measurements in Gas Dynamics and Combustion, Princeton University Press, 1954.
8. Liepmann, H. W., and Roshko, A., Elements of Gas Dynamics, p. 165, John Wiley and Sons, Inc., 1957.
9. Maldonado, C. D., Caran, A. P., and Olsen, H. N., "New Method for Obtaining Emission Coefficients from Emited Spectral Intensities. Part I--Circularly Symmetric Light Sources.", Journal of the Optical Society of America, Vol. 55, No. 10, pp. 1247-1254, October 1965.
10. Maldonado, C. D., "Note on Orthogonal Polynomials Which Are 'Invariant in Form' to Rotations of Axis", Journal of Mathematical Physics Vol. 6, No. 12, pp. 1935-1938, December 1965.
11. Maldonado, C. D. and Olsen, H. N., "New Method for Obtaining Emission Coefficients from Emited Spectral Intensities. Part II--Asymmetrical Sources", Journal of the Optical Society of America, Vol 56, No. 10, pp. 1305-1313, October 1966.
12. Matulka, R. D., The Application of Holographic Interferometry to the Determination of Asymmetric Three-Dimensional Density Fields in Free Jet Flow, Ph. D. Thesis, Naval Postgraduate School, June, 1970.
13. Matulka, R. D. and Collins D. J., "Determination of Three-Dimensional Density Fields from Holographic Interferograms", Journal of Applied Physics, Vol. 42, No. 3, March 1971.

14. Okayama, H. and Emori, Y., "Polarization Effects in Holography", Applied Physics Letters, Vol. 19, No. 9, pp. 359-360, 1 November 1971.
15. Olsen, H. N., Maldonado, C. D., Duckworth, G. D., and Caron, A. P., Investigation of the Interaction of an External Magnetic Field with an Electric Arc, Aerospace Research Laboratories Report ARL 66-0016, January 1966.
16. Olsen, H. N., Maldonado, C. D., and Duckworth, G. D., "A Numerical Method for Obtaining Internal Emission Coefficients from Externally Measured Spectral Intensities of Asymmetrical Plasmas", J. Quant. Spectrosc. Radiat. Transfer, Vol. 8, pp. 1419-1430, 1968.
17. Ragent, B. and Brown, R. M., editors, Holographic Instrumentation Applications, Conference held at Ames Research Center, Moffett Field, California, NASA SP-248, January 13-14, 1970.
18. Roe, P. L., Exploratory Flow Measurements in the Wing-Body Junction of a Possible Mach Four Vehicle, Royal Aircraft Establishment Technical Report No. 65257, November 1965.
19. Polutchko, R. J., Hypersonic Flow Field About a Blunt Slab Wing at Angle of Attack: Phase I, Aerospace Research Laboratories 64-213, December 1964.
20. Stewartson, K. and Treadgold, D. A., "Wing-Body Interference at Supersonic Speeds", Transonic Aerodynamics, AGARD Conference Proceedings No. 35, pp. 19-1--19-9, September 1968.
21. Stewartson, K., On Wing-Body Interference in Supersonic Flow, Aeronautical Research Council 27-715, 9 February 1966.
22. Stollery, J. K., Hypersonic Viscous Interaction--An Experimental Investigation of Flow over Flat Plates at Incidence and Around an Expansion Corner, Aerospace Research Laboratories 70-0125, July 1970.
23. Thomas, J. P., Investigation of the Pressure Distribution on a Blunt-Fin Blunt-Plate Combination at a Mach Number of 11.26, Aerospace Research Laboratories 66-0142, July 1966.
24. Thomas, J. P., Flow Investigation At a Fin-Plate Model at a Mach Number of 11.26, Aerospace Research Laboratories 67-0188, September 1967.
25. Weirich, R. L. and Vahl, W. A., Flow-Field Properties Near an Arrow-Wing-Body Model at Mach Numbers of 1.60, 2.36, and 2.96, NASA Technical Note D-4809, October 1968.
26. Winkelmann, A. E., "Flow Visualization Studies of a Fin Protuberance Partially Immersed in a Turbulent Boundary Layer at Mach 5", United States Naval Ordnance Laboratory NOLTR-70-93, 20 May 1970.
27. Winkelmann, A. E., "Aerodynamic Interaction Phenomena Produced by a Fin Protuberance Partially Immersed in a Turbulent Boundary Layer at Mach 5", AGARD Conference Proceedings No. 71, September 1970.